

A hand is shown from the palm side, holding a bright, jagged lightning bolt between the thumb and index finger. The lightning bolt is a mix of blue and pinkish-purple. The background is a blue grid pattern that transitions into a white grid pattern at the top right.

Aram H. Markosyan

MODELING

multiple time scales
in streamer discharges



Aram H. Markosyan

Aram H. Markosyan was born in Yerevan, Armenia on December 3, 1985. From 2002 to 2008 he studied Mathematics at Yerevan State University. He obtained his Bachelor of Science with honours, the latter in 2006 on a thesis titled “An application of variational inequalities to the monotone operator theory”, under supervision of Dr. G. Hakobyan. In 2008 he obtained the degree of Master of Science in Mathematics by defending his thesis entitled “Existence of the minimal element of the class of super solutions in the one-phase parabolic free boundary problem in convex domain” under supervision of Dr. M. Poghosyan.

In late 2008 he moved to Paris and enrolled in the Master of Science & Technologies (M2) program of Mathematical Modeling, PDE and Numerical Analysis (in French: Spécialité Mathématiques de la Modélisation, parcours “Analyse Numérique & Équations aux Dérivées Partielles”) at Jacques-Louis Lions Laboratory, University Pierre and Marie Curie (UPMC, Paris 6). In parallel to his studies, from the beginning of 2009 until the end of 2009, Aram H. Markosyan did his internship at Zeliade Systems under the supervision of CEO Dr. C. Martini. In late 2009, he defended his Master's thesis titled “SVI implied variance parameterization” under supervision of Dr. C. Martini (Zeliade Systems), Prof. Dr. O. Pironneau (Paris 6) and Prof. Dr. H. Berestycki (Paris 6).

From 2010 to 2014 he performed PhD research under supervision of Prof. Dr. U. Ebert, Dr. S. Dujko and Prof. Dr. W. Hundsdorfer on modeling multiple time scales in streamer discharges, at the Centrum Wiskunde & Informatica (CWI, Amsterdam).

ISBN 9789462591677



9 789462 591677

Modeling multiple time scales in streamer discharges

Modeling multiple time scales in streamer discharges

PROEFSCHRIFT

ter verkrijging van de graad van doctor aan de
Technische Universiteit Eindhoven, op gezag van de
rector magnificus prof.dr.ir. C.J. van Duijn, voor een
commissie aangewezen door het College voor
Promoties, in het openbaar te verdedigen
op maandag 19 mei 2014 om 16.00 uur

door

Aram Markosyan

geboren te Jerevan, Armenië

Dit proefschrift is is goedgekeurd door de promotoren en de samenstelling van de promotiecommissie is als volgt:

voorzitter: prof.dr. H.J.H. Clercx
promotor: prof.dr. U.M. Ebert
copromotor: dr. S. Dujko
leden: prof.dr. N.L. Aleksandrov (Moscow Institute of Physics
and Technology)
Prof.dr. R.P. Brinkmann (Ruhr-Universität Bochum)
prof.dr. C.W. Oosterlee (Technische Universiteit Delft)
prof.dr.ir. B. Koren
prof.dr.ir. O.J. Luiten

Dit onderzoek werd gesteund door project 10751 van Technologiestichting STW, dat deel uitmaakt van de Nederlandse Organisatie voor Wetenschappelijk Onderzoek (NWO). Het Centrum Wiskunde & Informatica (CWI) en STW hebben bijgedragen in de drukkosten van het proefschrift. Verder wil ik het CWI bedanken voor alle faciliteiten en ondersteuning.



ISBN 978-94-6259-167-7

Copyright © 2014 by A.H. Markosyan

All rights reserved. No part of the material protected by this copyright notice may be reproduced or utilized in any form or by any means, electronic or mechanical, including photocopying, recording or by any information storage and retrieval system, without the prior permission of the author.

Cover design: Gegham Sargsyan

Typeset by the author with the L^AT_EX Documentation System

Printed in The Netherlands by: Ipskamp Drukkers Print Service

To my parents, my sister, and my beloved fiancée Araks
Սիրով նվիրում եմ ծնողներին, Անուշիկ քույրիկին և Արաքս հարսնացուին:

Contents

Main Content

1	Introduction	1
1.1	Streamers	1
1.2	Multiple time scales in and after streamer discharges	3
1.3	The content of the thesis	3
2	Derivation of high-order fluid model for streamer discharges	5
2.1	Introduction	5
2.2	Derivation of first- and higher order fluid models	8
2.2.1	General considerations: Boltzmann equation and moment equations	8
2.2.2	The first-order or classical fluid model	9
2.2.3	Second order models including the energy balance equation	13
2.2.4	High order fluid model	14
2.3	Transport and reaction data	18
2.3.1	Evaluation of the transport data: Boltzmann equation analysis	18
2.3.2	Cross sections and transport data	21
2.3.3	Input data for the first order model	22
2.3.4	Input data for the high order model	24
2.4	First order streamer model with different transport data	26
2.4.1	Numerical methods, initial and boundary conditions.	26
2.4.2	Overview of simulation results with different transport data	27
2.4.3	Front velocities	29
2.4.4	Ionization levels behind the front	30
2.5	Conclusion	30
3	Numerical solution of high-order fluid model for streamer discharges in 1D and investigation of planar fronts	33

3.1	Introduction	33
3.2	Model description and numerical solution	36
3.2.1	The high order fluid model	36
3.2.2	1D hyperbolic system of balance laws	37
3.2.3	Initial and boundary conditions	38
3.3	MC particle model and first order fluid model	39
3.3.1	The MC particle model	39
3.3.2	The first order fluid model	39
3.4	Results and discussion	40
3.4.1	Simulation of planar fronts: overall comparison between the models	40
3.4.2	Electron energy profiles in different front regions within the different models	42
3.4.3	On the use of transport data in the high order fluid model .	49
3.4.4	Simulation of planar fronts with and without the energy flux term	50
3.4.5	Simulation of planar fronts with and without the high order tensor	52
3.5	Conclusion	54
4	Comparison of fluid models for streamer discharges with MC- PIC results	57
4.1	Introduction	57
4.2	Fluid models for streamer discharges	59
4.2.1	The first-order or classical model	61
4.2.2	The second-order model	62
4.2.3	The high-order model	64
4.3	The MC particle model	65
4.4	Transport parameters	65
4.4.1	What to do when $n_e \rightarrow 0$?	68
4.5	Simulation conditions	69
4.5.1	Boundary conditions	69
4.5.2	Initial conditions	69
4.5.3	Numerical method	69
4.5.4	Time stepping	70
4.6	Comparison results	70
4.6.1	Basic comparison of planar fronts in Ne	71
4.6.2	Comparison of average electron energies in different models	73
4.7	Discussion	75
4.8	Conclusions	76
5	Investigation of positive streamers by double pulse experiments, effects of repetition rate and gas mixture	77
5.1	Introduction	77
5.2	Experimental setup by S. Nijdam and E. Takahashi	79
5.3	General development	82

5.3.1	Air	82
5.3.2	Pure nitrogen	87
5.3.3	Pure argon	87
5.4	Duration of streamer continuation	90
5.4.1	Oxygen concentration effects	92
5.5	Modelling	93
5.5.1	Model description	93
5.5.2	Modelling results on streamer continuation	94
5.5.3	Other modelling results	99
5.6	Summary and conclusions	100
5.6.1	Continuation of old paths	100
5.6.2	Other phenomena	101
6	PumpKin: A tool to find principal pathways in plasma chemical models	103
6.1	Introduction	103
6.2	PumpKin algorithm	106
6.3	Code description and general requirements	106
6.3.1	Input and output	107
6.4	Examples	109
6.4.1	Species of interest	109
6.4.2	Dominant pathways or reduction	111
6.5	Conclusions	112
7	Conclusions and Outlook	113
7.1	High order fluid model	113
7.2	Plasma chemistry	114
	References	117
	 Appendices	
A	Discretization of the high order fluid model	139
B	PumpKin algorithm	141
B.1	Basic definitions	141
B.2	Description of the algorithm	143
B.2.1	Initialization.	143
B.2.2	Branching-points.	144
B.2.3	Merging pathways.	144
B.2.4	Deletion of insignificant pathways.	145
B.2.5	Sub-pathways.	145
C	List of reactions used in chemical model	147
	Summary	153

Acknowledgements	155
Curriculum Vitae	165
List of Publications	167

CHAPTER 1

Introduction

In science one tries to tell people, in such a way as to be understood by everyone, something that no one ever knew before. But in poetry, it is the exact opposite.

– PAUL DIRAC

There are sadistic scientists who hurry to hunt down errors instead of establishing the truth.

– MARIE CURIE

1.1 Streamers

Streamers are rapidly growing ionized filaments appearing in gases, liquids and solids. The propagation is driven by their own space charge field. The dynamics of the streamers is mostly controlled by the high-field region ahead of the *streamer head*. In a rather thin layer around the head the net charge is high and positive or negative depending on the polarity of the streamer. In figure 1.1 we show various parts of the streamer structure. The high field ahead of the head, which can reach 4-7 times the breakdown field, creates additional ionization that moves the streamer forward. The channel of the streamer is an electrically neutral plasma, with ionization densities going up to 10^{14} cm^{-3} in air at standard temperature and pressure (293 K, 1 bar). In air streamers propagate very fast: with velocities in the range of $10^5 - 10^7 \text{ m/s}$, where $3 \times 10^8 \text{ m/s}$ is the speed of light in the vacuum.

The concept of streamer discharges was introduced in the 1930's by Raether [179]. The theory was further promoted by Meek [135], Loeb [117, 118, 119, 120] and Raether [116], though the exact form of the space charge distribution and

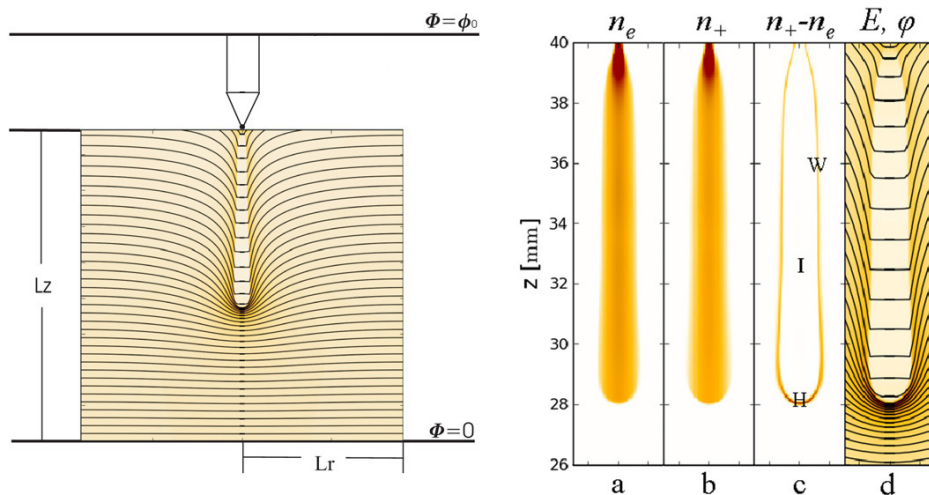


Figure 1.1: Simulation of positive streamer performed by [183] in air showing the various parts of the streamer structure. Full domain is shown in the left panel, panel a and b show electron and positive ion density respectively. Panel c shows the net charge density and marks the different parts of the streamer: H - streamer head, W - channel wall, I - streamer interior. Panel d shows the electric field strength (colour coded) and equipotential lines.

the amount of field enhancement became clear only in the early 80's with the first simulations [53].

Streamers occur widely in pulsed discharges, both in nature and in technology. As their size scales with inverse gas density, streamers occur in the limited volumes of plasma technological devices mostly at high gas densities, while our atmosphere also can host huge discharges at very low air densities at high altitudes; so-called sprite discharges [54, 64, 126] are streamers, they exist at altitudes of up to 90 km in our atmosphere, i.e. at pressures down to well below 10 μ bar. For a cluster issue on streamers, sprites and lightning, we refer to [49] and the 19 original papers therein, discussing common issues of streamer dynamics in atmospheric discharges and plasma technology, including discharge evolution and subsequent chemical reactions. Streamers are a key element in gas processing in so-called corona reactors [226, 237] as well as in high-voltage technology [202]; they are used for the treatment of polluted gases [227] and water [70] or for plasma-enhanced vapour deposition [11]. The plasma bullets observed in plasma jets in noble gases have now been identified with streamers [21, 86, 147, 148, 240, 241]. Studies of breakdown phenomena at atmospheric pressure in short non-uniform air gaps [145] or in microwave fields [32] benefit from related streamer studies. Streamers appear as well in resistive plate chambers used in high-energy physics, where the streamer mode of operation must be carefully controlled and optimized [39, 63, 89].

1.2 Multiple time scales in and after streamer discharges

A streamer is a multiscale phenomenon both in space and time. Multiple space-scales of streamer heads have been actively investigated by many authors, see [53, 55] and the references within. The fast time-scales of streamer dynamics are associated with the streamer inception and the propagation of the streamer head. Streamer inception is the stage when streamer initiates due to locally high electric fields [14, 25, 48, 168, 178]. When the streamer head moves, it leaves weakly ionized plasma in the streamer channel behind, which is full of chemically activated species. Another time scale of streamer dynamics is involved in the heating of the streamer channel. The heating process is a result of relaxation of the energies stored in the vibrational and electronically excited levels of molecules into the translational energy levels. This process depends very much on external conditions (such as pressure, background gas temperature, externally applied electric field etc.) and the initial energy input in the system. In the later phases, the localised heating causes the gas expansion and the mixing of the chemically activated radicals inside of the domain. The later property is essential for such industrial application as plasma assisted combustion, where different radicals and species need to be generated and efficiently mixed. Observations show that more time scales are associated with the gas expansion stages where turbulence is starting to play a significant role [33, 85, 99, 115, 124, 197, 203].

Depending on the external conditions (electric circuit configuration, gap distance, voltage duration etc.) streamer can initiate other types of discharges, like sparks, arcs, leaders etc. [5, 6, 56, 57, 132, 136, 144, 145, 184]. In that case, the processes described above will continue. Depending on the application and the timescales of application, one can be interested in fast or very slow mechanisms of chemistry or heating.

1.3 The content of the thesis

The chapters 2 and 3 are devoted to the derivation and numerical implementation of a high order fluid model for the head region of streamers. We have derived a new high order fluid model for streamer discharges based on first principles. The high order fluid model employs the first four moments of the Boltzmann equation. The system of equations is closed by approximating the highest order tensor with lower order moments, namely the average electron density and the average electron energy. Macroscopic quantities like the average electron energy and the average electron energy flux can be essential input for plasma chemical models.

In chapter 4 we compare the most frequently used fluid models to simulate streamer discharges, namely the first order classical drift-diffusion-reaction fluid model, the second order employing the local energy approximation and the high order fluid model. We compare results of fluid models with microscopic Particle-in-Cell Monte Carlo results.

In chapter 5 S. Nijdam and E. Takahashi have performed experiments in air and argon to investigate the effects of a preceding streamer discharge on a sub-

sequent discharge by applying two positive high voltage pulses in succession with pulse-to-pulse intervals (Δt) between 200 ns and 40 ms. They observed that the value of Δt for which we can still observe continuation of the first-pulse streamers during the second pulse, depends on oxygen concentration in nitrogen-oxygen mixtures, and has a maximum at an oxygen concentration of about 0.2%. We have applied zero dimensional plasma-chemical modelling to reproduce and explain these results.

We have developed a tool, called PumpKin, to find the dominant pathways in plasma chemical models, presented in chapter 6. The tool is based on the algorithm proposed by R. Lehmann [103]. PumpKin is a user friendly tool publicly available under the license GNU GPL (version 2) and can be obtained from the website <http://www.pumpkin-tool.org>.

Each chapter contains a very detailed introduction to the subject of the respective chapter.

CHAPTER 2

Derivation of high-order fluid model for streamer discharges

The beginning of knowledge is the discovery of something we do not understand.

– FRANK HERBERT

Any sufficiently advanced technology is indistinguishable from magic.

– ARTHUR C. CLARKE

Yes, we have to divide up our time like that, between our politics and our equations. But to me our equations are far more important, for politics are only a matter of present concern. A mathematical equation stands forever.

– ALBERT EINSTEIN

2.1 Introduction

Streamers are rapidly growing filaments of weakly ionized plasma, whose dynamics are controlled by highly localized space charge regions and steep plasma density gradients. The dynamics of the streamer ionization front are governed by electron

This chapter is based on the publication [47] *High-order fluid model for streamer discharges: I. Derivation of model and transport data* by Saša Dujko, Aram H. Markosyan, Ron D. White and Ute Ebert published in *Journal of Physics D: Applied Physics*, Volume 46, Number 47, Page 475202, 2013.

dynamics in electric fields above the breakdown value; therefore, the plasma is very far from equilibrium, and the neutral gas stays cold while the ionization front passes.

The progress of streamer simulations with fluid models has recently been reviewed in [125]. The main point for this paper is that essentially all these numerical studies are based on the classical fluid model, as we have called it in [110, 111, 112]. The classical fluid model for electron density contains a reaction term for impact ionization and attachment, a drift term accounting for electron displacement in the local field, and electron diffusion; the reaction term is typically taken as a function of the local electric field. The structure of this classical model with reaction, drift and diffusion is based on basic symmetry considerations and conservation laws; it has generally emerged as a purely phenomenological model in the course of the past century, though it was also derived later from the Boltzmann equation by Gogolides and Sawin [66].

On the other hand, cross-sections for the collisions of electrons with molecules have become available with growing accuracy [7, 36, 170, 171, 182]. They are the input either for the Boltzmann equation or for Monte Carlo models. These microscopic particle models have not yet been appropriately linked with the much older phenomenological fluid models. This becomes evident when comparing their solutions. A negative streamer ionization front in nitrogen represented by a Monte Carlo model cannot appropriately be described by a classical fluid model even if the transport and reaction coefficients for the fluid model are derived from the Monte Carlo model [107]. In [107], the coefficients for the fluid model were derived as so-called bulk coefficients; therefore, in this model the electron swarms evolve correctly, and ionization fronts in a given electric field propagate with the correct velocity, as they are so-called pulled fronts [107]. However, the electron density behind the ionization front is very low. As we will see in section 2.4.2 of this chapter, a classical fluid model evaluated with flux coefficients gives better ionization densities behind the front, but very low front velocities. A phenomenological extension of the classical fluid model with a gradient expansion considerably improves the approximation of the microscopic electron dynamics [4, 143], and it cures the deficiency of the local field approximation by including a dependence of the impact ionization rate on the local electron density gradient [110]. That the extended fluid model matches the Monte Carlo model well up to the moment of streamer branching, can also be seen in a recent comparison of three-dimensional model simulations in [112]. On the other hand, the model is still based on a local field approximation, therefore electron energies in the streamer interior are modelled erroneously as relaxing instantaneously to the low field in the streamer interior.

A full simulation by Monte Carlo models would deliver the physically most reliable results, but this is computationally extremely costly. As a compromise between accuracy and efficiency, hybrid methods [108, 110, 111, 112] have been developed in the past years to track the fast and energetic processes in the ionization front with a particle model, and to model the many electrons at lower fields in the streamer interior with a fluid model. Fluid models are also the most efficient for the long time evolution in the streamer interior where slow chemical

reactions and a slow thermalization of the deposited energy set in.

These demands on fast and quantitative streamer simulations ask for the development of a fluid model that accurately incorporates the microscopic electron dynamics contained in Boltzmann or Monte Carlo models. We will follow here the strategy to derive such a model not from phenomenological considerations, but through a systematic derivation from the Boltzmann equation.

This chapter is the first in an ongoing investigation of high-order fluid models for streamer discharges; it is focused on the derivation of first- and higher order fluid models and on the derivation and correct implementation of transport data in these models. Section 2.2 describes the derivation of models of different order. The starting point is the set of balance equations obtained as velocity moments of the Boltzmann equation. Then the derivation of the classical first-order model is briefly described, and previous approaches to higher order models are summarized. In section 2.2.4, our new high-order fluid model is derived in a systematic manner. The balance/moment equations are closed after the balance equation for the energy flux. This is done by approximating the high-order tensors in the energy flux balance equation by a product of two lower moments while the collision transfer terms are evaluated using momentum transfer theory. In section 2.3, electron transport properties as an input in fluid models are calculated using a multi-term theory for solving the Boltzmann equation [43, 234]. We pay particular attention to the accuracy of the calculation and the proper use in both the first- and high-order fluid models. The results of our multi-term solution of Boltzmanns equation are compared with those obtained by the publicly available Boltzmann solver BOLSIG+ developed by Hagelaar and Pitchford [74] for electrons in molecular nitrogen. BOLSIG+ is a popular Boltzmann solver based on a classical two-term theory, so we have been motivated to check its accuracy and integrity against the advanced and highly sophisticated multi-term Boltzmann solver developed by the group from the James Cook University and their associates [43, 150, 190, 234]. In section 2.4, we give the results for negative planar fronts obtained with the first- order, model with particular emphasis upon the consistent implementation of transport data. It should be noted that a full 3D streamer channel is characterized by a high field enhancement at its growing tip. This field enhancement is created by a thin space charge layer around its ionized interior that in turn largely suppresses the interior field. The thickness of the space charge layer is much smaller than its radius of curvature [51, 52, 107, 110, 111]. Therefore, when zooming into the front structure, the curvature can be neglected. Modelling this front structure is the largest challenge for a fluid model and therefore this is what we focus on in section 2.4. The results for various streamer properties obtained with different types of input data are compared. A thorough analysis of numerical streamer front solutions with our high-order model, and a comparison with Monte Carlo results is contained in chapter 3.

2.2 Derivation of first- and higher order fluid models

2.2.1 General considerations: Boltzmann equation and moment equations

Our starting point is the Boltzmann equation for charged particles in an electric field \mathbf{E}

$$\partial_t f_i + \mathbf{c} \cdot \nabla f_i + \frac{e_i}{m_i} \mathbf{E} \cdot \nabla_{\mathbf{c}} f_i = -J(f_i, f_0). \quad (2.1)$$

Here $f_i(\mathbf{r}, \mathbf{c}, t)$ is the distribution function in phase space at the position \mathbf{r} and velocity \mathbf{c} for each charged component i , ∇ is the differential operator with respect to space \mathbf{r} and $\nabla_{\mathbf{c}}$ with respect to velocity \mathbf{c} , e_i and m_i are charge and mass of species i , and t is time. The right-hand side of equation (2.1), $J(f_i, f_0)$, describes the collisions of charged particles with neutral molecules, accounting for elastic, inelastic, and non-conservative (e.g. ionizing or attaching) collisions, and f_0 is the velocity distribution function of the neutral gas (usually taken to be Maxwellian at temperature T_g).

Streamer discharges have a characteristic nonlinear coupling between densities of charged particles and electric field. The space charge modifies the field, and the field determines the drift, diffusion and rate coefficients. The electric field has to be calculated self-consistently with Poisson's equation

$$\nabla \cdot \mathbf{E} = \frac{1}{\epsilon_0} \sum_i e_i n_i(\mathbf{r}, t), \quad (2.2)$$

where ϵ_0 is the dielectric constant, and e_i and n_i are the charges and densities of species i that can be electrons and ions. As ions are much heavier than electrons, their motion is typically neglected within the ionization front, and the analysis focuses on the electron evolution. Thus, in what follows we suppress the charged particle index i in equation (2.1) and focus in the electron dynamics.

After solving equations (2.1) and (2.2), quantities of physical interest could be obtained as velocity ‘moments’ of the distribution functions, starting with the number density

$$n(\mathbf{r}, t) = \int f(\mathbf{r}, \mathbf{c}, t) d\mathbf{c}, \quad (2.3)$$

followed by higher order quantities

$$\langle \phi(\mathbf{c}) \rangle = \frac{1}{n(\mathbf{r}, t)} \int \phi(\mathbf{c}) f(\mathbf{r}, \mathbf{c}, t) d\mathbf{c}, \quad (2.4)$$

with $\phi(\mathbf{c}) = m\mathbf{c}$, $\frac{1}{2}mc^2, \dots$ furnishing the average velocity $\mathbf{v} = \langle \mathbf{c} \rangle$, average energy $\varepsilon = \langle \frac{1}{2}mc^2 \rangle$, and so on.

Equations (2.1) and (2.2) represent a non-linear coupled system of partial differential equations in 6-dimensional phase space and in time, with a complicated collision operator J . For a complete problem description, appropriate initial and boundary conditions on $f(\mathbf{r}, \mathbf{c}, t)$ in phase space must be implemented.

For streamers, it is very difficult to solve equations (2.1) and (2.2) due to the large gradients of electric fields and of charged particle densities at their fronts.

Moreover, the streamers create a self-consistent field enhancement at their tips which allow them to penetrate into regions where the background field is too low for efficient ionization processes to take place. From a kinetic theory point of view, this is a non-stationary, non-hydrodynamic and non-linear problem where space and time should be treated on an equal footing with velocity in equation (2.1). Clearly, the numerical solution of equations (2.1) and (2.2) for the full streamer problem is a formidable task and a fluid equation treatment is more tractable. In a fluid approach, the problem of solving the Boltzmann equation for f in phase-space is replaced by a set of low order approximate (velocity) moment equations of f [192, 193, 234].

Fluid equations may be derived either directly as moments of (2.1) or from first principles using physical arguments. Following the first approach, the set of moment/balance equations can be found by multiplying (2.1) by $\phi(\mathbf{c})$ and integrating over all velocities

$$\partial_t (n\langle\phi(\mathbf{c})\rangle) + \nabla \cdot (n\langle\mathbf{c}\phi(\mathbf{c})\rangle) - n\frac{e}{m}\mathbf{E} \cdot \langle\nabla\mathbf{c}\phi(\mathbf{c})\rangle = C_\phi, \quad (2.5)$$

where $\langle\rangle$ represents the average over the velocity \mathbf{c} of the charged particles, and C_ϕ is the collision term in the balance equation:

$$C_\phi = - \int \phi(\mathbf{c})J(f)d\mathbf{c}. \quad (2.6)$$

To derive the term $\langle\nabla\mathbf{c}\phi(\mathbf{c})\rangle$ with its negative sign, a partial integration over \mathbf{c} has been performed.

If one now takes $\phi(\mathbf{c})$ consecutively equal to 1, $m\mathbf{c}$, $\frac{1}{2}mc^2$ and $\frac{1}{2}mc^2\mathbf{c}$, etc., equation (2.5) generates an infinite series of equations, a full solution of which would be equivalent to calculating f itself. In practice, one truncates after a certain moment equation; in this process obviously some information of the Boltzmann equation is lost. Therefore we now discuss the derivation of first and second order fluid models with their truncations of the moment equations, and then we derive systematically our new high order fluid model.

2.2.2 The first-order or classical fluid model

First we derive the classical fluid model as an approximation from the Boltzmann equation. We use continuity and momentum balance equation, i.e., $\phi(\mathbf{c}) = 1$ and $m\mathbf{c}$, and truncate the set (2.5) at the momentum balance equation,

$$\partial_t n + \nabla \cdot (n\mathbf{v}) = C_1, \quad (2.7)$$

$$\partial_t (nm\mathbf{v}) + \nabla \cdot (nm\langle\mathbf{c}\mathbf{c}\rangle) - ne\mathbf{E} = C_{m\mathbf{c}}, \quad (2.8)$$

where $\mathbf{v} = \langle\mathbf{c}\rangle$ is the average local electron velocity. Now the velocities are decomposed into an average velocity \mathbf{v} plus random velocities $\mathbf{c} - \mathbf{v}$ with zero mean ($\langle\mathbf{c} - \mathbf{v}\rangle = 0$). On introducing the pressure tensor

$$\mathbf{P} = nm\langle(\mathbf{c} - \mathbf{v})(\mathbf{c} - \mathbf{v})\rangle, \quad (2.9)$$

equation (2.8) becomes

$$\partial_t (nm\mathbf{v}) + \nabla \cdot (nm\mathbf{v}\mathbf{v}) + \nabla \cdot \mathbf{P} - ne\mathbf{E} = C_{mc}, \quad (2.10)$$

where the following identity was used

$$\begin{aligned} \nabla \cdot (nm\langle \mathbf{c}\mathbf{c} \rangle) &= \nabla \cdot [nm(\mathbf{v}\mathbf{v} + \mathbf{v}\langle \mathbf{c} - \mathbf{v} \rangle + \langle \mathbf{c} - \mathbf{v} \rangle \mathbf{v} + \langle (\mathbf{c} - \mathbf{v})(\mathbf{c} - \mathbf{v}) \rangle)] \\ &= \nabla \cdot (nm\mathbf{v}\mathbf{v}) + \nabla \cdot (nm\langle (\mathbf{c} - \mathbf{v})(\mathbf{c} - \mathbf{v}) \rangle). \end{aligned} \quad (2.11)$$

The second term in the left-hand side of (2.10) can be expanded as

$$\nabla \cdot (nm\mathbf{v}\mathbf{v}) = nm(\mathbf{v} \cdot \nabla)\mathbf{v} + \mathbf{v}[\nabla \cdot (nm\mathbf{v})]. \quad (2.12)$$

Now we substitute (2.12) into (2.10), use the continuity equation (2.7) and introduce the convective time derivative

$$\frac{d}{dt} = \partial_t + \mathbf{v} \cdot \nabla, \quad (2.13)$$

which measures the rate of change in a reference frame moving with the mean drift velocity \mathbf{v} of the electrons. The momentum balance equation then obtains the form

$$nm\frac{d\mathbf{v}}{dt} = ne\mathbf{E} - \nabla \cdot \mathbf{P} + C_{mc} - m\mathbf{v}C_1. \quad (2.14)$$

The physical interpretation of this equation is straightforward: the rate of change of the mean electron velocity is due to the force of the electric field plus forces due to the pressure of the electron fluid itself and due to internal forces associated with the collisional interactions with a large number of neutral gas molecules. It should be emphasized, however, that the form with the convective derivative d/dt is not useful for the analysis of a full streamer problem where local fields and therefore local mean electron velocities \mathbf{v} vary largely in space and time.

Because the system has been truncated, the yet unspecified tensor \mathbf{P} (2.9) of electron pressure appears on the right-hand side of (2.14), and a closure assumption needs to be found. If the distribution of random velocities is close to isotropic, the diagonal terms of \mathbf{P} are equal and given by the scalar kinetic pressure p ,

$$\mathbf{P} \approx p\mathbf{I} = nkT, \quad (2.15)$$

where \mathbf{I} is the unity tensor, k is the Boltzmann constant and T is the electron temperature. It should be emphasized here that the isotropy of the velocity fluctuations and of the pressure is a strong assumption at the streamer tip where the electric fields are high and strong pressure gradients exist. In this streamer region the random spread of electrons along the field direction can differ significantly from the perpendicular direction.

The next simplifying assumption concerns the collision terms. An expression often used for momentum transfer by collision is

$$C_{mc} = -nm\nu_{\text{eff}}\mathbf{v}, \quad (2.16)$$

which assumes that the force per unit volume exerted on the electrons due to collisions with neutral molecules is proportional to the average electron velocity. The proportionality constant is called the effective momentum transfer collision frequency; it accounts for momentum exchange in elastic and inelastic collisions. With this simplifying assumption and neglecting the transfer of momentum in non-conservative collisions¹ relative to other momentum transfer collisions (which is usually a good approximation), the momentum balance equation (2.14) becomes

$$nm \frac{d\mathbf{v}}{dt} = ne\mathbf{E} - \nabla p - nm\nu_{\text{eff}}\mathbf{v}. \quad (2.17)$$

If the rate of momentum change $(d_t\mathbf{v})/\mathbf{v}$ is smaller than the rate of momentum transfer ν_{eff} , and if the gradients in electron energy can be neglected, one gets the following expression for the average flux of the electrons

$$\mathbf{\Gamma} = n\mathbf{v} = n\mu\mathbf{E} - D\nabla n, \quad (2.18)$$

where mobility and diffusion constant are given by

$$\mu = \frac{e}{m\nu_{\text{eff}}}, \quad D = \frac{kT}{m\nu_{\text{eff}}}, \quad (2.19)$$

if the system is close to equilibrium. In this case the Nernst-Townsend-Einstein relation

$$\frac{D}{\mu} = \frac{kT}{e} \quad (2.20)$$

is valid. The steady-state form of equation (2.17) is an acceptable approximation because the effective time constant for momentum transfer $\frac{1}{\nu_{\text{eff}}}$ at atmospheric pressure is generally much less than the time scale on which the local electric field varies within a streamer [87, 107].

Further from equilibrium as in the head of the streamer where the electric fields are high, the approximation (2.15) is not valid as the velocity fluctuations of the electrons are clearly anisotropic. Let us consider once more the special case where the average velocity of electrons is stationary. From equation (2.14) and neglecting momentum transfer in non-conservative collisions, we obtain

$$mn\nu_{\text{eff}}\mathbf{v} = en\mathbf{E} - \nabla \cdot \mathbf{P}, \quad (2.21)$$

and as a result for the flux we have

$$\mathbf{\Gamma} = n\mu\mathbf{E} - \frac{1}{\nu_{\text{eff}}} \nabla \cdot [n\langle(\mathbf{c} - \mathbf{v})(\mathbf{c} - \mathbf{v})\rangle]. \quad (2.22)$$

Comparing the last equation and equation (2.18), it is obvious that quantity

$$\mathbf{D}^* = \frac{\langle(\mathbf{c} - \mathbf{v})(\mathbf{c} - \mathbf{v})\rangle}{\nu_{\text{eff}}} \quad (2.23)$$

¹Non-conservative collisions do not conserve particle numbers as they account for ionization, attachment or recombination reactions.

is the reminiscence of the diffusion tensor often used in the drift-diffusion approximation instead of the diffusion constant. However, the physical interpretation of this quantity is not *a priori* clear. Though this quantity assumes the anisotropic nature of the temperature tensor, it reduces to the diffusion constant D when the effective momentum transfer collision frequency ν_{eff} is independent of the electron energy. For an energy-dependent effective momentum transfer collision frequency, the straightforward generalization of the Einstein relation for the diffusion constant (2.19) to the diffusion tensor \mathbf{D} or application of \mathbf{D}^* in the equation for the average flux (2.18) is misleading and reader is referred to [133, 186, 187] where the so-called generalized Einstein relation were introduced using the momentum and energy balance equations. However, the generalization of the diffusion constant D appearing in (2.18) to diffusion tensor \mathbf{D} is a very welcome step in fluid modeling of streamer discharges due to the often strong anisotropic nature of the diffusion tensor for certain gases and due to deviations of the electron velocity distribution function from a Maxwellian distribution of velocities in different spatial regions of the streamers.

When the above approximation for the particle flux is inserted into equation (2.7), we get the well known reaction drift diffusion expression for the charged particle motion in the discharge

$$\partial_t n + \nabla \cdot (\mu(\mathbf{E}) \mathbf{E} n - \mathbf{D}(\mathbf{E}) \cdot \nabla n) = C_1. \quad (2.24)$$

Originally this approximation was not derived from the Boltzmann equation, but derived on purely phenomenological grounds. It is clear that the equation must have the structure of a continuity equation with a source term for electron generation and loss. The parametric dependence of the source term is open at this point; within the classical model the source term is assumed to depend on local particle densities and on the local electric field. The second approximation concerns the electron velocity \mathbf{v} . On a time scale much larger than the collision frequency, the electron motion is overdamped, so the electrons must drift against the direction of the electric field according to the second term in (2.24). The stochastic and undirected motion is modeled in an *ad hoc* manner through the diffusion term; the fact that the diffusion correction is added to the drift term and not included in any other functional manner is not *a priori* clear and can actually be deduced from the above analysis.

In conclusion, the lowest level of fluid approximation, also called classical model or first order model, is given by the equations

$$\partial_t n = \nabla \cdot (\mathbf{D} \cdot \nabla n) + \nabla \cdot (\mu n \mathbf{E}) + n(\nu_I - \nu_A), \quad (2.25)$$

$$\partial_t n_p = n \nu_I, \quad (2.26)$$

$$\partial_t n_n = n \nu_A, \quad (2.27)$$

coupled to the Poisson equation for the electric field,

$$\nabla^2 \phi = \frac{e}{\epsilon_0} (n - n_p + n_n), \quad \mathbf{E} = -\nabla \phi. \quad (2.28)$$

Here n_p and n_n are positive and negative ion densities, while ν_I and ν_A are the ionization and attachment collision frequencies due to electron-molecule collisions,

and ϕ is the electric potential. The numerical solution of the system (2.25)-(2.28) requires the transport properties μ , \mathbf{D} , ν_I and ν_A as a function of the local electric field for the gas in question. The derivation and implementation of transport data is discussed in section 2.3. The numerical solutions of planar streamer fronts with these transport data are discussed in section 2.4.

2.2.3 Second order models including the energy balance equation

We now turn to models that include the second velocity moment of the Boltzmann equation, i.e., the energy balance equation. We will see that the closure of this equation is not a straight forward process, and we will discuss some approximations made in the literature. The results of a second order model and of our high order model for planar streamer fronts will be compared in chapter 3.

The first important steps beyond first order fluid models of streamer discharges, to our knowledge, were carried out by Abbas and Bayle [1, 2], and by Bayle and Carenbois [13]. They employed a second order model which involves the energy balance equation to explore the zone at the streamer tip where the electron energy is not determined anymore by the local electric field only. However, as pointed out by Kanzari *et al.* [87], the accuracy of their model was restricted by the drastic assumptions taken in their energy balance equation. They evaluated the source term in the energy balance equation and corresponding averages by assuming a Maxwellian distribution for the electrons. Guo and Wu [73] have developed a more sophisticated second order model in which the Langevin theory was used to simplify the collision source terms with *a priori* knowledge of the relaxation times of electron energy and momentum. Kanzari *et al.* [87] have made an important step further by calculating the source term in the energy equation in a more consistent way where the *ad hoc* assumptions for the distribution function were avoided. A similar approach was later used by Eichwald *et al.* [58] in their simulations of the streamer dynamics and of the radical formation in a pulsed corona discharge used for flue gas control. Their results showed that the average electron velocity in the streamer head is largely overestimated by the classical first order model. As a consequence, electron density and radical density in the ionized channel were up to 50% higher than with the second order model. The salient feature of their theory is the fact that the heat flux term in the energy balance equation was explicitly neglected, but this, unfortunately, is of questionable accuracy. We will illustrate in streamer simulations in chapter 3 that the energy flux plays an important role in determining the streamer behavior. Thus, particular care should be taken with the closure through specification of the energy flux. Even for charged particle swarms under non-hydrodynamic conditions one must be careful how to specify the heat flux vector [151, 192, 193, 234]. We now discuss how the fluid equations should be closed for streamers, while we stress that the method itself is applicable to a much wider range of phenomena.

2.2.4 High order fluid model

We now derive a fluid model including the energy flux equation, i.e., we truncate at the moment equation with the third power of velocity. We will argue that the energy flux equation is crucial for the success of the fluid model for streamers. Inserting different moments of \mathbf{c} into equation (2.5), one finds

$$\frac{\partial n}{\partial t} + \nabla \cdot n\mathbf{v} = C_1, \quad (2.29)$$

$$\frac{\partial}{\partial t} (nm\mathbf{v}) + \nabla \cdot (nm\langle \mathbf{c}\mathbf{c} \rangle) - ne\mathbf{E} = C_{m\mathbf{c}}, \quad (2.30)$$

$$\frac{\partial}{\partial t} \left(n \left\langle \frac{1}{2} mc^2 \right\rangle \right) + \nabla \cdot \left(n \left\langle \frac{1}{2} mc^2 \mathbf{c} \right\rangle \right) - ne\mathbf{E} \cdot \mathbf{v} = C_{\frac{1}{2}mc^2}, \quad (2.31)$$

$$\frac{\partial}{\partial t} \left(n \left\langle \frac{1}{2} mc^2 \mathbf{c} \right\rangle \right) + \nabla \cdot \left(n \left\langle \frac{1}{2} mc^2 \mathbf{c}\mathbf{c} \right\rangle \right) - ne\mathbf{E} \cdot \left\langle \frac{\partial}{\partial \mathbf{c}} \left(\frac{1}{2} mc^2 \mathbf{c} \right) \right\rangle = C_{\frac{1}{2}mc^2 \mathbf{c}}. \quad (2.32)$$

Different forms of these equations that some readers might be familiar with, are given in the appendix. It will be shown in section 2.2.4 that the explicit form of the high order tensors appearing in the divergence term of the energy flux equation (2.32) is not required.

This system of equations is exact at this stage, but not very useful and the reason is twofold. First, there are more unknowns than equations, the familiar problem of closure. The set of fluid equations can be increased to an arbitrary size merely by taking higher velocity moments of the Boltzmann equation. Second, the definition of the system requires the respective collision terms C_ϕ .

Collision processes

In contrast to Monte Carlo simulations or kinetic equations in which cross sections for charged particle scattering enter into the calculations in a fairly clear way, in fluid equations the collisions are treated in a variety of ways which are not necessarily consistent with the data itself and/or with the system under consideration. There are many examples which illustrate this issue and the reader is referred to [108, 192, 193] for a detailed discussion. In the context of streamer and breakdown studies beyond first order fluid models, it has become common practice to evaluate the collision terms and averages by assuming some particular form of the velocity distribution function, usually Maxwellian [13, 37, 66, 73, 206, 208].

Let us consider the form of the collision terms in the balance equations (2.29)-(2.32). In this work we characterize the elastic, inelastic and non-conservative collisions by corresponding average collision frequencies. A collision frequency $\nu(v_r)$ for collisions between charged particles and gas molecules is related to the cross section $\sigma(v_r)$ characterizing the process by

$$\nu(v_r) = n_g v_r \sigma(v_r), \quad (2.33)$$

where \mathbf{v}_r is the relative velocity and n_g is the number density of the neutral gas. Further, we deal with weakly ionized systems where the interactions of charged particles with one another is negligible.

Our calculation takes into account that the charged particles can loose energy and momentum even in elastic collisions with the gas molecules as the finite mass and the thermal energy of the molecules are taken into account. The momentum exchange in inelastic collisions is included and $\nu_m = \nu_m(v_r)$ denotes the total momentum transfer collision frequency while ν_α and $\nu_\alpha^{(s)}$ are inelastic and superelastic collision frequencies for the inelastic channel α . The total collision frequencies for attachment and ionization are denoted by $\nu_A = \nu_A(v_r)$ and $\nu_I = \nu_I(v_r)$, respectively. We consider only single ionization with ionization energy ϵ_I , but the resulting ion can be left in any one of its internal excited states, characterized by an excitation energy $\Delta\epsilon_I^{(i)}$ and a collision frequency $\nu_I^{(i)}$.

Momentum transfer theory

The momentum transfer theory has a long history in kinetic theory of gases and has proved very successful for describing charged particle transport in gases under the influence of electric and magnetic fields. It is discussed comprehensively in the textbook of Mason and McDaniel [133] and in references [106, 186, 191, 192, 193, 229, 234]. The main ideas can be briefly summarized as follows:

(1) We need to express the average collision frequencies as a function of the mean energy in the center-of-mass reference frame. Thus, we replace the variables

$$v_r \rightarrow \varepsilon = \frac{1}{2}\mu_r v_r^2, \quad (2.34)$$

in expressions for collisional frequencies

$$\nu = \nu(v_r) \rightarrow \tilde{\nu} = \tilde{\nu}(\varepsilon), \quad (2.35)$$

where ε is the energy measured in the center-of-mass reference frame and μ_r is the reduced mass.

(2) If we assume that the dominant contributions to the averages come from regions near the mean energy $\bar{\varepsilon}$, and that $\nu(\varepsilon)$ varies sufficiently slowly with ε , then a Taylor expansion

$$\tilde{\nu}(\varepsilon) = \tilde{\nu}(\bar{\varepsilon}) + \tilde{\nu}'(\bar{\varepsilon})(\varepsilon - \bar{\varepsilon}) + \dots, \quad (2.36)$$

is expected to be a reasonable approximation. For conservative collisional processes such as elastic and inelastic scattering, only the first term of the expansion (2.36) is considered. However, when energy-dependent non-conservative processes such as ionization and electron attachment are operative then the derivative term in (2.36) becomes the leading term and must be included.

(3) Using the momentum transfer approximation, the balance equations (2.29)-(2.32) get the form

$$\frac{\partial n}{\partial t} + \nabla \cdot n\mathbf{v} = -n(\tilde{\nu}_A - \tilde{\nu}_I), \quad (2.37)$$

$$\frac{\partial}{\partial t}(mn\mathbf{v}) + \nabla \cdot (mn\langle\mathbf{c}\mathbf{c}\rangle) - ne\mathbf{E} = -\mu_r n\tilde{\nu}_m\mathbf{v} - mn\mathbf{v}[\tilde{\nu}_I + \zeta\tilde{\nu}_A'], \quad (2.38)$$

$$\frac{\partial}{\partial t}(n\varepsilon) + \nabla \cdot (n\boldsymbol{\xi}) - ne\mathbf{E} \cdot \mathbf{v} = -n\tilde{\nu}_e \left[\left(\varepsilon - \frac{3}{2}kT_0 \right) + \Omega(\bar{\varepsilon}) \right] - n\varepsilon\tilde{\nu}_A, \quad (2.39)$$

$$\frac{\partial}{\partial t}(n\boldsymbol{\xi}) + \nabla \cdot \left(n \left\langle \frac{1}{2}mc^2 \mathbf{c} \mathbf{c} \right\rangle \right) - ne\mathbf{E} \cdot \left\langle \frac{\partial}{\partial \mathbf{c}} \left(\frac{1}{2}mc^2 \mathbf{c} \right) \right\rangle = -n\tilde{\nu}_m \boldsymbol{\xi}, \quad (2.40)$$

where ε is the average electron energy, $\boldsymbol{\xi}$ is the average electron energy flux and m_0 is the mass of gas molecules. ζ is given by [187, 229]:

$$\zeta = \frac{2}{3} \frac{m_0}{m + m_0} \left(\frac{1}{2}m\langle c^2 \rangle - \frac{1}{2}m|\mathbf{v}|^2 \right). \quad (2.41)$$

The average collision frequencies for momentum and energy transfer

$$\tilde{\nu}_m(\bar{\varepsilon}) = n_g \sqrt{\frac{2\varepsilon}{\mu_r}} \sigma_m(\bar{\varepsilon}), \quad (2.42)$$

$$\tilde{\nu}_e(\bar{\varepsilon}) = \frac{2\mu_r}{m + m_0} \tilde{\nu}_m(\bar{\varepsilon}), \quad (2.43)$$

are prescribed functions of the mean energy in the centre-of-mass frame

$$\bar{\varepsilon} = \frac{m_0\varepsilon + m\frac{3}{2}kT_0}{m + m_0}, \quad (2.44)$$

where k is Boltzmann's constant and T_0 is the neutral gas temperature. The term Ω represents the average energy lost in one energy relaxation time $\tilde{\nu}_e^{-1}$, through non-elastic processes and is given by [234]:

$$\Omega(\bar{\varepsilon}) = \frac{m_0}{m + m_0} \sum_{\alpha} \frac{(\tilde{\nu}_{\alpha} - \tilde{\nu}_{\alpha}^{(s)})}{\tilde{\nu}_e} \epsilon_{\alpha} + \sum_i \frac{\tilde{\nu}_I^{(i)}}{\tilde{\nu}_e} \Delta \epsilon_I^{(i)}. \quad (2.45)$$

The inelastic channels α are governed by threshold energies ϵ_{α} and collision frequencies for inelastic and superelastic processes $\tilde{\nu}_{\alpha}$ and $\tilde{\nu}_{\alpha}^{(s)}$, respectively. All collision frequencies describing the inelastic, non-conservative and superelastic collisions appearing in equations (2.37)-(2.40) are functions of $\bar{\varepsilon}$. It should be emphasized that the equations of continuity (2.37), of momentum balance (2.38) and of energy balance (2.39) are valid for charged particles of arbitrary mass while the energy flux equation (2.40) is obtained in the approximation of $m/m_0 \ll 1$. High-order corrections in momentum transfer theory corrections (e.g., high-order terms in the Taylor expansion (2.36)) could be added on the right-hand side of the system (2.37)-(2.40) if desired, without in any way changing the generality of the physical arguments associated with the closure assumptions presented below.

Solution regimes and closure assumptions

The closure of the system of equations (2.37)-(2.40) requires approximations or assumptions on the form of the pressure tensor. The standard approximation for light particles such as electrons is that the pressure tensor can be taken as a

scalar at the fluid level of approximation [186, 192, 193, 234]. This means that, $\bar{\varepsilon} \approx \varepsilon \gg \frac{1}{2}mv^2$, and the pressure tensor simplifies to

$$\mathbf{P} = nk\mathbf{T} \approx \frac{2}{3}n\varepsilon\mathbf{I}, \quad (2.46)$$

where \mathbf{T} is the so-called temperature tensor that characterizes energy fluctuations even if the system is not in thermal equilibrium. This form of the pressure tensor was employed in all previous swarm oriented studies [151, 186, 191, 192, 193, 229, 234], as well as in the recent fluid models of streamer discharges [58, 87]. However, if the velocity distribution significantly deviates from isotropy in velocity space, then this approximation is problematic. For ions, the distribution function in velocity space is always anisotropic (even if elastic collisions between ions and molecules are predominant) and hence any assumption on an isotropic pressure tensor is wrong for ions. This problem can be avoided by considering the temperature tensor balance equation but this in turn contains further unknowns. The reader is referred to [106] for how to treat charged particle swarms under spatially-homogeneous hydrodynamic conditions. In streamer studies, the ions are usually considered as immobile or they are modeled by a reaction-drift-diffusion and local field approximation which is a reasonable approximation on the time scale on which a streamer ionization front passes a given point in space.

The next step in the closure of the system of equations (2.37)-(2.40) concerns the energy flux balance equation (2.40). The third term can be simplified as follows:

$$\frac{\partial}{\partial \mathbf{c}} \left(\frac{1}{2} mc^2 \mathbf{c} \right) = mc \frac{\partial \mathbf{c}}{\partial \mathbf{c}} + \frac{1}{2} mc^2 \frac{\partial \mathbf{c}}{\partial \mathbf{c}} = m\mathbf{c}\mathbf{c} + \frac{1}{2} mc^2 \mathbf{I}, \quad (2.47)$$

where \mathbf{I} is the unity tensor. Assuming again as in (2.46) that the temperature tensor is isotropic, and hence that

$$\langle \mathbf{c}\mathbf{c} \rangle \approx \frac{\langle c^2 \rangle}{3} \mathbf{I}, \quad (2.48)$$

and after some algebra, the energy flux equation can be written as

$$\frac{\partial}{\partial t} (n\boldsymbol{\xi}) + \nabla \cdot \left(n \left\langle \frac{1}{2} mc^2 \mathbf{c}\mathbf{c} \right\rangle \right) - \frac{e}{m} \mathbf{E} \left(\frac{5}{3} n\varepsilon \right) = -n\tilde{\nu}_m \boldsymbol{\xi}. \quad (2.49)$$

The second term in the energy flux balance equation (2.49) or (2.40) is the divergence of the fourth power of the velocity averaged over the velocity distribution, $\langle c^2 \mathbf{c}\mathbf{c} \rangle$, while all other terms in the equation contain only the third power of velocity. Therefore this term, that we will call the quartic tensor, requires either the next equation in the sequence of moment equations or a closure approximation. This closure assumption must be physically transparent and consistent with the general structure of the equations. One way is to approximate the relevant term by a product of lower moments as

$$\langle c^2 \mathbf{c}\mathbf{c} \rangle \approx \beta \langle c^2 \rangle \langle \mathbf{c}\mathbf{c} \rangle \approx \beta \frac{4}{3m^2} \varepsilon^2 \mathbf{I}, \quad (2.50)$$

where we used (2.48) for the second equality. β is a parametrization factor, generically close to unity, when the higher order correlation term $\langle c^2 \mathbf{c} \mathbf{c} \rangle - \langle c^2 \rangle \langle \mathbf{c} \mathbf{c} \rangle$ can be neglected.

With these closure assumptions the system of fluid equations (2.37)-(2.40) for the electrons becomes:

$$\frac{\partial n}{\partial t} + \nabla \cdot n \mathbf{v} = -n(\tilde{\nu}_A - \tilde{\nu}_I), \quad (2.51)$$

$$\frac{\partial}{\partial t}(n \mathbf{v}) + \frac{2}{3m} \nabla(n \varepsilon) - n \frac{e}{m} \mathbf{E} = -n \mathbf{v} \left(\tilde{\nu}_m + \tilde{\nu}_I + \frac{2}{3m} \varepsilon \tilde{\nu}_A' \right), \quad (2.52)$$

$$\frac{\partial}{\partial t}(n \varepsilon) + \nabla \cdot (n \boldsymbol{\xi}) - e \mathbf{E} \cdot (n \mathbf{v}) = -n \tilde{\nu}_e \left[\left(\varepsilon - \frac{3}{2} k T_0 \right) + \Omega \right] - n \varepsilon \tilde{\nu}_A, \quad (2.53)$$

$$\frac{\partial}{\partial t}(n \boldsymbol{\xi}) + \nabla \cdot \left(\beta \frac{2n}{3m} \varepsilon^2 \right) - \frac{5}{3} n \varepsilon e \mathbf{E} = -\tilde{\nu}_m(n \boldsymbol{\xi}). \quad (2.54)$$

The parameter β that appears in the energy flux equation is a quantity close to unity, but can be used to fit the neglected higher order correlations. Variations of this parameter will be discussed in chapter 3.

The system of equations (2.51)-(2.54) has the following properties: (i) If the parameter β is specified and if the collision terms are given then the system of equations contains no further unknowns can be numerically solved for the density, average velocity, average energy and energy flux. (ii) The equations contain mean-energy collisional rates that should be carefully derived and implemented as elaborated in the next section. (iii) Attachment enters the momentum and energy balance equation in terms of the derivative of the attachment collision frequency while for ionization only the ionization collision frequency is present. (iv) The above equations are set for a single component gas; the generalization to gas mixtures proceeds through the generalization of the collision term to a sum of terms appropriately weighted according to the mole fractions of the respective species.

2.3 Transport and reaction data

2.3.1 Evaluation of the transport data: Boltzmann equation analysis

Here we discuss how to evaluate and implement electron transport properties in both first and high order fluid models. In plasma modeling, transport coefficients of electrons and/or ions may be obtained either from swarm experiments, from solutions of the Boltzmann equation, or from Monte Carlo simulations. We note that swarm transport data are usually given in the literature in the form of tables as a function of reduced electric field, E/n_0 [192, 234]. In fluid plasma modeling, however, several important issues have to be considered before directly implementing data from the literature.

First, transport coefficients are defined far from boundaries, sources and sinks of charged particles where the so-called hydrodynamic conditions prevail [43, 44,

46, 98, 150, 190, 234]. Under hydrodynamic conditions, the space-time dependence of the distribution function is expressible in terms of linear functionals of $n(\mathbf{r}, t)$. A sufficient functional relationship between the distribution function $f(\mathbf{r}, \mathbf{c}, t)$ and $n(\mathbf{r}, t)$ in the case of weak gradients is the well-known expansion

$$f(\mathbf{r}, \mathbf{c}, t) = \sum_{s=0}^{\infty} f^{(s)}(\mathbf{c}) \odot (-\nabla)^s n(\mathbf{r}, t), \quad (2.55)$$

where $f^{(s)}(\mathbf{c})$ are tensors of rank s and \odot denotes an s -fold scalar product. Direct application of transport properties measured/calculated in different experimental arrangements where often non-hydrodynamic conditions are present explicitly or implicitly, is problematic and should be avoided. Typical example of swarm data obtained under non-hydrodynamic conditions are those measured/calculated under the steady-state Townsend (SST) conditions [189, 196]. Before direct application of SST data one must perform careful swarm analysis and convert the SST data into the hydrodynamic transport coefficients. Details of this procedure are presented in [42].

Second, care must be taken when non-conservative collisions are significant. In the presence of non-conservative collisions there are two sets of transport coefficients, the bulk and the flux [188, 234]. Assuming the functional relationship (2.55) the flux $\mathbf{\Gamma}$ and source term C_1 (usually denoted by $S(\mathbf{r}, t)$ in previous swarm oriented studies [43, 44, 46, 234]) appearing in the equation of continuity (2.7) can be expanded

$$\mathbf{\Gamma}(\mathbf{r}, t) = n\mathbf{W}^{(*)} - \mathbf{D}^{(*)} \cdot \nabla n, \quad (2.56)$$

$$S(\mathbf{r}, t) = S^{(0)}n(\mathbf{r}, t) - \mathbf{S}^{(1)} \cdot \nabla n(\mathbf{r}, t) + \mathbf{S}^{(2)} : \nabla \nabla n(\mathbf{r}, t), \quad (2.57)$$

where $\mathbf{W}^{(*)}$ and $\mathbf{D}^{(*)}$ define, respectively, the flux drift velocity and flux diffusion tensor while $\mathbf{S}^{(k)}$ are expansion coefficients of the source term. Substitution of expansions (2.56) and (2.57) into the continuity equation (2.7) yields the diffusion equation

$$\frac{\partial n}{\partial t} + \mathbf{W} \cdot \nabla n - \mathbf{D} : \nabla \nabla n = -R_a n, \quad (2.58)$$

which defines the bulk transport coefficients

$$R_a = -S^{(0)}, \quad (2.59)$$

$$\mathbf{W} = \mathbf{W}^{(*)} + \mathbf{S}^{(1)}, \quad (2.60)$$

$$\mathbf{D} = \mathbf{D}^{(*)} - \mathbf{S}^{(2)}, \quad (2.61)$$

where R_a is the loss rate, \mathbf{W} is the bulk drift velocity and \mathbf{D} is the bulk diffusion tensor.

The basic difference between the bulk and flux transport coefficients should now be apparent. The bulk drift velocity is displacement of the mean position of the electron swarm and it characterizes the motion of the total ensemble of electrons. The presence of the electric field results in a spatial variation in the energy throughout the swarm. Under such conditions, the presence of non-conservative

collisions (ionization/ attachment) may lead to a change in the position of the center-of-mass of the swarm. This effect on the bulk drift velocity is denoted by $\mathbf{S}^{(1)}$. On the other hand, the flux drift velocity $\mathbf{W}^{(*)}$ represents the rate of change of the position of the center-of-mass due to the electric field only and can be interpreted as the mean velocity of the electrons. Likewise the flux diffusion tensor $\mathbf{D}^{(*)}$ represents the rate of spreading of the swarm due to the electric field \mathbf{E} and gradients in density ∇n . The presence of non-conservative collisions may result in the variation of ∇n throughout the swarm and a subsequent variation in the rate of change of the mean squared width of the swarm. Such effects are expressed by the second rank tensor $\mathbf{S}^{(2)}$. The most appropriate procedure in plasma modeling would be to use the experimental swarm data (e.g. bulk values) for the analysis of the validity of the cross section and then to calculate the flux quantities which are necessary as input data in fluid modeling. More about duality of the hydrodynamic transport coefficients and their implementation in fluid modeling can be found in the references [43, 44, 46, 171, 192, 234].

Third, while the first order fluid model requires electron transport data as a function of local reduced electric field, what really appears in high order fluid models are mean-energy-dependent collisional rates. Since momentum transfer theory is used to determine the collision terms in the fluid equations, the most appropriate procedure would be to systematically reduce these fluid equations down to the swarm limit assuming the hydrodynamic regime. From this set of equations, one can then find relationships between collisional transfer rates and the mean energy, in a self-consistent manner. This method was employed in previous works of Robson and co-workers (see for example [192] and references therein), but we apply here a slightly different approach. Instead of using the so-called generalized Einstein relation to determine the mean energy from the transverse diffusion coefficient [186, 192], the mean energy is directly calculated from the multi term solution of Boltzmann's equation. The correspondence between the mean energy and E/n_0 is then used to find the correspondence between the mean energy and other relevant transport data. The momentum transfer collision rate is obtained from

$$\nu_m = \frac{e}{m\mu(\varepsilon)}, \quad (2.62)$$

where $\mu(\varepsilon)$ is the electron mobility which is here a function of the mean energy. The energy-transfer collision frequency is calculated from equation (2.43). Thus our procedure of determining the electron transport data as an input for high order fluid models is entirely consistent with the work of Boeuf and Pitchford [20].

The electron transport data employed in this work are calculated using a multi term theory for solving the Boltzmann equation. The methods and techniques are by now standard and the reader is referred to our previous works [43, 44, 234]. Among many important aspects, we highlight the following important steps:

- No assumptions on symmetries in velocity space are made, and the directional dependence of the phase-space distribution function in velocity space

is represented in terms of a spherical harmonic expansion:

$$f(\mathbf{r}, \mathbf{c}, t) = \sum_{l=0}^{\infty} \sum_{m=-l}^l f(\mathbf{r}, c, t) Y_m^{[l]}(\hat{\mathbf{c}}), \quad (2.63)$$

where $Y_m^{[l]}(\hat{\mathbf{c}})$ are spherical harmonics and $\hat{\mathbf{c}}$ represents the angles of \mathbf{c} . In contrast to the classical two term theory (where the sum over l is performed only up to $l = 1$), the number of spherical harmonics is not restricted, and our method therefore is a truly multi term approach. The differences between two-term approximation and our full multi term approach for electron transport in nitrogen are illustrated in section 2.3. The inadequacies of a Legendre polynomial expansion (when density gradients are not parallel to the field) are highlighted in our previous publications [43, 234] and avoided in this work.

- As discussed above, under hydrodynamic conditions a sufficient representation of the space dependence is an expansion in terms of powers of the density gradient operator.
- The velocity (energy) dependence of the phase-space distribution function is represented by an expansion about a Maxwellian at an arbitrary temperature in terms of Sonine polynomials.

Using the appropriate orthogonality relations for the spherical harmonics and for the modified Sonine polynomials, the Boltzmann equation is converted into a hierarchy of coupled equations for the moments of the distribution function. These equations are solved numerically and all transport and rate coefficients are expressed in terms of moments of the distribution function [43, 234].

2.3.2 Cross sections and transport data

In this section, transport and reaction coefficients for electrons in N_2 at a temperature of 298 K are calculated as an input for first and high order fluid models. The first order model is based on the local field approximation; it requires mobility, diffusion coefficient and ionization rate as a function of the reduced electric field E/n_0 (where n_0 is the gas number density). Compared to our previous work [44], we extend the electric field range up to 3000 Td (1 Td = 10^{-21} Vm²). The high order fluid model requires average collision frequencies for momentum and energy transfer in elastic and inelastic collisions, and rate coefficients for all collision processes as a function of the mean electron energy.

We use the cross sections for electron scattering in N_2 provided by Stojanović and Petrović [215]. For elastic collision processes we use the original Boltzmann collision operator while for inelastic processes we employ the generalization of Wang-Chang *et al.* [31]. The ionization collision operator is detailed in [150]. We assume that the ratio between the energy of the scattered electron and the total available energy in an ionizing collision is equally distributed between 0 and 1; the same holds then, of course, for the ejected electron. We remark that at the

high electron energies in the streamer tip, the assumptions on the energy division can considerably influence transport profiles. Furthermore, scattering is assumed to be isotropic. This can be problematic for high values of E/n_0 (generally for $E/n_0 \geq 1000$ Td for electrons in N_2) when electrons scatter predominantly in the forward direction [111, 173]. However, the errors in the calculated transport coefficients and rate coefficients are acceptable in fluid modeling for streamers in the range of the reduced electric fields E/n_0 considered in this work after appropriate renormalization of cross-sections for the scattering angle distribution [111].

We present both *bulk* and *flux* coefficients obtained by our multi term solution of the Boltzmann equation, and we compare them with the coefficients obtained by the public available Boltzmann solver BOLSIG+ derived from the same cross sections. BOLSIG+ is based on the two term approximation [74] and provides exclusively flux transport data.

2.3.3 Input data for the first order model

Figure 2.1(a) shows the electron mobility (multiplied by the gas number density) as a function of the reduced electric field E/n_0 . We observe that bulk and flux quantities start to differ visibly above a reduced field of approximately 150 Td, this means that the ionization processes start to be significant at this value of the field. As E/n_0 increases further, the effect becomes more pronounced, until the bulk mobility exceeds the flux mobility by approximately 30% at 3000 Td. The difference between bulk and flux mobility is the consequence of the spatial variation of the average electron energy within an electron swarm [43, 107, 150]. If the ionization rate is an increasing function of electron energy (as is the case for the parameters considered here), electrons are preferentially created in regions of higher energy resulting in a shift in the centre of mass position as well as in a modification of the spread about the centre of mass. In nitrogen up to 3000 Td, the electrons are preferentially created at the leading edge of an electron swarm and hence the bulk mobility is larger than the flux mobility.

Figure 2.1(a) shows as well that the flux data obtained by our multi term solution of Boltzmann's equation and by the BOLSIG+ code agree well. Only for E/n_0 below about 3 Td, the BOLSIG+ mobility is higher than our flux mobility. As we have successfully compared our multi term results with Monte Carlo results that include the thermal energy of the background molecules as well, the results shown in figure 2.1(a) suggest that the BOLSIG+ code should be carefully tested in the limit of thermal energies.

Figure 2.1(b) shows the diffusion coefficients (multiplied by the gas number density) as a function of the reduced field E/n_0 . The bulk and flux values of the longitudinal and transverse diffusion coefficients are compared with the isotropic diffusion coefficient calculated by the BOLSIG+ code. As for the mobility, flux and bulk data start to deviate for E/n_0 above approximately 150 Td, indicating again the onset of ionization effects. The diffusion coefficients are more sensitive to the ionization processes than the mobility; the differences between bulk and flux data can reach almost 50% for E/n_0 approaching 3000 Td. For a more thorough analysis of the explicit influence of ionization processes on the diffusion

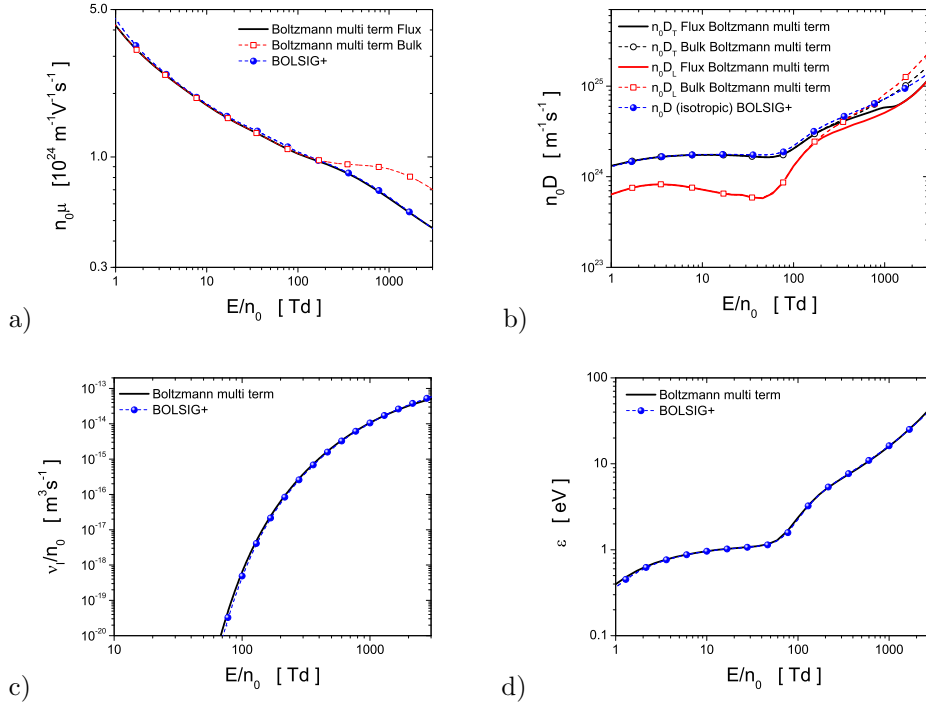


Figure 2.1: (a) Mobility, (b) longitudinal and transverse diffusion coefficient, and (c) ionization rate of electrons in N_2 as a function of the reduced electric field E/n_0 , as an input for the first order model. Shown are flux and bulk data obtained by our multi term solution of the Boltzmann equation, and flux data obtained by the BOLSIG+ code. BOLSIG+ provides only an isotropic diffusion coefficient for panel (b). Panel (d) shows the variation of mean energy with E/n_0 .

coefficients one must consider the second order variations in the average energy along the swarm. This is beyond the scope of this work and we defer this to a future study.

Figure 2.1(b) clearly shows the anisotropy of the diffusion tensor, i.e. $D_L \neq D_T$; for the range of E/n_0 considered here, the transverse diffusion coefficient is always larger than the longitudinal diffusion coefficient. This is due to the spatial variation of the average energy within the swarm and to the energy dependence of the collision frequency. The theory of anisotropic diffusion in an electric field is now textbook material (see for example [84]) and rather than a detailed discussion of the origin of this phenomenon, we prefer to highlight the implementation of the diffusion coefficients in fluid models of streamer discharges. For E/n_0 below approximately 30 Td, our results for the flux component of the transverse diffusion coefficient and those obtained by the BOLSIG+ code agree very well. For E/n_0 above 30 Td, however, BOLSIG+ with its two term approximation is clearly above our multi term solution. Here one should bear in mind that BOLSIG+ treats the

diffusion processes under the spatially homogeneous conditions and hence the transverse diffusion coefficient obtained under the spatially-inhomogeneous conditions should be used for comparisons. On the other hand, our one-dimensional fluid model requires the longitudinal diffusion coefficient as an input as we consider the spatial variations of the electron density and average electron energy only along the field direction. Therefore, particular care needs to be taken with implementation of the diffusion coefficients in fluid models of streamer discharges.

Figure 2.1(c) shows that the ionization rate (divided by the gas number density) differs between the two term and the multi term calculations by up to 30 %. It is interesting to note that the two term approximation is less accurate in the energy region dominated by the vibrational excitation of N_2 and for energies well above the ionization threshold. Surprisingly, for the electric field range between approximately 200 and 600 Td the two term approximation increases in accuracy. In this energy region the cross sections for inelastic processes are much smaller than for elastic collisions. Similar but not identical observations have been made by Phelps and Pitchford [173].

Figure 2.1(d) shows the variation of the mean energy with E/n_0 . The properties of the cross sections are reflected in the profile of the mean energy. The initial slow rise indicates the influence of low-threshold rotational and vibrational processes. The sharp rise for mean energies starting approximately from 50 Td indicates the ‘turning off’ of the vibrational processes. Our results and those obtained by the BOLSIG+ code agree very well. The mean energy is determined from the balance between the gain from the field and the loss by collisions with the molecule. This quantity is directly used in high order fluid modeling of streamer discharges. Though it does not appear in the first order fluid models, unlike other transport coefficients such as the drift velocity (mobility), diffusion coefficients, and ionization rate, we often find that a knowledge of the mean energy is necessary to explain certain phenomena.

2.3.4 Input data for the high order model

The density normalized average collision frequencies for momentum transfer in elastic collisions and the average energy loss in one energy relaxation time $\tilde{\nu}_e^{-1}$, through non-elastic processes as a function of mean electron energy are shown in figure 2.2. Bulk and flux frequencies obtained with the multi term approach are compared with flux values calculated with BOLSIG+. The flux values of the two approaches for $\tilde{\nu}_m/n_0$ agree well. The differences between bulk and flux values of $\tilde{\nu}_m/n_0$ are a direct consequence of the differences between bulk and flux mobilities (see figure 2.1(a)). Similar arguments can be used to explain the difference between bulk and flux components of Ω . This quantity should be viewed as a ‘measure’ of energy transfer in inelastic collisions in one energy relaxation time $\tilde{\nu}_e^{-1}$. It is directly proportional to mobility and hence its bulk dominate the corresponding flux component for higher mean electron energies. Differences between flux values of the two approaches for Ω follow directly from internal errors of the two term approximation used to solve Boltzmann’s equation in the BOLSIG+ code.

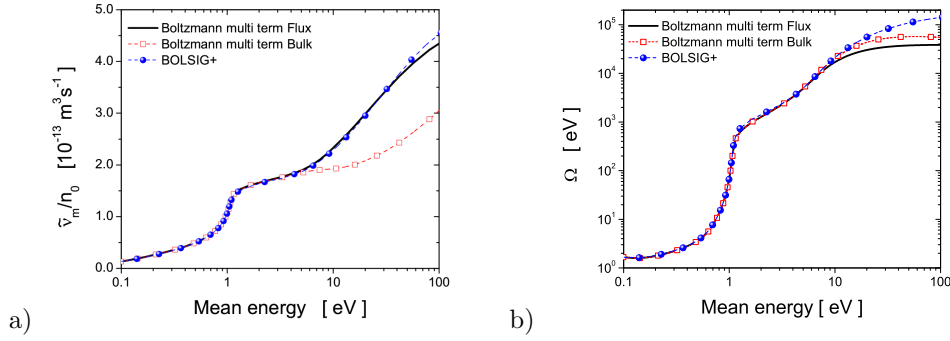


Figure 2.2: Density normalized average collision frequency for momentum transfer in elastic collisions $\tilde{\nu}_m/n_0$ (a) and the average energy lost in one energy relaxation time $\tilde{\nu}_e^{-1}$, through non-elastic processes Ω (b) as a function of the mean energy of electrons in N_2 , as an input for the high order model. The three curves in each panel show the flux and bulk data obtained by our multi term solution for the Boltzmann equation and the flux data obtained by the BOLSIG+ code.

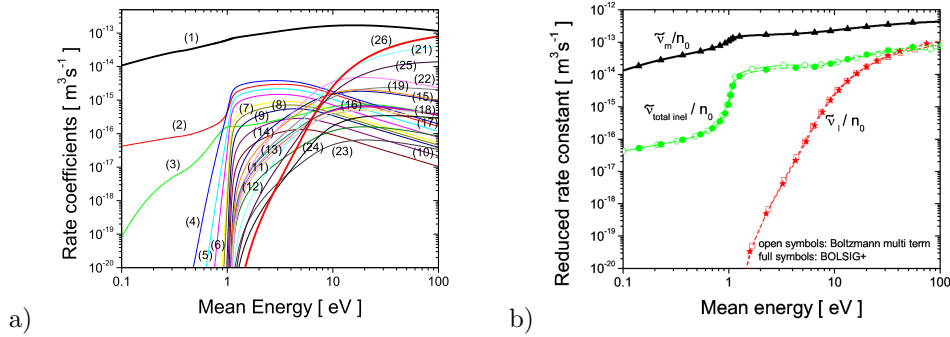


Figure 2.3: Rate coefficients in N_2 as a function of the electron energy, calculated with the multi term solution of the Boltzmann equations. (a) Rates for the cross sections listed in [173, 215]: momentum transfer in elastic collisions (1), rotational excitation (2), vibrational excitations (3-11), electronic excitation $A^3\Sigma_u^+ v = (0-4)$ (12), $A^3\Sigma_u^+ v = (5-9)$ (13), $B^3\Pi$ (14), $W^3\Delta$ (15), $A^3\Sigma_u^+ v > 10$ (16), $B'^3\Sigma_u^-$ (17), $a'^1\Sigma_u^-$ (18), $a^1\Pi_g$ (19), $w^1\delta_u$ (20), $C^3\Pi_u$ (22), $E^3\Sigma_g^+$ (23), $a''^1\Sigma_g^+$ (24), sum of singlets (25), dissociation [34] (21), ionization (26); and (b) density normalized momentum transfer rate, density normalized total inelastic rate and ionization rate.

Figure 2.3(a) shows the rate coefficients as a function of the mean electron energy for all collision processes. Figure 2.3(b) compares the density normalized average collision frequency for momentum transfer in elastic collisions, the density normalized total inelastic rate (sum of all rates for inelastic processes without ionization) and the ionization rate. All results are obtained with the solution of

Boltzmann's equation. On figure 2.3(b) the results obtained by the BOLSIG+ code are also included. The ionization rate is significant for relatively high mean energies (i.e., high E/n_0) and is essential for modeling of streamers. Excepting rates for dissociation (21), electronic excitation (25) and ionization (26), the following feature is observed in the mean energy-profiles of the rate coefficients: at some point their increase with the mean energy slows down until a maximum is reached and then they start to decrease. Under conditions considered in this work, the ionization rate monotonically increase with the mean energy and in the limit of 100 eV it approaches to the rate for momentum transfer in elastic collisions. In the low energy range, however, rotational and vibrational excitations have the most important role. In particular, for electron energies less than approximately 0.1 eV, the processes of rotational excitation control the energy transfer in the system and should be carefully considered. In conclusion, collisional rates for inelastic processes enter the energy balance equation describing the change in the average energy of electrons. The knowledge of the rate coefficients is of key importance to calculate the kinetics of various plasma chemical processes and densities of excited species and thus used in much broader context of plasma modeling.

2.4 First order streamer model with different transport data

Here we present simulations of planar negative ionization fronts in N_2 using the first order fluid model, while simulation results with the high order fluid model are presented in chapter 3.

2.4.1 Numerical methods, initial and boundary conditions.

In this subsection we briefly describe the numerical method, and the initial and boundary conditions used to solve equations (2.25)-(2.28) in one spatial dimension. The calculations are carried out in N_2 at atmospheric pressure and at the ambient temperature of 298 K. The 1D simulations are started with the same initial Gaussian type distribution for electrons and ions

$$n(x)|_{t=0} = n_i \exp \left[-\frac{(x - x_0)^2}{\sigma^2} \right], \quad (2.64)$$

in a gap parameterized with the coordinate $x \in [0, L]$, with $L = 1.2$ mm. We have chosen $n_i = 2 \times 10^{18} \text{ m}^{-3}$, $x_0 = 8 \times 10^{-4} \text{ m}$ and $\sigma = 2.9 \times 10^{-5} \text{ m}$. The externally applied electric field is positive in the x direction, therefore electrons drift to the left. The field is fixed in the non-ionized region at the left boundary $x = 0$, providing a fixed electric field for the negative streamer ionization front to penetrate. In this work we consider reduced electric fields of 350 Td, 460 Td, 590 Td, 770 Td and 1000 Td.

To investigate the sensitivity of streamer properties to the definition and accuracy of the transport data, we employ three different sets of data for μ , D and

ν_I : bulk and flux data obtained by our Boltzmann equation analysis and the flux data obtained by the BOLSIG+ code.

The finite volume method is used to spatially discretize the system (2.25)-(2.28) on a uniform grid with 1000 points. More details will be outlined in chapter 3 where numerical methods for solving the high order fluid equations are presented in a comprehensive way. To approximate the spatial derivatives in (2.25) we use the second-order central difference discretization while the time derivatives are approximated with the Runge-Kutta 4 method [83]. The continuity equation for the electron density has a second order spatial derivative, and therefore it requires two boundary conditions. For $x = 0$ we use a homogeneous Neumann boundary condition ($\partial_x n = 0$), so that electrons that arrive at this boundary may flow out of the system. For $x = L$ we employ a homogeneous Dirichlet boundary condition ($n = 0$) to ensure that there is no outflow of electrons from the system. In any case, it should be noted that the electrons are well separated from the boundaries, therefore the actual boundary conditions do not matter. In equation (2.26) the time derivative is approximated with the Runge-Kutta 4 method using the same time step as in equation (2.25). In the 1D case, equation (2.28) has the form

$$\partial_x E = \frac{e}{\epsilon_0}(n - n_{ion}), \quad (2.65)$$

from which we can determine the electric field E by integrating over x and using the fixed value of E at $x = 0$.

2.4.2 Overview of simulation results with different transport data

Figure 2.4 displays the spatio-temporal evolution of electron and ion densities and of the electric field when the reduced electric field ahead of the front is fixed to 590 Td (or equivalently to 145 kV/cm in N_2 at atmospheric pressure and temperature of 298 K). Calculations are performed for three different sets of transport data as indicated in the figures. We start with a Gaussian density distribution as described above. Though the transition from avalanche to streamer has been discussed many times within the past 80 years [107, 137, 138, 180], the characteristics and main physical processes are discussed here to investigate the sensitivity to different transport data.

In the early stage of evolution, we see that both the electron and the ion densities grow due to electron impact ionization. If this was the only mechanism, the electric field would remain unchanged and the ionization would continue indefinitely. However, the electrons drift in the direction opposite to the electric field while the positive ions would slowly drift in the opposite direction; as their mobility is so much smaller, this motion is actually neglected here and in most other streamer studies. As a consequence, the charge separation starts to distort the initially homogeneous electric field. Now figure 2.4 shows that the ionization profiles at time 0.06 ns obtained with the bulk transport data are somewhat wider while their height is less than with our flux and BOLSIG+ data. This follows from the fact that the bulk mobility and diffusion constant are higher than the corresponding flux data and hence the centre of mass moves faster and the

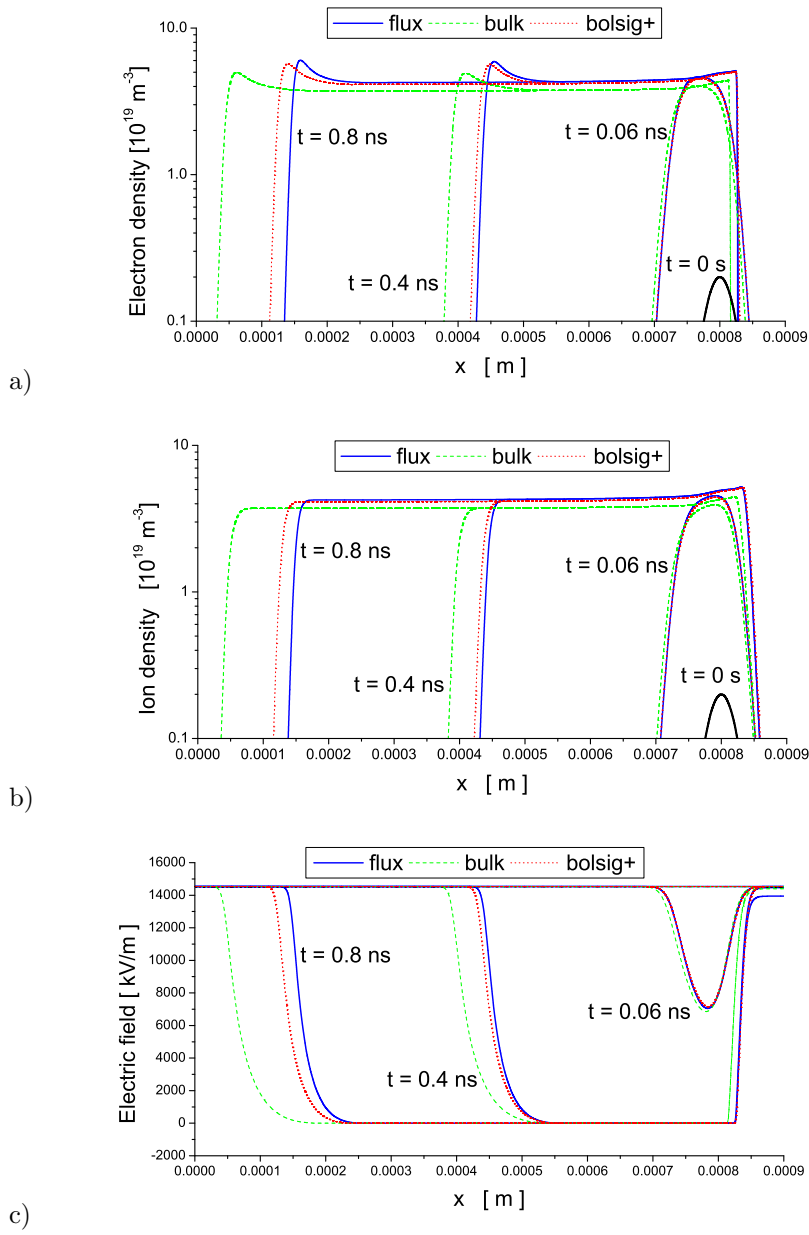


Figure 2.4: Evolution of (a) the electron density, (b) the ion density and (c) the electric field in a negative planar ionization front in N_2 with a reduced electric field of 590 Td ahead of the front. Shown are the spatial profiles obtained with three different sets of input data as indicated in the graph.

electron package spreads faster. As the ionization rate is the same in both cases, the height of the profiles obtained with the bulk data must be less than with the flux and BOLSIG+ data. As the evolution continues, the electric field in the ionised region gets completely screened, and further ionization processes cannot occur in this region anymore. The transition from avalanche to streamer is then completed. We mention in passing that the complete screening of the interior field is due to the 1D set-up and to the fact, that the field ahead of the front does not change in time.

2.4.3 Front velocities

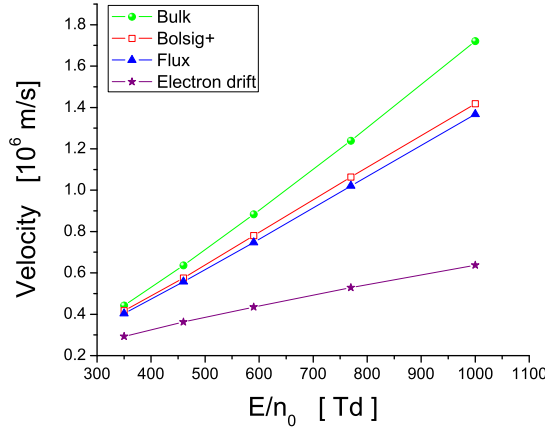


Figure 2.5: Velocities of planar fronts obtained by three different sets of input data as a function of the reduced electric field. The flux drift velocity of electrons is also included.

When the streamers have approached an approximately uniformly translating state, we see that the streamers obtained with bulk data propagate faster than those obtained with flux and BOLSIG+ data, in agreement with earlier studies [107, 110, 112]. In section 2.3.1 it was already discussed, that in general flux transport data should be used in fluid equations derived systematically from the Boltzmann equation; however, in the particular case of streamer ionization fronts with their pulled dynamics simulated with the half-phenomenological classical streamer model, the bulk coefficients approximate the front velocity better, with the drawback that the ionization level behind the front is too small [107, 110, 112].

In figure 2.5 we display velocities of planar fronts as a function of E/n_0 . In order to calculate the streamer velocity we have followed the evolution of a certain level ($2n_i$) of the electron density at the streamer front. We compare the velocities obtained with different input data. The flux drift velocity as a function of E/n_0 is also shown. First, we see that the planar fronts move much faster than the electrons. This follows from the fact that the velocity of a planar front is the

sum of the drift in the electric field at the front edge plus a term accounting for diffusion, for creation of additional electrons due to impact ionization and for the electron density profile [52]. The difference between front velocity and electron drift velocity increases with E/n_0 , up to more than a factor of 2 for the highest field displayed here.

We remark that according to analytical theory [50, 52], the front velocities in planar configurations (where the field does not decay ahead of the front) depend for a long time on initial conditions, and if the initial condition decays less than $e^{-\Lambda^*|x|}$, $\Lambda^* = \sqrt{\nu_I/D}$, it will determine the front velocity for arbitrarily long times. For this reason, we here do not compare numerical with analytical results [107].

We finally note that the front velocities calculated with bulk transport data are up to 30 % higher than with flux data. This illustrates the sensitivity of the model to the input data. On the other hand, the velocities differ much less between our flux data and those obtained with BOLSIG+. To explore this issue in more detail, additional tests are required, particularly for atomic and molecular systems with large anisotropy of the velocity distribution function in velocity space.

2.4.4 Ionization levels behind the front

We now explore how the ionization degree behind the front depends on the transport data, and we compare with the analytical approximation

$$n_{e,\text{back}} \leq \frac{\epsilon_0}{e} \int_0^{E_{\text{max}}} \frac{\nu_I(E)}{E\mu(E)} dE. \quad (2.66)$$

This approximation becomes an identity, if diffusion can be neglected [52]; and it is an upper bound, if diffusion is taken into account [107]. This analytical result has been derived for planar fronts, and it is independent of the front velocity.

In figure 2.6 we compare the ionization levels behind the fronts calculated with the three different sets of transport data and with the analytical upper bound, using our flux data. We see that the approximation (2.66) indeed serves as such a bound, but is furthermore also a very good approximation of the numerical results, when using the same transport data. The errors of the two term approximation are negligible indicating a weak sensitivity of the ionization level to the isotropy of the distribution function in velocity space that is assumed in BOLSIG+. The ionization level with bulk data is considerably lower. Generally, it is evident that the ionization level is much less sensitive to the type of transport data than the front velocity. Similar observations have been made in [107].

2.5 Conclusion

In this chapter we have derived a high order fluid model for streamer discharges. Our goal has been to develop a comprehensive theory at a level of sophistication appropriate for the electron energy distributions very far from equilibrium and for the steep electron density gradients that characterize a streamer front. The first

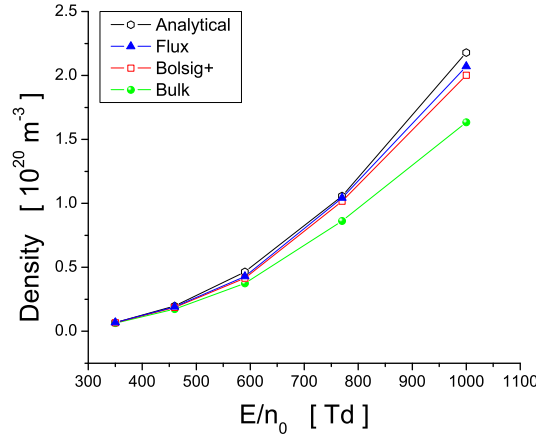


Figure 2.6: Ionization levels behind planar fronts as a function of the reduced electric field. results are shown with three different sets of input data and with the analytical approximation (2.66) calculated with flux data.

steps are reported in the present chapter, which deals with theoretical foundations and phenomenology. After examining the application of the Boltzmann equation, we have proceeded to the evaluation of the velocity moments of Boltzmann's equation. To make contact with previous works and to place our theory in a much broader context, we have demonstrated how to derive the classical drift-diffusion approximation often used in the plasma modeling community to model streamer discharges. Then we have introduced our more sophisticated high order fluid approach, proceeding directly from Boltzmann's equation and systematically discussing the critical assumptions required to close the system of equations and to evaluate the collision terms involved. Momentum transfer theory has been used to approximate collision terms in the high order fluid model while high order tensors appearing in the energy flux equation have been specified in terms of previous moments. In contrast to previous works, it has been emphasized that the energy flux equation plays a pivotal role for the correct description of streamer dynamics. The fluid equations obtained as velocity moments of the Boltzmann equation have been closed in the local mean energy approximation and coupled to the Poisson equation to calculate the modification of the electric field by space charges. The numerical solutions of the high order fluid model for planar fronts and their discussion are deferred to the following chapter.

The second important aspect of this chapter concerns the application of transport data in fluid models of streamer discharges. In order to illustrate this issue, we have used the first order fluid model to investigate the temporal evolution of negative planar fronts in pure nitrogen. We have focused on the way in which the inherent streamer properties such as the velocity of a streamer or the ionization level behind the front are influenced by different transport data employed as an

input in fluid equations. Our primary goal was to show which aspects of kinetic theory developed for swarm physics and particularly which segments of data would be important for further improvement of streamer models. It was shown and illustrated that the direct application of transport data from the literature without knowledge of origin and nature of the data is problematic and can often lead to significant errors in the profiles of various streamer properties. In this respect, the origin and nature of transport data must be known and, if appropriate, suitably modified before implementation in the fluid models. This is particularly important for collisional transfer rates required as input in high order fluid model. We have also discussed the validity of transport data obtained by a two term theory for solving the Boltzmann equation. Our general sentiment was that two term data are well acceptable in fluid modeling of streamers, though additional testing is required for gases with large anisotropy of the velocity distribution function in velocity space.

CHAPTER 3

Numerical solution of high-order fluid model for streamer discharges in 1D and investigation of planar fronts

There are no such things as applied sciences, only applications of science.

– LOUIS PASTEUR

The greatest challenge to any thinker is stating the problem in a way that will allow a solution.

– BERTRAND RUSSELL

3.1 Introduction

Streamer discharges occur in nature and technology, predominantly in pulsed high voltage discharges; at their rapidly propagating tips electric fields well above the break-down value are maintained that create high electron energies and reaction rates. Streamers occur in lightning and sprites [49, 54, 64, 123] as well as in industrial applications such as lighting [61, 113, 208], treatment of polluted gases and water [227], disinfection [226], plasma jets and bullets [21, 121, 147, 148, 241] and

This chapter is based on the publication [131] *High-order fluid model for streamer discharges: II. Numerical solution and investigation of planar fronts* by Aram H. Markosyan, Saša Dujko and Ute Ebert published in *Journal of Physics D: Applied Physics*, Volume 46, Number 47, Page 475203, 2013.

plasma assisted combustion [210, 212]. Further optimization and understanding of such applications depends on an accurate knowledge of the electron dynamics during streamer development.

A Monte Carlo technique is able to track the electron distribution in phase space, yielding both electron density profiles and electron energy distribution. However, a full particle model long has been computationally too demanding or too inaccurate due to the used super-particle techniques, and even now the parameter range of simulations is limited. For recent progress in particle and hybrid models we refer to [107, 110, 111, 112, 125]. Due to the computational costs and limitations of particle models, up to today mainly fluid approximations have been used to model the structure and evolution of streamer discharges in two or three spatial dimensions. These fluid models were restricted almost exclusively to the hydrodynamic reaction drift diffusion approximation combined with the local field approximation, though the short-comings of this model have been acknowledged and documented [13, 58, 73, 87, 107, 108, 109, 110, 112, 143]. They arise from the fact that within the streamer front the electron density develops large spatial gradients and a complex interaction with the field. This in turn limits the use of the local field approximation as the electron energy does not immediately relax to the value determined by the local field, but depends upon the electric field in a wider spatial range.

The aim of the preceding and the present chapter is to develop and test a better fluid approximation for streamer discharges in gaseous media. In the previous chapter 2 we have derived a high order fluid model, whose predictions for streamer dynamics will be tested in the present chapter. The high order fluid model contains equations for the electron density, for the average electron velocity, for the average electron energy and for the average electron energy flux. It was obtained from velocity moments of the Boltzmann equation and closed in the local mean energy approximation. Momentum transfer theory [187, 229, 234] was used to evaluate the collisional terms in the balance equations, and particular emphasis was placed upon the correct representation of momentum and energy transfer in energy-dependent non-conservative collisions. The system was truncated at the level of the energy flux balance and simplifying approximations were introduced in the momentum and energy flux balance equations in order to close the system. In particular, in the momentum balance equation it was assumed that the distribution of velocities is isotropic assuming isotropy of the temperature and pressure tensors. Thus, the pressure tensor was reduced to a scalar kinetic pressure. Furthermore, the same approximation was used in the energy flux balance equation. If one assumes an isotropic distribution of velocities then the contribution of higher terms including the high order heat flux tensor and the high order pressure tensor is relatively small and could be neglected. However, the energy flux transported by the convective particle motion should be treated and implemented carefully. The high order tensor in the energy flux balance equation is expressed in terms of lower moments using the simplifying assumption that the pressure tensor is isotropic. Thus with such a treatment of the random motion and the high order terms associated with the energy flux of the drift motion, we have obtained a complete and closed system of fluid equations sufficient to

determine all macroscopic streamer properties.

In the present chapter the system of fluid equations derived in the previous chapter 2 is solved numerically for a negative planar streamer ionization front and compared with results of a PIC/MC particle model and of the first order fluid model. The comparison with the particle model confirms that our high order fluid model approximates the particle behaviour very well. The comparison with the commonly used first order fluid model of reaction drift diffusion type shows the short-comings of this classical model. This concerns the front velocities, the ionization levels behind the front as well as the electron energy distribution in the high field region ahead of the front and in the ionized low field region in the streamer interior. Actually the inaccurate ionization level in the streamer interior in the first order fluid model is a direct consequence of the inaccuracies of the electron energy distribution [107, 110]. Inaccurate electron densities and energies also have direct consequences for the gas chemistry in the streamer interior [62, 127, 162, 176, 177]. In addition to the accuracy and comprehensiveness of our high order fluid model, its firm theoretical foundation is certainly an additional favouring factor.

We begin by presenting in section 3.2 the differential equations governing the electron density, the average electron velocity, the average electron energy and the average electron energy flux. Then we discuss the numerical algorithm used for the solution of the differential equations. The specific elements of this discussion include a brief mathematical reminder on hyperbolic systems, the implementation of initial and boundary conditions and the discretization in space and time. Our numerical analysis is performed in a 1D model, because in the present chapter we are not interested in a streamer morphology and related phenomena where a full multidimensional model is required. We use a PIC/MC method as an alternative technique to verify our high order fluid model. Following the recent work of Li *et al.* [107, 110, 111], in section 3.3 we give a brief description of this method with particular emphasis upon the construction of planar fronts in the particle model. The high order fluid model is then applied in section 3.4 where examples of planar fronts in pure nitrogen are presented. The effects of photoionization are not considered and present theory can be applied to negative fronts in discharges where photoionization is very weak (high-purity nitrogen is a good example). Results demonstrating the validity of a high order fluid model compared with the PIC/MC are shown. Following the previous chapter 2, we demonstrate the importance of a consistent implementation of transport data in fluid models, but now instead of using the first order model as in the previous chapter 2, we employ our high order model. Along similar lines, the accuracy of the two term approximation for solving Boltzmanns equation in the context of high order fluid studies of the streamer discharges is examined. We pay particular attention to the role of the electron energy flux. For illustrative purposes, calculated results for the planar fronts based on a high order model with energy flux and those calculated without energy flux, are compared over a range of electric fields in order to verify the physical arguments associated with the solution regimes and closure assumptions outlined in the previous chapter 2. Next, we examine the closure assumption associated with the explicit influence of the high order tensor

appearing in the energy flux equation on the streamer dynamics. We conclude that the explicit contribution of the high order tensor in the energy flux equation is negligible and it makes a notable difference only in the velocity of the planar fronts. In summary, in this chapter we present the numerical solution of a high order fluid model, test and verify it on the more microscopic PIC/MC model, and discuss how inherent streamer properties deviate when simpler fluid models are used.

3.2 Model description and numerical solution

3.2.1 The high order fluid model

In the previous chapter 2 we have developed a high order fluid model for streamer discharges. The balance equations were obtained as velocity moments of the Boltzmann equation while the collisional terms were evaluated using momentum transfer theory. We have truncated the system of fluid equations at the level of energy flux balance by reducing the pressure tensor to a scalar kinetic pressure and by neglecting the high order terms associated with the flux of thermal motion. The energy flux of the drift motion, however, is included. For more details of the derivation we refer to [47]. The derived model consists of a set of differential equations for the electron density n , for the average electron velocity \mathbf{v} , for the average electron energy ε and for the average electron energy flux $\boldsymbol{\xi}$:

$$\frac{\partial n}{\partial t} + \nabla \cdot n\mathbf{v} = -n(\tilde{\nu}_A - \tilde{\nu}_I), \quad (3.1)$$

$$\frac{\partial}{\partial t}(n\mathbf{v}) + \frac{2}{3m}\nabla(n\varepsilon) - n\frac{e}{m}\mathbf{E} = -n\mathbf{v}(\tilde{\nu}_m + \tilde{\nu}_I + \frac{2}{3m}\varepsilon\tilde{\nu}_a'), \quad (3.2)$$

$$\frac{\partial}{\partial t}(n\varepsilon) + \nabla \cdot (n\boldsymbol{\xi}) - e\mathbf{E} \cdot (n\mathbf{v}) = -n\tilde{\nu}_e \left[\left(\varepsilon - \frac{3}{2}kT_0 \right) + \Omega \right] - n\varepsilon\tilde{\nu}_A, \quad (3.3)$$

$$\frac{\partial}{\partial t}(n\boldsymbol{\xi}) + \nabla \cdot \left(\beta \frac{2n}{3m}\varepsilon^2 \right) - \frac{5}{3}n\varepsilon e\mathbf{E} = -\tilde{\nu}_m n\boldsymbol{\xi}, \quad (3.4)$$

where \mathbf{E} is the electric field, m and e are electron mass and charge, T_0 is gas temperature and k is the Boltzmann constant. The average collision frequencies for momentum $\tilde{\nu}_m$ and energy transfer in elastic collisions $\tilde{\nu}_e$ are given by equations (2.42) and (2.43) of the previous chapter 2 while $\tilde{\nu}_I$ and $\tilde{\nu}_A$ are the ionization and attachment rate coefficients. The term Ω represents the average energy lost in one energy relaxation time $\tilde{\nu}_e^{-1}$ and is given by equation (4.26) of the previous chapter 2. β is a parameter introduced to approximate the high order tensors in the energy flux equation in terms of lower moments (see equation (2.50) of the previous chapter 2).

Taking into account the rapid growth and propagation of the streamers with orders of the electron drift velocity and the relatively slow drift velocity of ions, the ions are approximated as immobile, as usually done when streamer ionization

fronts are analyzed. Therefore, the charge densities n_{ion} due to the positive and negative ions change only due to ionization and attachment:

$$\frac{\partial n_{ion}}{\partial t} = -n(\tilde{\nu}_A - \tilde{\nu}_I). \quad (3.5)$$

In order to account for the space charge effects, the system (3.1)-(3.5) is coupled with the Poisson equation for the potential ϕ which then enables the calculation of the electric field \mathbf{E} :

$$\nabla^2 \phi = -\frac{e}{\epsilon_0}(n_{ion} - n), \quad \mathbf{E} = -\nabla \phi, \quad (3.6)$$

where ϵ_0 is the dielectric constant.

3.2.2 1D hyperbolic system of balance laws

In the present chapter we simulate the propagation of negative streamer fronts in pure N_2 at atmospheric pressure and at an ambient temperature of 298 K in 1D. As N_2 is a non-attaching gas, electron attachment does not appear in the source terms of our system (3.1)-(3.6). The effects of superelastic collisions are not taken into account and we consider only single ionization with ionization energy ϵ_I . The electron dynamics of equations (3.1)-(3.4) in 1D is given by the following nonlinear system of balance laws:

$$\frac{\partial \mathbf{u}}{\partial t} + \mathbf{A}(\mathbf{u}) \frac{\partial \mathbf{u}}{\partial x} = \mathbf{F}(\mathbf{u}), \quad (3.7)$$

where the primitive variables are

$$\mathbf{u} = (n, nv, n\varepsilon, n\xi)^T, \quad (3.8)$$

the matrix $\mathbf{A}(\mathbf{u})$ is

$$\mathbf{A}(\mathbf{u}) = \begin{pmatrix} 0 & 1 & 0 & 0 \\ 0 & 0 & \frac{2}{3m} & 0 \\ 0 & 0 & 0 & 1 \\ -\beta \frac{2\varepsilon^2}{3m} & 0 & \beta \frac{4\varepsilon}{3m} & 0 \end{pmatrix}, \quad (3.9)$$

and the source term is

$$\mathbf{F}(\mathbf{u}) = \begin{pmatrix} n\tilde{\nu}_I \\ \frac{nqE}{m} - nv(\tilde{\nu}_m + \tilde{\nu}_I) \\ qEnv - n\tilde{\nu}_e \left[\left(\varepsilon - \frac{3}{2}kT_0 \right) + \Omega \right] \\ \frac{5qE}{3m} n\varepsilon - n\xi\tilde{\nu}_m \end{pmatrix}. \quad (3.10)$$

The equation for the ions (3.5) is without electron attachment

$$\frac{\partial n_{ion}}{\partial t} = n\tilde{\nu}_I, \quad (3.11)$$

while the Poisson equation (3.6) in 1D has the following simple form:

$$\frac{\partial E}{\partial x} = \frac{e}{\epsilon_0}(n_{ion} - n). \quad (3.12)$$

Hence, the streamer dynamics in 1D for a non-attaching gas is described by the system of equations (3.7)-(3.12).

Now we can apply the theory for hyperbolic systems of balance laws [104, 105, 140] to our system (3.7)-(3.9). The matrix $\mathbf{A}(\mathbf{u})$ has four eigenvalues:

$$\begin{aligned} \lambda_{1,2} &= \pm \gamma \sqrt{\beta - \sqrt{\beta(\beta - 1)}}, \\ \lambda_{3,4} &= \pm \gamma \sqrt{\beta + \sqrt{\beta(\beta - 1)}}, \end{aligned} \quad (3.13)$$

where $\gamma = \sqrt{\frac{2\epsilon}{3m}}$. All eigenvalues are real and distinct when

$$\beta = 0 \quad \text{or} \quad \beta \geq 1. \quad (3.14)$$

This means that the system (3.7) is *hyperbolic* if the condition (3.14) holds. Although the eigenvalues (3.13) are simple, the corresponding right and left eigenvectors have a rather complicated form, which makes it impossible to work with the vector of Riemann invariants.

3.2.3 Initial and boundary conditions

The electric field $\mathbf{E} = E\hat{e}_x$ (where \hat{e}_x is the unit vector in the x direction) drives the dynamics. We take E as a positive value; therefore electrons drift to the left, and negative streamer ionization fronts move to the left as well. To create steady propagation conditions for the negative front, the electric field on the left boundary $x = 0$ is fixed to the time independent value E_0

$$E(0, t) = E_0 > 0. \quad (3.15)$$

The electric field for $x > 0$ is calculated by integrating equation (3.12) numerically over x , with (3.15) as a boundary condition. The right boundary is located at $x = L$; in all calculations we set the system length L to 1.2 mm and we use 1500 grid points. sec3.2.3 All simulations are started with the same initial Gaussian type distribution for electrons and ions

$$n(x)|_{t=0} = n_i \exp \left[-\frac{(x - x_0)^2}{\sigma^2} \right], \quad (3.16)$$

where we have chosen $n_i = 2 \times 10^{18} \text{ m}^{-3}$, $x_0 = 0.8 \text{ mm}$ and $\sigma = 0.029 \text{ mm}$. The initial conditions for the average electron velocity, average electron energy and average electron energy flux are taken to be spatially homogeneous. The actual values of these quantities are calculated using a multi term solution of Boltzmann's equation, as already discussed in the chapter 2.

As discussed in the appendix, we use homogeneous Neumann boundary conditions for all components of \mathbf{u} at both ends of the system, so that all electron quantities may flow out of the system. Only for the electron density at $x = L$ we employ a homogeneous Dirichlet boundary condition to prevent electrons from diffusing out. However, all calculations end before the ionization reaches the boundary, that means, before the boundary conditions start to become relevant.

Further details on the numerical discretization of the system can be found in the appendix. Extended mathematical and/or numerical studies of the system (3.7) are deferred to a future work.

3.3 MC particle model and first order fluid model

In the next section, we will compare the simulation results of our high order model with those of the PIC/MC particle model and with the first order fluid model. Here these models are briefly described.

3.3.1 The MC particle model

A Monte Carlo model following the motion of individual electrons contains the full physics that is to be approximated by a fluid model. The successful comparison of a fluid model with such a particle model validates the fluid model; of course, the same cross-sections have to be used in both models.

The construction of a planar front is straight forward in fluid models, as the spatial derivatives are simply evaluated in one direction. However, in the particle model electrons move in all three spatial dimensions and hence, the three-dimensional setting has to be restricted as in previous work [107]. An essentially one-dimensional setting is achieved by considering only a small transversal area \mathbf{T} of the front and by imposing periodic boundary conditions at the lateral boundaries. The electric field is calculated only in the forward direction x through

$$E_x(x, t) = E_x(x_0, t) + \int_{x_0}^x dx' \int_{\mathbf{T}} \frac{dy dz}{\mathbf{T}} \frac{e(n_{ion} - n)(x', y, z, t)}{\epsilon_0}, \quad (3.17)$$

where E_x is the electric field in the x -direction, and x_0 is an arbitrary position. Therefore, fluctuations of the transversal field due to density fluctuations in the transversal direction are not included. The density fluctuations projected onto the forward direction depend on the transversal area \mathbf{T} over which the averages are taken.

3.3.2 The first order fluid model

The first order fluid model is the multiply used reaction drift diffusion model that also was called the “classical fluid model” in our previous work [110] [112]; in these previous papers, it was already shown that the model can only serve as a first approximation, but cannot reproduce the results of a particle simulation quantitatively. The steps of derivation of this model were discussed and criticized

in the previous chapter 2. The model is based on the hydrodynamic reaction drift diffusion approximation

$$\frac{\partial n}{\partial t} - \frac{\partial}{\partial x} \left(n\mu E + D \frac{\partial n}{\partial x} \right) = n\nu_I, \quad (3.18)$$

where μ and D are electron mobility and diffusion coefficient, respectively. Transport coefficients used as an input in this model are functions of the local electric field as discussed in the chapter 2. In order to account for the space charge effects, equation (3.18) is coupled to the equations for ion density (3.11) and for the electric field (3.12). For the purpose of comparison, we use the same numerical schemes to discretize equation (3.18) and the same initial and boundary conditions as introduced above for the high order model.

3.4 Results and discussion

In this section we present and compare the simulations results obtained with our high order fluid model, with the PIC/MC method and with the first order fluid model. We consider the configuration described in Section 3.2.3. The transport coefficients required as an input in both the first and the high order fluid model are given in chapter 2. They were calculated from cross sections for electron scattering in N_2 through a multi term solution of the Boltzmann equation. Details of the calculation together with the prescription how to use the data in modeling are given in the same article. It is important to emphasize that the same collisional cross sections for electrons in N_2 are used in all models presented in this chapter.

3.4.1 Simulation of planar fronts: overall comparison between the models

Figure 3.1 shows the temporal evolution of the electron and ion densities and of the electric field in N_2 , when the electric field ahead of the front is 590 Td (or equivalently 145 kV/cm at atmospheric pressure and at a temperature of 298 K). The initially Gaussian electron density shows the behavior observed many times in past: first, it grows due to the ionization processes; then charge separation occurs in the electric field due to the drift of oppositely charged particles in opposite directions, and the initially homogeneous electric field is distorted; and finally, when the field in the ionized region becomes more and more screened, the ionization stops in the ionized region and the typical ionization front profiles of electron and ion densities and of the electric field are established. The initial ionization avalanche is then said to have developed into a streamer.

We note that the results of the high order fluid model and of the PIC/MC simulation agree very well. The streamer velocity is almost the same, as well as the electric field and the electron/ion density. Conversely, when the first order fluid model is applied, the streamer velocity is lower, with a lower electron density in the streamer head and in the streamer channel. In figure 3.2 we show how the streamer velocity depends on the applied reduced electric field E/n_0 . In order to calculate the streamer velocity we have followed the evolution of a certain level

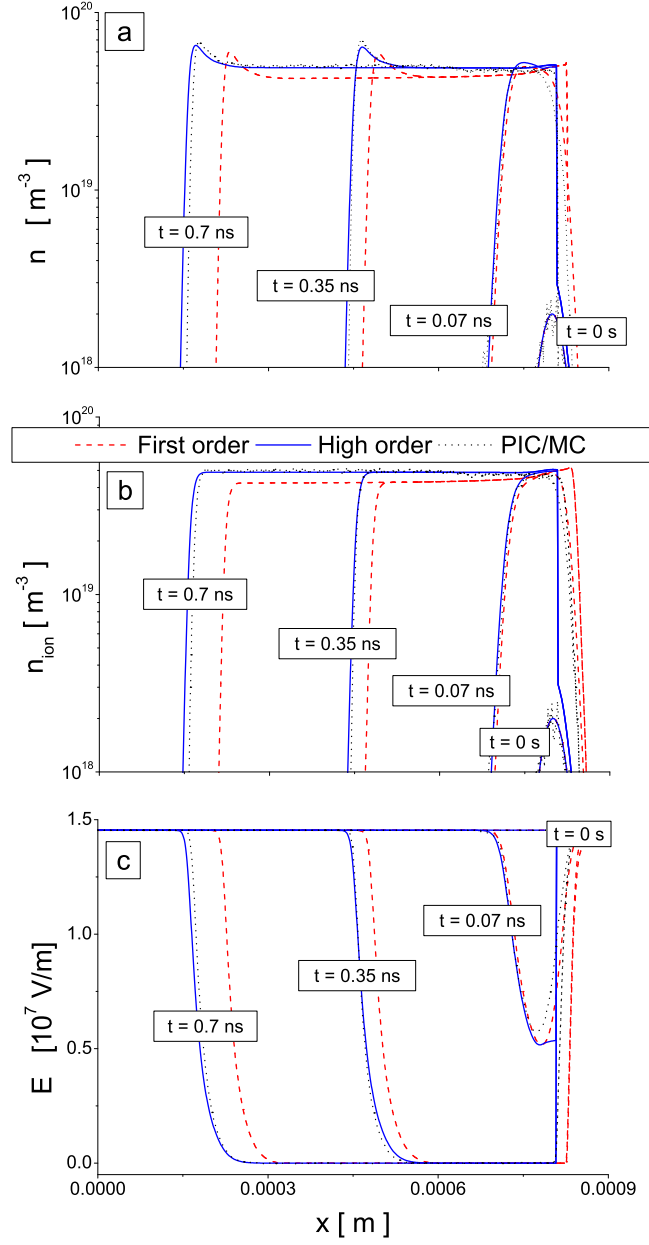


Figure 3.1: Temporal evolution of the electron density (a), ion density (b) and electric field (c) in a planar front in N_2 . Shown are the spatial profiles obtained with three different models as indicated on the graph. Flux transport data are used as an input in fluid models. The externally applied reduced electric field is 590 Td.

($2n_i$) of the electron density at the streamer front. We see that for increasing E/n_0 the differences of the streamer velocities between the first order and the high order fluid model increase slightly. On the other hand, the velocities of the high order fluid model and the PIC/MC agree very well. Similar trends are observed for the electron density behind the ionization front. While the first order model generally underestimates this electron density, the high order model approximates the PIC/MC results much better. This agreement holds in the full range of fields E/n_0 explored, while the differences between first order model and MC model increase with increasing E/n_0 .

In some aspects the results presented in figures 3.1 and 3.2 are consistent with observations by Li *et al.* [107, 110] and by Kanzari *et al.* [87]. In particular, Li *et al.* [107, 110, 112] already have found considerable differences in velocities and ionization densities between MC particle model and classical fluid model; they have proposed an extension of the first order fluid model in [110], based on a phenomenological gradient expansion suggested in [4, 143] to get a better agreement of the fluid model with the results of the particle model. The extended fluid model of Li and co-workers uses a density gradient expansion of the source term to approximate the spatial non-locality of the ionization processes at the streamer front. However, this model overestimates the particle results for the electron density in the streamer channel when the field is below 125 kV/cm (for standard temperature and pressure of the background gas) by up to 4 %, while for an electric field of up to 200 kV/cm, the extended fluid model underestimates the particle results by up to 9 % [110]. On the other hand, the differences in the electron density behind the ionization front between our systematically derived high order fluid model and the PIC/MC model do not exceed 5% for electric fields of up to 245 kV/cm as considered in this work, thus demonstrating that we correctly derived and implemented our high order fluid model.

3.4.2 Electron energy profiles in different front regions within the different models

We now focus on the characteristic differences in the profiles of the electron density. Figure 3.3 shows the profiles of the average electron energy for all three models, as well as the profiles of the electric field and of the electron density at $t = 0.7$ ns for the first order model only. In the first order model, the average electron energy is assumed to adapt to the electric field instantaneously, therefore it was derived from the local electric field for the plot. However, the profile of the average energy obtained by the high order fluid and PIC/MC models is more complex.

We distinguish three different spatial regimes, the streamer head where most ionization occurs and where electron density and electric field have large gradients, the region ahead of the front where the electric field is high and the electron density vanishes, and the streamer interior where the electron density is finite and the electric field is low or vanishing.

First, figure 3.3 shows that in the streamer head the average electron energy given by the high order fluid and PIC/MC methods are higher than in the first

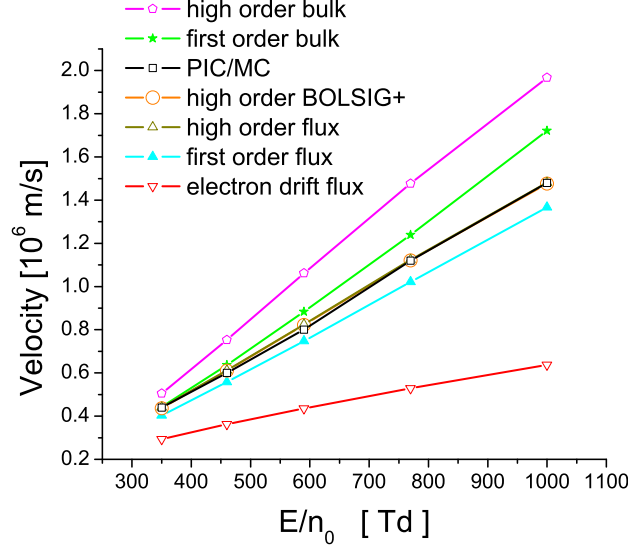


Figure 3.2: Velocities of planar fronts as a function of the electric field obtained with the first and the high order fluid model and with the PIC/MC method; different sets of input data are used as indicated on the graph. The electron flux drift velocity as a function of E/n_0 is also included. We remark that the negative sign of all velocities is removed here.

order fluid model. Since the ionization rate in this energy range is an increasing function of the electron energy, it is clear that the higher the average electron energy, the higher is the ionization rate. These observations are consistent with those made by Li *et al.* [107, 110].

Second, in the region ahead of the front the average energy in the high order model has a slope which reflects the so-called non-local effects. In this region, the PIC/MC method is not efficient as there are not enough particles to sample the spatially resolved average electron energy correctly. It must be emphasized that the spatial variation of the average electron energy is present even in the avalanche phase where an initial spatially homogeneous electric field is not distorted due to space charge effects. According to arguments given in [107], the leading edge of an ionization front has essentially the same dynamics and therefore also the same energy slope as an electron swarm. In the past, many swarm oriented studies have been performed to explore the effects of spatial variation of the average energy through the swarm and many phenomena have been discovered [46, 169, 232, 234]. Almost certainly, one of the most striking phenomena is the difference between the flux and the bulk transport data which follows directly from spatially dependent nonconservative collisions (ionization and/or electron attachment) resulting from a spatial variation of average electron energies within the swarm [44, 46, 150, 234].

Third, figure 3.3 shows strong disagreement between the average energy in the first order model and the average energies predicted by high order fluid and

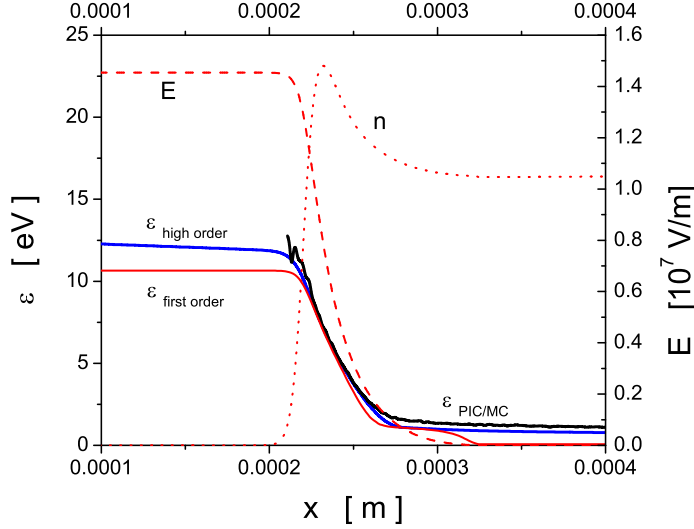


Figure 3.3: The average electron energy in three different models at time 0.7 ns. Profiles of the electric field and the electron number density from the first order fluid model are also included to indicate the location of the front. Calculations are performed for E/n_0 of 590 Td.

PIC/MC methods in the streamer interior. Within the first order fluid model the average electron energy attains approximately the thermal value. This follows directly from the local field approximation and from our Boltzmann equation calculation of the mean energy in the limit of vanishing electric field. It should be emphasized that thermal effects of background molecules are included in our Boltzmann equation analysis. In contrast to the first order fluid model, the average electron energy given by high order fluid and PIC/MC methods are significantly higher. This is another manifestation of the non-local effects, but this time, these phenomena take place in the streamer channel. As the velocity of the front is higher than the electron drift velocity even in the streamer head region, electrons slowly relax to lower energies in the lower or vanishing field in the streamer interior. This causes the spatial decay of average electron energy in high order fluid and PIC/MC model, that can be observed in figure 3.3. This decrease of the average electron energy follows directly from the energy dependence of the collision frequency for energy relaxation in elastic and inelastic collisions.

Another interesting feature is the disagreement between the high order and the PIC/MC results for the average electron energy in the streamer channel. We believe that this disagreement arises from the limitations associated mainly with the high order fluid model. Although our PIC/MC method does not treat thermal effects of the background molecules, electron energies are too high for this to be significant. Most probably this disagreement arises from an increased anisotropy of the distribution function which in turn limits the adequacy of the closure as-

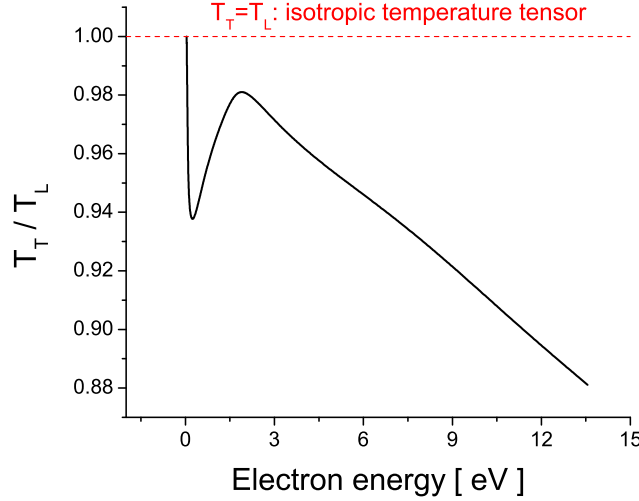


Figure 3.4: The ratio between transverse and longitudinal components of the temperature tensor as a function of electron energy in N_2 based on the multi term approach for the Boltzmann equation.

sumptions associated with the pressure tensor. Indeed, the average energy in the streamer channel varies between 0.5 and 1 eV and exactly in the same energy region the cross sections for vibrational excitation grow rapidly in magnitude (a few orders of magnitude in a very narrow energy range) while the cross section for momentum transfer in elastic collisions varies relatively slowly with the electron energy. This will induce strong anisotropy of the distribution function, and it is clear that the assumption of the isotropy of the temperature tensor is certainly problematic under these conditions. These physical arguments are verified on figure 3.4 where the ratio between transverse and longitudinal components of the temperature tensor for electrons in N_2 is shown. It shows a minimum in the profile between 0.5 and 1 eV which is a clear sign of an increasing anisotropy of the distribution function in velocity space. It should be emphasized that for the range of electric fields considered in this work, the different average energies in the streamer channel observed in high order fluid or PIC/MC model cannot induce significant changes in the electron density. Another physical argument which can be used to address the differences between the average electron energies in the streamer channel is associated with the accuracy of the PIC/MC method. In the energy range around 1 eV one must carefully follow the electrons in a PIC/MC simulation. If the time step between two successive collisions is too big then the energy losses due to rapidly increasing cross sections for vibrational excitation are not going to be included accurately. This is of less importance for the collisional processes whose cross sections do not vary so rapidly with the electron energy. One way to overcome this problem is to reduce the time step in a PIC/MC method

but the penalty is a significant increase in the computation time. It is clear that additional testing and calculations are required to resolve this issue.

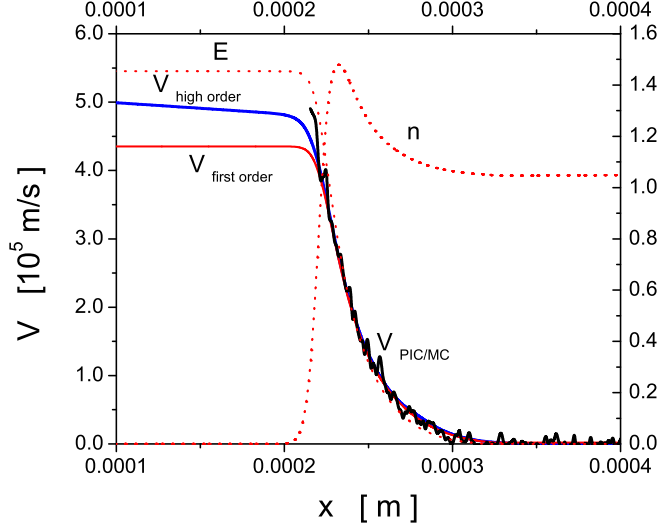


Figure 3.5: Profiles of the average electron velocity in the first and the high order fluid models and of the PIC/MC model at time 0.7 ns. Profiles of the electric field and of the electron number density from the first order model are also included to indicate the location of the front. Calculations are performed for E/n_0 of 590 Td. We remark that all velocities are negative, and their absolute value has been plotted.

Figure 3.5 shows the average electron velocity through the streamer front. As for the average electron energy, in the first order model the average velocity of electrons is obtained from the profile of the electric field assuming the local field approximation. We see that the average velocity of electrons follows changes in the electric field instantaneously: in the outer streamer region where the electric field is constant the average velocity has also a constant value while in the streamer channel the average velocity is essentially zero. When considering the profiles of the average velocity derived by the high order model, one may observe the characteristic slope of this quantity in the outer region of the streamer while in the streamer channel it vanishes. This stands in contrast to the profile of the average energy. The relaxation of the average velocity is determined by the momentum transfer collision frequency which is a factor of 2.5×10^4 larger than the collision frequency for energy transfer. This means that the relaxation of the average velocity is much faster and hence in contrast to the average electron energy this quantity relaxes very rapidly. Figure 3.5 shows a good agreement between results derived by fluid models and by the PIC/MC method. As in the case of the average electron energy, the PIC/MC method is not suitable for the determination of the average velocity of electrons in the region ahead of the front because in this region only a few electrons exist.

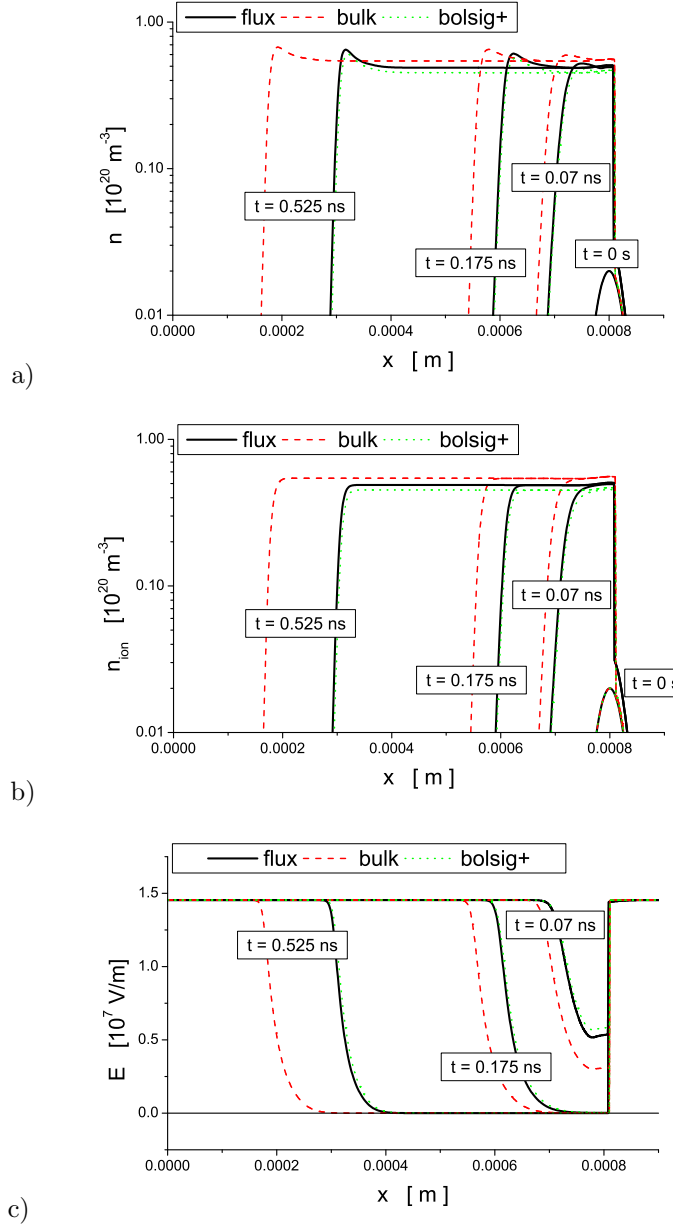


Figure 3.6: Temporal evolution of (a) the electron density, (b) the ion density and (c) the electric field in a planar negative ionization front in N_2 with a reduced electric field E/n_0 of 590 Td ahead of the front. Displayed are the spatial profiles obtained with three different sets of input data as indicated in the graph.

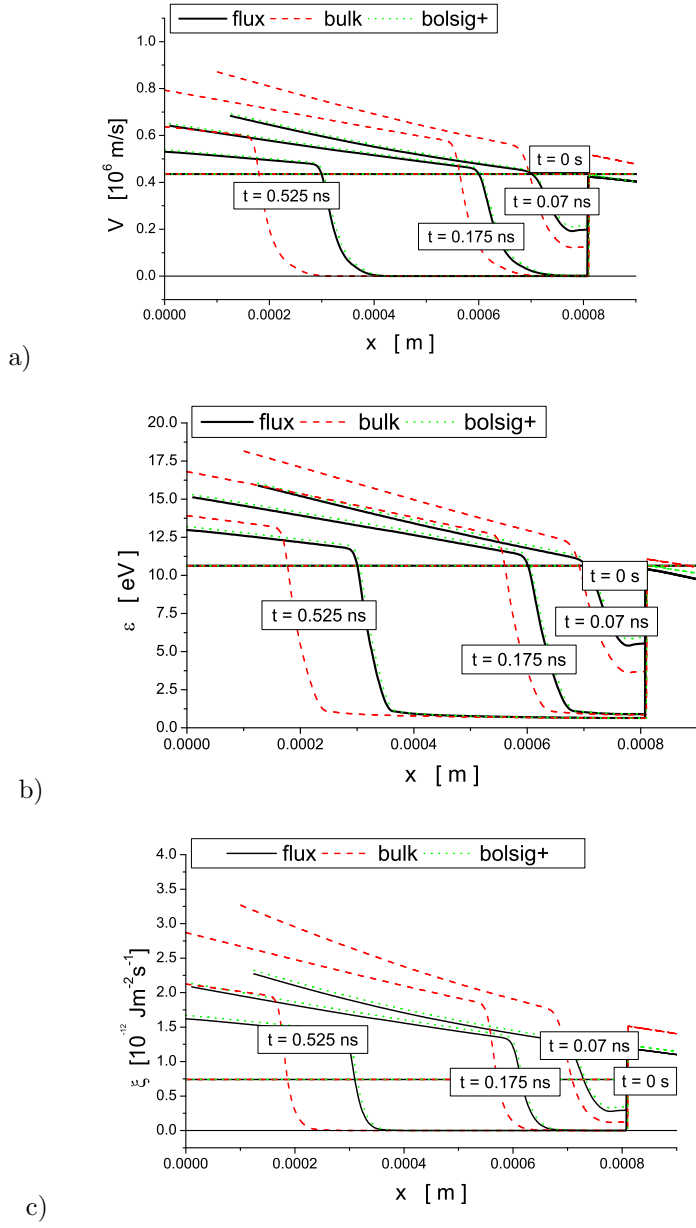


Figure 3.7: The same simulations and plots as in the previous figure, but now for (a) the average electron velocity v , (b) the average electron energy ϵ , and (c) the average electron energy flux ξ . Again, velocity v and energy flux ξ here are negative quantities, and their absolute value is plotted.

3.4.3 On the use of transport data in the high order fluid model

Another important issue in streamer modeling concerns the choice of transport data in fluid models. The origin of, and the difference between bulk and flux transport coefficients in the context of streamer studies have been recently discussed in [44, 110, 111]. In this section we consider the implications of the transport coefficient duality in the context of our high order fluid model for streamers. We also discuss to what extent the differences between transport coefficients obtained by the two term approximation for solving Boltzmann's equation and those obtained by a multi term theory affect the accuracy of streamer models.

Figure 3.6 shows the temporal evolution of the electron and ion densities and of the electric field in a streamer front when the reduced electric field ahead of it is 590 Td. The calculations are performed for three different sets of input data as indicated in the figures. The inadequacy of using bulk data in the high order model is clearly evident (having in mind the very good agreement between the profiles obtained with the flux data and with the PIC/MC method, as shown in the previous section): the streamer velocity is higher and the electron/ion density in the streamer head and in the streamer channel is higher than with the flux transport data. For increasing electric field the discrepancies in the streamer velocity increase further, as illustrated in figure 3.2. Similar trends have been observed in the chapter 2 where planar fronts were modeled with the first order fluid model. In both models, streamers with bulk data are faster and the electron/ion density is higher in both the streamer head and the streamer channel. This follows directly from the fact that in N_2 the bulk mobility of the electrons is larger than the flux mobility. On the other hand, as already shown in section 3.4.1 we observe an excellent agreement between our high order profiles obtained with the flux data and those predicted by a PIC/MC method.

Figure 3.7 displays the temporal evolution of the average electron velocity, of the average electron energy and of the averaged electron energy flux under the influence of electric field of 590 Td for different times as indicated on the graph. The inadequacy of using bulk data is again evident. In the early stage of the streamer development (when the electric field is not entirely screened), the average electron energy calculated using the bulk data is higher in all relevant streamer regions. When the transition process from an avalanche to a streamer is finished, we see a clear discrepancy between the average energies in the region ahead of the streamer front. As simulated planar fronts with bulk data are faster, the corresponding profiles of the average energy are shifted forward. However, for a fully developed streamer, there are no significant deviations between the average energies in the streamer channel. In this region the electric field is screened, and the average energies are slowly thermalizing although not fully relaxed as shown in previous section. The average electron velocity behaves exactly in the same manner as the average electron energy when comparing results with flux or bulk data. The only difference is associated with the fact that the average velocity of electrons is almost fully relaxed in the streamer channel regardless of the type of data used in calculations. The average electron energy flux shows similar behavior.

In earlier streamer investigations it has not been generally investigated to what

extent the two term Boltzmann equation results for various transport coefficients affect the accuracy of the model predictions. The limitations of the two term approximation for solving Boltzmann's equation have been illustrated many times in past in the context of swarm studies [45, 171, 233, 234]. Here the question arises of whether a similar conclusion can be drawn for streamers taking into account that the streamer development is a non-linear, non-stationary and non-hydrodynamic problem where space charge effects are important and where the electron energy varies from thermal values in the streamer channel up to a few tens of eV in the outer region of the streamer for the fields considered here. It is clear that the anisotropy of the velocity distribution function may be considerable in various streamer regions and hence we will compare profiles for different streamer properties using the two term and multi term results for transport data as an input in modeling.

Figure 3.6 (a) shows that the ionization level behind the streamer front calculated using the BOLSIG+ transport data is lower while the streamer velocity is the same. Surprisingly, the profiles of the electric field, the average electron energy and the average electron velocity obtained with the multi term flux data or with the BOLSIG+ data agree very well. This is a clear indication that internal errors of the two term approximation associated with the ionization rate can be directly used to understand the differences in the profiles of the electron and ion densities in the streamer channel (see figure 2.4 (c) in the chapter 2). However, this conclusion cannot be generalized to other gases or other conditions than those studied here. As pointed out recently by White and co-workers [233, 234] one may never be sure about the accuracy of the two term approximation as various transport properties show different sensitivity with respect to this approximation in different energy ranges. For example, the inadequacy of the two term approximation has been recently demonstrated for CF_4 [171] and CH_4 [233]. In the chapter 2, it was shown that the velocity of a streamer in the first order fluid model is significantly affected by choosing either the two term or the multi term solution. Therefore, when high precision is required the best option is to use a multi term approach and/or a Monte Carlo simulation technique to calculate the input data for fluid models regardless of their order.

3.4.4 Simulation of planar fronts with and without the energy flux term

In this section, we compare the results of the high order fluid model with and without the energy flux term (3.4). In the model without the energy flux term the energy flux ξ in the energy balance equation (3.3) is set to zero, and therefore the energy flux balance equation (3.4) does not need to be considered. This approach was already used in the case of streamer corona discharge dynamics [58, 87] and for analysis of ionization wave dynamics in low-temperature plasma jets [241]. Figures 3.8 and 3.9 show the streamer properties for a reduced electric field E/n_0 of 350 Td at time $t = 1.5$ ns. First, we see that the high order fluid model with the energy flux term gives higher electron and ion densities within the streamer channel than without the energy flux. For increasing E/n_0 these differences increase further, as shown in figure 3.10(a). The electric field exhibits the typical streamer behavior;

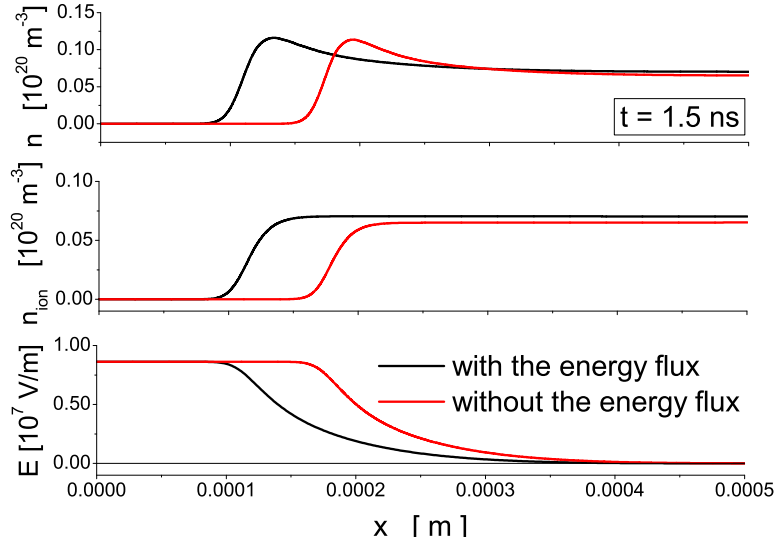


Figure 3.8: Electron density, ion density and electric field in N_2 in an external electric field of 350 Td. The two lines indicate solutions of the high order fluid model with and without the energy flux term at the same instance of time. The initial condition is the same, and the flux transport data are used.

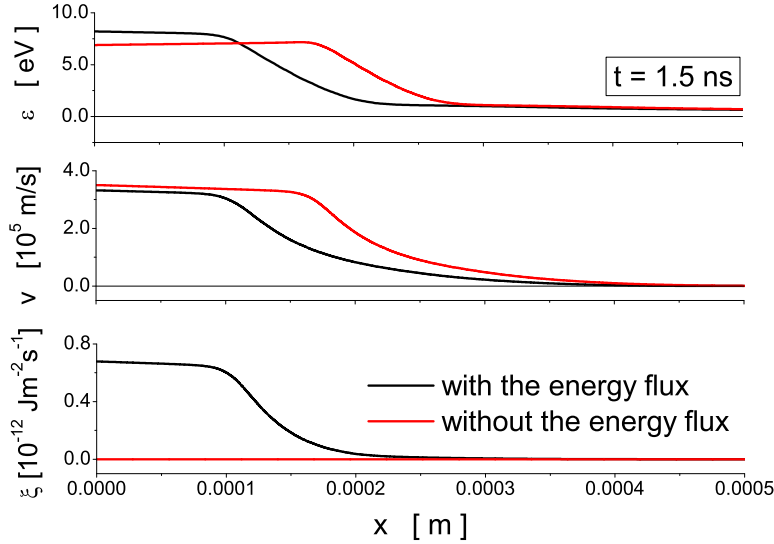


Figure 3.9: The same instant and plot as in Fig. 3.8, but now average electron energy, negative average electron velocity and negative average electron energy flux are plotted.

the observed differences between the high order fluid models with and without the energy flux term follow from the time delay needed for the space charge to

become high enough and distort the externally applied spatially homogeneous electric field in these two models. This property is even more evident for the streamer velocity shown in figure 3.10(b). Figures 3.8 and 3.9 show clearly that in our simulation conditions the streamer front propagates faster in the high order fluid model with the energy flux term.

Furthermore, the average electron energy and the average electron velocity ahead of the streamer depends clearly on the fact whether the electron energy flux is included or not. The average electron energy has a steep gradient between the outer streamer region and the streamer channel. In this spatially narrow region the energy decreases from the range between 10 and 20 eV to essentially thermal values in the streamer channel. It is clear that the correct treatment of the energy flux in the high order fluid model is critical for an accurate energy transport between the different streamer regions. In view of the close agreement between the present results with the energy flux term and those predicted by a PIC/MC method, established in the previous sections, we must conclude that the high order fluid model without the energy flux term is qualitatively right but quantitatively wrong under the conditions simulated.

3.4.5 Simulation of planar fronts with and without the high order tensor

In this section we investigate the influence of the high order tensor in the energy flux equation. In order to truncate the system after the energy flux equation, in the chapter 2 this tensor was expressed by a product of two lower order tensors times a parameter β . In all previous sections, we used $\beta = 1$ which is a natural guess. Here we investigate how the simulation results depend on β .

Figure 3.11 shows the profiles of the electron density, the electric field, the average electron energy and the average electron flux for a reduced electric field E/n_0 of 350 Td at time 1.5 ns. One can immediately see that increasing the parameter β increases the velocity of the streamer very slightly. All other quantities remains essentially unaltered in the streamer channel indicating their weak sensitivity with respect to β . Only in the limit of the highest electric field considered here, the streamer properties in the channel respond slightly to the variation of the parameter β . Ahead of the streamer front, however, we observe variations in the streamer properties even for the reduced electric field of 350 Td. As expected, the most sensitive quantity with respect to variations in β is the average electron energy flux.

In section 3.2.2, we have derived that our high order model is well posed if $\beta = 0$ or $\beta \geq 1$. We have solved our system for a range of values for β and reduced electric fields E/n_0 and it was found that $\beta = 1$ ensures the best agreement between profiles obtained by the high order fluid model and by the PIC/MC method. This validates the closure assumption associated with the contribution of high order tensors in the energy flux equation, as discussed in the chapter 2. Furthermore, if we analyze the profiles of various streamer properties for $\beta = 0$, the simulation results agree very well with those derived by the PIC/MC method. The importance of this is twofold. First, the influence of the high order tensors in the energy flux equation is less than initially expected. Second, taking $\beta = 0$ is a

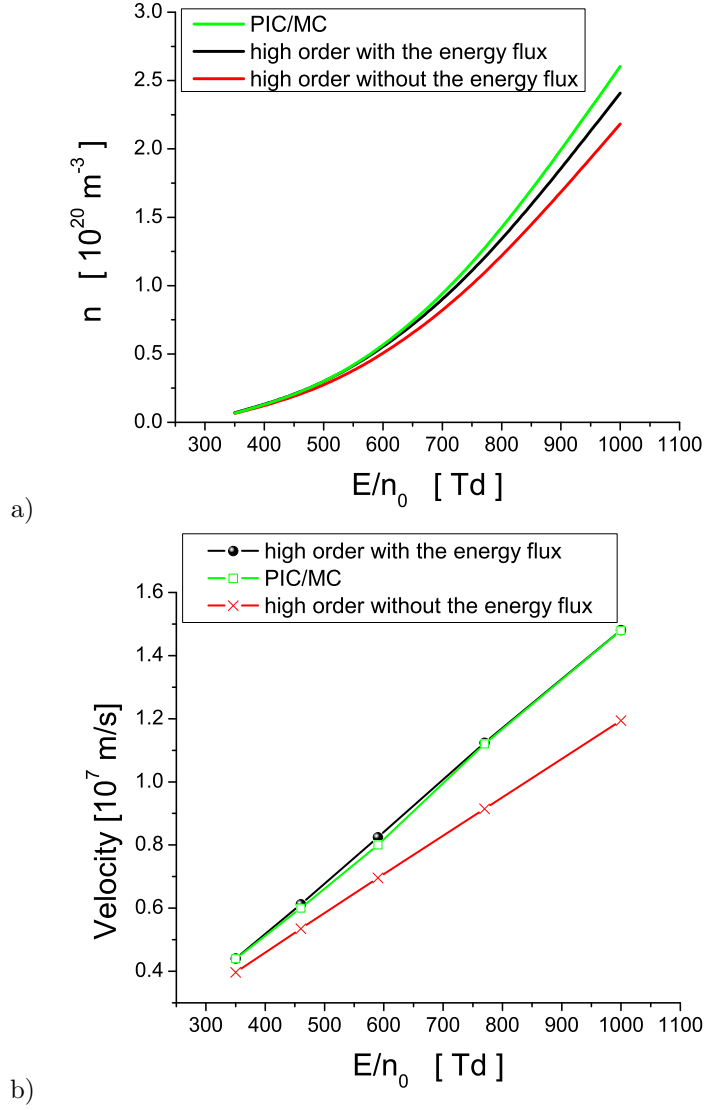


Figure 3.10: (a) The ionization level behind the planar front, and (b) the absolute value of the front velocity as a function of the reduced electric field E/n_0 ahead of the front. Results are shown for the high order fluid model with or without the energy flux term, as well as for the PIC/MC model. Flux transport data are used as an input in the fluid models.

very good approximation, and it will significantly reduce the computation costs for the differential equations in 3D.

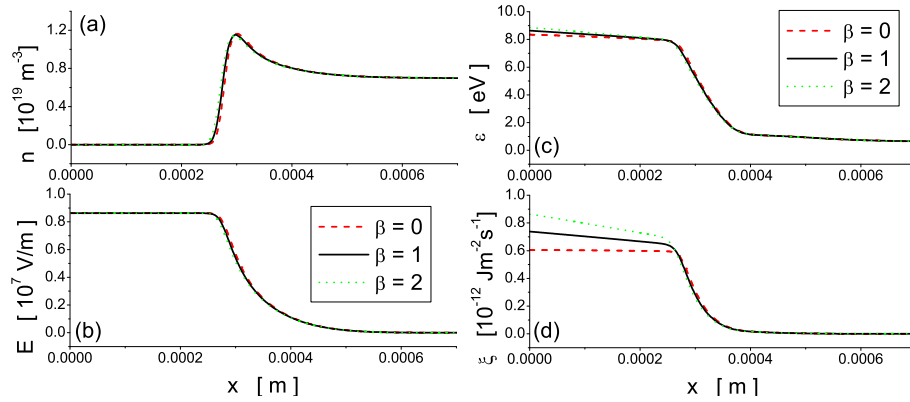


Figure 3.11: Profiles of (a) electron density, (b) electric field, (c) average electron energy, and (d) average electron energy flux for $\beta = 1$, $\beta = 2$ and $\beta = 3$. The results are shown for E/n_0 of 350 Td at time 1.5 ns.

3.5 Conclusion

In the previous chapter 2 we have derived the equations and the transport and reaction parameters of a high order fluid model for streamer discharges. In the present chapter we have briefly presented an accurate and efficient way to numerically solve the high order fluid model. These numerical schemes are then used to study the propagation of negative streamer fronts in N_2 . Then we compared the high order fluid model and the first order fluid model with a PIC/MC model. While the first order model is very commonly used for streamer simulations, it can be clearly seen that the high order model is a much better approximation of the full particle dynamics. This concerns not only quantitative, but also qualitative differences. In particular we observe:

- (a) The non-local effects in the profile of the average electron energy are present both in the PIC/MC-model and in the high order model, but are missing in the first order model due to the local field approximation. The slope of the average electron energy in the region ahead of the streamer is related to the spatial variation of the average electron energy in the avalanche phase of the streamer development. And the slope of the average electron energy in the streamer channel is striking and an inherent property of a streamer as well, as the electrons can not immediately relax to the low or vanishing field in the streamer interior.
- (b) Bulk and flux transport coefficients for electrons can differ substantially in so-called non-conservative regions where ionization, attachment, detachment and recombination takes place. Here one needs to take care which coefficients to implement. Streamers in nitrogen with bulk data are faster and create a much higher electron density in the streamer channel. When the streamers in nitrogen are calculated with BOLSIG+ data, their velocity is not affected. However, in the streamer channel and in the streamer head we have found differences between the electron densities in our high order fluid model when we inserted either BOLSIG+

data or our flux data for the electron transport coefficients.

(c) When we conducted streamer simulations with our high order model, either including or excluding the energy flux, various streamer properties showed that the energy flux term cannot be neglected. Streamers without energy flux term are slower and create a lower electron density in the streamer channel. In the region ahead of the streamer, the average electron energy and the average electron velocity also change when the energy flux is neglected.

(d) The validity of the closure assumption associated with the treatment of high order terms in the energy flux equation is studied through the variation of the parameters used to parameterize the expression in which high order tensors are expressed in terms of lower order moments. We have pointed out that although the average electron energy and average electron energy flux in the outer region of the streamer are influenced by this parameter, the demand for a strict consideration of the high order tensor in the energy flux equation may be relaxed. This follows from the fact that it is almost impossible to notice the differences in the streamer velocity and electron density in the streamer channel for different parameters used to parameterize the high order terms.

Though in the present chapter, we have tested our model on planar fronts, the theory of the high order model has been developed in the previous chapter 2 without restrictions for the full three-dimensional setting. An important aspect to be addressed in the future is our closure assumption for the pressure tensor that we assumed to be isotropic. This restriction will be removed in future work.

Finally we would like to emphasize that though this study has concentrated on electron dynamics mainly in planar streamer fronts, the theory and the associated numerical solution of the system of differential equations are equally valid for ions up to the energy balance equation. Therefore we have derived a new modeling frame work that is widely applicable in reactive plasmas in full 3D.

CHAPTER 4

Comparison of fluid models for streamer discharges with MC-PIC results

In mathematics you do not understand things. You just get used to them.

– JOHANN VON NEUMANN

If a man will begin with certainties, he shall end in doubts; but if he will be content to begin with doubts he shall end in certainties.

– SIR FRANCIS BACON

In all affairs it is a healthy thing now and then to hang a question mark on the things you have long taken for granted.

– BERTRAND RUSSELL

4.1 Introduction

Streamers are fast ionizing waves that are non-linearly controlled by space charge effects. Streamer discharges occur in nature (lightening and sprites [49, 123, 167]) and technology (plasma-assisted combustion [212], plasma medicine [92], disinfection [226] etc.). The development of models and simulation techniques

This chapter is based on the preprint *Comparison of fluid models for streamer discharges with MC-PIC results* by Aram H. Markosyan, Jannis Teunissen, Saša Dujko and Ute Ebert to be submitted to *Plasma Sources Science and Technology*.

has been an ongoing process for more than five decades. All these models can be classified as one of the following types: particle, kinetic, fluid and hybrid.

Particle models follow particles and thereby give direct information about the electron distribution in phase space [107, 110]. These models have few underlying assumptions or approximations, and therefore give accurate predictions under a wide range of conditions, but they are computationally very expensive.

The second type of models are the so-called kinetic models, that couple the full Boltzmann equation with the Poisson equation. Recent advances in both computing power and algorithms have made these fully kinetic simulations possible [9, 91].

The third type of models are the plasma fluid models, which describe the electron dynamics in plasma based on macroscopic quantities like electron density, electron average velocity, electron average energy etc. Fluid models are constructed by taking the velocity moments of the Boltzmann equation. Depending on the number of moments considered and the closure assumptions, various fluid models have been derived over last two decades [16, 47, 58, 66, 87]. Fluid models require less computational resources compared to particle models yet provide reasonably good results.

Finally, hybrid models try to combine the strengths of the fluid and particle approaches, by using both models in the same simulation. Li *et al* [110] have used a particle model to follow the individual electrons around the head of a negative streamer, while using a fluid approximation in the rest of the domain. The progress in hybrid modelling has recently been reviewed by Kushner [100].

In the present chapter we consider the most popular first and the second order fluid models together with the newly developed high order fluid model, and we compare them with a particle model. The goal of this work is to compare how well these models can simulate 1D ionization waves. In the chapter 3 we already have compared the high order and the first order models with the particle model in nitrogen. We have concluded that the results obtained with the high order model agreed very well with the particle model. In this chapter simulations are performed in the noble gas Ne at standard temperature and pressure (STP). The reason is that unlike a molecular gas N_2 , Ne has very few inelastic channels and the thresholds for these processes are quite high. These means that non-local phenomena, like a high energy level in the streamer channel (despite of fully screened electric field in the channel), are more pronounced. Due to this high energies in the channel, Ne is highly used in industry (neon lamps, plasma medicine etc.). In section 4.2, we summarize the origin of these fluid models, namely to the Boltzmann equation, introduced previously in the section 2.2.1. In the next consecutive subsections 4.2.1 and 4.2.3 we briefly summarize the derivations and the assumptions of the first and high order fluid models, which have been introduced earlier in great detail in the chapter 2. In subsection 4.2.2 we present the second order fluid model. We shortly discuss the particle model in section 4.3 which was already introduced in detail in section 3.3. In section 4.4 we present the transport parameters for neon which are used by the fluid models. The simulation conditions that we use for comparing the models are discussed in section 4.5, and the results of the comparison are given in section 4.6. In section

4.7 we discuss our results in more detail and we give our conclusions in section 4.8.

4.2 Fluid models for streamer discharges

The dynamics of charged particles, in particular electrons, under the influence of external forces, in this case electric field, can be described microscopically by the Boltzmann equation or by the Particle-in-Cell Monte Carlo (PIC/MC) technique. While the latter one follows individual particles in phase space [221], the former one describes the ensemble of particles by the distribution function, or phase density, $f_i(\mathbf{r}, \mathbf{c}, t)$ in phase space (\mathbf{r}, \mathbf{c}) for each charged component i at time t . The evolution of distribution function is described by the Boltzmann equation introduced in the chapter 2.2.1 and in the references [43, 201, 234, 238]:

$$\partial_t f_i + \mathbf{c} \cdot \nabla f_i + \frac{e_i}{m_i} \mathbf{E} \cdot \nabla_{\mathbf{c}} f_i = -J(f_i, f_0). \quad (4.1)$$

where ∇ is the differential operator with respect to space \mathbf{r} and $\nabla_{\mathbf{c}}$ with respect to velocity \mathbf{c} , e_i and m_i are charge and mass of species i , and t is time. The right-hand side of equation (4.1), $J(f_i, f_0)$, describes the collisions of charged particles with neutral molecules, accounting for elastic, inelastic, and non-conservative (e.g. ionising or attaching) collisions, and f_0 is the velocity distribution function of the neutral gas (usually taken to be Maxwellian at fixed temperature).

If we work under electrostatic conditions, then space charge effects can be accounted for by coupling the Boltzmann equation to the Poisson equation:

$$\nabla^2 V = -\frac{1}{\epsilon_0} \sum_i q_i n_i(\mathbf{r}, t), \quad (4.2)$$

so that the electric field can be calculated by:

$$\mathbf{E} = -\nabla V, \quad (4.3)$$

where ϵ_0 is the dielectric permittivity, and q_i and n_i are the charges and densities of species i (electrons, ions, excited states etc.). One should note that the Boltzmann equation provides a complete description of the distribution in phase space of species i , while the density n_i in equation (4.2) is a macroscopic (averaged) quantity. The number density n_i can be directly calculated from the distribution function $f_i(\mathbf{r}, \mathbf{c}, t)$:

$$n_i(\mathbf{r}, t) = \int f_i(\mathbf{r}, \mathbf{c}, t) d\mathbf{c}. \quad (4.4)$$

The most common techniques for solving the Boltzmann equation are the moment and the path integral methods. In moment methods the distribution function is usually expanded in terms of spherical harmonics to resolve its angular dependence in velocity space [43, 234]. In the path integral method the distribution function is converted to an integral equation along the free path and

the solution is usually found by the direct integration [207]. One ought to mention approaches based on a Monte Carlo method for direct numerical integration of the Boltzmann equation [94, 165, 195]. Direct numerical solution of the Boltzmann equation using a computational mesh in phase space (both in physical and velocity spaces) is very challenging [91]. Advances in computational techniques such as Adaptive Mesh Refinement (AMR) have made it possible to significantly reduce the number of computational cells needed [17, 175]. The application of AMR to solve the Boltzmann equation shows promising results [9, 91]. In [9, 91], the Discrete Velocity Method (DVM) [139] is used to discretize velocity space, so that the velocity distribution can be calculated for all points of physical space.

Unfortunately, the system (4.1)-(4.3) can typically not be solved with direct numerical simulations. An alternative approach is to consider the velocity moments of distribution function:

$$\langle \phi(\mathbf{c}) \rangle = \frac{1}{n(\mathbf{r}, t)} \int \phi(\mathbf{c}) f(\mathbf{r}, \mathbf{c}, t) d\mathbf{c}, \quad (4.5)$$

with $\phi(\mathbf{c}) = 1, m\mathbf{c}, \frac{1}{2}mc^2, \frac{1}{2}mc^2\mathbf{c}, \dots$ giving the average velocity $\mathbf{v} = \langle \mathbf{c} \rangle$, average energy $\varepsilon = \langle \frac{1}{2}mc^2 \rangle$, average electron energy flux $\boldsymbol{\xi} = \langle \frac{1}{2}mc^2\mathbf{c} \rangle$ and so on. $\langle \cdot \rangle$ represents the average over the velocity \mathbf{c} of the charged particles. Using this approach, the set of moment equations can be found by multiplying (4.1) by $\phi(\mathbf{c})$ and integrate over the velocity space:

$$\partial_t (n\langle \phi(\mathbf{c}) \rangle) + \nabla \cdot (n\langle \mathbf{c}\phi(\mathbf{c}) \rangle) - n\frac{e}{m}\mathbf{E} \cdot \langle \nabla \mathbf{c}\phi(\mathbf{c}) \rangle = C_\phi, \quad (4.6)$$

where C_ϕ is the collision term:

$$C_\phi = - \int \phi(\mathbf{c}) J(f) d\mathbf{c}. \quad (4.7)$$

To derive the term $\langle \nabla \mathbf{c}\phi(\mathbf{c}) \rangle$, a partial integration over \mathbf{c} has been performed.

The complete knowledge of the distribution function allows to compute all of its moments, but the inverse is true as well: if all moments are known, the distribution can be reconstructed. In practice, we can consider only a finite set of equations (4.6). Obviously, this will lead to the loss of some information. For small Knudsen numbers, i.e. the mean free path of electrons is much less than the characteristic dimensions of the discharge, the knowledge of a small number of moments is sufficient to describe the state of the gas with reasonable accuracy [216]. Even in this case, unfortunately, any finite set of moment equations is not determined and some closure assumption should be made.

Equation (4.6) represents a set of hydrodynamic balance laws or fluid equations: the mass balance ($\phi(\mathbf{c}) = 1$), the momentum balance ($\phi(\mathbf{c}) = m\mathbf{c}$), the energy balance ($\phi(\mathbf{c}) = \frac{1}{2}mc^2$), etc. The hydrodynamic or continuum description is applicable to the modelling of streamer discharges as the Knudsen number is low.

In the following subsections we present different models with respect to the number of moments considered. Except for the high order model, these models have been frequently used over the last few decades.

4.2.1 The first-order or classical model

The first order model, also called classical model, is the simplest and most used model considered in this work [10, 30, 40, 47, 52, 66, 96, 97, 138, 164, 228]. For the full derivation we refer to [47, 66]. This model considers only the first two balance laws from the system (4.6):

$$\partial_t n + \nabla \cdot (n\mathbf{v}) = C_1, \quad (4.8)$$

$$nm \frac{d\mathbf{v}}{dt} = ne\mathbf{E} - \nabla \cdot \mathbf{P} + C_{m\mathbf{c}} - m\mathbf{v}C_1, \quad (4.9)$$

where $\mathbf{v} = \langle \mathbf{c} \rangle$ is the average local electron velocity, C_1 and $C_{m\mathbf{c}}$ are the collisional term, $\mathbf{P} = nm \langle (\mathbf{c} - \mathbf{v})(\mathbf{c} - \mathbf{v}) \rangle$ is the pressure tensor and $\frac{d}{dt} = \partial_t + \mathbf{v} \cdot \nabla$ is the convective time derivative. Now the velocities are decomposed into an average velocity \mathbf{v} plus random velocities $\mathbf{c} - \mathbf{v}$ with zero mean ($\langle \mathbf{c} - \mathbf{v} \rangle = 0$).

At this stage no assumptions have been made and the system (4.8)-(4.9) is incomplete, as the pressure tensor \mathbf{P} , momentum transfer by collision $C_{m\mathbf{c}}$ and the production term C_1 are not specified, hence it can not be directly solved. In order to close the system (4.8)-(4.9) and to obtain the classical drift-diffusion-reaction model the following assumptions have to be made :

1. the distribution of random velocities is close to isotropic, hence $\mathbf{P} \approx p \mathbf{I} = nkT \mathbf{I}$, where \mathbf{I} is the unity tensor, k is the Boltzmann constant and T is the electron temperature. This is a very strong assumption for streamer discharges, where at the streamer tip the electric field is locally very high and strong pressure gradients exists,
2. $C_{m\mathbf{c}} = -nm\nu_{\text{eff}}\mathbf{v}$, where ν_{eff} is the effective momentum transfer collision frequency, which accounts for momentum transfer exchange only in elastic and inelastic collisions. The momentum transfer exchange due to non-conservative (ionisation, attachment, recombination, photoionisation, etc.) collisions is omitted,
3. $C_1 = n\nu_I$, where ν_I is the ionisation collision frequencies due to electron-molecule collisions
4. the rate of momentum change $(d_t\mathbf{v})/\mathbf{v}$ is smaller than the rate of momentum transfer ν_{eff} ,
5. the gradients in electron energy are neglected,
6. the system is close to equilibrium and the Nernst-Townsend-Einstein relation $D/\mu = kT/e$ is valid,
7. all transport properties are functions of the local electric field, i.e. the Local Field Approximation (LFA) is valid.

Under the assumptions above the equation (4.9) can be written in the following form:

$$n\mathbf{v} = n\mu\mathbf{E} - D\nabla n, \quad (4.10)$$

where the mobility and diffusion constant are given by the following expressions:

$$\mu = \frac{e}{m\nu_{\text{eff}}}, \quad D = \frac{kT}{m\nu_{\text{eff}}}. \quad (4.11)$$

If we assume that the mobility and diffusion of ions are negligible compared with electron mobility and diffusion, we can rewrite the system (4.8)-(4.9) in the following form:

$$\partial_t n = \nabla \cdot (\mu(E)n\mathbf{E} + D(E) \cdot \nabla n) + n\nu_I(E), \quad (4.12)$$

$$\partial_t n_{\text{ion}} = n\nu_I, \quad (4.13)$$

where $E = |\mathbf{E}|$, n_{ion} is ion density. The transport properties μ , D and ν_I are the functions of the local electric field. Of course, the system (4.12)-(4.13) is coupled to the Poisson equation (4.2)-(4.3) which in 1D has the following simple form:

$$\frac{\partial E}{\partial x} = \frac{e}{\epsilon_0}(n_{\text{ion}} - n). \quad (4.14)$$

We would like to remark that when LFA is derived from the Boltzmann equation (4.1), the diffusion coefficient, strictly speaking, is a scalar. But in the case of streamer discharges, the diffusion tensor is highly anisotropic, as the electron velocity distribution function is non-Maxwellian. A few authors have considered anisotropic diffusion [59, 110]. Particularly, in [59] the effect of anisotropic diffusion on branching phenomena of negative streamers is investigated.

In [4, 110, 143] a phenomenological extension of LFA based on gradient expansion of electron density is provided. It provides better results than the classical LFA [110].

4.2.2 The second-order model

The second order model considers also the energy balance equation. Depending on the closure assumption, one can obtain conceptually different second-order models. In this section we discuss the model called LEA (Local Energy Approximation) and originating, to our knowledge, from [1, 2, 13], which successfully has been used by many others in different applications [19, 20, 37, 58, 73, 74, 75, 76, 90, 110, 181, 224, 231]. It contains the equations (4.8), (4.9) and the energy balance equation:

$$\partial_t(n\varepsilon) + \nabla \cdot \mathbf{\Gamma}_\varepsilon = \mathbf{E} \cdot n\mathbf{v} - C_\varepsilon, \quad (4.15)$$

where $\mathbf{\Gamma}_\varepsilon$ is the average electron energy flux:

$$\mathbf{\Gamma}_\varepsilon = n\varepsilon\mathbf{v} + \mathbf{P} \cdot \mathbf{v} + \mathbf{q}, \quad (4.16)$$

where $\mathbf{q} = \frac{1}{2}nm\langle (\mathbf{c} - \mathbf{v})^2 (\mathbf{c} - \mathbf{v}) \rangle$ is the heat flux vector and C_ε is the collisional operator.

At this stage the system (4.8), (4.9), (4.15) is exact (free of assumptions) and incomplete. To close the system the following assumptions are made:

1. the assumptions (i)-(vi) from the section 4.2.1 are applied to the system (4.8), (4.9), i.e we have the equation (4.12), but with transport parameters depending on local average electron energy,
2. the total energy transfer (losses) is due to the elastic and inelastic collisions:

$$C_\varepsilon = n \sum_j k_j \varepsilon_j, \quad (4.17)$$

where k_j and ε_j are the collision rate coefficient and energy loss per electron per collision (elastic, inelastic) for the collision process denoted by j ,

3. the pressure tensor in equation (4.16) is simplified to $\mathbf{P} = nk\mathbf{T} \approx \frac{2}{3}n\varepsilon\mathbf{I}$,
4. the heat flux vector \mathbf{q} is assumed to be proportional to the gradient of the electron average energy $\mathbf{q} = -\frac{5}{3}nD\nabla\varepsilon$, where D is the diffusion coefficient,
5. all transport properties are functions of the local average electron energy, i.e. the Local Energy Approximation (LEA) is valid. In future we refer to this second order model as to LEA.

Under the assumptions above, the LEA model can be written in the following way:

$$\partial_t n = \nabla \cdot \mathbf{\Gamma} + n\nu_I(\varepsilon), \quad (4.18)$$

$$\partial_t(n\varepsilon) = \frac{5}{3}\nabla \cdot (\varepsilon\mathbf{\Gamma}) + \mathbf{E} \cdot \mathbf{\Gamma} - n \sum_j k_j \varepsilon_j, \quad (4.19)$$

$$\partial_t n_{ion} = n\nu_I, \quad (4.20)$$

where $\mathbf{\Gamma} = n\mu(\varepsilon)\mathbf{E} - D(\varepsilon)\nabla n$. Of course, in this case as well, the system (4.18)-(4.20) is coupled with the Poisson equation (4.14). As illustrated by Hagelaar and Pitchford [74], this model is consistent with the classical theory for electron transport based on the two term approximation for solving the Boltzmann equation.

The LEA model is one of the most popular second-order models. Depending on the closure assumptions, one can obtain different second-order models. In chapter 3 we have investigated the importance of the energy flux equation by deriving a second-order model with neglected energy flux term. A similar system has been derived by Kanzari *et al* [87]. Eichwald *et al* [58] used a similar approach to simulate streamer dynamics and radical formation in a pulsed corona discharge used for flue gases. Guo and Wu [73] have developed a more sophisticated second order model in which the Langevin theory was used to simplify the collision source terms with *a priori* knowledge of the relaxation times of electron energy and momentum. Another, recent, second order model has been derived by Becker *et al* [15] as a simplification of their "four-moment" model [16]. They illustrate that this simplification can be done without loss of accuracy, if the characteristic frequency of the electric field alteration in the discharge is small in comparison with the momentum dissipation frequency of the electrons [16]. In [15] the authors have emphasised that fluid models are able to describe nonlocal phenomena caused by electron energy transport, if the energy transport is consistently described. The same conclusions are derived in the chapter 3.

4.2.3 The high-order model

Presently, the most complex model, developed only recently [47, 131], is the high order fluid model. The infinite system of moment equations (4.6) is truncated at the level of energy flux balance by approximating pressure tensor with a scalar kinetic pressure. The collisional terms were evaluated using momentum transfer theory [186, 192, 234]. For more details of the derivation we refer to chapter 2. The high order fluid model consists of a balance laws for the electron density n , for the average electron velocity \mathbf{v} , for the average electron energy ε and for the average electron energy flux $\boldsymbol{\xi}$:

$$\frac{\partial n}{\partial t} + \nabla \cdot n\mathbf{v} = n\nu_I, \quad (4.21)$$

$$\frac{\partial}{\partial t}(n\mathbf{v}) + \frac{2}{3m}\nabla(n\varepsilon) - n\frac{e}{m}\mathbf{E} = -n\mathbf{v}(\nu_m + \nu_I), \quad (4.22)$$

$$\frac{\partial}{\partial t}(n\varepsilon) + \nabla \cdot (n\boldsymbol{\xi}) - e\mathbf{E} \cdot (n\mathbf{v}) = -n\nu_e \left[\left(\varepsilon - \frac{3}{2}kT_0 \right) + \Omega \right], \quad (4.23)$$

$$\frac{\partial}{\partial t}(n\boldsymbol{\xi}) + \nabla \cdot \left(\beta \frac{2n}{3m} \varepsilon^2 \right) - \frac{5}{3}n\varepsilon e\mathbf{E} = -\nu_m n\boldsymbol{\xi}, \quad (4.24)$$

where \mathbf{E} is the electric field, m and e are electron mass and charge, T_0 is gas temperature and k is the Boltzmann constant. The average collision frequencies for momentum ν_m and energy transfer in elastic collisions ν_e are defined in [47] while ν_I is the ionization rate coefficients. The term Ω represents the average energy lost in one energy relaxation time ν_e^{-1} and is given in [47]. β is a parameter introduced to approximate the high order tensors in the energy flux equation in terms of lower moments [47].

In the system (4.21)-(4.24) the following assumptions are present:

1. $C_1 = n\nu_I$,
2. the momentum transfer approximation is employed [47] to evaluate collisional terms,
3. the pressure tensor is simplified to $\mathbf{P} = nk\mathbf{T} \approx \frac{2}{3}n\varepsilon\mathbf{I}$,
4. the temperature tensor is isotropic, and hence $\langle \mathbf{c}\mathbf{c} \rangle \approx \frac{\langle c^2 \rangle}{3} \mathbf{I}$
5. the higher order tensor $\langle c^2 \mathbf{c}\mathbf{c} \rangle$ appearing in the energy flux balance equation can be expressed by a product of the lower order moments as $\langle c^2 \mathbf{c}\mathbf{c} \rangle \approx \beta \langle c^2 \rangle \langle \mathbf{c}\mathbf{c} \rangle c^2 \frac{1}{3} \langle c^2 \rangle \approx \beta \frac{4}{3m^2} \varepsilon^2 \mathbf{I}$. β is a parametrization factor, generically close to unity, when the higher order correlation term $\langle c^2 \mathbf{c}\mathbf{c} \rangle - \langle c^2 \rangle \langle \mathbf{c}\mathbf{c} \rangle$ can be neglected [47, 131],
6. following original papers [47, 131], in this work β is considered to be equal to 1.

An alternative approach has been proposed by Becker *et al* [16].

4.3 The MC particle model

As a reference model we use a Particle-in-Cell Monte Carlo (PIC/MC) code. Because the motion of individual electrons is simulated with a particle code, it contains the full physics that is to be approximated by a fluid model. The successful comparison of a fluid model with such a particle model validates the fluid model; of course, the same cross-sections have to be used for both models.

The construction of a planar front is straight forward in fluid models, as the spatial derivatives are simply evaluated in one direction. However, in the particle model electrons move in all three spatial dimensions and hence, the three-dimensional setting has to be restricted as in previous work [107, 131].

4.4 Transport parameters

In this section we briefly discuss how the transport data for electrons are calculated and implemented in our fluid models of negative planar streamer fronts. The electron transport data employed in this work are calculated using a multiterm theory for solving the Boltzmann equation. The methods and techniques are by now standard and the readers are referred to [43, 234]. In particular, in the presence of nonconservative collisions there are two types of transport coefficients flux and bulk, and one has to take care that the correct quantity is used in any particular modeling situation (see section 2.3 for discussion).

Calculations of transport data at a temperature of 293 K are performed for reduced electric fields (E/n_0) ranging from $10^{-4} - 10^3$ Td. The first-order model is based on the local field approximation; it requires mobility, diffusion coefficient and ionization rate as a function of the reduced electric field E/n_0 (where n_0 is the gas number density). The second-order model is based on the local mean energy approximation and the transport data, including electron mobility, diffusion coefficient and ionization rate as well as rate coefficients for relevant processes are functions of the electron mean energy. The correspondence between the mean energy and E/n_0 is used to find the correspondence between the mean energy and other relevant transport data. The high-order fluid model requires average collision frequencies for momentum and energy transfer in elastic and inelastic collisions, and rate coefficients for all collision processes as a function of the mean electron energy. As for the second-order model, the correspondence between the mean energy and E/n_0 is used to find the correspondence between the mean energy and collision frequencies. The momentum transfer collision frequency has not been determined directly from the cross sections but rather from the following equation:

$$\nu_m = \frac{e}{m\mu(\varepsilon)}, \quad (4.25)$$

where e and m are the electron charge and mass, respectively, and $\mu(\varepsilon)$ is the electron mobility which is here a function of the mean energy. Since momentum transfer theory [47, 234] is used to determine the transfer of energy in the fluid equations, we use the following expression for the average energy loss in one energy

relaxation time ν_e^{-1} , through nonelastic processes [47, 234]

$$\Omega(\varepsilon) = \frac{m_0}{m + m_0} \sum_{\alpha} \frac{(\nu_{\alpha} - \nu_{\alpha}^{(s)})}{\nu_e} \epsilon_{\alpha} + \sum_i \frac{\nu_I^{(i)}}{\nu_e} \Delta \epsilon_I^{(i)}. \quad (4.26)$$

The inelastic channels α are governed by threshold energies ϵ_{α} and collision frequencies for inelastic and superelastic processes ν_{α} and $\nu_{\alpha}^{(s)}$, respectively. All collision frequencies (including the ionization collision frequencies $\nu_I^{(i)}$) are function of the electron mean energy. The collision frequency for energy transfer in elastic collisions ν_e is defined by Eq. (43) by Dujko *et al.* [47].

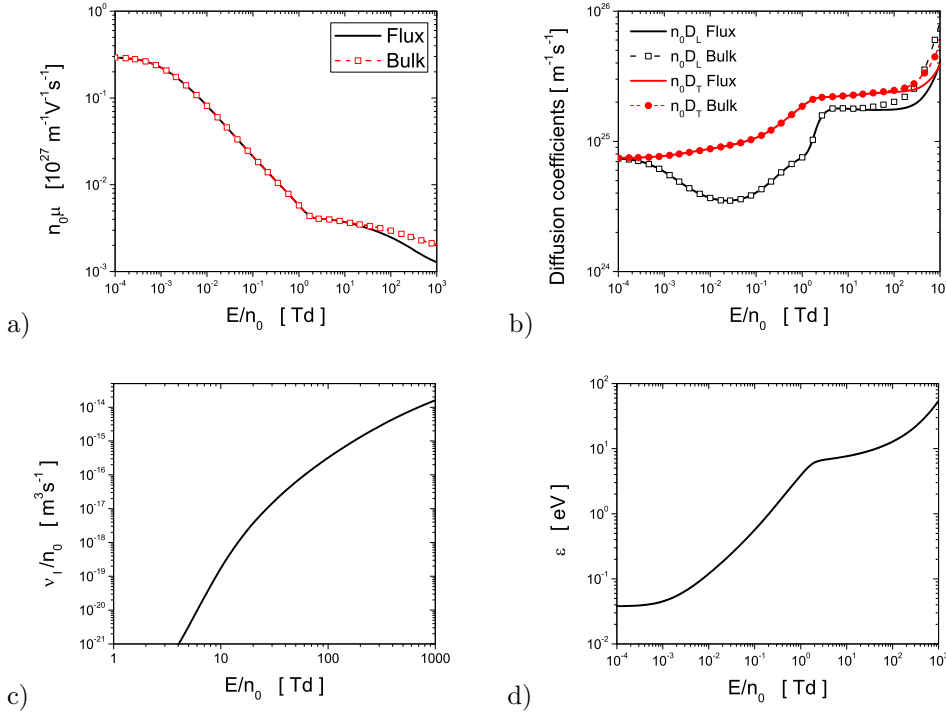


Figure 4.1: (a) Mobility, (b) longitudinal and transverse diffusion coefficient, and (c) ionization rate of electrons in Ne as a function of the reduced electric field E/n_0 , as an input for the first-order model. Shown are flux and bulk data obtained by our multi-term solution of the Boltzmann equation. Variation of the mean energy with E/n_0 is shown on panel (d).

Finally, the PIC/MC model requires a set of cross sections for electron scattering in Ne. This work considers negative planar streamer fronts in Ne using the cross section set of [77], which includes seven cross sections for electronic excitations and cross section for ionization as well as cross section for momentum transfer in elastic collisions. Transport data required as input in our various fluid

models are calculated using the same set of cross sections for electron scattering in Ne.

Figure 4.1(a) shows the electron mobility (multiplied by the gas number density) as a function of the reduced electric field E/n_0 . We observe that bulk and flux quantities start to differ visibly above a reduced field of approximately 10 Td, this means that the ionization processes start to be significant at this value of the field. As E/n_0 increases further, the effect becomes more pronounced, until the bulk mobility exceeds the flux mobility by approximately 40% at 1000 Td. From the E/n_0 -profiles of the diffusion coefficients (see figure 4.1(b)), however, we see that the diffusion coefficients are more sensitive to the explicit effects of ionization processes; the differences between bulk and flux data are higher than 50% for E/n_0 approaching 1000 Td.

Variation of the mean energy and ionization rate coefficient are shown on panels 4.1(c) and 4.1(d) respectively. We see that the ionization rate becomes significant at higher values of E/n_0 when sufficient electrons have enough energy to undergo ionization. From the profiles of the mean energy, we observe four distinct regions of transport as E/n_0 increases. First, there is an initial plateau region where the electron energy is thermal ($3kT/2 \approx 0.038$ eV). Second, there is a region of sharp rise as the electrons start to rapidly gain the energy from the electric field. Third, there is a second small plateau region due to large energy loss of the electrons as the inelastic channels become important. Finally, there is another region of rapid rise, as both the elastic and inelastic processes drop off with high energy, and the electrons start to rapidly gain energy from the strong electric field.

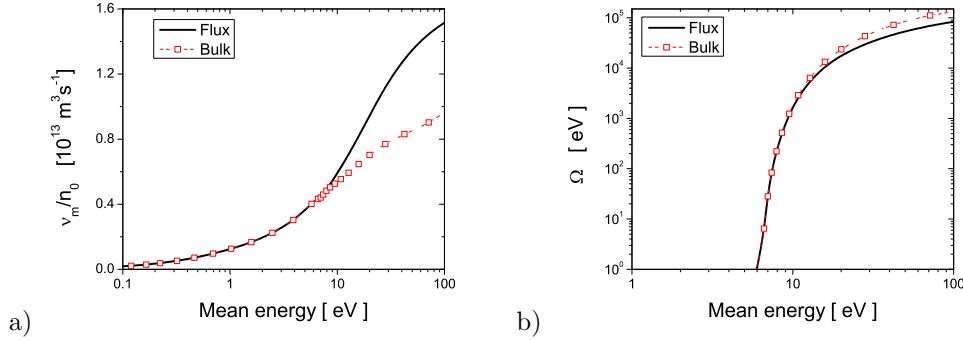


Figure 4.2: Density normalized average collision frequency for momentum transfer in elastic collisions ν_m (a) and the average energy lost in one energy relaxation time ν_e^{-1} , through nonelastic processes (b) as a function of the mean energy of electrons in Ne, as an input for the high-order model.

Figures 4.2(a) and (b) display the density normalized average collision frequencies for momentum transfer in elastic collisions and the average energy loss in one energy relaxation time ν_e^{-1} , through nonelastic processes, respectively. The differences between bulk and flux values of these two quantities are clearly evident

and follow from the differences of bulk and flux mobilities.

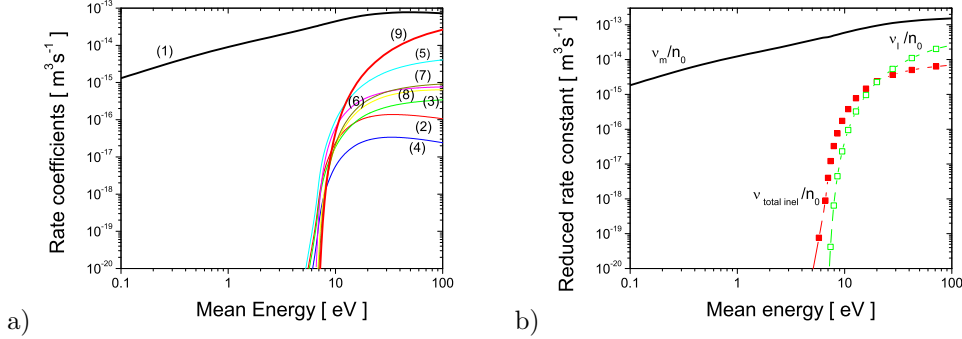


Figure 4.3: Rate coefficients (1-momentum transfer in elastic collisions, 2-8 electronic excitations and 9-ionization) in neon as a function of the electron energy, calculated with the multi-term solution of the Boltzmann equation and (b) density normalized momentum transfer rate, density normalized total inelastic rate and ionization rate.

Figure 4.3(a) shows the rate coefficients as a function of the mean electron energy for all collision processes. Figure 4.3(b) compares the density normalized average collision frequency for momentum transfer in elastic collisions, the density normalized total inelastic rate (sum of all rates for inelastic processes without ionization) and the ionization rate. The ionization rate is significant for relatively high mean energies (i.e. high E/n_0) and is essential for streamer modeling. From figure 4.3(b) we see that the ionization rate dominates the total inelastic rate for mean energies higher than 25 eV which reflects the energy dependence and magnitude of the cross sections for ionization and electronic excitation.

4.4.1 What to do when $n_e \rightarrow 0$?

In many plasma fluid models the transport coefficients depend on the mean energy. However, the models typically contain equations for the evolution of the energy density ($Q = n\varepsilon$). To get the mean energy at every point, we would like to simply compute

$$\varepsilon = Q/n. \quad (4.27)$$

Unfortunately, this simple expression leads to problems where n goes to zero, not only because one can not divide by zero numerically, but also because round-off errors get large. Therefore, we use the following regularization:

$$\varepsilon = \frac{Q + \eta_0 \varepsilon_f(E)}{n + \eta_0}, \quad (4.28)$$

where $\varepsilon_f(E)$ is the relaxed mean energy in an electric field of strength E , and η_0 is a small density. Using equation (4.28) instead of equation (4.27) makes no difference where $n \gg \eta_0$. But where $n \lesssim \eta_0$, using (4.28) ensures that the mean

energy is approximately relaxed to the background electric field. In simulations we use the value of η_0 to be 10^{-5} m^{-3} .

4.5 Simulation conditions

In this work we consider 1D geometry and we simulate negative planar fronts. All fluid models are simulated in noble gas Ne at standard temperature and pressure (STP). The electric field $\mathbf{E} = E\hat{e}_x$ (where \hat{e}_x is the unit vector in the x direction) drives the dynamics. We take E as a positive value; therefore electrons drift to the left, and negative streamer ionization fronts move to the left as well.

4.5.1 Boundary conditions

To create steady propagation conditions for the negative front, the electric field on the left boundary $x = 0$ is fixed to the time independent value E_0 :

$$E(0, t) = E_0 > 0. \quad (4.29)$$

The electric field for $x > 0$ is calculated by integrating equation (4.14) numerically over x , with (4.29) as a boundary condition. The right boundary is located at $x = L$; in all calculations we set the system length L to 1.8 mm and we use 1500 grid points.

As in case of N_2 from section 3.2.3, homogeneous Neumann boundary conditions are imposed for all conserved variables in all models for both ends of the system, so that all electron quantities may flow out of the system. Only for the electron density at $x = L$ we employ a homogeneous Dirichlet boundary condition to prevent electrons from diffusing out. However, all calculations end before the ionization reaches the boundary, that means, before the boundary conditions start to become relevant.

4.5.2 Initial conditions

We start all simulations with the same initial Gaussian distribution for electrons and ions

$$n(x)|_{t=0} = n_0 \exp \left[-\frac{(x - x_0)^2}{\sigma^2} \right], \quad (4.30)$$

where we have chosen $n_0 = 2 \times 10^{18} \text{ m}^{-3}$, $x_0 = 1.6 \text{ mm}$ and $\sigma = 2.94 \times 10^{-5} \text{ mm}$. The initial conditions for the average electron velocity, average electron energy and average electron energy flux are taken to be spatially homogeneous. These quantities are assumed to be relaxed to the background electric field when the simulation starts, with the values for the field given by a multi term solution of Boltzmann's equation, as already discussed in section 4.4.

4.5.3 Numerical method

The advective terms in LEA and LFA models are numerically discretised using the same upwind-based scheme with Koren flux limiter function [93] and the

diffusive terms are calculated with second-order central differences [83, 104]. The high order model is discretised using first-order upwind scheme. Although we use very fine grid consisting of 1500 points, the order of the numerical of the high order model is very low (first-order). Presently we are working on improvement of the accuracy. Several previous works have been devoted to the comparison of the accuracy of numerical schemes for advection problems in different situations (see e.g. [23, 194, 209, 235, 239]). The scope of present chapter does not cover the effects of the numerical schemes on a streamer properties (see section 4.7 for discussion).

4.5.4 Time stepping

For the time integration we used the classical fourth-order Runge-Kutta 4 (RK4) scheme [83]. With such an explicit time stepping method, there are typically at least three restrictions on Δt [12, 83, 138]:

$$\Delta t < C_a \Delta x / v \quad \text{CFL condition,} \quad (4.31)$$

$$\Delta t < C_d \Delta x^2 / D_e \quad \text{explicit diffusion limit,} \quad (4.32)$$

$$\Delta t < \varepsilon / (\mu_e n_e e) \quad \text{dielectric relaxation limit,} \quad (4.33)$$

where Δx is the spatial step size, D_e the diffusion coefficient, ε the permittivity, μ_e the electron mobility, n_e the electron density and e the elementary charge. C_a and C_d are the maximal Courant numbers for advection and diffusion equations [35]. Courant number depends on the particular time-integration method and space discretization. Unlike the first two conditions, the last conditions does not depend on the transport scheme used for the electrons.

The CFL time step restriction for the high order fluid model is given by the following formula

$$\Delta t \leq C_h \frac{2\Delta x}{\beta} \sqrt{\frac{3m}{2 \max \varepsilon}}, \quad (4.34)$$

where C_h is the maximal Courant number [131].

In this article we focus on the accuracy of the models, not on their computational efficiency. Therefore, we have simply used a very small constant time step of 0.5 ps for all models, satisfying all the above conditions.

4.6 Comparison results

In this section we compare the simulation results obtained with the fluid models and the PIC/MC model. As mentioned before, the simulations are performed in Ne at STP. We consider the following externally applied electric fields: 130, 170, 210, 350 and 460 Td.

Before we proceed to the actual comparisons, we would like to emphasize one more time that transport data derived from the same collisional cross-sections as used in the particle model have been used in all the tests presented in the next section.

4.6.1 Basic comparison of planar fronts in Ne

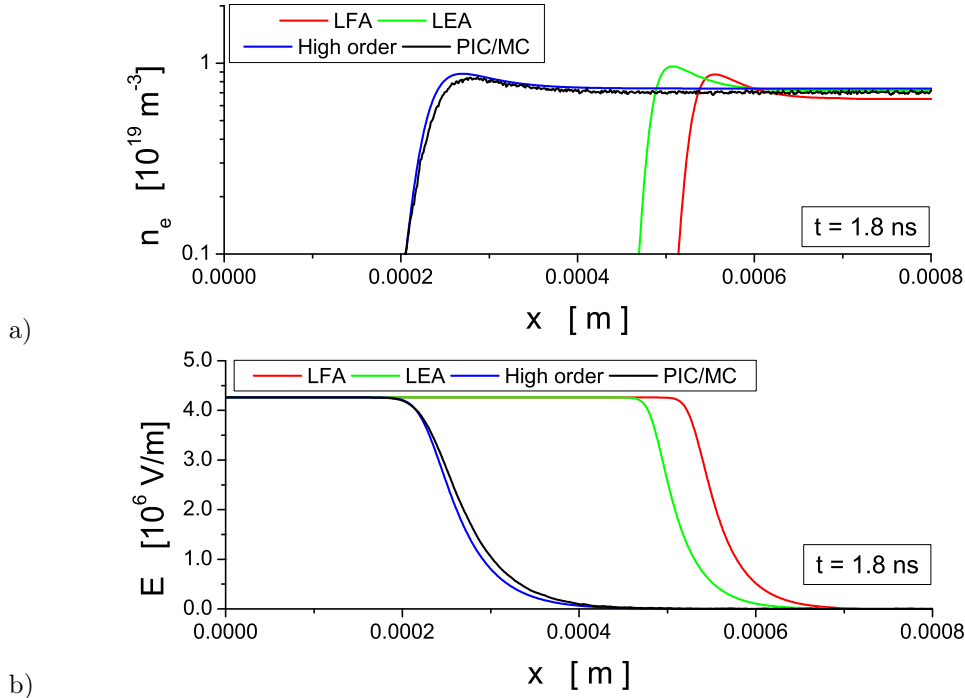


Figure 4.4: Electron density (a) and electric field (b) for all four models in Ne in an external electric field of 170 Td at time 1.8 ns.

Figure 4.4 shows the electron density and the electric field profiles in Ne for the LFA, LEA and high order model. As a reference model we include the PIC/MC profiles as well. The profiles are shown at 1.8 ns. The electric fields in all profiles preserve the classical shape of cathode directed ionization wave, with a high electric field at the front [87, 107, 131]. Due to space charge effects and the 1D configuration, the electric field inside of discharge channel is completely screened. The typical electron overshoot at the front of the discharge is present in all considered models.

The results of the high order fluid model are in good agreement with the PIC/MC results. The streamer head positions obtained by the LFA and LEA models deviate more from the PIC/MC results. This shortcoming of LFA has been reported by many authors [58, 87, 107, 110]. Li *et al* [110] have achieved relatively good agreement between PIC/MC and LFA by using a so-called ‘extended fluid model’. Our simulation results for the LFA and LEA models are in good agreement with the results by Eichwald *et al* [58], where a more sophisticated second order model was compared with LEA and LFA. Unfortunately, Eichwald *et al* did not compare their results with PIC/MC simulations.

Figure 4.5 shows the velocities of planar fronts as a function of the external re-

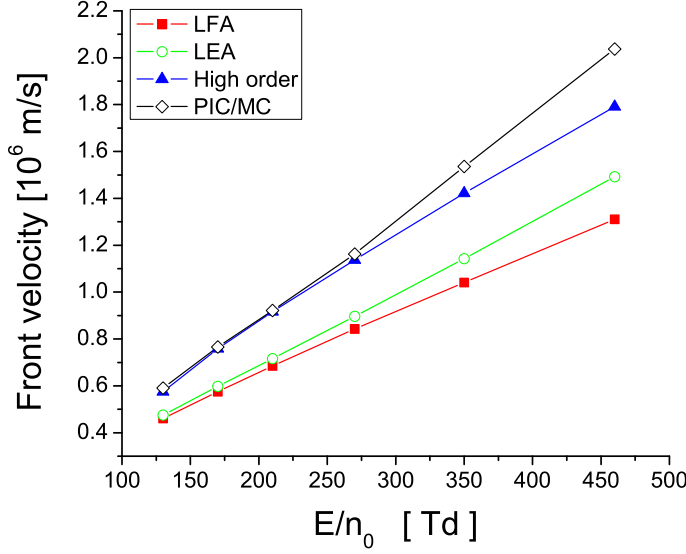


Figure 4.5: Velocities of planar fronts as a function of the electric field obtained with all the models in Ne. We remark that the negative sign of all velocities is removed here.

duced electric field for Ne. These velocities are calculated at the end of simulation time by following the time evolution of a certain level ($2 \cdot n_0$, see equation 4.30) of the electron density at the streamer front. All models show better agreement with PIC/MC for lower E/n_0 . Overall, the LFA and LEA models show the worst agreement with PIC/MC among the models considered. On the other hand, for higher values of reduced electric field, LEA shows better results than LFA. The results of the high order model agree quite well with PIC/MC. Figure 4.5 shows how one can improve the agreement of the results with PIC/MC by increasing the number of the moment equations (4.6) or, in other words, by increasing the complexity of the model. The LEA and LFA results deviate significantly for high E/n_0 . This improvement can be explained by the fact that the transport parameters used by the LEA model depend on the local average electron energy, while in the case of LFA they depend on the local electric field. We will continue this discussion in the next sections.

In the figure 4.6 we show the relative difference of the electron density in the streamer channel compared with PIC/MC as a function of E/n_0 . The LFA model overestimates the electron density by up to 18%. The high order model underestimates the electron density by up to 5%. The LEA model performs the best in predicting the electron density in the channel. This model underestimates the electron density by up to 6%.

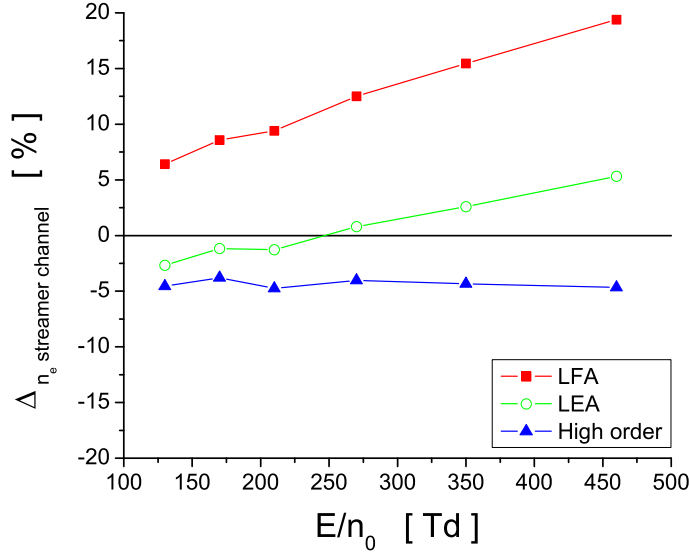


Figure 4.6: The relative differences of the electron densities in the channel of the negative planar fronts from all fluid models compared with PIC/MC as a function of reduced electric field in Ne.

4.6.2 Comparison of average electron energies in different models

In most applications it is crucial to correctly calculate the space resolved profiles of the average electron energies. LEA and high order fluid model can calculate such profiles as, unlike LFA, they contain an equation for the electron energy density. If we assume that in the LFA model the electron energy instantaneously relaxes to the electric field, we can calculate electron energies directly from the field. Figure 4.7 shows that this assumption is wrong. The profiles of average electron energies for the four models (LFA, LEA, high order and PIC/MC) are presented after 1.2 ns in Ne at 270 Td. We have also included the profiles of the electric field and the electron density obtained from the high order model to indicate the streamer head position. We have shifted all profiles and aligned them with the particle model for comparison.

We divide our discussion of the results in three parts, linked to spatial regions: the streamer head, where large gradients in the electron density and the electric field are present, the streamer channel, where the electric field is completely screened, and the region ahead of streamer head. We discuss all these regions separately.

Figure 4.7 shows that the energy profiles in streamer head agree very well between the PIC and the high order model. It is remarkable to note that in figure 4.7 the slope of the decay of the electron energies for the PIC/MC and high order model are identical. A similar observation is valid for the slopes of

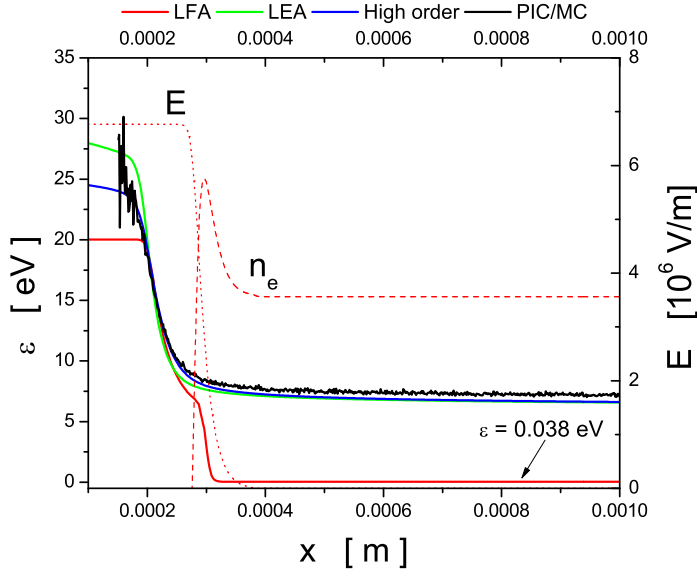


Figure 4.7: The average electron energy in four different models in Ne at time 1.2 ns. Profiles of the electric field and the electron number density from the high order fluid model are also included to indicate the location of the front. For clarity, all profiles are shifted and aligned with PIC/MC profile. Calculations are performed for E/n_0 of 270 Td.

the LFA and LEA model: both LEA and LFA are decaying at the same rate. This is a clear manifestation of the inconsistent assumptions on the flux terms in the electron balance and the average electron energy balance equations present in both LFA and LEA models. This region is the most sensitive region to the assumptions on the shape of electron energy distribution function (EEDF), like close to Maxwellian etc.. Hence, for the proper description of the features present in the streamer head the momentum and average energy flux balance equations should be consistently modelled.

The region ahead of streamer head is qualitatively well described by LEA model in the figure 4.7. Very good agreement is established between PIC/MC and high order model. The particle model suffers from a lack of electrons that creates stochastic noise. In all models, except in LFA, the average electron energy has a slope, which reflects the so-called non-local effects. This slope is present from a very early stage on as discussed in [107, 131].

The LFA model completely fails to describe the energy in the streamer channel. The reason is that in this region electric field is totally screened and hence LFA predicts the electron energy to take the thermal value 0.038 eV. This is unacceptable as in figure 4.7 the particle model predicts it to be around 7 eV. These high energy values are another manifestation of non-local effects. As the velocity of the front is higher than the electron drift velocity even in the streamer head

region, electrons slowly relax to lower energies in the lower or vanishing field in the streamer interior. This causes the spatial decay of average electron energy in the high-order fluid and PIC/MC models, that can be observed in figure 4.7. On the other hand, there is a very good agreement between predictions of the average electron energies of LEA, high order and PIC/MC. The small disagreement between high order and particles models in the channel is discussed in [131].

4.7 Discussion

In the previous section, we have compared three fluid models with Monte Carlo simulations. For all models we have used input data based on the same cross sections. Furthermore, we have used similar boundary conditions and the same initial conditions, grid resolution and time stepping. But is that enough to say that our conclusions are ‘final’? We do not think so. The present work should be considered as the average user’s (modeller’s) experience. The results in section 4.6 show the performance of the fluid models for streamer simulations using a specific implementation with specific simulations conditions.

Since fluid models of different order have different mathematical morphologies and as they are non-linearly coupled with the Poisson equation, the choice of or the sensitivity of results to numerical scheme, grid size, time step restriction, boundary conditions, spatial dimensions and dimensionality of space can affect overall results and corresponding conclusions. In higher dimensions (i.e. 2D or 3D) grid choice, i.e. structured or unstructured, or the presence of adaptive (or static) grid refinement will produce more and more uncertainties. In the case of adaptive grid refinement one should study the influence of the refinement criterion on the simulation results [219]. The choice of mesh adaptation can be also an issue [80, 81]. In higher dimensions the uncertainties associated with (complex) geometries and roughnesses of the interfaces are becoming very critical. It is very hard to predict how stable a certain model will behave under these more realistic conditions.

One more source of uncertainty are the transport coefficients. Small differences in cross-sections may produce large differences in plasma parameters [22]. The sensitivity of models to the differences in transport coefficients should be investigated.

The complexity of models depends on the considered number of moments of the Boltzmann equation. Or in other words, the more physics we put in a model, the more complex it becomes: the more equations should be solved, the more initial and boundary conditions should be specified, in general the more computational resources are required etc. One can conclude that with the increase of the complexity of the system the associated uncertainties are rising. In this case, it is up to the modeller to decide for a given type of discharge and under given conditions (geometries, parameter range, etc.) how complex a system to consider.

The integral part of any plasma simulation should be verification and validation (V&V) [158, 185]. Indeed, for just this purpose, there has recently been an

explicit call for ensuring the fidelity of future simulation tools [197, 221, 222]. In the field of radio frequency discharges some pioneering work is done by Surendra [217]. Turner *et al* [220] have developed benchmark solutions for capacitive discharges and showed that a number of independently developed particle-in-cell simulations can reproduce the benchmark solutions. In particular, the swarm literature contains many models suitable for benchmarking plasma models in the free-diffusion limit [43, 172, 192, 234].

Therefore, we believe that uncertainty quantification together with V&V should be the next step in the modelling of low-pressure plasmas. This techniques are successfully adopted by related fields such as computational fluid dynamics, computational finance, climate modelling, astrophysics etc. [18, 27, 38, 142, 157, 159].

4.8 Conclusions

We have compared the performance of three plasma fluid models: a first order model based on the local field approximation, a second order model based on the local energy approximation and a high order model. The test problems we considered were 1D ionization waves in neon, in a wide range of electric fields. As a reference model, we have used a Particle-in-Cell Monte Carlo code. Our comparisons show that the second order model describes the electron density and the average electron energy in streamer channel well, although it underestimates the streamer front velocity. The classical model is the simplest model considered. Despite the simplifying assumptions present in the model and the strong recommendations by Grubert *et al* [72] to use the second order instead of the first order model, we find that using the classical model gives reasonably good results. Of course, it can not calculate the electron energy, but if one is interested in general characteristics like velocity, ionization level or general shape of the discharge, this model can be the first choice. The high order fluid model is overall in closest agreement with the Particle-in-Cell Monte Carlo results.

CHAPTER 5

Investigation of positive streamers by double pulse experiments, effects of repetition rate and gas mixture

To avoid situations in which you might make mistakes may
be the biggest mistake of all.

– PETER MCWILLIAMS

Important thing in science is not so much to obtain new facts
as to discover new ways of thinking about them.

– SIR WILLIAM BRAGG

5.1 Introduction

It has been observed by multiple groups that streamer discharges are in many ways influenced by preceding discharges [154, 155, 161, 205]. From these and other studies, it is clear that species produced by such discharges play an important role in inception and propagation of streamers. In most cases it is assumed that the dominant effect of preceding discharges is the creation of (background) ionization. Immediately after a discharge (depending on composition and pressure) the background ionization consists primarily of free electrons and positive

This chapter is based on the publication [156] *Investigation of positive streamers by double pulse experiments, effects of repetition rate and gas mixtures* by Sander Nijdam, Eiichi Takahashi, Aram H. Markosyan, Ute Ebert published in *Plasma Sources Science and Technology*, Volume 23, Number 2, Page 025008, 2014.

ions. For longer timescales this generally changes to positive and negative ions due to electron attachment or recombination (again, depending on composition and pressure). When the positive and negative species are not distributed equally this will lead to space-charge which can also influence subsequent streamer discharges by its resulting electric field. Other species that can play a role besides charged species are radicals (e.g. N and O), metastables (e.g. $\text{N}_2(\text{A}^3\Sigma_u^+)$ and $\text{Ar}(4s)$) as well as other products like NO and OH.

One way of studying the effects of initial conditions on a streamer discharge is to create background ionization with an independent source like a laser [218], x-rays [134] or radioactive compounds [155]. This has the advantage that it decouples the production of ionization (and other important long-lived species) from the streamers.

Here, we will investigate the effects of a preceding streamer discharge on a subsequent discharge by applying two positive high voltage pulses in succession with pulse-to-pulse intervals (Δt) between 200 ns and 40 ms. This allows us to study the effect of the preceding discharge on a very large range of time scales. At low values of Δt the time scale is of similar order as the characteristic time of the total streamer development (and the duration of the applied pulse). Therefore we can also learn things about streamer development in general. Values of Δt around 100 μs to 1 ms correspond to repetitive streamer discharges with 1 to 10 kHz repetition frequency that are often used in commercial streamer and plasma-jet applications [101, 212, 236]. Finally, at $\Delta t \geq 10$ ms the discharges start to resemble the 'single pulse' discharges often used to study streamer development.

The advantage of applying two pulses instead of a continuous pulse train is that it is much easier to see the effects of a single pulse discharge on the next discharge and that it allows the huge range of Δt that was discussed above. It is experimentally extremely challenging to build a pulse source with a variable repetition frequency between 10 Hz and 50 MHz while maintaining the same pulse shape and amplitude. Creation of two identical pulses with variable interval is much easier.

Walsh *et al* [149, 230] have shown in experiments with atmospheric pressure plasma-jets in helium that, for jets extending beyond the guiding tube, the propagation can be temporarily halted by 'neutralizing' the applied voltage by applying the same voltage to two external electrodes surrounding the jet. This resembles the application of two consecutive pulses to a single electrode like in our experiments.

In this chapter we will discuss the following topics: in section 5.2 we give the details and parameters of our experiment and methods. Section 5.3 treats the general development of streamer discharges created with two pulses as function of the time gap Δt between pulses by means of ICCD imaging. This is done for three gases: artificial air, pure nitrogen and pure argon for various pressures and pulse widths and amplitudes. In section 5.4 we focus on the value of Δt for which we can still observe continuation of the first-pulse streamers during the second pulse and how this depends on gas conditions, most notably on the variation of

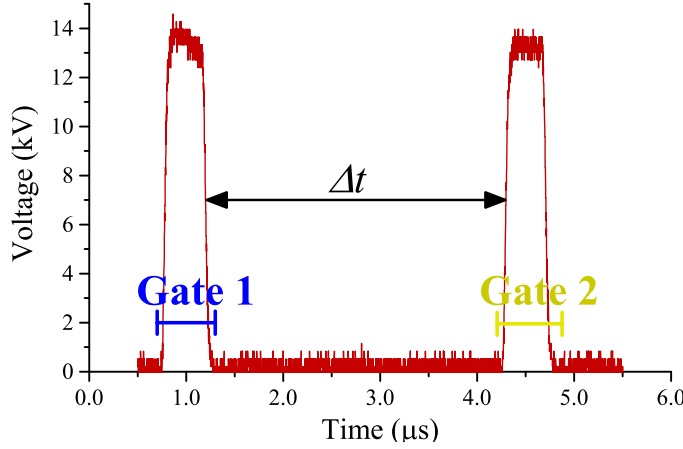


Figure 5.1: Typical shape of the two subsequent voltage pulses with the pulse-to-pulse interval Δt indicated. Indications of the opening (gate) times of the two different ICCD cameras are shown in blue and yellow respectively.

the oxygen concentration in nitrogen-oxygen mixtures. The experimental results are then compared to plasma-chemical modelling results in section 5.5. Finally we will summarize our results and draw conclusions in section 5.6.

5.2 Experimental setup by S. Nijdam and E. Takahashi

All experiments are performed in a 103 mm point-plane gap mounted inside a vacuum vessel. This vessel is filled with artificial air, pure nitrogen, pure argon and air-nitrogen mixtures at pressures between 67 and 533 mbar. When using pure nitrogen or argon, the vessel is flushed at a rate of roughly 1 standard litre per minute to improve gas purity in the experiments. The purity of all of the source gases is specified as 6.0 (less than 1 ppm impurities). However, because of leakage and/or out-gassing, we estimate the impurity level during experiments at about 5 ppm¹. On the pointed tungsten tip with a tip radius of 15 μm , a pair of positive voltage pulses is applied repeatedly. Such a pulse pair consists of two nearly identical pulses with pulse-to-pulse intervals (Δt) between 200 ns and 40 ms. The pulse pairs are applied with a repetition frequency of 0.7 Hz. The individual pulses that make up the pulse pairs are relatively rectangular shaped with pulse lengths of 200–700 ns, rise/fall times of about 15 ns and pulse amplitudes 7–17 kV. An example of such a pulse-pair is shown in figure 5.1, where the definition of Δt is indicated as well.

The streamer-discharges induced by the two voltage pulses are imaged by two separate, nearly-identical ICCD cameras. These cameras are mounted so that they image exactly the same plane, by means of a half-mirror (see figure 5.2).

¹Calculated by dividing the measured leak/out-gassing rate of $5 \cdot 10^{-6}$ standard litres per minute by the applied gas flow of 1 standard litre per minutes.

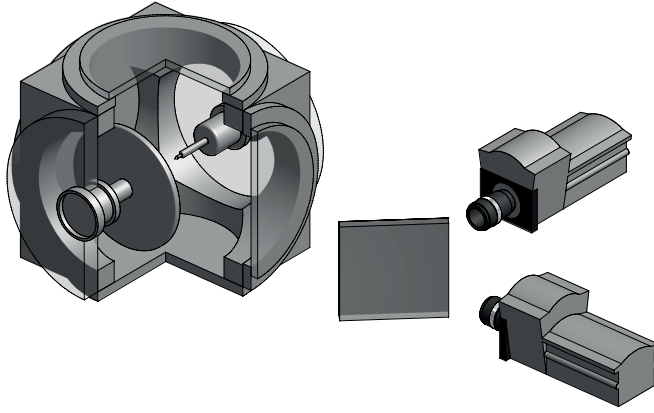


Figure 5.2: Schematic illustration of vacuum vessel, half-mirror and two ICCD-cameras. Part of the vacuum vessel has been cut from the rendering to show the tip and plate. In all presented images the recorded images are rotated anti-clockwise by 90° so that the electrode tip is shown on top.

During post-processing the images are rotated so that the electrode tip is always located at the top of the image. The gate of one camera is opened during the first voltage pulse; the gate of the other camera is opened during the second voltage pulse (see gate indications in figure 5.1).

A typical example of an image-pair produced by the two cameras is shown in figures 5.3a and b, where the images are acquired during the first and second pulse respectively. These two images are then laid over each other as a new image where the blue channel (component) of the RGB-pixels represents the first pulse image and the red and green channels represent the second pulse image. A pixel with the red and green channels equally bright and the blue channel off will appear yellow, while a pixel with all three channels fully illuminated will appear white. Therefore areas that only emit during the first pulse are blue, areas that only emit during the second pulse are yellow and areas that emit during both pulses are white. All linear combinations of yellow and blue are possible. The result of this operation on figures 5.3a and b is shown in figure 5.3c.

In the example from figure 5.3a-c it is clear that the (blue) streamer channels created by the first pulse continue their path (in yellow) during the second pulse. The area around the electrode tip, as well as some areas on the edge of the inception cloud emit again during the second pulse (and are therefore coloured white).

Figure 5.3d shows a superimposed image with both cameras gated around the first pulse (under different conditions than in figure 5.3a-c). They should therefore get exactly the same image. This shows that the two cameras are aligned properly as almost all lines are white and only a slight yellow/blue offset is visible.

Note that in all images the intensities of both cameras are chosen arbitrarily.

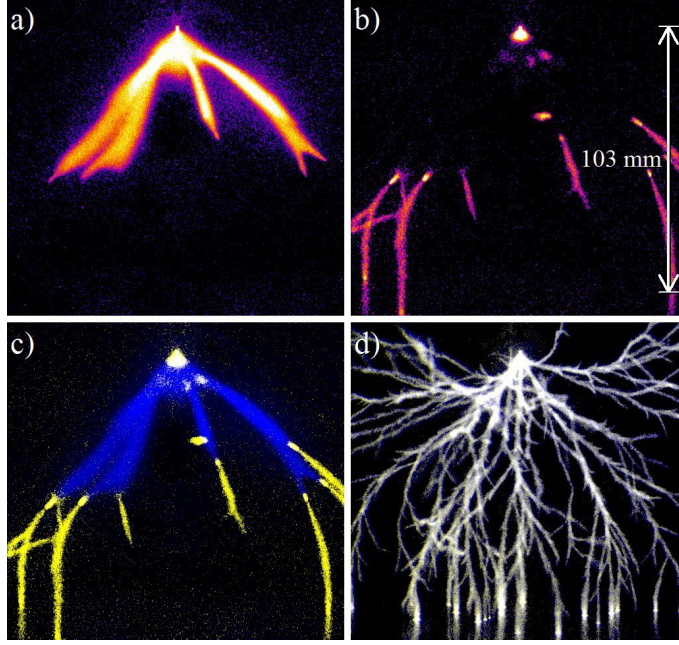


Figure 5.3: Illustration of the two-camera overlay technique. a) and b) show false-colour representations of the captured frames from camera 1 and 2 respectively, recorded during one voltage pulse pair (conditions: 6.8 % O_2 in N_2 , 133 mbar gas, 13.6 kV, 200 ns pulses with $\Delta t = 500$ ns) . In c) the images from a) and b) are superimposed in blue and yellow respectively. d) shows a similar overlay of a discharge under different conditions, with both camera gate times set at the first pulse only (conditions: pure N_2 , 133 mbar gas, 13.6 kV, 400 ns pulse).

The same intensity on the image does not imply that the original streamers have the same intensity. This was done for several reasons: Firstly the two cameras are slightly different and do not have the same gain factors. Secondly there was a half-mirror between the vessel and the cameras which has different losses for transmission and reflection and finally because the streamer morphology is best imaged with the maximum contrast per image. For these reasons we have used automatic contrast and brightness algorithms to process the final output images. This may also explain the slight blue tint in figure 5.3d.

In all cases, observations are performed on two-dimensional images of the three-dimensional discharge structures. Therefore it is not always possible to draw conclusions on the exact relation between first and second discharge from one image. To do this properly one would need a stereoscopic set-up [152] to observe the full three-dimensional relation between the paired images. Nevertheless, observation of multiple images under the same conditions can give good insight in the morphology and the relation between the paired discharges. All observations discussed in this chapter are based upon multiple images per parameter setting (usually 10 images), but only a limited subset of these images is presented here.

5.3 General development

We have studied the morphology of the discharge induced by the voltage pulse pairs as function of pulse-to-pulse interval (Δt) for a variety of gases, pressures and voltage pulse lengths and amplitudes. In general the development during the second pulse as function of Δt is similar for all conditions, although there are variations in details. We will first discuss the full development for one set of conditions in air. Next we will look into the effects of pulse length, voltage and pressure on this development. Finally we will look at pure nitrogen and pure argon.

5.3.1 Air

An example of the development of the discharges during the two pulses in 133 mbar air with relatively short pulses and a large variation in Δt is given in figure 5.4. The discharges generated by the first pulse are, except for stochastic variations, similar for all values of Δt . These first-pulse discharges consist of a so-called inception cloud that breaks up into a few (typically five or six) streamer channels which mostly terminate either at the moment the first pulse is stopped or when the (bottom) cathode plate has been reached. In the conditions from figure 5.4 the pulse duration has been chosen so that the streamers terminate roughly halfway between electrode tip and cathode plate.

We can describe the development of the discharge during the second pulse as function of Δt for the conditions of 5.4 with the following six stages:

- (i) At very short pulse-to-pulse intervals ($\Delta t < 700$ ns), the second-pulse streamers continue where the first-pulse streamers stopped at the end of the first pulse. At the new starting point a structure resembling a small scale in-

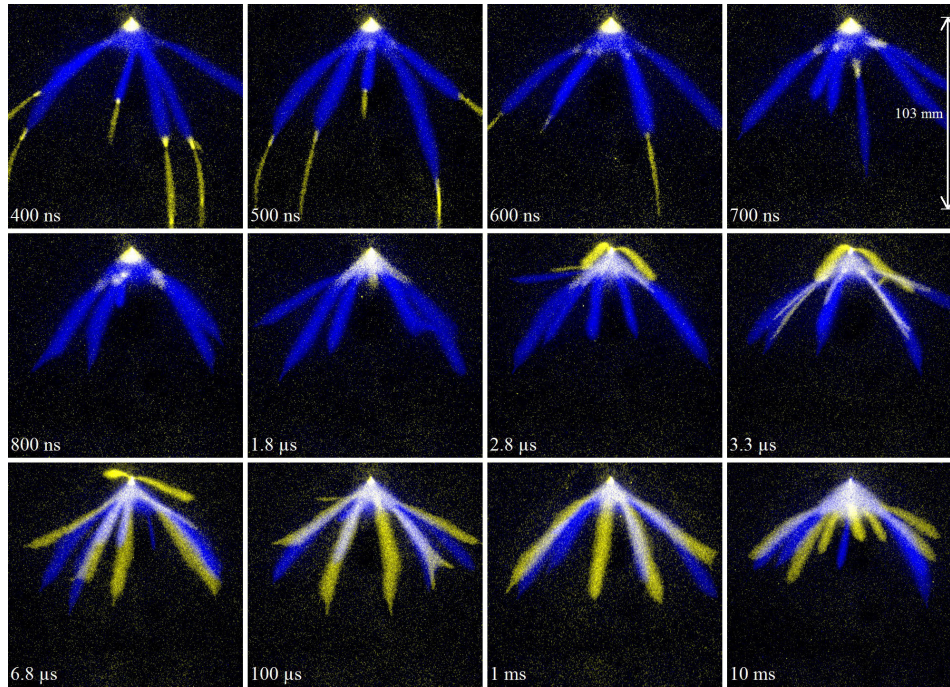


Figure 5.4: Superimposed discharge-pair images for varying Δt (as indicated in the images). Images taken in 133 mbar artificial air with pulses of 13.6 kV amplitude and 200 ns pulse length.

ception cloud is visible. The extended streamer channels become shorter, thinner and fewer for increasing Δt .

Furthermore, the regions around the tip and the positions where the first streamers originally emerged from the inception cloud both emit light again, as can be seen from their white colour.

- (ii) At $\Delta t \geq 700$ ns the continuation channels are no longer continued during the second pulse. Instead the re-glowing points at the edge of the inception cloud become more pronounced and eventually (at $\Delta t = 1.8$ μ s) grow together with the emitting region around the tip.
- (iii) At $\Delta t \geq 2.5$ μ s the first new streamer channels start to appear. These channels avoid the entire old inception cloud region and move around it.
- (iv) At $\Delta t = 3.3$ μ s more new channels appear. These new channels seem to follow the edges of the old channels. They are clearly thinner than both the old channels and the other new channels that avoid the inception cloud. Note that at $\Delta t = 1.8$ μ s a few short channels with similar morphology are also visible. Analysis of a large number of images at these conditions has shown a preference for the bottom side (with respect to the orientation of the presented images) of the old streamer channels.
- (v) At larger values of Δt the new channels increase in width until they have roughly the same width as the original channels around $\Delta t = 5.8$ μ s and start to overlap more with the parent channels. For increasing Δt they also start to become less dependent on the location of the first-pulse streamers. However, up to $\Delta t = 1.0$ ms a large number of the second-pulse streamers still follows the first-pulse streamers, although not always exactly. Under these conditions the inception cloud during the second pulse is significantly smaller than during the first pulse.
- (vi) Around $\Delta t = 10$ ms the second discharge has become fully independent of the first discharge. The inception cloud sizes as well as the thickness and position distributions of the streamers are now the same for the two pulses. Furthermore, the position of the streamers during the second pulse no longer shows a correlation with the positions during the first pulse.

Note that these six stages cannot always be distinguished exactly and that the exact transition between stages is often difficult to pinpoint.

Interpretation The structures that are visible in stage (i) resemble the findings of Walsh *et al.* [230] where atmospheric pressure plasma-jets in helium also continue their path after the applied external field was suppressed for a short period. We will discuss the stage (i) streamer continuation and its interpretation in depth in sections 5.4 and 5.5.2.

The re-emission of light from some regions during stages (i) to (iv) is probably similar to a secondary streamer. A more detailed investigation has revealed that during the second pulse the re-glowing of the points around the tip and the original

inception cloud occurs early in the pulse, while the continuation of the old channels starts from about 50 to 100 ns after the pulse start. Note that it is very likely that parts of the old channels that do not re-emit during the second pulse still carry (dark) current. Because their conductivity is still high no high fields can exist and current will not produce any light. For larger Δt the conductivity decreases and therefore the secondary streamers become more pronounced.

The new channels avoiding the old ones that appear in stage (iii) appear similar to the streamer morphology treated in [154], where new streamers avoid the pre-ionized area generated by a previous discharge. Similar behaviour was found by Briels *et al.* [24] where long voltage pulses were applied to a point plane gap in ambient air and so-called late streamers are visible that avoid the area occupied by earlier streamers. In both these cases as well as in the results presented here the new streamers move around the area that was pre-ionized by the preceding streamers or inception cloud. This is probably caused by the high conductivity in this area which will quickly shield any electric field and therefore inhibit the formation of an ionization front. The position of the new channels at the edge of the old ones in stage (iv) seems to be related to this: the inside of the old channels is still too highly ionized for discharge propagation but the edges have an ionization density which is preferable for streamer propagation. The preference for the bottom side of the channels may be due to the higher background field in this region (closer proximity to the cathode plane). Alternatively, as was proposed by Mark Kushner at the GEC 2013, the outer regions of the old channels may contain higher concentrations of O_2^- and may therefore be more attractive for streamer propagation. In stage (v) the new channels can slowly penetrate the area of the old channels due to the decrease in conductivity.

Longer pulses When longer (400 ns) voltage pulses instead of 200 ns pulses are applied the development of the second-pulse streamer as function of Δt is very similar (see figure 5.5). The only differences are related to the fact that the first-pulse streamers have already crossed the gap. Therefore the occurrence of channel-continuation for small values of Δt (stage (i)) is rare as this only occurs on the few branches that did not cross the channel during the first pulse. However, the branches that did cross show something else: during the second voltage pulse the cathode-spots (the ‘feet’ of the channels) from the first discharge light up again. This effects lasts to about $\Delta t = 1 \mu s$. Furthermore, re-glowing of the spots at the edge of the original inception cloud is more pronounced with these longer pulses and the new channels start to occur for smaller values of Δt than with the shorter pulse (compare at $\Delta t = 2.6 \mu s$ from figure 5.5 to at $\Delta t = 2.8 \mu s$ from figure 5.4).

When changing voltage and pressure, the effects on the first and second pulse morphologies are in general predictable (see figure 5.6): at higher voltages more and thicker streamers occur while at higher pressures fewer and thinner streamers occur. Furthermore, the different stages of development occur at lower values of Δt for higher pressures and vice-versa. More details on the effects of parameter settings on streamer continuation will be given in section 5.4.

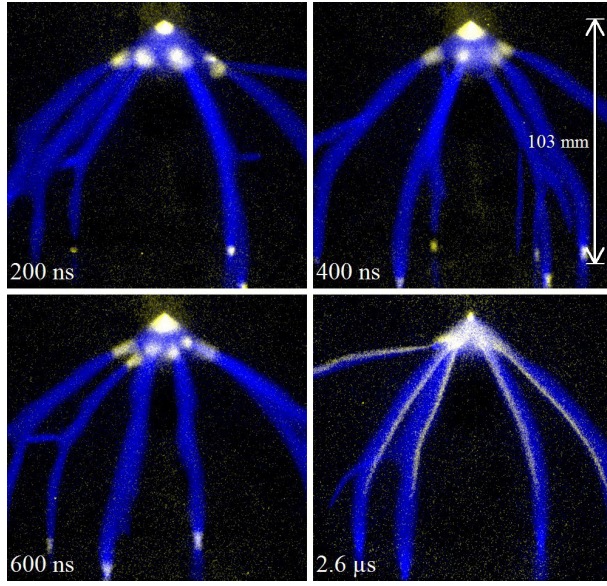


Figure 5.5: Superimposed discharge-pair images for varying values of Δt . Images taken in 133 mbar artificial air with pulses of 13.6 kV amplitude and 400 ns length.

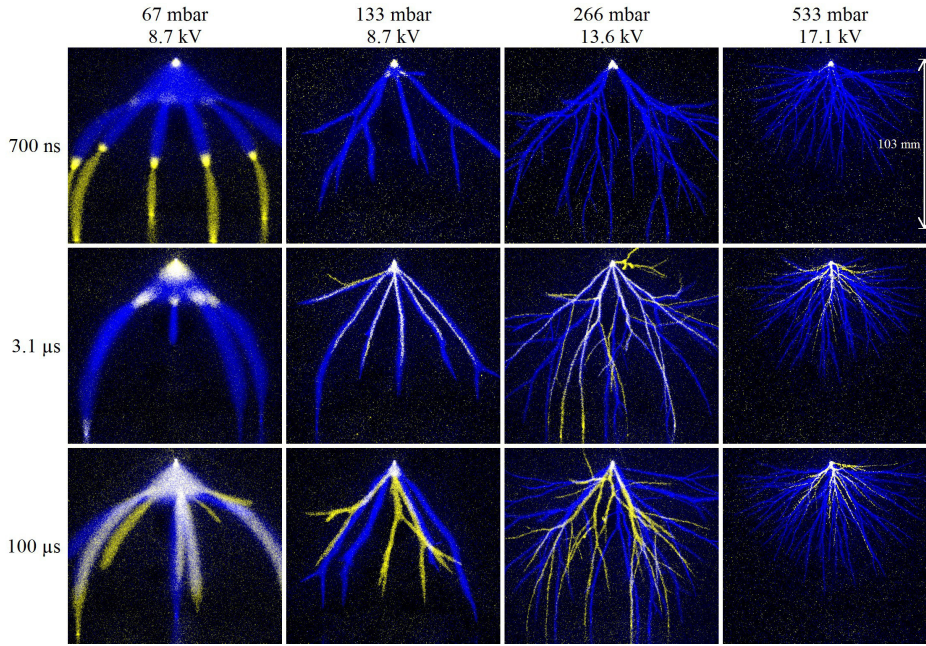


Figure 5.6: Superimposed discharge-pair images for varying values of Δt (indicated on the left), pressure and voltage pulse amplitude (indicated on top). Images taken in artificial air with pulses of 400 ns length.

5.3.2 Pure nitrogen

The same measurements as treated above on air have also been performed on pure nitrogen. As was mentioned before, the expected purity in pure nitrogen is about 5 ppm. This purity is less than in previous work [153] but still ensures an oxygen concentration that is four to five orders of magnitude lower than in air.

A selection of measurement results obtained in pure nitrogen is given in figure 5.7. In general, the behaviour of double-pulse streamers in nitrogen is very similar to that in air although there are also some notable differences:

- As usual, streamers in nitrogen are thinner and branch more than streamers in air.
- The inception cloud in nitrogen is much smaller than in air, therefore at pressures above 100 mbar it is not possible to distinguish the spots on the edge of the inception cloud.
- The maximum value of Δt for which streamer continuation still occurs (stage (i)) is about 1.5 to 2 times higher than in air. More details will be given in section 5.4.
- The value of Δt at which new channels start to occur (stages (iii) and (iv)) is much longer in pure nitrogen than in air. For the case of 133 mbar, 8.7 kV, 400 ns new channels (following the side of the old ones, stage (iv)) become clearly present around $\Delta t = 3 \mu\text{s}$ in air while in pure nitrogen this only starts to occur around $\Delta t = 30 \mu\text{s}$.
- Even at very high values of Δt (10 ms and above) many second-pulse streamers still follow the rough paths of first-pulse streamers (stage (v)). In air this only occurs up to $\Delta t = 1 \text{ ms}$ and in general is less obvious. At $\Delta t = 40 \text{ ms}$ in nitrogen the second discharge seems independent of the first.

One thing not shown in figure 5.7, but very obvious in the total set of measurement images is the large variation from pulse-pair to pulse-pair in pure nitrogen: the value of Δt at which a certain phenomenon occurs can vary by about a factor 2 between pulse-pairs while in air the behaviour was much more stable. This makes a quantitative study of these phenomena in nitrogen more difficult than in air. Nevertheless it is still possible to see the trends of streamer morphology as function of time, but quantitative measurements of properties can easily have error margins of 20 % or more.

5.3.3 Pure argon

A third gas we have investigated next to artificial air and pure nitrogen is argon. The expected purity of argon is identical to that of nitrogen. Because streamer discharges in argon can easily lead to the occurrence of a spark, the applied voltages and pulse durations were limited and the lowest pressure used was 133 mbar. This prevents a spark that can potentially damage the electrodes as well as the intensifier in the ICCD cameras.

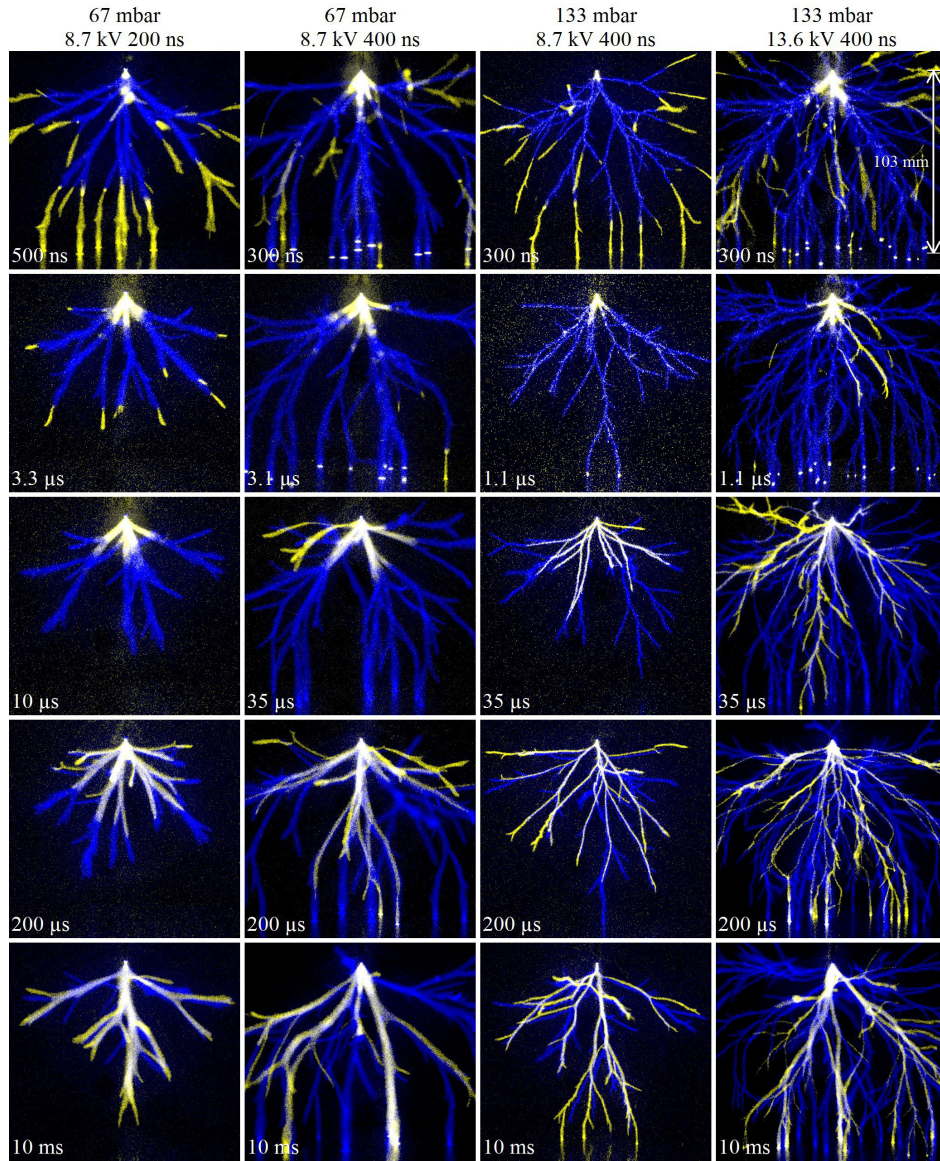


Figure 5.7: Superimposed discharge-pair images for varying values of Δt (indicated on the images), pressure and voltage pulse amplitude and length (indicated on top). Images taken in pure nitrogen.

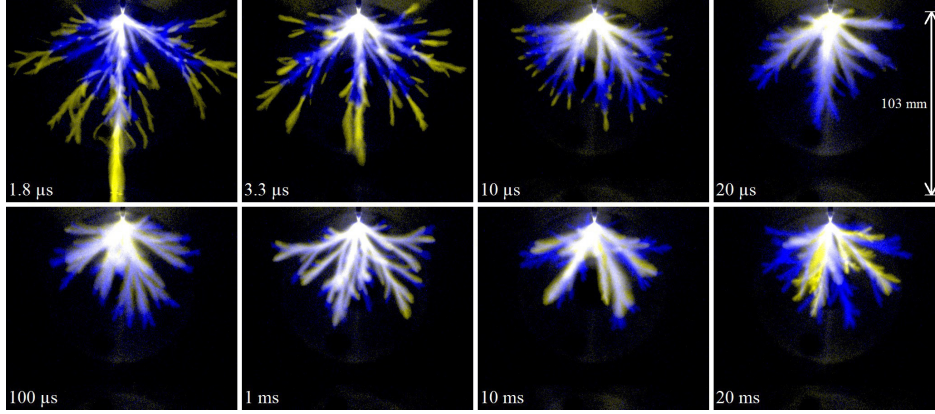


Figure 5.8: Superimposed discharge-pair images for varying values of Δt (as indicated in the images). Images taken in 133 mbar pure argon with pulses of 8.7 kV amplitude and 200 ns length.

An overview of double-pulse discharges in 133 mbar argon with a pulse of 8.7 kV amplitude and 200 ns length is given in figure 5.8. The double-pulse discharges in argon have many similarities with discharges in air and nitrogen; however there are again some notable differences:

- The continuation of first-pulse streamers during the second pulse (stage (i)) takes much longer. While in air and nitrogen the maximum value of Δt for continuation under similar conditions is less than 2 μs , in argon it is about 15 μs . A more detailed comparison will be given in section 5.4.
- The decay of excited argon-levels is slower than the decay of the dominant emitting channels in nitrogen (partly due to energy-pooling by metastables). Therefore the old channels keep emitting light, even when no second pulse is given. This means that for lower values of Δt it is impossible to distinguish between light from the still emitting excited species created during the first pulse and newly excited species created during the second pulse. This (partly) explains the large white sections in the centre of the discharge for $\Delta t \lesssim 100 \mu\text{s}$.
- At values of Δt between 100 μs and 1 ms the second-pulse streamer channels seem to follow the old channels like in nitrogen and air (stages (iv) and (v)). However, the large number of channels makes it difficult to tell whether they exactly follow the old paths or, like in nitrogen and air, hug the edges of the old paths.
- The first-pulse discharges show a very feather-like morphology, as is always visible in argon under similar conditions [153, 218]. However, up to $\Delta t = 10 \text{ ms}$ the second-pulse streamers (except for the continuing first-pulse streamers) are very smooth. This fits well with previous work on the effects of pre-ionization on pure argon and nitrogen streamer morphology [155, 218].

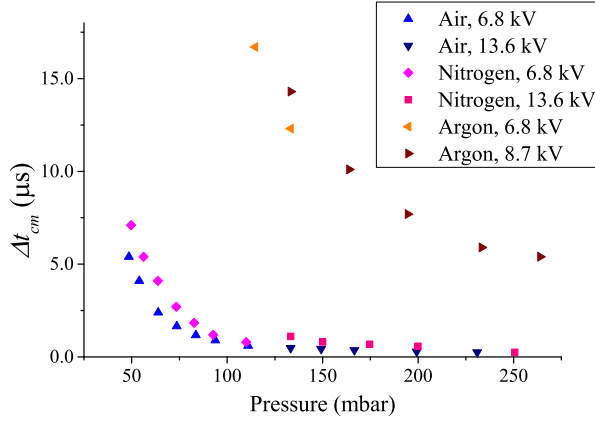


Figure 5.9: Maximum pulse-to-pulse interval for which continuation still occurs (Δt_{cm}) in artificial air, pure nitrogen and pure argon as function of gas pressure for different pulse voltages as indicated. All measurements were performed with a pulse length of 300 ns.

- Between $\Delta t = 100 \mu\text{s}$ and $\Delta t = 1 \text{ ms}$ the second-pulse channels get more narrow, however, between $\Delta t = 1 \text{ ms}$ and $\Delta t = 10 \text{ ms}$ they become wider again. The first effect can probably be attributed to a decrease in background-ionization levels inside the channel, while the second effect may be explained by diffusion of the remaining (low levels) of background ionization.

5.4 Duration of streamer continuation

In a more quantitative study of the important time-scales in our experiment, we have measured the maximum value of Δt , for which the continuation of streamers is still observed, or, in other words, the value of Δt determining the border between stages (i) and (ii). We label this quantity Δt_{cm} . It was measured as function of pressure for all gases involved and as function of oxygen concentration in nitrogen-oxygen mixtures at a fixed pressure. Because the continuation does not stop instantly at a certain Δt , Δt_{cm} is defined as the value of Δt for which in 50% of the images some form of continuation is visible.

Similar parameters for the occurrence of other phenomena as function of Δt have also been considered, most notably the time when the first new streamers start to occur. However, the jitter of these phenomena (that happen for larger Δt) can be as large as a factor of ten, especially in pure nitrogen. This makes it nearly impossible to make a coherent data set of such phenomena.

Measured values of Δt_{cm} as function of pressure for three different gases are plotted in figure 5.9. It was not possible to measure Δt_{cm} over the entire pressure range with the same voltage pulse amplitude, at lower pressures a too high voltage pulse would lead to streamers that cross the gap during the first pulse and therefore no continuation would be visible. A too low voltage pulse at higher

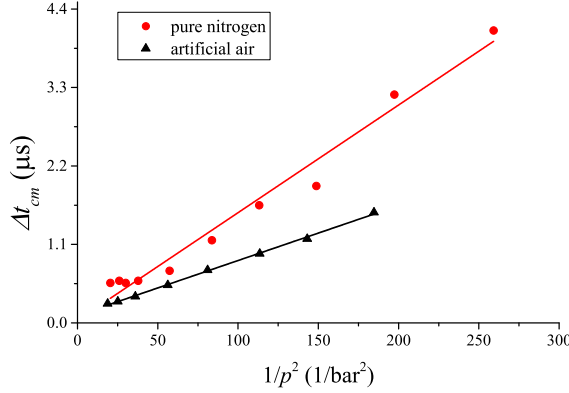


Figure 5.10: Δt_{cm} in artificial air and nitrogen as function of $1/p^2$ with V_{max}/p kept constant at 77.7 and 74.5 V/mbar for nitrogen and air respectively. The voltage pulse length was kept at 200 ns for both gases. For both gases a linear fit is included.

pressures would lead to no or very short and thin streamers where continuation is difficult to see. Therefore the applied voltage pulse was varied over the pressure range, as indicated in the figure.

As could already be concluded from the images shown in the previous section, Δt_{cm} is much larger for argon than for nitrogen or artificial air.

In order to avoid the effects of changing the reduced electric field too much (E/n) we have also measured Δt_{cm} in artificial air and pure nitrogen as function of pressure while varying the applied voltage V_{max} so that V_{max}/p remains constant. We assume constant temperature so that n scales with p according to the ideal gas law. Note that this does not imply that everything scales perfectly with V_{max}/p but just that the total streamer length² remains roughly constant and that streamer inception is ensured. In this way it is possible to measure Δt_{cm} over a large pressure range without the need for abrupt changes in applied voltage.

Unsurprisingly, in the measurements presented in figure 5.9 Δt_{cm} increases with decreasing pressure for all three gases. The most obvious cause of the stopping of streamer continuation is a decrease in streamer channel conductivity by various electron loss processes. Many of the rate-limiting reactions involved in the electron loss processes are three particle reactions (involving an electron or an ion and two neutral particles) they scale with $1/n^2$, so we can expect that Δt_{cm} also scales with $1/n^2$ with n the neutral density. Therefore we have plotted Δt_{cm} in artificial air and nitrogen as function of $1/p^2$ in figure 5.10. In section 5.5.2 we will treat the relevant electron loss reactions in more detail.

As was expected we can observe a linear relation between Δt_{cm} and $1/p^2$, although the fitted lines do not exactly cross zero. Unfortunately, because of the

²Streamer length depends here on streamer velocity and pulse duration. Because streamer velocity scales with E/n , the streamer length remains roughly constant for a given pulse duration when V_{max}/p is kept constant.

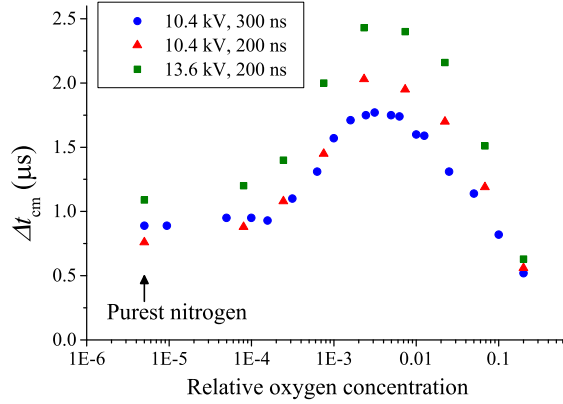


Figure 5.11: Δt_{cm} as function of oxygen concentration for different oxygen-nitrogen mixtures. All measurements were performed at 133 mbar with the pulse amplitudes and durations as indicated. The points drawn at 5 ppm oxygen concentration are actually measured in pure nitrogen gas (within experimental limitations).

tendency of argon discharges to form a spark, only a limited pressure range could be explored and it was not possible to measure Δt_{cm} for constant V_{max}/p .

5.4.1 Oxygen concentration effects

Figures 5.9 and 5.10 show that although Δt_{cm} is larger for nitrogen than for artificial air, the difference is relatively small, especially in comparison with argon. However, if the value of Δt_{cm} would only be influenced by electron attachment to molecular oxygen, we would expect an increase of Δt_{cm} of at least a few orders of magnitude between air and pure nitrogen. To investigate this in more detail, we have measured and plotted Δt_{cm} as function of oxygen concentration. This was done by starting with artificial air and then repeatedly replacing 50 to 70 % of the gas in the vessel with pure nitrogen, always returning to the starting pressure to measure Δt_{cm} . The results of this procedure are plotted in figure 5.11.

We observe that when we decrease the oxygen concentration of artificial air at 133 mbar by mixing in more and more pure nitrogen, Δt_{cm} increases as expected. However, this effect reaches a maximum at an oxygen concentration of about 0.2 %. For lower oxygen concentrations Δt_{cm} decreases again and stabilizes around 0.01 % oxygen. A similar effect has also been found in other streamer measurements: Ono and Oda [160] observed a maximum in time-integrated discharge current for oxygen concentrations (in nitrogen) around 0.2–1.0 %, not far from the maximum found here although they measured at 1000 mbar instead of our 133 mbar.

Note that although we have calculated from the leak-rate that the amount of impurities in our purest nitrogen is less than 5 ppm, we cannot be entirely sure. It is possible that leaks or impurities in our gas-handling system lead to higher impurity levels. This would mean that the leftmost points in figure 5.11 shift to

the right and the plateau below 0.01 % oxygen could be an artefact of our set-up.

5.5 Modelling

The development of the discharge during the second pulse depends on density and distribution of various species (electrons, ions, metastables, etc.) left over from the first-pulse discharge. If we fix a computational cell inside of the discharge, neglect drift and diffusion of the species and follow only the temporal dynamics, we can apply zero-dimensional modelling to study the left overs of the first-pulse discharge. By varying the N₂:O₂ ratio we can simulate experimental results from sections 5.3.1 and 5.3.2.

5.5.1 Model description

A zero-dimensional model is used to describe the dynamics of species

$$\frac{d[n_i]}{dt} = S_i, \quad (5.1)$$

where the source term S_i is the total rate of production or destruction of the species i in various processes; it depends on the local electric field. A modification of the kinetic file for N₂-O₂ mixtures from ZDPlasKin [62, 163] is used that consists of 650 reactions (listed in the supplementary data) and of the 53 species and states listed in table 6.1. The plasma chemical processes in N₂-O₂ mixtures are mainly taken from [28]. Constant rates for electron-neutral interactions are calculated using the BOLSIG+ solver that is contained in the package [74]. The list of species and reactions was automatically converted into the system of ordinary differential equations (5.1) and solved numerically using the ZDPlasKin tool. The QtPlasKin visualization software was used for the analysis of the results [122].

In order to run ZDPlasKin, the calculation of the electric field has to be brought into the structure of equation (5.1), but the field profile should also be consistent with the local electron density. We have solved this problem by 1. neglecting the leading edge of the ionization front, and by 2. using the conservation of the total current.

$$\nabla \cdot (\varepsilon_0 \partial_t E + j) = 0, \quad (5.2)$$

where j is the electric current; in our case it is $j = -e j_e$ with

$$j_e = -\mu(|E|) E n_e, \quad (5.3)$$

where e , $\mu(|E|)$ and n_e are the charge, electron mobility in N₂ and density of electrons, respectively. Electron mobilities are obtained from [44, 47], where the multi term solution of Boltzmann's equation was used. If we approximate the weakly curved front by a planar front [55] and the electric field in the non-ionised region does not change in time, i.e. in zero-dimensional configuration, we get

$$\frac{dE}{dt} = \frac{\varepsilon_0}{e} \mu(|E|) E n_e. \quad (5.4)$$

Table 5.1: *Species considered in the model*

Ground neutrals
N, N ₂ , O, O ₂ , O ₃
NO, NO ₂ , NO ₃
N ₂ O, N ₂ O ₅
Positive ions
N ⁺ , N ₂ ⁺ , N ₃ ⁺ , N ₄ ⁺
O ⁺ , O ₂ ⁺ , O ₄ ⁺
NO ⁺ , N ₂ O ⁺ , NO ₂ ⁺ , O ₂ ⁺ N ₂
Excited neutrals
N ₂ (A ³ Σ _u ⁺ , B ³ Π _g , C ³ Π _u , a' ¹ Σ _u ⁻)
N(² D, ² P), O(¹ D, ¹ S)
O ₂ (a ¹ Δ _g , b ¹ Σ _g ⁺ , 4.5 eV)
O ₂ (X ³ , <i>v</i> = 1 - 4), N ₂ (X ¹ , <i>v</i> = 1 - 8)
Negative ions
e, O ⁻ , O ₂ ⁻ , O ₃ ⁻ , O ₄ ⁻
NO ⁻ , NO ₂ ⁻ , NO ₃ ⁻ , N ₂ ⁻ O

As said above, we neglect the leading edge of the front and start integrating at the maximum of the electric field. As [146] reviews, the maximal electric fields in simulated positive streamers in STP air vary between 120 and 180 kV/cm, so we use 150 kV/cm. This scales to $E(0) = 20$ kV/cm at 133 mbar according to the similarity laws that approximate the fast processes in streamer heads very well. We assume the electron density at the maximal electric field to be $n_e(0) = 7.1 \cdot 10^{11} \text{ cm}^{-3}$. We initialise the densities of the positive ions N₂⁺ and O₂⁺ such that the plasma is neutral $n_e(0) = n_{\text{N}_2^+}(0) + n_{\text{O}_2^+}(0)$. while keeping the initial ratio $n_{\text{N}_2^+}(0) : n_{\text{O}_2^+}(0) = \text{N}_2:\text{O}_2$. The initial densities of all other ions, excited species and ground neutrals (except N₂ and O₂) are assumed to be zero.

This approximation allows us to integrate equations (5.1) and (5.4) together in the form required by ZDPlasKin, and to get a decay of the electric field that is consistent with the local conductivity. We integrate the equations until the electric field reaches 0.67 kV/cm which is the so-called stability field for positive streamers in air at 133 mbar. We remark that though we have recently criticized this concept in [128], our simulations still show that the average electric field inside a streamer tree reaches such a value. When the stability field is reached, we continue to integrate equation (5.1), but now in a constant electric field of 0.67 kV/cm until the end of the voltage pulse, and then in a vanishing field.

5.5.2 Modelling results on streamer continuation

The modelled development of n_e as function of time for artificial air, 0.2 % oxygen in nitrogen and pure nitrogen at 133 mbar is given in figure 5.12. In this figure also

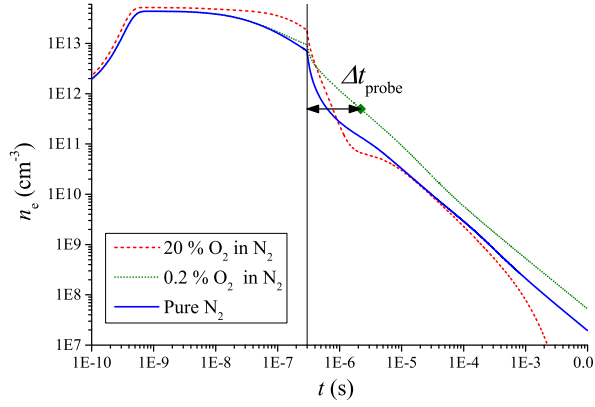


Figure 5.12: Modelled development of electron density as function of time for three different gas mixtures at 133 mbar. Pulse duration: 300 ns, initial electron density: $7.1 \cdot 10^{11} \text{ cm}^{-3}$, maximum electric field on streamer tip: 20 kV/cm, field in streamer channel: 0.67 kV/cm. The end of the pulse is indicated with the vertical line and the quantity Δt_{probe} is indicated for the 0.2 % oxygen mixture with a probing density of $5 \cdot 10^{11} \text{ cm}^{-3}$.

the quantity Δt_{probe} is indicated (for the 0.2 % oxygen mixture). This quantity represents the time between the end of the pulse (the moment the field goes to zero) and the moment a certain probe electron density has been reached. We assume that the conductivity of the channel depends only on electron density and that a certain critical conductivity is required for the streamers to continue their old path during the second pulse. Therefore we can find this critical density by comparing different Δt_{probe} results with the measured Δt_{cm} values. This is done in figure 5.13. The shape of the Δt_{cm} and Δt_{probe} curves are remarkably similar: both rise quickly from artificial air towards decreasing oxygen content, have a maximum around 0.2 % oxygen, decrease for even lower oxygen concentrations and then level off again around 100 ppm oxygen. This indicates that the measured curves are no artefact of the measurement method, but can be explained by plasma chemical processes. The modelling results shown for 0.1 ppm oxygen concentration are virtually identical to results in pure nitrogen.

Note that except for the chosen electron density probing values, no fitting parameters were used in the model. Therefore, even this relatively simple, zero-dimensional model with rate coefficients that can still have large uncertainties is able to predict the shape of Δt_{cm} . Only at oxygen concentrations below 100 ppm we observe that the model results are always below the measured results. From the comparison of the model and measurement results we can conclude that the electron density required for continuation of old streamer paths is around $5 \cdot 10^{11} \text{ cm}^{-3}$ under the conditions presented here.

The reason for the shape of the Δt_{probe} and Δt_{cm} curves can be understood by studying the various electron loss mechanisms. In figure 5.14 the cumulative electron losses by the eight most important electron loss reactions up to the moment that $n_e = 5 \cdot 10^{11} \text{ cm}^{-3}$ are plotted as function of oxygen concentration. In this

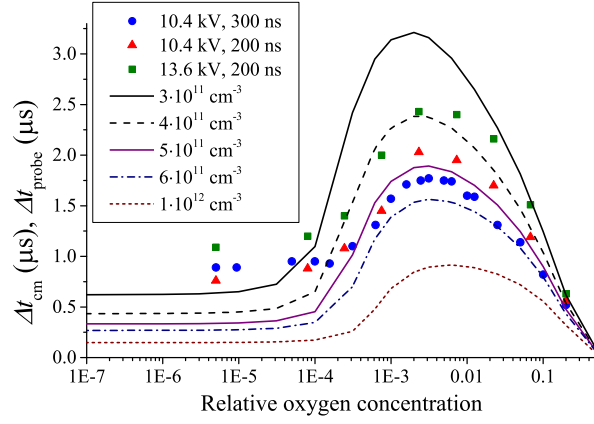


Figure 5.13: Measured data from figure 5.11 combined with modelling results of Δt_{probe} with varying probe electron densities as indicated in the legend for the conditions from figure 5.12.

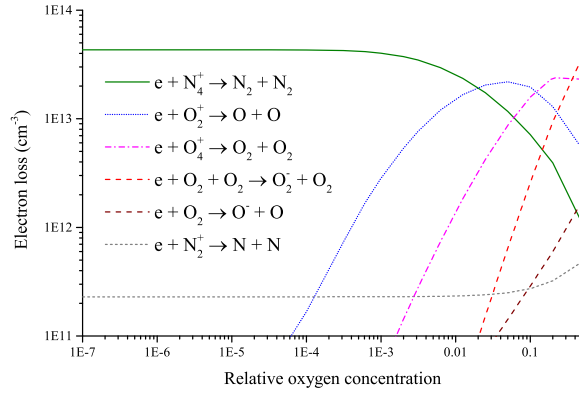


Figure 5.14: Modelled cumulative electron losses by the eight dominant electron loss processes as function of oxygen concentration for the conditions from figure 5.12. Losses are integrated over time between the start of the simulation and the moment n_e reaches a probing value of $5 \cdot 10^{11} \text{ cm}^{-3}$.

figure the dissociative attachment reactions with N_2^+ and O_2^+ leading to ground state atoms are grouped with similar reactions leading to $O(^1D)$ and $N(^2D)$ states although they are calculated separately in the actual model.

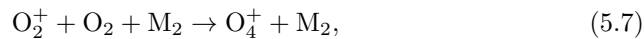
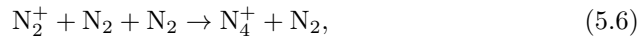
The figure shows that at low oxygen concentrations (below about 2 %) the electron loss is dominated by dissociative recombination with N_4^+ , while above an oxygen concentration of about 100 ppm also other reactions play a significant role. At high oxygen concentrations the electron loss is dominated by electron attachment to molecular oxygen and by dissociative recombination with O_4^+ . All these three processes are relatively fast and thereby can explain the fast decrease in conductivity at high and low oxygen concentrations. However, at intermediate oxygen concentrations, a significant part of the electrons (the major part between 2 and 12 % oxygen) are lost through dissociative recombination with O_2^+ , which is a much slower process than the dominant reactions at high and low oxygen concentrations.

In air, the main pathway of positive ions is as follows:



as described by Aleksandrov and Bazelyan [3] and also found in our model results. In this case the electron loss is dominated by the fast dissociative recombination with O_4^+ as was discussed above. At high nitrogen and oxygen concentrations this total pathway including recombination is very fast. At low oxygen concentrations the pathway stops at N_4^+ , which also recombines rapidly with free electrons. However, at intermediate oxygen concentrations there is enough oxygen to form O_2^+ but not enough to form reasonable quantities of O_4^+ . As, at 133 mbar, the recombination rate of electrons with O_2^+ is much lower than with O_4^+ , the total recombination rate is lower at these intermediate concentrations, which is exactly what we observe in our Δt_{cm} measurements. This is supported by the modelled development of the major ionic species as is plotted in figure 5.15.

As was shown in section 5.4, when V_{max}/p is kept constant we observe an almost linear relation between Δt_{cm} and $1/p^2$. This was attributed to three body processes responsible for the electron loss. This is not immediately obvious from the list of dominant reactions in figure 5.14 where the attachment of electrons to molecular oxygen is the only three body reaction. However, also the creation of N_4^+ and O_4^+ requires three body reactions. The dominant production reactions for these species are:



with M either O or N. Therefore it is not surprising that Δt_{cm} scales approximately with $1/p^2$.

However, if we look at the calculated values of Δt_{probe} plotted in figure 5.16, there is no perfect linear relation between Δt_{probe} and $1/p^2$. This may be caused by the constant electric fields that were applied in the model and that lead to lower than proportional Δt_{probe} for increasing $1/p^2$. This can also be observed

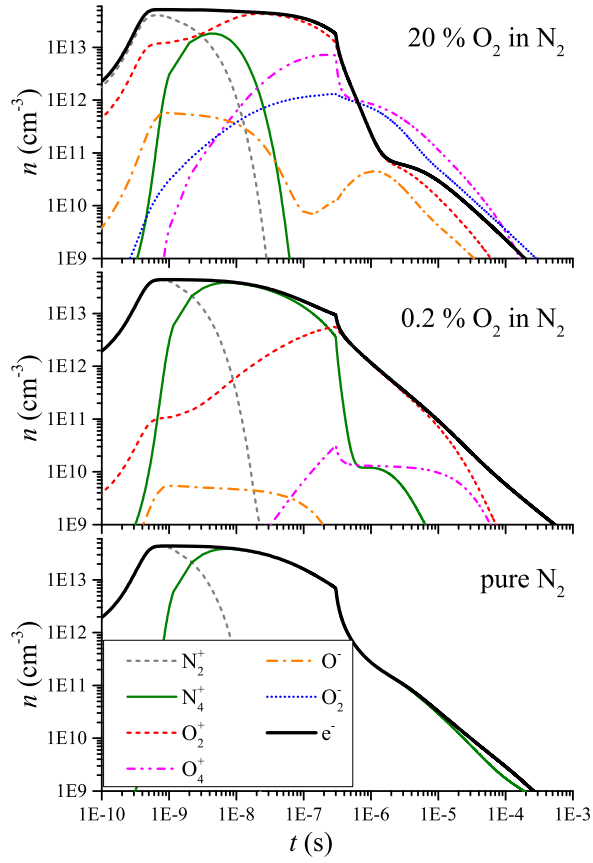


Figure 5.15: Modelled development of the densities of the major ionic species and the electrons in three different gas mixtures for the conditions indicated in figure 5.12.

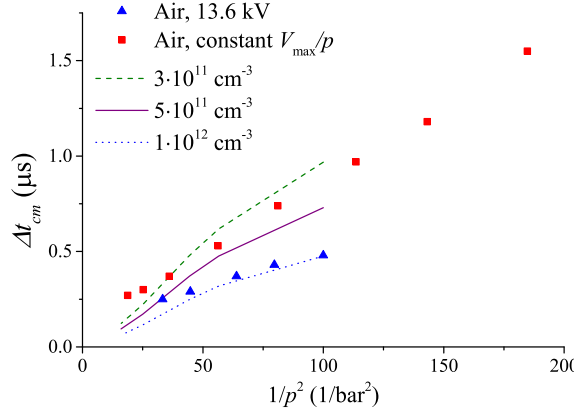


Figure 5.16: Measured Δt_{cm} as function of $1/p^2$ in artificial air with 13.6 kV, 300 ns pulses (triangles), Δt_{cm} at constant V_{max}/p (squares, same data as plotted in figure 5.10) compared with modelling results with 250 ns pulse lengths for different probe electron densities.

from the accompanying measurement results at fixed applied voltage (triangles in the figure). Unfortunately, the model did not converge for pressures below 100 mbar.

5.5.3 Other modelling results

The experiments have shown that in 133 mbar artificial air or pure nitrogen, new streamers start to occur around $\Delta t \approx 2.5 \mu\text{s}$ and $\Delta t \approx 35 \mu\text{s}$ respectively. From the modelled development of n_e (see figure 5.12) we cannot fully understand these timescales: there is no probing value of n_e that gives such a difference in Δt_{probe} . In general the values of Δt_{probe} for artificial air and pure nitrogen are quite similar for any n_e for probing times below a few hundred microseconds. When looking at the total ionization density as function of time (e.g. the sum of electrons and all negative ions) the results get further away from the observation: the ionization degree is higher in air than in nitrogen at any time after the pulse. This is because in air the electrons attached to oxygen have to be added to the electron density which increases it significantly. Therefore we can conclude that the occurrence of new streamers cannot be directly linked to either electron or ionization density.

In section 5.3.2 we observed that in pure nitrogen streamers can follow the path of their predecessors even at $\Delta t \geq 10 \text{ ms}$ while in artificial air this is only observed up to $\Delta t \approx 1 \text{ ms}$ and even then this occurs much less often. This fits well with the modelled n_e development which in air starts to drop much quicker than in nitrogen after about $t = 100 \mu\text{s}$. This also holds for the total ionization degree, which, although (in air) is higher than the electron density, it shows the same trend and drops below the one for nitrogen at about 1.3 ms.

All mentioned numbers are for a pressure of 133 mbar and room temperature. Of course electrons will also be lost through (ambipolar) diffusion, which will start

to play a role around millisecond timescales and is not incorporated in our model.

5.6 Summary and conclusions

5.6.1 Continuation of old paths

In this work we have shown that the application of two consecutive pulses is a valuable tool to improve our understanding of streamer discharges and the interaction between repetitive discharges. We have found that it is possible to "reignite" a streamer with a second high voltage pulse so that it continues its old path. This is only possible for relatively short durations ($\Delta t \leq \Delta t_{\text{cm}}$) after the first pulse. The measured values of Δt_{cm} are between 0.5 and 15 μs at 133 mbar depending on the gas mixture. In nitrogen-oxygen mixtures we have observed that Δt_{cm} exhibits a maximum around 0.2 % oxygen in nitrogen. For lower and higher oxygen concentrations Δt_{cm} decreases. When modelling the decrease of electron density after a streamer discharge we find the same pattern. For probe electron densities around $5 \cdot 10^{11} \text{ cm}^{-3}$ the decay times fit very well with our measurements. Therefore we conclude that the maximum in Δt_{cm} , and the continuation of old paths in general, can be explained by a loss of conductivity in the streamer channel due to the loss of free electrons and that, under our conditions, the minimum n_e for continuation is about $5 \cdot 10^{11} \text{ cm}^{-3}$ at 133 mbar.

The reason that there is a maximum in Δt_{cm} , which means a minimum in total electron loss rate, is that at these oxygen concentrations the major loss process is recombination with O_2^+ , while at lower/higher oxygen concentrations the electron loss is dominated by recombination with N_4^+ and O_4^+ respectively, combined with attachment at high oxygen concentrations. These three processes are all faster than recombination with O_2^+ which explains the maximum in Δt_{cm} .

Höft *et al* [79] have found an increase in discharge decay time when changing the oxygen concentration in nitrogen from 20 % to 0.1 % in a pulsed atmospheric pressure dielectric barrier discharge. This is in line with our observations. Figure 5.17 shows that the development of n_e at atmospheric pressure follows a similar general trend as observed at lower pressures: n_e decays fastest for artificial air, is slower for lower oxygen concentrations, but is again somewhat faster for pure nitrogen. However, the difference between air and pure nitrogen is much larger than at lower pressures due to the much faster three body attachment at atmospheric pressure. Also the maximum in Δt_{probe} for probe densities below $1 \cdot 10^{12} \text{ cm}^{-3}$ now occurs at 0.01 % oxygen, instead of 0.2 % as was found at 133 mbar³. Höft *et al* conclude that the decay time increases with decreasing oxygen concentration, and our observations generalize their findings at atmospheric pressure and oxygen concentrations above 0.01 %. According to our modelling, an extension of these measurements to higher purity nitrogen should show a maximum in decay time and a decrease when going to very pure nitrogen.

It is probable that this mechanism can also explain the maximum in integrated current density (and light emission) found by Ono and Oda [160] at oxygen

³We have calculated the development of n_e at atmospheric pressure for only five oxygen concentrations so the real maximum can be higher or lower than 0.01 % oxygen.

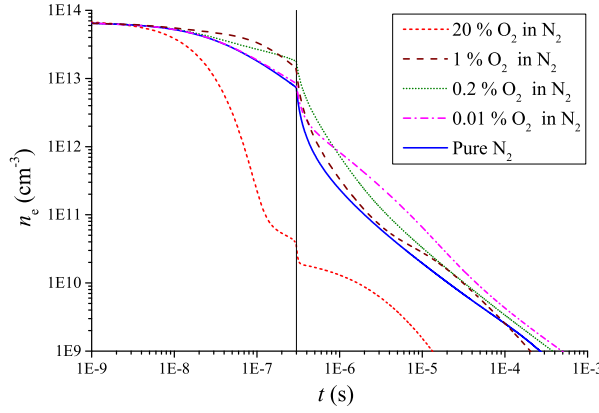


Figure 5.17: Modelled development of electron density as function of time for five different gas mixtures at 1000 mbar. Pulse duration: 300 ns, initial electron density: $7.1 \cdot 10^{11} \text{ cm}^{-3}$, maximum electric field on streamer tip: 20 kV/cm, field in streamer channel: 0.67 kV/cm. The end of the pulse is indicated with the vertical line.

concentrations around 0.2–1.0 % in atmospheric pressure point-plane discharges. They explain the increase of current when adding small amounts of oxygen to pure nitrogen by the increased streamer diameter and photo-ionization. Too much oxygen would lead to electron attachment and therefore reduces the current. This is in line with our modelling results, although it disregards the effects of recombination with O_4^+ . The increase in current with small oxygen additions also matches our modelling results at atmospheric pressure (figure 5.17) which shows the highest electron density during the pulse ($t < 300 \text{ ns}$) for oxygen concentrations of 0.2 and 1 %.

Walsh *et al* [149, 230] also presented a similar continuation phenomenon in atmospheric pressure plasma-jets in helium but did not discuss the maximum continuation time as it was limited by the applied voltage pulse length.

5.6.2 Other phenomena

Besides the continuation of streamers for short pulse-to-pulse intervals, we have observed a few other interesting phenomena at longer pulse-to-pulse intervals. When the interval is long enough to prevent streamer continuation (i.e., the conductivity has dropped enough), the remaining ionization still prevents new streamers to occur. We attribute this to the too high ionization degree which, though too low for continuation, is still high enough to shield the electrode tip and prevent streamer formation. During this period we only observe some re-glowing or secondary streamers in the area of the first discharge, especially the edge between inception cloud and streamers as well as the cathode spots for the cases where the first streamers have crossed the gap.

After some time (pulse-pulse intervals of a few to some tens of microseconds, corresponding to electron densities of $10^{10} - 10^{11} \text{ cm}^{-3}$ at 133 mbar) new streamers

start to occur. The first of these still avoid the entire area occupied by the first-pulse discharge. For slightly larger values of Δt the new streamers penetrate the area of the first-pulse discharge. These new streamers are much thinner than the first-pulse streamers and follow the outside of the paths of the original channels. This is similar to the streamers observed in [154] that also follow the edge of a pre-ionized region. Apparently the streamers cannot enter the area of high leftover ionization of the old channel because they cannot enhance the field there but preferentially follow the intermediate ionization levels present at the edge of these channels.

For still larger values of Δt (tens to hundreds of microseconds corresponding to electron densities of $10^9 - 10^{10} \text{ cm}^{-3}$ at 133 mbar) the new streamers grow in size and start to overlap more with the first-pulse channels. Finally, at even larger values of Δt (electron densities below 10^8 cm^{-3} at 133 mbar) they become fully independent of the first-pulse channels. This transition is very gradual and in most cases some second-pulse channels still follow a first-pulse channel while others do not. In nitrogen the following of first-pulse streamers occurs much longer than in artificial air. This is caused by the faster loss of electrons in air by electron attachment which, at longer timescales, dominates over recombination as it scales with n_e instead of with $n_e n_+$.

All these later-stage phenomena can be explained by the same two mechanisms: streamers prefer and follow elevated levels of background ionization but cannot propagate through areas with too high background ionization.

CHAPTER 6

PumpKin: A tool to find principal pathways in plasma chemical models

Machines take me by surprise with great frequency.

– ALAN TURING

If I have seen further it is by standing on the shoulders of
giants.

– ISAAC NEWTON

6.1 Introduction

Complex chemical models are increasingly demanded by many fields of science. Thanks to the availability of cheap computing power, scientists routinely use models composed of hundreds, if not thousands, of interacting chemical species. Many of these models have a direct relevance for our society’s most pressing problems; for example the chemical modeling of the atmosphere plays a significant role in the study of global climatic change [26]. Another example is provided by combustion, where a better understanding of the chemical interactions would lead to better and more efficient fuel use [223].

The demand for complex chemical models is also growing within the plasma physics community. This tendency arises from the recent development of plasma

This chapter is based on the preprint *PumpKin: A tool to find principal pathways in plasma chemical models* by Aram H. Markosyan, Alejandro Luque, Francisco J. Gordillo Vázquez, Ute Ebert, revised for *Computer Physics Communications*.

applications involving complex chemical processes, as well as a growing interest in the role of atmospheric electricity on the global chemical balance of our atmosphere [8, 68, 69, 166, 204].

The early work by Kossyi et al published in 1992 [95] can be considered as one of the very first attempts to build a complex kinetic scheme (of about 450 reactions) to study the non-equilibrium plasma kinetics during electric discharges in synthetic air ($\text{N}_2\text{-O}_2$ mixtures). In the last 20 years, the employed kinetic schemes have gained in complexity due to the new challenges posed to the scientific community.

For instance, complex kinetic schemes were proposed [41, 65] to understand the plasma remediation (through DBD discharges) of SO_2 and N_xO_y (mainly NO and NO_2) resulting from combustion of coal fired electrical power plants and mobile emission sources such as diesel trucks and cars. In addition, the identification of key pathways in the non-equilibrium plasma kinetics of hydrogen-air and hydrocarbon-air mixtures is of great importance for the advance of plasma assisted combustion (PAC) where hundreds of species and thousands of reactions are usually implemented [211, 212].

More recently (since 2005), cold atmospheric pressure plasma jets (APPJs) have been shown as promising tools for biomedical applications [102]. Many of the APPJ plasma species (mixture of air and a noble gas) enable the plasma to disinfect and, consequently, it has become important to study the chemical processes of the plasma jets in order to understand the plasma-induced effects on biological samples. Different models incorporating kinetic schemes of very high complexity have been developed [114, 141, 242] including one with almost 2000 reactions [225]; however, none of these works use a systematic tool to trace and analyse the relative importance of the many kinetic pathways considered.

Finally, it is worth mentioning also present studies about the possible electrical activity in the atmospheres of exoplanets. In this regard, a recent work by Helling et al [78] shows first results of the dependence of the electric breakdown conditions in giant gas exoplanets on the local gas-phase chemistry. These preliminary results suggest that different intra-cloud discharges (local corona discharges and large-scale sparks near and above the cloud tops) dominate at several heights inside the mineal clouds of exoplanets. A tool like PumpKin would clearly help in the analysis of the key gas-phase kinetic pathways controlling the atmospheric chemistry driven by the possible electrical activity in extrasolar planets.

In most cases, when we use a chemical model, we are concerned with the production or consumption of some long-lived species. However, short-lived species very often mediate the chemical interactions between the species of interest so we must also include them in the model. After the model is run, we would like to analyze the result by summarizing only the interactions between long-lived species. This can be done by combining reactions that produce and consume the fast species into a so-called *pathway*. For example, given a fast species B and the reactions $A \rightarrow B$, $B \rightarrow C$ these can be combined into the net reaction $A \rightarrow C$ that recycles the species B .

This separation between time-scales is even more acute in the context of plasma physics and, in particular, in the study of electrical discharges, where

also the mechanism driving the chemistry is strongly inhomogeneous in time. This introduces an additional separation of time-scales, in this case external to the chemical processes. For example, many plasma applications at atmospheric pressure rely on nanosecond pulsed discharges, where we deal with a strong, repetitively pulsed electric field lasting for some nanoseconds. We may be nevertheless interested in the effects of this electric field on much longer time scales of some milliseconds or more.

Many software tools exist to integrate numerically the evolution of arbitrary chemical reaction systems [29, 67, 88, 163, 174, 198]. In the plasma context, a tool such as ZDPlaskin [163] incorporates the Boltzmann equation solver BOLSIG+ [74] and thus it is compatible with reaction rates that depend on an evolving electron energy distribution, driven by a time-dependent electric field.

However, few automated tools exist to analyze the output of these codes in terms of the separation between long-lived and short-lived species mentioned above. Recently Lehmann [103] proposed an algorithm to find the most relevant pathways in a given chemical system. With a focus on atmospheric chemistry, this algorithm has been applied successfully to investigate the destruction of ozone in the Earth's atmosphere [71] as well as the formation [213] and stability [214] of CO₂ in the lower Martian atmosphere. Unfortunately, Lehmann [103] didn't provide the source code of his implementation of the algorithm to the public access.

We present here the software tool PumpKin (pathway reduction method for plasma kinetic models) that reimplements Lehmann's algorithm with a focus on plasma chemical models. PumpKin is an open-source tool available to all interested researchers, provided that proper reference is made in publications reporting results obtained using this software. The code and its user manual can be downloaded from the web site <http://www.pumpkin-tool.org>.

It is worth mentioning that there exists first principle tools (based on quantum chemical calculations) such as the global reaction route mapping (GRRM) using the new ADDF (for one reactant) and AFIR (for two or more reactants) methods for searching elemental reactant pathways recently published by Maeda et al [129]. Tools such GRRM with the new ADDF and AFIR search methods are of fundamental importance to determine the elemental (chemical) pathways resulting in some product species as a consequence of the chemical interaction of one (ADDF method), or two or more (AFIR method) reactants. However, our tool (PumpKin) takes for granted the elemental pathways (searched by GRRM through ADDF and AFIR) giving the products of each of the kinetic processes considered (taken from the scientific literature). Thus, PumpKin focuses on the net (or global) reaction pathways producing selected species, as illustrated in section 4 (examples) for NO and O₃⁻, rather than on the search of possible elemental pathways resulting from the interaction of given reactants which is the principal goal of first principle tools such as GRRM.

The rest of this chapter is organized as follows. Section 6.2 describes the general algorithm of PumpKin. The tool is described in section 6.3 where we discuss input and output, as well as technical requirements to run PumpKin. Several examples and use cases are illustrated in section 6.4. Our conclusions are

detailed in section 6.5.

6.2 PumpKin algorithm

In this section we briefly describe the algorithm underlying the PumpKin tool. For a more detailed description and further discussions about the algorithm we refer our users to Lehmann's original paper [103] and to the Users Manual of PumpKin.

Given a model consisting of a set of reactions between several chemical species and the average rates of these reactions, obtained by solving of the model, PumpKin calculates a set of *pathways* and their effective rates. A pathway is a linear combination of reactions, each of them weighted by a natural number. PumpKin builds pathways that have a zero net production of fast species, defined as those with a chemical lifetime much shorter than the time of interest of the model.

To construct a list of pathways, PumpKin proceeds as follows. It starts from a set of pathways consisting of one reaction each, including all the reactions in the model. The list of pathways is then updated in steps, each step treating a fast species (named *branching point* in [103]). At a given point, the next branching point to treat is selected as the species with the shortest lifetime relative to the present list of pathways; then the pathways producing the chosen species are combined with pathways that consume it. The resulting pathways recycle the branching point species, in the sense that they have a zero net production of it. Then, in order to avoid a too large set of pathways, pathways with a low rate are eliminated. Finally, some pathways are decomposed into more elementary ones. This process is repeated for all fast species, defined as those with a lifetime shorter than a user-specified τ .

6.3 Code description and general requirements

The PumpKin tool is written in the programming language C++. Originally it has been developed and tested on Mac OS X 10.8.5 using Xcode (versions 4.6.3 and 5.0) with LLVM compilers 4.2 and 5.0. Later it has been successfully compiled with GCC (versions above 4.2) on Mac OS X and Linux. Windows users should have installed the Cygwin tool (www.cygwin.com), which provides a Linux look and feel environment for Windows. Here are the general requirements:

- To build PumpKin, the GNU version of make (GNUmake) must be installed. The PumpKin makefile requires GNU make version 3.77 or later. GNU software can be downloaded from many places, including www.gnu.org/software/make/.
- A C++ compiler is required. PumpKin makes heavy use of the ISO/IEC 14882 C++ Standard. Some compilers are not fully compliant with this specification, although most are. PumpKin has been compiled and tested with

Table 6.1: Species considered in the model

N, N ₂ , O, O ₂ , O ₃
NO, NO ₂ , NO ₃
N ₂ O, N ₂ O ₅
N ⁺ , N ₂ ⁺ , N ₃ ⁺ , N ₄ ⁺
O ⁺ , O ₂ ⁺ , O ₄ ⁺
NO ⁺ , N ₂ O ⁺ , NO ₂ ⁺ , O ₂ ⁺ N ₂
N ₂ (A ³ Σ _u ⁺ , B ³ Π _g , C ³ Π _u , a' ¹ Σ _u ⁻)
N(² D, ² P), O(¹ D, ¹ S)
O ₂ (a ¹ Δ _g , b ¹ Σ _g ⁺ , 4.5 eV)
O ₂ (X ³ , <i>v</i> = 1 - 4), N ₂ (X ¹ , <i>v</i> = 1 - 8)
e, O ⁻ , O ₂ ⁻ , O ₃ ⁻ , O ₄ ⁻
NO ⁻ , NO ₂ ⁻ , NO ₃ ⁻ , N ₂ O ⁻

- GNU g++ 3.32 or higher.
- LLVM 3.2 or higher
- GLPK (GNU linear programming kit) must be installed [130]. This provides PumpKin a solution of large-scale linear programming (LP) problems. GLPK can be downloaded from website www.gnu.org/software/glpk/. We have tested PumpKin with GLPK recent version 4.32.

The recommended system requirements depend on the choice of parameters discussed in section 6.3.1. As a reference, in a MacBook Pro 15-inch (Mid 2010) with a CPU Intel Core i5 at 2.4 GHz, 4 GB (1067 MHz DDR3) of RAM memory and the operating system Mac OS X 10.8.5, it can analyse a chemical system consisting of 650 reactions and 53 species from the table 6.1, with the largest possible `tau_lifetime` and `f_min` = 1000 (see section 6.3.1), in about 30 seconds. When the input files are large, PumpKin will require more time to load them into the computer memory.

6.3.1 Input and output

To determine the chemical pathways, PumpKin requires from the user the stoichiometric matrix and kinetic data for the full chemical reaction system, namely:

- chemical reactions R_j , $j = 1, \dots, n_R$, involving between species S_i , $i = 1, \dots, n_S$, where n_R and n_S are the number of chemical reactions and species, respectively,
- stoichiometric coefficients s_{ij} , which represent the number of molecules of species S_i produced (or negative number of molecules of S_i consumed) by reaction R_j ,
- a time evolution of concentrations $c_i(t_l)$ and reactions rate $r_j(t_l)$, where $l = 1, \dots, n_T$ and $t_0 = t_1 \leq \dots \leq t_{n_T} = t_{end}$,

The code is independent of the units chosen by the user. Conventionally, $c_i(t_l)$ is specified in units of [molec. cm⁻³] and r_j in units of [molec. cm⁻³ s⁻¹]. A user should also provide an input file similar to the following table

```

interest = 1
t_init = 0.0
t_end = 1.0e-3
max_bp = 0
tau_lifetime = 0.9e-5          (*)
max_path = 1500
f_min = 0,
```

where:

- `interest` - an index of the species of interest S_{interest} , if the user is interested in the production and/or consumption of S_{interest} , otherwise the user should specify `interest` as a non-positive number,
- `[t_init, t_end]` - a time interval $[t_{\text{init}}, t_{\text{end}}] \subseteq [0, T]$ where PumpKin will perform the analysis,
- `max_bp` - if positive, the maximum number of branching points considered, otherwise it is disregarded,
- `tau_lifetime` - if positive, a lifetime threshold in units of [s], otherwise it is disregarded,
- `max_path` - if positive, the maximum number of pathways considered per branching point treatment, i.e. the only the first `max_path` pathways with higher rate will be considered, otherwise is neglected,
- `f_min` - if positive, pathway rate threshold in the unit of [molec. cm⁻³s⁻¹], i.e. pathways with a rate smaller than `f_min` will be deleted, otherwise is neglected.

The order of parameters in the input file should be exactly like in the table (*). The names of parameters are not important.

Currently, PumpKin by default can read an output of ZDPlasKin. The PumpKin package is provided with an example of input files. The output of PumpKin with these input files is discussed in section 6.4.

Depending on whether the user has specified the `interest` parameter as a positive integer (the index of the species of interest) or as a non-positive number (the user does not have any species of interest), one of the following results will be printed:

`interest > 0`: PumpKin will output all the pathways (and their rates) producing or consuming the species of interest S_{interest} , as well as the relative production or consumption compared with the initial concentration of S_{interest} . The output will contain information such as how much S_{interest}

has been produced or consumed by the pathways that are deleted by PumpKin using parameters `f_min` or `max_path`.

`interest ≤ 0`: Pumpkin will output all the pathways (and their rates) sorted by rate. In some cases, this number can be very large, so we decided to limit it to 100, which of course can be easily changed inside the PumpKin source code. The output will also contain information such as how much of any species has been produced or consumed by the pathways that are deleted by PumpKin (by user) using parameters `f_min` or `max_path`.

6.4 Examples

PumpKin is provided with two sets of input files. Both examples are the outputs of the zero-dimensional plasma kinetic solver ZDPlasKin used also in the previous chapter 5. We use a zero-dimensional model to describe the dynamics of species under a constant electric field. The following system of ordinary differential equations (ODEs) is used to describe the interaction between the species

$$\frac{d[n_i]}{dt} = S_i, \quad (6.1)$$

where the source term S_i is the total production and destruction rate of species i in various processes. The adapted version of the kinetic file for N₂-O₂ mixtures (dry air) from ZDPlasKin [62, 163] is used. A complete list of plasma chemical precesses in N₂-O₂ mixtures is taken mainly from [28]. Transport parameters and rate coefficients for electron-neutral interactions are calculated using the BOLSIG+ solver built-in into ZDPlasKin. As initial value of the electron density we take $n_e(0) = 4.0 \cdot 10^{13} \text{ cm}^{-3}$.

The list of species and reactions was automatically converted into a system of ordinary differential equations (6.1) and solved numerically using the ZDPlasKin tool. The user can visualize the results of ZDPlasKin using a software Qt-Plaskin [122].

6.4.1 Species of interest

As a first example we assume the background electric field to be a constant 10 kV/cm at standard temperature and pressure (STP). We run our chemical model up to 1 ms with ZDPlasKin. The output is stored in the folder called `Input_10`, where the input parameters specified by the user are in the file `input.txt`, which

looks as follows

```

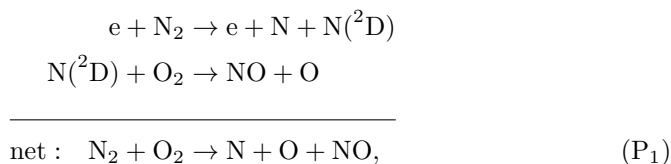
interest = 40
t_init = 5.0e-11
t_end = 0.9e-3
max_bp = 0
tau_lifetime = 0.9e-5
max_path = 1500
f_min = 0.

```

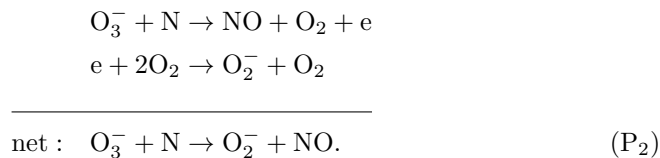
In this subsection we will modify only the species of interest.

NO

If we run PumpKin for the species NO, PumpKin will output 2 pathways responsible for the production:



and



The pathway (P₁) will produce 52% and pathway (P₂) 41% of the total NO-production, with corresponding rates of $3 \cdot 10^{13}$ and $2.4 \cdot 10^{13} \text{ cm}^{-3}\text{s}^{-1}$.

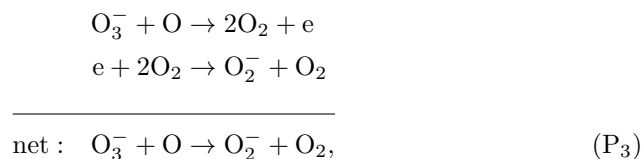
The following reaction will be responsible for 72% of the destruction of NO:



and has a rate of $1.5 \cdot 10^{13} \text{ cm}^{-3}\text{s}^{-1}$.

O₃⁻

If we run PumpKin and choose O₃⁻ as the species of interest, we obtain the following pathway responsible for 94% of O₃⁻-destruction

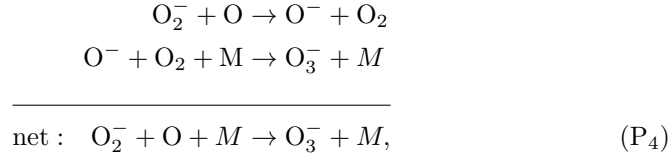


with a rate $3.1 \cdot 10^{16} \text{ cm}^{-3} \text{ s}^{-1}$.

On the other hand, O_3^- -production will be dominated by the following reaction and pathway



and



where M is any neutral. The pathway (P₄) will produce 18% of O_3^- , with a rate $1.4 \cdot 10^{16} \text{ cm}^{-3} \text{ s}^{-1}$ and the reaction (R₂) will produce 69% of O_3^- , with a rate $5.3 \cdot 10^{16} \text{ cm}^{-3} \text{ s}^{-1}$.

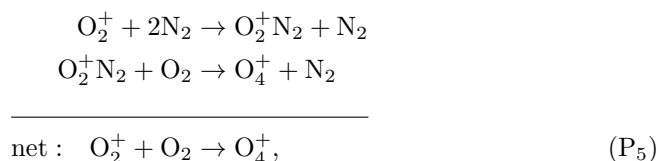
6.4.2 Dominant pathways or reduction

In the second example of input file we consider the electric field to be a constant 20 kV/cm at STP. We run the chemical model up to 2 μs . The output is stored in the folder called Input_20, where the input parameters the specified in the file input.txt as follows

```
interest = 0
t_init = 5.0e-11
t_end = 2.0e-6
max_bp = 0
tau_lifetime = 2.0e-7
max_path = 1500
f_min = 1.0e+5.
```

The user can benefit from this execution mode in two ways. First by initializing max_bp by some positive N number we can eliminate from the system the first N fastest species. This can significantly reduce the number of species considered in the kinetics. Of course, this depends on the timescale of interest of the user. The second way to use this execution mode, is to list the most important pathways sorted by their rate. This also depends on the user's election of where to cut and how many pathways to consider. As a reference, the highest rate of pathway is $2.4 \cdot 10^{23} \text{ cm}^{-3} \text{ s}^{-1}$ and the 240th pathway has a rate of $9.9 \cdot 10^{17} \text{ cm}^{-3} \text{ s}^{-1}$. On the other hand, 26 branching points are already considered, which means that these species are considered as short-lived and recycled. If the user has no interest in these species, he can neglect them. For instance, in this example the first branching point, i.e. the fastest species, is $\text{O}_2^+ \text{N}_2$ with a lifetime of $8.5 \cdot 10^{-11} \text{ s}$. After treating this branching point, PumpKin will generate new

pathways recycling it. Among these newly created pathways the following one has one of the highest rates



with a rate of $3.9 \cdot 10^{19} \text{ cm}^{-3} \text{ s}^{-1}$. Thus, we see that the pathway (P₅) uses the species O₂⁺N₂ only as an intermediate species. PumpKin is pointing here that the chemical model can be reduced by replacing the two original reactions in (P₅) with a single net reaction. The density of O₂⁺N₂ does not need to be tracked any longer and therefore the model requires the solution of one equation less.

6.5 Conclusions

The present paper introduces the PumpKin package, a tool to analyse and reduce complex plasma chemical models. The user can analyse the underlying mechanisms of production or/and consumption of the species of interest. The idea is to investigate the relevant chemistry at a given time scale. We have provided two examples of the use of PumpKin as an introduction for potential users that would apply the code to their own models. The present implementation reads only the output format of ZDPlasKin. In principle, though, PumpKin can be extended to read output from other applications.

CHAPTER 7

Conclusions and Outlook

How much easier it is to be critical than to be correct.

– BENJAMIN DISRAELI

An opinion should be the result of thought, not a substitute for it.

– JEF MALLET

Conclusions and suggestions for future work have been given at the end of each chapter. The main findings of this thesis are summarised here.

7.1 High order fluid model

We have derived a new high order fluid model for streamer discharges, based on first principles. The high order fluid model employs the first four moments of the Boltzmann equation. The system is closed by approximating the highest order tensor with lower order moments, namely the average electron density and the average electron energy, in the last equation. We also have sketched the derivation of the lower order models. The source terms of the high order fluid model are evaluated using momentum transfer theory. We have calculated transport data using a multi term Boltzmann solver and the publicly available two term solver (BOLSIG+). The non-local effects in the profile of the average electron energy are present both in the Particle-in-Cell Monte Carlo model and in the high order model, but are missing in the first order model due to the local field approximation. The slope of the average electron energy in the region ahead of the streamer is related to the spatial variation of the average electron energy in the avalanche phase of the streamer development. These observations are consistent with those made by Li *et al.* [107, 110]. In chapter 4 we discussed fluid models for streamer

discharges of arbitrary order. In particular, we summarised the origins and the assumptions underlying each fluid model, including the second order model. We compare them with Particle-in-Cell Monte Carlo in Ne under varying externally applied electric fields. We have concluded that the high order fluid model must be used in order to accurately simulate the streamer head and the region ahead of the streamer. Our comparisons show that the second order model describes very well the electron density and the average electron energy in a streamer channel, although it largely underestimates streamer front propagation velocity.

We have derived a high order fluid model in three spatial dimensions, and we have simulated the streamers in one dimension. The resulting hyperbolic system should be investigated in higher spatial dimensions. The mathematical properties of the system are currently under investigation. The high order model should be extended even further to include the ion motion and the chemistry in the streamer channel, which will also allow the investigation of the heating dynamics. The temperature and pressure effects on the properties of streamers should be investigated [82]. Furthermore, the assumptions on the isotropy of the temperature tensor and absence of the super-elastic collisions, metastables and photo-ionization could be eliminated. Besides, the high order model has never been tested to simulate positive streamers. We have shown that the high order fluid model simulates the streamer head with great accuracy. This fact can be used to couple the high order fluid model with Particle-in-Cell Monte Carlo in a hybrid framework similar to the model developed by Li *et al.* [109]. The region ahead of the streamer head is lacking electrons and only few highly energetic ones are present. This means, generally speaking, the in this region the fluid approximation is failing. Here is where Particle-in-Cell Monte Carlo can be used to capture the electron dynamics properly. The other parts of the streamer body can be accurately represented by the fluid description.

7.2 Plasma chemistry

S. Nijdam and E. Takahashi have performed experiments in $\text{N}_2:\text{O}_2$ mixtures and argon to investigate the effects of a preceding streamer discharge on a subsequent discharge by applying two positive high voltage pulses in succession with pulse-to-pulse intervals (Δt) between 200 ns and 40 ms. They observed that the value of Δt for which we can still observe continuation of the first-pulse streamers during the second pulse depends on the oxygen concentration in nitrogen-oxygen mixtures and has a maximum at an oxygen concentration of about 0.2%. Our zero dimensional plasma-chemical model reproduces and explains the experimental results.

We have developed a tool, called PumpKin, to find the dominant pathways in plasma chemical models. The tool is based on the algorithm proposed by R. Lehmann [103]. PumpKin is user friendly tool publicly available under the license GNU GPL (version 2), and it can be obtained from the website <http://www.pumpkin-tool.org>.

PumpKin is a new tool and many possible use-cases are still unknown even for

me. Publicity will help to reveal many applications from different fields. On my behalf, the graphical user interface (GUI) is presently in the development stage and before printing this thesis it will be realised. Another important component to be added is the visualisation of results using the open source tool called Graphviz [60]. The philosophy (or the license) behind of PumpKin assumes that the scientist-enthusiasts will include many other features and improve the user's experience.

References

- [1] I. Abbas and P. Bayle. A critical analysis of ionising wave propagation mechanisms in breakdown. *J. Phys. D*, 13:1055, 1980. doi: 10.1088/0022-3727/13/6/015.
- [2] I. Abbas and P. Bayle. Non-equilibrium between electrons and field in a gas breakdown ionising wave. I. Macroscopic model. *J. Phys. D*, 14:649, 1981. doi: 10.1088/0022-3727/14/4/019.
- [3] N. L. Aleksandrov and E. M. Bazelyan. Ionization processes in spark discharge plasmas. *Plasma Sour. Sci. Technol.*, 8:285, 1999. doi: 10.1088/0963-0252/8/2/309.
- [4] N. L. Aleksandrov and I. V. Kochetov. Electron rate coefficients in gases under non-uniform field and electron density conditions. *J. Phys. D*, 29:1476, 1996. doi: 10.1088/0022-3727/29/6/011.
- [5] N. L. Aleksandrov, E. M. Bazelyan, I. V. Kochetov, and N. A. Dyatko. The ionization kinetics and electric field in the leader channel in long air gaps. *J. Phys. D*, 30:1616, 1997. doi: 10.1088/0022-3727/30/11/011.
- [6] N. L. Aleksandrov, E. M. Bazelyan, N. A. Dyatko, and I. V. Kochetov. Streamer breakdown of long air gaps. *Plasma Physics Reports*, 24:541, 1998.
- [7] K. Anzai, H. Kato, M. Hoshino, H. Tanaka, Y. Itikawa, L. Campbell, M. J. Brunger, S. J. Buckman, H. Cho, F. Blanco, G. Garcia, P. Limão-Vieira, and O. Ingólfsson. Cross section data sets for electron collisions with H₂, O₂, CO, CO₂, N₂O and H₂O. *Eur. Phys J. D*, 66:36, 2012. doi: 10.1140/epjd/e2011-20630-1.
- [8] E. Arnone, A. Kero, B. M. Dinelli, C.-F. Enell, N. F. Arnold, E. Papandrea, C. J. Rodger, M. Carlotti, M. Ridolfi, and E. Turunen. Seeking sprite-

- induced signatures in remotely sensed middle atmosphere NO_2 . *Geophys. Res. Lett.*, 35:L05807, 2008. doi: 10.1029/2007GL031791.
- [9] R. R. Arslanbekov, V. I. Kolobov, and A. A. Frolova. Kinetic solvers with adaptive mesh in phase space. In M. Mareschal and A. Santos, editors, *American Institute of Physics Conference Series*, volume 1501 of *American Institute of Physics Conference Series*, page 294, 2012. doi: 10.1063/1.4769527.
 - [10] N. Y. Babaeva and G. V. Naidis. Two-dimensional modelling of positive streamer dynamics in non-uniform electric fields in air. *J. Phys. D*, 29:2423, 1996. doi: 10.1088/0022-3727/29/9/029.
 - [11] S. E. Babayan, J. Y. Jeong, V. J. Tu, J. Park, G. S. Selwyn, and R. F. Hicks. Deposition of silicon dioxide films with an atmospheric-pressure plasma jet. *Plasma Sour. Sci. Technol.*, 7:286, 1998. doi: 10.1088/0963-0252/7/3/006.
 - [12] Michael S. Barnes, Tina J. Cotler, and Michael E. Elta. Largesignal timedomain modeling of lowpressure rf glow discharges. *Journal of Applied Physics*, 61(1), 1987.
 - [13] P. Bayle and B. Cornebois. Propagation of ionizing electron shock waves in electrical breakdown. *Phys. Rev. A*, 31:1046, 1985. doi: 10.1103/PhysRevA.31.1046.
 - [14] M. Becerra. Glow corona generation and streamer inception at the tip of grounded objects during thunderstorms: revisited. *J. Phys. D*, 46(13):135205, 2013. doi: 10.1088/0022-3727/46/13/135205.
 - [15] M. M. Becker and D. Loffhagen. Enhanced reliability of drift-diffusion approximation for electrons in fluid models for nonthermal plasmas. *AIP Advances*, 3(1):012108, 1 2013. ISSN 2158-3226. doi: 10.1063/1.4775771.
 - [16] Markus M. Becker and Detlef Loffhagen. Derivation of Moment Equations for the Theoretical Description of Electrons in Nonthermal Plasmas. *Advances in Pure Mathematics*, 3:343–352, 2013.
 - [17] M. J. Berger and P. Colella. Local adaptive mesh refinement for shock hydrodynamics. *J. Comput. Phys.*, 82:64, 1989. doi: 10.1016/0021-9991(89)90035-1.
 - [18] Keith Beven and Andrew Binley. The future of distributed models: Model calibration and uncertainty prediction. *Hydrological Processes*, 6(3):279–298, 7 1992. ISSN 08856087. doi: 10.1002/hyp.3360060305.
 - [19] A. N. Bhoj and M. J. Kushner. Avalanche process in an idealized lamp: II. Modelling of breakdown in Ar/Xe electric discharges. *J. Phys. D*, 37:2510, 2004. doi: 10.1088/0022-3727/37/18/007.

- [20] J. P. Boeuf and L. C. Pitchford. Two-dimensional model of a capacitively coupled rf discharge and comparisons with experiments in the Gaseous Electronics Conference reference reactor. *Phys. Rev. E*, 51:1376, 1995. doi: 10.1103/PhysRevE.51.1376.
- [21] J.-P. Boeuf, L. L. Yang, and L. C. Pitchford. Dynamics of a guided streamer ("plasma bullet") in a helium jet in air at atmospheric pressure. *J. Phys. D*, 46(1):015201, 2013. doi: 10.1088/0022-3727/46/1/015201.
- [22] Deepak Bose, M. V. V. S. Rao, T. R. Govindan, and M. Meyyappan. Uncertainty and sensitivity analysis of gas-phase chemistry in a CHF_3 plasma. *Plasma Sources Science and Technology*, 12(2):225, 5 2003. ISSN 0963-0252. doi: 10.1088/0963-0252/12/2/314.
- [23] D. Bouche, G. Bonnaud, and D. Ramos. Comparison of numerical schemes for solving the advection equation. *Applied Mathematics Letters*, 16(2):147 – 154, 2003. ISSN 0893-9659. doi: [http://dx.doi.org/10.1016/S0893-9659\(03\)80024-1](http://dx.doi.org/10.1016/S0893-9659(03)80024-1).
- [24] T. M. P. Briels, J. Kos, E. M. van Veldhuizen, and U. Ebert. Circuit dependence of the diameter of pulsed positive streamers in air. *J. Phys. D*, 39:5201, 2006. doi: 10.1088/0022-3727/39/24/016.
- [25] T. M. P. Briels, E. M. van Veldhuizen, and U. Ebert. Time Resolved Measurements of Streamer Inception in Air. *IEEE Trans. Plasma Sci.*, 36:908, 2008. doi: 10.1109/TPS.2008.920223.
- [26] N. Butchart, I. Cionni, V. Eyring, T. G. Shepherd, D. W. Waugh, H. Akiyoshi, J. Austin, C. Brühl, M. P. Chipperfield, E. Cordero, M. Dameris, R. Deckert, S. Dhomse, S. M. Frith, R. R. Garcia, A. Gettelman, M. A. Giorgetta, D. E. Kinnison, F. Li, E. Mancini, C. McLandress, S. Pawson, G. Pitari, D. A. Plummer, E. Rozanov, F. Sassi, J. F. Scinocca, K. Shibata, B. Steil, and W. Tian. Chemistry-Climate Model Simulations of Twenty-First Century Stratospheric Climate and Circulation Changes. *Journal of Climate*, 23:5349, 2010. doi: 10.1175/2010JCLI3404.1.
- [27] A. C. Calder, B. Fryxell, T. Plewa, R. Rosner, L. J. Dursi, V. G. Weirs, T. Dupont, H. F. Robey, J. O. Kane, and B. A. Remington. On validating an astrophysical simulation code. *The Astrophysical Journal Supplement Series*, 143(1):201, 2002.
- [28] M Capitelli, Ferreira C. M., Gordiets B. F., and Osipov A. I. *Plasma Kinetics in Atmospheric Gases*. Springer Verlag, Berlin, Germany, 2000.
- [29] G. D. Carver, P. D. Brown, and O. Wild. The ASAD atmospheric chemistry integration package and chemical reaction database. *Comput. Phys. Commun.*, 105:197, 1997. doi: 10.1016/S0010-4655(97)00056-8.
- [30] S. Celestin, Z. Bonaventura, B. Zeghondy, A. Bourdon, and P. Ségur. The use of the ghost fluid method for Poisson's equation to simulate streamer

- propagation in point-to-plane and point-to-point geometries. *J. Phys. D*, 42(6):065203, 2009. doi: 10.1088/0022-3727/42/6/065203.
- [31] CS Wang Chang, J de Boer, G W Ford, and George Eugène Uhlenbeck. *Studies in statistical mechanics*, volume 5. North-Holland, 1970.
- [32] B. Chaudhury, J.-P. Boeuf, G.-Q. Zhu, and O. Pascal. Physics and modelling of microwave streamers at atmospheric pressure. *J. Appl. Phys.*, 110(11):113306, 2011. doi: 10.1063/1.3665202.
- [33] Thomas Christen. Radiation and nozzle-ablation models for CFD simulations of gas circuit breakers. In *Electric Power Equipment-Switching Technology (ICEPE-ST), 2011 1st International Conference on*, pages 471–474. IEEE, 2011.
- [34] P. C. Cosby. Electron-impact dissociation of oxygen. *J. Chem. Phys.*, 98:9560, 1993. doi: 10.1063/1.464387.
- [35] Richard Courant, Kurt Friedrichs, and Hans Lewy. Über die partiellen differenzengleichungen der mathematischen physik. *Mathematische Annalen*, 100(1):32–74, 1928.
- [36] R. W. Crompton. Benchmark Measurements of Cross Sections for Electron Collisions: Electron Swarm Methods. *Adv. At. Mol. Opt. Phys.*, 33:97, 1994. doi: 10.1016/S1049-250X(08)60034-8.
- [37] M. Davoudabadi, J. S. Shrimpton, and F. Mashayek. On accuracy and performance of high-order finite volume methods in local mean energy model of non-thermal plasmas. *J. Comput. Phys.*, 228:2468, 2009. doi: 10.1016/j.jcp.2008.12.015.
- [38] Hidde de Jong. Modeling and simulation of genetic regulatory systems: A literature review. *Journal of Computational Biology*, 9(1):67–103, 1 2002. ISSN 1066-5277. doi: 10.1089/10665270252833208.
- [39] U. Denni, G. Felici, M. A. Frani, A. Mengucci, G. Papalino, M. Spinetti, and A. Paoloni. Streamer studies in Resistive Plate Chambers. *Nuclear Instruments and Methods in Physics Research A*, 640:76, 2011. doi: 10.1016/j.nima.2011.03.008.
- [40] S. K. Dhali and P. F. Williams. Two-dimensional studies of streamers in gases. *J. Appl. Phys.*, 62:4696, 1987. doi: 10.1063/1.339020.
- [41] R. Dorai and M. J. Kushner. Consequences of propene and propane on plasma remediation of NO_x . *J. Appl. Phys.*, 88:3739, 2000. doi: 10.1063/1.1288511.
- [42] S. Dujko, R. D. White, and Z. L. Petrović. Monte Carlo studies of non-conservative electron transport in the steady-state Townsend experiment. *J. Phys. D*, 41(24):245205, 2008. doi: 10.1088/0022-3727/41/24/245205.

- [43] S. Dujko, R. D. White, Z. L. Petrović, and R. E. Robson. Benchmark calculations of nonconservative charged-particle swarms in dc electric and magnetic fields crossed at arbitrary angles. *Phys. Rev. E*, 81(4):046403, 2010. doi: 10.1103/PhysRevE.81.046403.
- [44] S. Dujko, U. Ebert, R. D. White, and Z. L. Petrović. Boltzmann Equation Analysis of Electron Transport in a N₂-O₂ Streamer Discharge. *Japanese Journal of Applied Physics*, 50(8):080000, 2011. doi: 10.1143/JJAP.50.08JC01.
- [45] S. Dujko, R. D. White, Z. L. Petrović, and R. E. Robson. A multi-term solution of the nonconservative Boltzmann equation for the analysis of temporal and spatial non-local effects in charged-particle swarms in electric and magnetic fields. *Plasma Sour. Sci. Technol.*, 20(2):024013, 2011. doi: 10.1088/0963-0252/20/2/024013.
- [46] S. Dujko, R. D. White, Z. M. Raspopović, and Z. L. Petrović. Spatially resolved transport data for electrons in gases: Definition, interpretation and calculation. *Nuclear Instruments and Methods in Physics Research B*, 279:84, 2012. doi: 10.1016/j.nimb.2011.10.067.
- [47] S. Dujko, A. H. Markosyan, R. D. White, and U. Ebert. High-order fluid model for streamer discharges: I. Derivation of model and transport data. *J. Phys. D*, 46:475202, 2013. doi: 10.1088/0022-3727/46/47/475202.
- [48] L. Dumitrescu, O. Lesaint, N. Bonifaci, A. Denat, and P. Notingher. Study of streamer inception in cyclohexane with a sensitive charge measurement technique under impulse voltage. *Journal of Electrostatics*, 53(2):135 – 146, 2001. ISSN 0304-3886. Selected Papers of the International Workshop on Electrical Conduction, Convection and Breakdown in Fluids.
- [49] U. Ebert and D. D. Sentman. Streamers, sprites, leaders, lightning: from micro- to macroscales. *J. Phys. D*, 41(23):230301, 2008. doi: 10.1088/0022-3727/41/23/230301.
- [50] U. Ebert and W. van Saarloos. Front propagation into unstable states: universal algebraic convergence towards uniformly translating pulled fronts. *Physica D Nonlinear Phenomena*, 146:1, 2000. doi: 10.1016/S0167-2789(00)00068-3.
- [51] U. Ebert, W. van Saarloos, and C. Caroli. Streamer Propagation as a Pattern Formation Problem: Planar Fronts. *Phys. Rev. Lett.*, 77:4178, 1996. doi: 10.1103/PhysRevLett.77.4178.
- [52] U. Ebert, W. van Saarloos, and C. Caroli. Propagation and structure of planar streamer fronts. *Phys. Rev. E*, 55:1530, 1997. doi: 10.1103/PhysRevE.55.1530.
- [53] U. Ebert, C. Montijn, T. M. P. Briels, W. Hundsdorfer, B. Meulenbroek, A. Rocco, and E. M. van Veldhuizen. The multiscale nature of streamers.

- Plasma Sour. Sci. Technol.*, 15:118, 2006. doi: 10.1088/0963-0252/15/2/S14.
- [54] U. Ebert, S. Nijdam, C. Li, A. Luque, T. Briels, and E. van Veldhuizen. Review of recent results on streamer discharges and discussion of their relevance for sprites and lightning. *J. Geophys. Res. (Space Phys)*, 115:A00E43, 2010. doi: 10.1029/2009JA014867.
 - [55] U. Ebert, F. Brau, G. Derks, W. Hundsdorfer, C.-Y. Kao, C. Li, A. Luque, B. Meulenbroek, S. Nijdam, V. Ratushnaya, L. Schäfer, and S. Tanveer. Multiple scales in streamer discharges, with an emphasis on moving boundary approximations. *Nonlinearity*, 24:1, 2011. doi: 10.1088/0951-7715/24/1/C01.
 - [56] O. Eichwald, P. Bayle, Y. Yousfi, and M. Jugroot. Modeling and three dimensional simulation of the neutral dynamics in an air discharge confined in a microcavity. II. Analysis of the wall and geometry effects. *J. Appl. Phys.*, 84:4716, 1998. doi: 10.1063/1.368714.
 - [57] O. Eichwald, M. Yousfi, P. Bayle, and M. Jugroot. Modeling and three-dimensional simulation of the neutral dynamics in an air discharge confined in a microcavity. I. Formation and free expansion of the pressure waves. *J. Appl. Phys.*, 84:4704, 1998. doi: 10.1063/1.368713.
 - [58] O. Eichwald, O. Ducasse, N. Merbahi, M. Yousfi, and D. Dubois. Effect of order fluid models on flue gas streamer dynamics. *J. Phys. D*, 39:99, 2006. doi: 10.1088/0022-3727/39/1/015.
 - [59] O. Eichwald, H. Bensaad, O. Ducasse, and M. Yousfi. Effects of numerical and physical anisotropic diffusion on branching phenomena of negative-streamer dynamics. *J. Phys. D*, 45:385203, 2012. doi: 10.1088/0022-3727/45/38/385203.
 - [60] John Ellson, Emden Gansner, Lefteris Koutsofios, Stephen North, Gordon Woodhull, Short Description, and Lucent Technologies. Graphviz open source graph drawing tools. In *Lecture Notes in Computer Science*, pages 483–484. Springer-Verlag, 2001.
 - [61] P. Flesch. *Light and Light Sources: High-Intensity Discharge Lamps*. Physica-Verlag, 2007. ISBN 9783540326854.
 - [62] A. Flitti and S. Pancheshnyi. Gas heating in fast pulsed discharges in N₂-O₂ mixtures. *European Physical Journal Applied Physics*, 45(2):021001, 2009. doi: 10.1051/epjap/2009011.
 - [63] P. Fonte. Applications and new developments in resistive plate chambers. *IEEE Transactions on Nuclear Science*, 49:881, 2002. doi: 10.1109/TNS.2002.1039583.
 - [64] M. Füllekrug, E. A. Mareev, and M. J. Rycroft. *Sprites, Elves and Intense Lightning Discharges*. 2006.

- [65] A. C. Gentile and M. J. Kushner. Reaction chemistry and optimization of plasma remediation of N_xO_y from gas streams. *J. Appl. Phys.*, 78:2074, 1995. doi: 10.1063/1.360185.
- [66] E. Gogolides and H. H. Sawin. Continuum modeling of radio-frequency glow discharges. I. Theory and results for electropositive and electronegative gases. *J. Appl. Phys.*, 72:3971, 1992. doi: 10.1063/1.352250.
- [67] D.G. Goodwin. Cantera: Object-oriented software for reacting flows, (2002). <http://www.cantera.org>.
- [68] F. J. Gordillo-Vázquez. Air plasma kinetics under the influence of sprites. *J. Phys. D*, 41(23):234016, 2008. doi: 10.1088/0022-3727/41/23/234016.
- [69] F. J. Gordillo-Vazquez. Vibrational kinetics of air plasmas induced by sprites. *J. Geophys. Res. (Space Phys)*, 115:A00E25, 2010. doi: 10.1029/2009JA014688.
- [70] L. Grabowski, E. van Veldhuizen, A. Pemen, and W. Rutgers. Corona Above Water Reactor for Systematic Study of Aqueous Phenol Degradation. *Plasma Chem. Plasma Process.*, 26:3–17, 2006. ISSN 0272-4324. doi: 10.1007/s11090-005-8721-8. 10.1007/s11090-005-8721-8.
- [71] J. L. Grenfell, R. Lehmann, P. Mieth, U. Langematz, and B. Steil. Chemical reaction pathways affecting stratospheric and mesospheric ozone. *Journal of Geophysical Research (Atmospheres)*, 111(10):D17311, September 2006. doi: 10.1029/2004JD005713.
- [72] G. K. Grubert, M. M. Becker, and D. Loffhagen. Why the local-mean-energy approximation should be used in hydrodynamic plasma descriptions instead of the local-field approximation. *Phys. Rev. E*, 80(3):036405, 2009. doi: 10.1103/PhysRevE.80.036405.
- [73] J.-M. Guo and C.-H. J. Wu. Two-dimensional nonequilibrium fluid models for streamers. *IEEE Trans. Plasma Sci.*, 21:684, 1993. doi: 10.1109/27.256788.
- [74] G. J. M. Hagelaar and L. C. Pitchford. Solving the Boltzmann equation to obtain electron transport coefficients and rate coefficients for fluid models. *Plasma Sour. Sci. Technol.*, 14:722, 2005. doi: 10.1088/0963-0252/14/4/011.
- [75] G.J.M. Hagelaar and G.M.W. Kroesen. Speeding up fluid models for gas discharges by implicit treatment of the electron energy source term. *Journal of Computational Physics*, 159(1):1 – 12, 2000. ISSN 0021-9991. doi: <http://dx.doi.org/10.1006/jcph.2000.6445>.
- [76] S. Hamaguchi. Modeling and simulation methods for plasma processing. *IBM Journal of Research and Development*, 43(1.2):199–215, 1 1999. ISSN 0018-8646. doi: 10.1147/rd.431.0199.

- [77] M. Hayashi. private communication, 2000.
- [78] C. Helling, M. Jardine, C. Stark, and D. Diver. Ionization in Atmospheres of Brown Dwarfs and Extrasolar Planets. III. Breakdown Conditions for Mineral Clouds. *Astrophys. J.*, 767:136, 2013. doi: 10.1088/0004-637X/767/2/136.
- [79] H. Höft, M. Kettlitz, T. Hoder, K.D. Weltmann, and R. Brandenburg. The influence of O₂ content on the spatio-temporal development of pulsed driven dielectric barrier discharges in O₂/N₂ gas mixtures. *J. Phys. D: Appl. Phys.*, 46(9):095202, 2013. doi: 10.1088/0022-3727/46/9/095202.
- [80] Weizhang Huang. Variational Mesh Adaptation: Isotropy and Equidistribution. *Journal of Computational Physics*, 174(2):903 – 924, 2001. ISSN 0021-9991. doi: 10.1006/jcph.2001.6945.
- [81] Weizhang Huang and Weiwei Sun. Variational mesh adaptation II: error estimates and monitor functions. *Journal of Computational Physics*, 184(2):619 – 648, 2003. ISSN 0021-9991. doi: 10.1016/S0021-9991(02)00040-2.
- [82] T. Huiskamp, A. J. M. Pemen, W. F. L. M. Hoebe, F. J. C. M. Beckers, and E. J. M. van Heesch. Temperature and pressure effects on positive streamers in air. *J. Phys. D*, 46(16):165202, 2013. doi: 10.1088/0022-3727/46/16/165202.
- [83] W. Hundsdorfer and J.G. Verwer. *Numerical Solution of Time-Dependent Advection-Diffusion-Reaction Equations*. Springer Series in Computational Mathematics. Springer, 2003. ISBN 9783540034407.
- [84] L.G.H. Huxley and R.W. Crompton. *The diffusion and drift of electrons in gases*. Wiley series in plasma physics. Wiley, 1974. ISBN 9780471425908.
- [85] A. A. Iordanidis and C. M. Franck. Self-consistent radiation-based simulation of electric arcs: II. Application to gas circuit breakers. *J. Phys. D*, 41(13):135206, 2008. doi: 10.1088/0022-3727/41/13/135206.
- [86] N. Jiang, A. Ji, and Z. Cao. Atmospheric pressure plasma jet: Effect of electrode configuration, discharge behavior, and its formation mechanism. *J. Appl. Phys.*, 106(1):013308, 2009. doi: 10.1063/1.3159884.
- [87] Z. Kanzari, M. Yousfi, and A. Hamani. Modeling and basic data for streamer dynamics in N₂ and O₂ discharges. *J. Appl. Phys.*, 84:4161, 1998. doi: 10.1063/1.368630.
- [88] R. J. Kee, F. M. Rupley, and J. A. Miller. The Chemkin Thermodynamic Data Base. Technical report, March 1990.
- [89] L. Khosravi Khorashad, M. Eskandari, and A. Moshaii. Simulation of resistive plate chamber in streamer mode operation. *Nuclear Instruments and Methods in Physics Research A*, 628:470, 2011. doi: 10.1016/j.nima.2010.07.027.

- [90] H. C. Kim, F. Iza, S. S. Yang, M. Radmilovic-Radjenov, and J. K. Lee. Particle and fluid simulations of low-temperature plasma discharges: benchmarks and kinetic effects. *J. Phys. D*, 38:283, 2005. doi: 10.1088/0022-3727/38/19/R01.
- [91] V. I. Kolobov and R. R. Arslanbekov. Towards adaptive kinetic-fluid simulations of weakly ionized plasmas. *J. Comput. Phys.*, 231:839, 2012. doi: 10.1016/j.jcp.2011.05.036.
- [92] M. G. Kong, G. Kroesen, G. Morfill, T. Nosenko, T. Shimizu, J. van Dijk, and J. L. Zimmermann. Plasma medicine: an introductory review. *New Journal of Physics*, 11(11):115012, 2009. doi: 10.1088/1367-2630/11/11/115012.
- [93] B. Koren. A robust upwind discretization method for advection, diffusion and source terms. *Notes on Numerical Fluid Mechanics*, 45:117–138, January 1993.
- [94] H. Kosina, M. Nedjalkov, and S. Selberherr. A Stable Backward Monte Carlo Method for the Solution of the Boltzmann Equation. In I. Lirkov, S. Margenov, J. Wasniewski, and P. Yalamov, editors, *Large-Scale Scientific Computing*, volume 2907 of *Lecture Notes in Computer Science*, pages 170–177. Springer Berlin Heidelberg, 2004. ISBN 978-3-540-21090-0. doi: 10.1007/978-3-540-24588-9_18.
- [95] I. A. Kossyi, A. Y. Kostinsky, A. A. Matveyev, and V. P. Silakov. Kinetic scheme of the non-equilibrium discharge in nitrogen-oxygen mixtures. *Plasma Sour. Sci. Technol.*, 1:207, 1992. doi: 10.1088/0963-0252/1/3/011.
- [96] A. A. Kulikovskiy. The structure of streamers in N_2 . II. Two-dimensional simulation. *J. Phys. D*, 27:2564, 1994. doi: 10.1088/0022-3727/27/12/018.
- [97] A. A. Kulikovskiy. Two-dimensional simulation of the positive streamer in N_2 between parallel-plate electrodes. *J. Phys. D*, 28:2483, 1995. doi: 10.1088/0022-3727/28/12/015.
- [98] K. Kumar, H. R. Skullerud, and R. E. Robson. Kinetic theory of charged particle swarms in neutral gases. *Australian Journal of Physics*, 33:343, 1980.
- [99] AL Kupershtokh and DA Medvedev. Simulations of gas-dynamic flows during streamers propagation at liquid dielectrics breakdowns. In *Electrical Insulation, 1998. Conference Record of the 1998 IEEE International Symposium on*, volume 2, pages 611–614. IEEE, 1998.
- [100] M. J. Kushner. Hybrid modelling of low temperature plasmas for fundamental investigations and equipment design. *J. Phys. D*, 42(19):194013, 2009. doi: 10.1088/0022-3727/42/19/194013.

- [101] M. Laroussi and T. Akan. Arc-Free Atmospheric Pressure Cold Plasma Jets: A Review. *Plasma Processes and Polymers*, 4(9):777–788, 2007. ISSN 1612-8869. doi: 10.1002/ppap.200700066.
- [102] M. Laroussi and X. Lu. Room-temperature atmospheric pressure plasma plume for biomedical applications. *Appl. Phys. Lett.*, 87(11):113902, 2005. doi: 10.1063/1.2045549.
- [103] R. Lehmann. An algorithm for the determination of all significant pathways in chemical reaction systems. *Journal of Atmospheric Chemistry*, 47(1):45–78, 2004. ISSN 0167-7764. doi: 10.1023/B:JOCH.0000012284.28801.b1.
- [104] Randall J LeVeque. *Finite volume methods for hyperbolic problems*, volume 31. Cambridge university press, 2002.
- [105] Randall J LeVeque. *Finite difference methods for ordinary and partial differential equations: steady-state and time-dependent problems*. Siam, 2007.
- [106] B. Li, R. D. White, R. E. Robson, and K. F. Ness. Transport Coefficients in Crossed E and B Fields: Empirical Relations and Nonconservative Collisional Effects. *Annals of Physics*, 292:179, 2001. doi: 10.1006/aphy.2001.6171.
- [107] C. Li, W. J. M. Brok, U. Ebert, and J. J. A. M. van der Mullen. Deviations from the local field approximation in negative streamer heads. *J. Appl. Phys.*, 101(12):123305, 2007. doi: 10.1063/1.2748673.
- [108] C. Li, U. Ebert, W. J. M. Brok, and W. Hundsdorfer. Spatial coupling of particle and fluid models for streamers: where nonlocality matters. *J. Phys. D*, 41(3):032005, 2008. doi: 10.1088/0022-3727/41/3/032005.
- [109] C. Li, U. Ebert, and W. Hundsdorfer. 3D hybrid computations for streamer discharges and production of runaway electrons. *J. Phys. D*, 42(20):202003, 2009. doi: 10.1088/0022-3727/42/20/202003.
- [110] C. Li, U. Ebert, and W. Hundsdorfer. Spatially hybrid computations for streamer discharges with generic features of pulled fronts: I. Planar fronts. *J. Comput. Phys.*, 229:200, 2010. doi: 10.1016/j.jcp.2009.09.027.
- [111] C. Li, U. Ebert, and W. Hundsdorfer. Spatially hybrid computations for streamer discharges : II. Fully 3D simulations. *J. Comput. Phys.*, 231:1020, 2012. doi: 10.1016/j.jcp.2011.07.023.
- [112] C. Li, J. Teunissen, M. Nool, W. Hundsdorfer, and U. Ebert. A comparison of 3D particle, fluid and hybrid simulations for negative streamers. *Plasma Sour. Sci. Technol.*, 21(5):055019, 2012. doi: 10.1088/0963-0252/21/5/055019.
- [113] G. G. Lister, J. E. Lawler, W. P. Lapatovich, and V. A. Godyak. The physics of discharge lamps. *Reviews of Modern Physics*, 76:541, 2004. doi: 10.1103/RevModPhys.76.541.

- [114] D. X. Liu, P. Bruggeman, F. Iza, M. Z. Rong, and M. G. Kong. Global model of low-temperature atmospheric-pressure He + H₂O plasmas. *Plasma Sour. Sci. Technol.*, 19(2):025018, 2010. doi: 10.1088/0963-0252/19/2/025018.
- [115] Z. Liu, E. M. van Veldhuizen, E. J. M. van Heesch, and A. J. M. Pemen. Strong Density Gradients in Postdischarges in Argon and Air. *IEEE Trans. Plasma Sci.*, 39:2092, 2011. doi: 10.1109/TPS.2011.2156418.
- [116] L. B. Loeb. Ionizing Waves of Potential Gradient. *Science*, 148:1417–1426, June 1965. doi: 10.1126/science.148.3676.1417.
- [117] L.B. Loeb. *Fundamental Processes of Electrical Discharge in Gases*. John Wiley & Sons, 1939.
- [118] Leonard B. Loeb and Arthur F. Kip. Electrical discharges in air at atmospheric pressure the nature of the positive and negative pointtoplane coronas and the mechanism of spark propagation. *Journal of Applied Physics*, 10(3), 1939.
- [119] Leonard B. Loeb and J. M. Meek. The mechanism of spark discharge in air at atmospheric pressure. ii. *Journal of Applied Physics*, 11(7), 1940.
- [120] Leonard B. Loeb and John M. Meek. The mechanism of spark discharge in air at atmospheric pressure. i. *Journal of Applied Physics*, 11(6), 1940.
- [121] X. Lu, M. Laroussi, and V. Puech. On atmospheric-pressure non-equilibrium plasma jets and plasma bullets. *Plasma Sour. Sci. Technol.*, 21(3):034005, 2012. doi: 10.1088/0963-0252/21/3/034005.
- [122] A. Luque. Computer code QPlaskin. <http://www.trappa.es/content/software>.
- [123] A. Luque and U. Ebert. Sprites in varying air density: Charge conservation, glowing negative trails and changing velocity. *Geophys. Res. Lett.*, 37:L06806, 2010. doi: 10.1029/2009GL041982.
- [124] A. Luque and U. Ebert. Electron density fluctuations accelerate the branching of positive streamer discharges in air. *Phys. Rev. E*, 84(4):046411, 2011. doi: 10.1103/PhysRevE.84.046411.
- [125] A. Luque and U. Ebert. Density models for streamer discharges: Beyond cylindrical symmetry and homogeneous media. *J. Comput. Phys.*, 231:904, 2012. doi: 10.1016/j.jcp.2011.04.019.
- [126] A. Luque and F. J. Gordillo-Vázquez. Mesospheric electric breakdown and delayed sprite ignition caused by electron detachment. *Nature Geoscience*, 5:22, 2012. doi: 10.1038/ngeo1314.
- [127] A. Luque and F. J. Gordillo-Vázquez. Mesospheric electric breakdown and delayed sprite ignition caused by electron detachment. *Nature Geoscience*, 5, 2012. doi: 10.1038/ngeo1357.

- [128] Alejandro Luque and Ute Ebert. Growing discharge trees with self-consistent charge transport: the collective dynamics of streamers. *New Journal of Physics*, 16(1):013039, 2014.
- [129] Satoshi Maeda, Koichi Ohno, and Keiji Morokuma. Systematic exploration of the mechanism of chemical reactions: the global reaction route mapping (grm) strategy using the addf and afir methods. *Phys. Chem. Chem. Phys.*, 15:3683–3701, 2013. doi: 10.1039/C3CP44063J.
- [130] A. Makhorin. GNU Linear Programming Kit, 4.9. <http://www.gnu.org/software/glpk/>.
- [131] A. H. Markosyan, S. Dujko, and U. Ebert. High-order fluid model for streamer discharges: II. Numerical solution and investigation of planar fronts. *J. Phys. D*, 46:475203, 2013. doi: 10.1088/0022-3727/46/47/475203.
- [132] E. Marode. The Glow-To-Arc Transition. In *NATO Advanced Science Institutes (ASI) Series B*, volume 93 of *NATO Advanced Science Institutes (ASI) Series B*, page 119, 1983. doi: 10.1007/978-1-4615-9311-9_3.
- [133] E. A. Mason and E. W. McDaniel. Transport properties of ions in gases. *NASA STI/Recon Technical Report A*, 89:15174, 1988.
- [134] D. Mathew, H. M. J. Bastiaens, K. J. Boller, and P. J. M. Peters. Effect of preionization, fluorine concentration, and current density on the discharge uniformity in F₂ excimer laser gas mixtures. *J. Appl. Phys.*, 102(3):033305, 2007. doi: 10.1063/1.2767869.
- [135] J. M. Meek. A theory of spark discharge. *Phys. Rev.*, 57:722–728, Apr 1940. doi: 10.1103/PhysRev.57.722.
- [136] A Kh Mnatsakanyan and GV Naidis. The vibrational-energy balance in a discharge in air. *High Temp.(Engl. Transl.);(United States)*, 23(4), 1986.
- [137] C. Montijn and U. Ebert. Diffusion correction to the Raether Meek criterion for the avalanche-to-streamer transition. *J. Phys. D*, 39:2979, 2006. doi: 10.1088/0022-3727/39/14/017.
- [138] C. Montijn, W. Hundsdorfer, and U. Ebert. An adaptive grid refinement strategy for the simulation of negative streamers. *J. Comput. Phys.*, 219: 801, 2006. doi: 10.1016/j.jcp.2006.04.017.
- [139] A.B. Morris, P.L. Varghese, and D.B. Goldstein. Monte carlo solution of the boltzmann equation via a discrete velocity model. *Journal of Computational Physics*, 230(4):1265 – 1280, 2011.
- [140] Keith W Morton. *Numerical solution of partial differential equations: an introduction*. Cambridge University Press, 2005.

- [141] T. Murakami, K. Niemi, T. Gans, D. O’Connell, and W. G. Graham. Chemical kinetics and reactive species in atmospheric pressure helium-oxygen plasmas with humid-air impurities. *Plasma Sour. Sci. Technol.*, 22(1): 015003, 2013. doi: 10.1088/0963-0252/22/1/015003.
- [142] James M. Murphy, David M. H. Sexton, David N. Barnett, Gareth S. Jones, Mark J. Webb, Matthew Collins, and David A. Stainforth. Quantification of modelling uncertainties in a large ensemble of climate change simulations. *Nature*, 430(7001):768–772, 8 2004. ISSN 0028-0836. doi: 10.1038/nature02771.
- [143] G. V. Naidis. Effects of nonlocality on the dynamics of streamers in positive corona discharges. *Technical Physics Letters*, 23:493, 1997. doi: 10.1134/1.1261717.
- [144] G. V. Naidis. Simulation of streamer-to-spark transition in short non-uniform air gaps. *J. Phys. D*, 32:2649, 1999. doi: 10.1088/0022-3727/32/20/311.
- [145] G. V. Naidis. Dynamics of streamer breakdown of short non-uniform air gaps. *J. Phys. D*, 38:3889, 2005. doi: 10.1088/0022-3727/38/21/009.
- [146] G. V. Naidis. Positive and negative streamers in air: Velocity-diameter relation. *Phys. Rev. E*, 79(5):057401, 2009. doi: 10.1103/PhysRevE.79.057401.
- [147] G. V. Naidis. Modelling of streamer propagation in atmospheric-pressure helium plasma jets. *J. Phys. D*, 43:402001, 2010. doi: 10.1088/0022-3727/43/40/402001.
- [148] G. V. Naidis. Modelling of plasma bullet propagation along a helium jet in ambient air. *J. Phys. D*, 44(21):215203, 2011. doi: 10.1088/0022-3727/44/21/215203.
- [149] G. V. Naidis and J. L. Walsh. The effects of an external electric field on the dynamics of cold plasma jets-experimental and computational studies. *J. Phys. D*, 46(9):095203, 2013. doi: 10.1088/0022-3727/46/9/095203.
- [150] K. F. Ness and R. E. Robson. Velocity distribution function and transport coefficients of electron swarms in gases. II. Moment equations and applications. *Phys. Rev. A*, 34:2185, 1986. doi: 10.1103/PhysRevA.34.2185.
- [151] P. Nicoletopoulos and R. E. Robson. Periodic Electron Structures in Gases: A Fluid Model of the “Window” Phenomenon. *Phys. Rev. Lett.*, 100(12): 124502, 2008. doi: 10.1103/PhysRevLett.100.124502.
- [152] S. Nijdam, J. S. Moerman, T. M. P. Briels, E. M. van Veldhuizen, and U. Ebert. Stereo-photography of streamers in air. *Appl. Phys. Lett.*, 92(10): 101502, 2008. doi: 10.1063/1.2894195.

- [153] S. Nijdam, F. M. J. H. van de Wetering, R. Blanc, E. M. van Veldhuizen, and U. Ebert. Probing photo-ionization: experiments on positive streamers in pure gases and mixtures. *J. Phys. D*, 43(14):145204, 2010. doi: 10.1088/0022-3727/43/14/145204.
- [154] S. Nijdam, K. Miermans, E. M. van Veldhuizen, and U. Ebert. A Peculiar Streamer Morphology Created by a Complex Voltage Pulse. *IEEE Trans. Plasma Sci.*, 39:2216, 2011. doi: 10.1109/TPS.2011.2158661.
- [155] S. Nijdam, G. Wormeester, E. M. van Veldhuizen, and U. Ebert. Probing background ionization: positive streamers with varying pulse repetition rate and with a radioactive admixture. *J. Phys. D*, 44:455201, 2011. doi: 10.1088/0022-3727/44/45/455201.
- [156] S Nijdam, E Takahashi, A H Markosyan, and U Ebert. Investigation of positive streamers by double-pulse experiments, effects of repetition rate and gas mixture. *Plasma Sources Science and Technology*, 23(2):025008, 2014.
- [157] William L. Ob, Sharon M. DeLand, Brian M. Rutherford, Kathleen V. Diegert, and Kenneth F. Alvin. Estimation of total uncertainty in modeling and simulation. *Sandia Report SAND2000-0824*, Albuquerque, NM, 2000.
- [158] William L. Oberkampf and Christopher J. Roy. *Verification and validation in scientific computing*. Cambridge University Press, Cambridge; New York, 2010. ISBN 0521113601.
- [159] William L. Oberkampf, Sharon M. DeLand, Brian M. Rutherford, Kathleen V. Diegert, and Kenneth F. Alvin. Error and uncertainty in modeling and simulation. *Reliability Engineering & System Safety*, 75(3):333 – 357, 2002. ISSN 0951-8320. doi: 10.1016/S0951-8320(01)00120-X.
- [160] R. Ono and T. Oda. Formation and structure of primary and secondary streamers in positive pulsed corona discharge-effect of oxygen concentration and applied voltage. *J. Phys. D*, 36:1952, 2003. doi: 10.1088/0022-3727/36/16/306.
- [161] D. Z. Pai, D. A. Lacoste, and C. O. Laux. Transitions between corona, glow, and spark regimes of nanosecond repetitively pulsed discharges in air at atmospheric pressure. *J. Appl. Phys.*, 107(9):093303, 2010. doi: 10.1063/1.3309758.
- [162] S. Pancheshnyi. Role of electronegative gas admixtures in streamer start, propagation and branching phenomena. *Plasma Sour. Sci. Technol.*, 14: 645, 2005. doi: 10.1088/0963-0252/14/4/002.
- [163] S Pancheshnyi, B. Eismann, G.J.M. Hagelaar, and L.C. Pitchford. Computer code ZDPlasKin (University of Toulouse, LAPLACE, CNRS-UPS-INP, Toulouse, France, 2008). <http://www.zdplaskin.laplace.univ-tlse.fr>.

- [164] S. Pancheshnyi, P. Ségur, J. Capeillère, and A. Bourdon. Numerical simulation of filamentary discharges with parallel adaptive mesh refinement. *J. Comput. Phys.*, 227:6574, 2008. doi: 10.1016/j.jcp.2008.03.020.
- [165] L. Pareschi and G. Russo. Asymptotic Preserving Monte Carlo Methods for the Boltzmann Equation. *Transport Theory and Statistical Physics*, 29: 415–430, 1998.
- [166] F. C. Parra-Rojas, A. Luque, and F. J. Gordillo-Vázquez. Chemical and electrical impact of lightning on the Earth mesosphere: The case of sprite halos. *J. Geophys. Res. (Space Phys)*, 118:5190, 2013. doi: 10.1002/jgra.50449.
- [167] V. Pasko. Theoretical modeling of sprites and jets. In M. Füllekrug, E. A. Mareev, and M. J. Rycroft, editors, *Sprites, Elves and Intense Lightning Discharges*, volume 225 of *NATO Science Series II: Mathematics, Physics and Chemistry*, pages 253–311. Springer Netherlands, 2006. ISBN 978-1-4020-4627-8. doi: 10.1007/1-4020-4629-4_12.
- [168] A. Pedersen, T. Christen, A. Blaszczyk, and H. Boehme. Streamer inception and propagation models for designing air insulated power devices. In *Electrical Insulation and Dielectric Phenomena, 2009. CEIDP '09. IEEE Conference on*, pages 604–607, 2009. doi: 10.1109/CEIDP.2009.5377740.
- [169] Z. L. Petrović, Z. M. Raspopović, S. Dujko, and T. Makabe. Kinetic phenomena in electron transport in radio-frequency fields. *Appl. Surf. Sci.*, 192: 1, 2002. doi: 10.1016/S0169-4332(02)00018-1.
- [170] Z. L. Petrovic, M. Suvakov, Z. Nikitovic, S. Dujko, O. Sasic, J. Jovanovic, G. Malovic, and V. Stojanovic. Kinetic phenomena in charged particle transport in gases, swarm parameters and cross section data. *Plasma Sour. Sci. Technol.*, 16:1, 2007. doi: 10.1088/0963-0252/16/1/S01.
- [171] Z. L. Petrović, S. Dujko, D. Marić, G. Malović, Ž. Nikitović, O. Šašić, J. Jovanović, V. Stojanović, and M. Radmilović-Radenović. Measurement and interpretation of swarm parameters and their application in plasma modelling. *J. Phys. D*, 42(19):194002, 2009. doi: 10.1088/0022-3727/42/19/194002.
- [172] Z Lj Petrović, S Dujko, D Marić, G Malović, Ž Nikitović, O Šašić, J Jovanović, V Stojanović, and M Radmilović-Raenović. Measurement and interpretation of swarm parameters and their application in plasma modelling. *Journal of Physics D: Applied Physics*, 42(19):194002, 2009.
- [173] A. V. Phelps and L. C. Pitchford. Anisotropic scattering of electrons by N₂ and its effect on electron transport. *Phys. Rev. A*, 31:2932, 1985. doi: 10.1103/PhysRevA.31.2932.
- [174] N. R. Pinhão. Recent developments on PLASMAKIN - a software package to model the kinetics in gas discharges. *Journal of Physics Conference Series*, 162(1):012006, 2009. doi: 10.1088/1742-6596/162/1/012006.

- [175] T. Plewa, T.J. Linde, and V.G. Weirs. *Adaptive Mesh Refinement - Theory and Applications: Proceedings of the Chicago Workshop on Adaptive Mesh Refinement Methods, Sept. 3-5, 2003*. Lecture Notes in Computational Science and Engineering. Springer, 2005. ISBN 9783540270393.
- [176] N. A. Popov. Investigation of the Mechanism for Rapid Heating of Nitrogen and Air in Gas Discharges. *Plasma Physics Reports*, 27:886, 2001. doi: 10.1134/1.1409722.
- [177] N. A. Popov. Formation and development of a leader channel in air. *Plasma Physics Reports*, 29:695, 2003. doi: 10.1134/1.1601648.
- [178] J. Qin, S. J. Celestin, V. P. Pasko, J. Li, and S. A. Cummer. Impact of successive lightning strokes on the initiation and propagation of sprite streamers. *AGU Fall Meeting Abstracts*, page A3, 2011.
- [179] H. Raether. Die entwicklung der elektronenlawine in den funkenkanal. *Zeitschrift fr Physik*, 112(7-8):464–489, 1939. ISSN 0044-3328. doi: 10.1007/BF01340229.
- [180] H. Raether. *Electron avalanches and breakdown in gases*. Butterworths advanced physics series: Monographs on ionization and electrical discharges in gases. Butterworths, 1964.
- [181] Y.P. Raizer, M.N. Shneider, and N.A. Yatsenko. *Radio-Frequency Capacitive Discharges*. Taylor & Francis, 1995. ISBN 9780849386442.
- [182] Gorur G Raju. *Gaseous Electronics: Tables, Atoms, and Molecules*. CRC Press, 2011.
- [183] V. Ratushnaya. Electrodynamic characterization of long positive streamers in air. in preparation.
- [184] J. A. Riouset, V. P. Pasko, and A. Bourdon. Air-density-dependent model for analysis of air heating associated with streamers, leaders, and transient luminous events. *J. Geophys. Res. (Space Phys)*, 115:A12321, 2010. doi: 10.1029/2010JA015918.
- [185] P.J. Roache. *Verification and Validation in Computational Science and Engineering*. Hermosa Publishers, 1998. ISBN 9780913478080.
- [186] R. E. Robson. Generalized Einstein relation and negative differential conductivity in gases. *Australian Journal of Physics*, 37:35, 1984.
- [187] R. E. Robson. Physics of reacting particle swarms in gases. *J. Chem. Phys.*, 85:4486, 1986. doi: 10.1063/1.451769.
- [188] R. E. Robson. Transport phenomena in the presence of reactions: Definition and measurement of transport coefficients. *Australian Journal of Physics*, 44:685, 1991.

- [189] R. E. Robson. The Steady State Townsend Experiment - Comparison of Boltzmann Equation and Diffusion Equation Analysis. *Australian Journal of Physics*, 48:347, 1995.
- [190] R. E. Robson and K. F. Ness. Velocity distribution function and transport coefficients of electron swarms in gases: Spherical-harmonics decomposition of Boltzmann's equation. *Phys. Rev. A*, 33:2068, 1986. doi: 10.1103/PhysRevA.33.2068.
- [191] R. E. Robson and K. F. Ness. Physics of reacting particle swarms. III. Effects of ionization upon transport coefficients. *J. Chem. Phys.*, 89:4815, 1988. doi: 10.1063/1.455675.
- [192] R. E. Robson, R. D. White, and Z. L. Petrović. Colloquium: Physically based fluid modeling of collisionally dominated low-temperature plasmas. *Reviews of Modern Physics*, 77:1303, 2005. doi: 10.1103/RevModPhys.77.1303.
- [193] R. E. Robson, P. Nicoletopoulos, B. Li, and R. D. White. Kinetic theoretical and fluid modelling of plasmas and swarms: the big picture. *Plasma Sour. Sci. Technol.*, 17(2):024020, 2008. doi: 10.1088/0963-0252/17/2/024020.
- [194] A.D. Rubio, A. Zalts, and C.D. El Hasi. Numerical solution of the advectionreactiondiffusion equation at different scales. *Environmental Modelling & Software*, 23(1):90 – 95, 2008. ISSN 1364-8152. doi: <http://dx.doi.org/10.1016/j.envsoft.2007.05.009>.
- [195] D.W. Ruth and A.K. MacPherson. On iterative and Monte Carlo solutions of the Boltzmann equation. *Zeitschrift für angewandte Mathematik und Physik ZAMP*, 25(2):189–194, 1974. ISSN 0044-2275. doi: 10.1007/BF01591320.
- [196] Y. Sakai, H. Tagashira, and S. Sakamoto. The development of electron avalanches in argon at high E/N values. I. Monte Carlo simulation. *J. Phys. D*, 10:1035, 1977. doi: 10.1088/0022-3727/10/7/010.
- [197] S. Samukawa, M. Hori, S. Rauf, K. Tachibana, P. Bruggeman, G. Kroesen, J. C. Whitehead, A. B. Murphy, A. F. Gutsol, S. Starikovskaia, U. Kortshagen, J.-P. Boeuf, T. J. Sommerer, M. J. Kushner, U. Czarnetzki, and N. Mason. The 2012 Plasma Roadmap. *J. Phys. D*, 45(25):253001, 2012. doi: 10.1088/0022-3727/45/25/253001.
- [198] A. Sandu and R. Sander. Technical note: Simulating chemical systems in Fortran90 and Matlab with the Kinetic PreProcessor KPP-2.1. *Atmospheric Chemistry & Physics*, 6:187, 2006.
- [199] R. Schuster and S. Schuster. Refined algorithm and computer program for calculating all non-negative fluxes admissible in steady states of biochemical reaction systems with or without some flux rates fixed. *Computer applications in the biosciences: CABIOS*, 9(1):79–85, 1993.

- [200] S. Schuster, C. Hilgetag, J.H. Woods, and D.A. Fell. Reaction routes in biochemical reaction systems: Algebraic properties, validated calculation procedure and example from nucleotide metabolism. *Journal of Mathematical Biology*, 45(2):153–181, 2002. ISSN 0303-6812. doi: 10.1007/s002850200143.
- [201] Alan A Sebastian and J M Wadehra. Time-dependent behaviour of electron transport in methane-argon mixtures. *Journal of Physics D: Applied Physics*, 38(10):1577, 2005.
- [202] M. Seeger, L. Niemeyer, and M. Bujotzek. Leader propagation in uniform background fields in SF₆. *J. Phys. D*, 42(18):185205, 2009. doi: 10.1088/0022-3727/42/18/185205.
- [203] M. Seeger, M. Schwinne, R. Bini, N. Mahdizadeh, and T. Votteler. Dielectric recovery in a high-voltage circuit breaker in SF₆. *J. Phys. D*, 45:395204, 2012. doi: 10.1088/0022-3727/45/39/395204.
- [204] D. D. Sentman, H. C. Stenbaek-Nielsen, M. G. McHarg, and J. S. Morrill. Correction to “Plasma chemistry of sprite streamers”. *J. Geophys. Res. (Atmos.)*, 113:D14399, 2008. doi: 10.1029/2008JD010634.
- [205] T. Shao, G.S. Sun, P. Yan, J. Wang, W.Q. Yuan, Y.H. Sun, and S.C. Zhang. An experimental investigation of repetitive nanosecond-pulse breakdown in air. *J. Phys. D: Appl. Phys.*, 39(10):2192–2197, MAY 21 2006. ISSN 0022-3727. doi: 10.1088/0022-3727/39/10/030.
- [206] Wenxia Sima, Qingjun Peng, Qing Yang, Tao Yuan, and Jian Shi. Study of the characteristics of a streamer discharge in air based on a plasma chemical model. *Dielectrics and Electrical Insulation, IEEE Transactions on*, 19(2):660–670, 2012. ISSN 1070-9878. doi: 10.1109/TDEL.2012.6180261.
- [207] H R Skullerud and S Kuhn. On the calculation of ion and electron swarm properties by path integral methods. *Journal of Physics D: Applied Physics*, 16(7):1225, 1983.
- [208] A. Sobota, F. Manders, E. M. van Veldhuizen, J. van Dijk, and M. Haverlag. The Role of Metastables in the Formation of an Argon Discharge in a Two-Pin Geometry. *IEEE Trans. Plasma Sci.*, 38:2289, 2010. doi: 10.1109/TPS.2010.2056934.
- [209] Zbyněk Sokol. Comparison of several numerical schemes applied to advection equations. *Quarterly Journal of the Royal Meteorological Society*, 125(553):213–224, 1999. ISSN 1477-870X. doi: 10.1002/qj.49712555312.
- [210] S. M. Starikovskaia. Plasma assisted ignition and combustion. *J. Phys. D*, 39:265, 2006. doi: 10.1088/0022-3727/39/16/R01.
- [211] S. M. Starikovskaia, A. Y. Starikovskii, and D. V. Zatsépin. Hydrogen oxidation in a stoichiometric hydrogen-air mixture in the fast ionization wave. *Combustion Theory Modelling*, 5:97, 2001. doi: 10.1088/1364-7830/5/1/306.

- [212] A. Starikovskiy and N. Aleksandrov. Plasma-assisted ignition and combustion. *Progress in Energy and Combustion Science*, 39(1):61 – 110, 2013. ISSN 0360-1285.
- [213] J. W. Stock, C. S. Boxe, R. Lehmann, J. L. Grenfell, A. B. C. Patzer, H. Rauer, and Y. L. Yung. Chemical pathway analysis of the Martian atmosphere: CO₂-formation pathways. *Icarus*, 219:13–24, May 2012. doi: 10.1016/j.icarus.2012.02.010.
- [214] J. W. Stock, J. L. Grenfell, R. Lehmann, A. B. C. Patzer, and H. Rauer. Chemical pathway analysis of the lower Martian atmosphere: The CO₂ stability problem. *Plan. Spac. Sci.*, 68:18, 2012. doi: 10.1016/j.pss.2011.03.002.
- [215] V. D. Stojanovic and Z. L. Petrovic. Comparison of the results of Monte Carlo simulations with experimental data for electron swarms in N₂ from moderate to very high electric field to gas density ratios (E/N). *J. Phys. D*, 31:834, 1998. doi: 10.1088/0022-3727/31/7/013.
- [216] H. Struchtrup. *Macroscopic Transport Equations for Rarefied Gas Flows: Approximation Methods in Kinetic Theory*. Interaction of Mechanics and Mathematics. Springer, 2006. ISBN 9783540323860.
- [217] M. Surendra. Radiofrequency discharge benchmark model comparison. *Plasma Sources Science and Technology*, 4(1):56, 2 1995. ISSN 0963-0252. doi: 10.1088/0963-0252/4/1/007.
- [218] E. Takahashi, S. Kato, A. Sasaki, Y. Kishimoto, and H. Furutani. Controlling branching in streamer discharge by laser background ionization. *J. Phys. D*, 44(7):075204, 2011. doi: 10.1088/0022-3727/44/7/075204.
- [219] R. Trompert and J. Verwer. Analysis of the Implicit Euler Local Uniform Grid Refinement Method. *SIAM Journal on Scientific Computing*, 14(2): 259–278, 1993. doi: 10.1137/0914017.
- [220] M. M. Turner, A. Derzsi, Z. Donkó, D. Eremin, S. J. Kelly, T. Lafleur, and T. Mussenbrock. Simulation benchmarks for low-pressure plasmas: Capacitive discharges. *Physics of Plasmas*, 20(1):013507, 2013. doi: 10.1063/1.4775084.
- [221] Miles Turner. Verification and Validation in Low Temperature Plasma Physics. *Bulletin of the American Physical Society*, 58, 2013.
- [222] MM Turner and M Vukovic. Overview of Verification and Validation in Low Temperature Plasma Physics. *Bulletin of the American Physical Society*, 57, 2012.
- [223] S. Turns. *An Introduction to Combustion: Concepts and Applications*. McGraw-Hill, New York, USA, 2012.

- [224] J. van Dijk, K. Peerenboom, M. Jimenez, D. Mihailova, and J. van der Mullen. The plasma modelling toolkit Plasimo. *J. Phys. D*, 42(19):194012, 2009. doi: 10.1088/0022-3727/42/19/194012.
- [225] W. Van Gaens and A. Bogaerts. Kinetic modelling for an atmospheric pressure argon plasma jet in humid air. *J. Phys. D*, 46(26):275201, 2013. doi: 10.1088/0022-3727/46/27/275201.
- [226] E. J. M. van Heesch, G. J. J. Winands, and A. J. M. Pemen. Evaluation of pulsed streamer corona experiments to determine the O^* radical yield. *J. Phys. D*, 41(23):234015, 2008. doi: 10.1088/0022-3727/41/23/234015.
- [227] E. M. van Veldhuizen. *Electrical Discharges for Environmental Purposes: Fundamentals and Applications*. Nova Science Publishers, New York, 2000.
- [228] P. A. Vitello, B. M. Penetrante, and J. N. Bardsley. Simulation of negative-streamer dynamics in nitrogen. *Phys. Rev. E*, 49:5574, 1994. doi: 10.1103/PhysRevE.49.5574.
- [229] S. B. Vrhovac and Z. L. Petrović. Momentum transfer theory of nonconservative charged particle transport in mixtures of gases: General equations and negative differential conductivity. *Phys. Rev. E*, 53:4012, 1996. doi: 10.1103/PhysRevE.53.4012.
- [230] J. L. Walsh, F. Iza, N. B. Janson, and M. G. Kong. Chaos in atmospheric-pressure plasma jets. *Plasma Sour. Sci. Technol.*, 21(3):034008, 2012. doi: 10.1088/0963-0252/21/3/034008.
- [231] Sima Wen-Xia, Peng Qing-Jun, Yang Qing, Yuan Tao, and Shi Jian. Local electron mean energy profile of positive primary streamer discharge with pin-plate electrodes in oxygen/nitrogen mixtures. *Chinese Physics B*, 22(1):015203, 1 2013. ISSN 1674-1056. doi: 10.1088/1674-1056/22/1/015203.
- [232] R. D. White, K. F. Ness, and R. E. Robson. Development of swarm transport theory in radio-frequency electric and crossed electric and magnetic fields. *Appl. Surf. Sci.*, 192:26, 2002. doi: 10.1016/S0169-4332(02)00019-3.
- [233] R. D. White, R. E. Robson, B. Schmidt, and M. A. Morrison. Is the classical two-term approximation of electron kinetic theory satisfactory for swarms and plasmas? *J. Phys. D*, 36:3125, 2003. doi: 10.1088/0022-3727/36/24/006.
- [234] R. D. White, R. E. Robson, S. Dujko, P. Nicoletopoulos, and B. Li. Recent advances in the application of Boltzmann equation and fluid equation methods to charged particle transport in non-equilibrium plasmas. *J. Phys. D*, 42(19):194001, 2009. doi: 10.1088/0022-3727/42/19/194001.
- [235] Mark H. Wilcoxson and Vasilios I. Manousiouthakis. Simulation of a three-moment fluid model of a two-dimensional radio frequency discharge. *Chemical Engineering Science*, 51(7):1089 – 1106, 1996. ISSN 0009-2509. doi: 10.1016/S0009-2509(96)80008-X.

- [236] G. J. J. Winands, K. Yan, A. J. M. Pemen, S. A. Nair, Z. Liu, and E. J. M. van Heesch. An Industrial Streamer Corona Plasma System for Gas Cleaning. *IEEE Trans. Plasma Sci.*, 34:2426, 2006. doi: 10.1109/TPS.2006.881278.
- [237] G. J. J. Winands, Z. Liu, A. J. M. Pemen, E. J. M. van Heesch, and K. Yan. Analysis of streamer properties in air as function of pulse and reactor parameters by ICCD photography. *J. Phys. D*, 41(23):234001, 2008. doi: 10.1088/0022-3727/41/23/234001.
- [238] R. Winkler, D. Loffhagen, and F. Sigeneger. Temporal and spatial relaxation of electrons in low temperature plasmas. *Applied Surface Science*, 192(14):50 – 71, 2002. ISSN 0169-4332. doi: [http://dx.doi.org/10.1016/S0169-4332\(02\)00020-X](http://dx.doi.org/10.1016/S0169-4332(02)00020-X). Advance in Low Temperature {RF} Plasmas.
- [239] Paul Woodward and Phillip Colella. The numerical simulation of two-dimensional fluid flow with strong shocks. *Journal of Computational Physics*, 54(1):115 – 173, 1984. ISSN 0021-9991. doi: [http://dx.doi.org/10.1016/0021-9991\(84\)90142-6](http://dx.doi.org/10.1016/0021-9991(84)90142-6).
- [240] Z. Xiong and M. J. Kushner. Atmospheric pressure ionization waves propagating through a flexible high aspect ratio capillary channel and impinging upon a target. *Plasma Sour. Sci. Technol.*, 21(3):034001, 2012. doi: 10.1088/0963-0252/21/3/034001.
- [241] M. Yousfi, O. Eichwald, N. Merbahi, and N. Jomaa. Analysis of ionization wave dynamics in low-temperature plasma jets from fluid modeling supported by experimental investigations. *Plasma Sour. Sci. Technol.*, 21(4):045003, 2012. doi: 10.1088/0963-0252/21/4/045003.
- [242] Q.-Z. Zhang, Y.-X. Liu, W. Jiang, A. Bogaerts, and Y.-N. Wang. Heating mechanism in direct current superposed single-frequency and dual-frequency capacitively coupled plasmas. *Plasma Sour. Sci. Technol.*, 22(2):025014, 2013. doi: 10.1088/0963-0252/22/2/025014.

APPENDIX A

Discretization of the high order fluid model

Know how to solve every problem that has ever been solved.

– RICHARD FEYNMAN

In this appendix we briefly describe the discretization of our system of differential equations. The finite volume method is used to discretize the system (3.7)-(3.12) in space. The basic principle of the control volume method is to maintain the conservative properties of the system (3.7) over every volume element. We introduce control volumes or cells V_j as follows:

$$V_j := [j\Delta x, (j+1)\Delta x], \quad x_j := \left(j + \frac{1}{2}\right) \Delta x, \quad j = 0, 1, \dots, M-1, \quad (\text{A.1})$$

where $\Delta x = L/M$ is the spatial grid size while L is the length of the simulation domain.

The numerical solution $\bar{\mathbf{u}}_j(t)$ has to be interpreted as an approximation of the average value of $\mathbf{u}(x, t)$ over the control volume V_j at time t , i.e.

$$\bar{\mathbf{u}}_j(t) = \frac{1}{\Delta x} \int_{V_j} \mathbf{u}(x, t) dx. \quad (\text{A.2})$$

To approximate the spatial derivative in (3.7) we use the second-order central difference discretization [83],

$$\frac{\partial \mathbf{u}(x, t)}{\partial x} = \frac{1}{2\Delta x} (\mathbf{u}(x + \Delta x, t) - \mathbf{u}(x - \Delta x, t)) + \mathcal{O}(\Delta x^2), \quad (\text{A.3})$$

which has already been used in previous first order fluid models and associated codes (see for example [107]). Hence, the equation (3.7) can be re-written in difference form:

$$\frac{\partial \bar{\mathbf{u}}_j(t)}{\partial t} + \frac{1}{2\Delta x} \mathbf{A}(\bar{\mathbf{u}}_j(t))(\bar{\mathbf{u}}_{j+1}(t) - \bar{\mathbf{u}}_{j-1}(t)) = \mathbf{F}(\bar{\mathbf{u}}_j(t)), \quad (\text{A.4})$$

where $i = 1, 2, \dots, M - 2$.

As discussed in the main text, homogeneous Neumann or Dirichlet boundary conditions are imposed: At the left boundary, $i = 0$, we impose a homogeneous Neumann boundary condition

$$\frac{\partial \mathbf{u}(0, t)}{\partial x} = 0 \quad \text{or} \quad \bar{\mathbf{u}}_{-1}(t) = \bar{\mathbf{u}}_0(t). \quad (\text{A.5})$$

In this manner, we provide the value $\bar{\mathbf{u}}_{-1}(t) = \mathbf{u}(-\frac{1}{2}\Delta x, t)$ at $i = -1$ which exceeds the computational domain. At the right boundary, $i = M - 1$, we impose a homogeneous Dirichlet boundary condition for the electron number density, while for the other components of \mathbf{u} we impose homogeneous Neumann boundary conditions to obtain a value for $\bar{\mathbf{u}}_M(t) = \mathbf{u}(L + \frac{1}{2}\Delta x, t)$.

To approximate the electric potential φ (3.6) we use the same strategy as for the primitive variables \mathbf{u} , i.e. φ is averaged over control volumes. Hence, the electric field $E(x, t)$ is discretized on the edges of the control volume, denoted by $E(x_{j-\frac{1}{2}}, t)$. But since we consider a 1D case, the electric field follows directly from the charge densities by integrating equation (3.12) along the x -direction:

$$E(x, t) = E(0, t) + \frac{e}{\epsilon_0} \left(\int_0^x (n_{ion}(x', t) - n(x', t)) dx' \right). \quad (\text{A.6})$$

We then can calculate $E(x_j, t)$ by:

$$E(x_j, t) = \frac{1}{2}(E(x_{j-\frac{1}{2}}, t) + E(x_{j+\frac{1}{2}}, t)). \quad (\text{A.7})$$

Now we are going to consider the ODE system (A.4). To approximate the time derivatives we use classical RK4 (Rounge-Kutta 4) time-integration scheme [83], which is a fourth order method. This is an explicit method which always has a bounded stability domain. In our case the stability condition has the following form:

$$\max_{1 \leq i \leq 4} |\lambda_i \Delta t / 2\Delta x| \leq C, \quad (\text{A.8})$$

or by taking into account $\beta \geq \sqrt{\beta + \sqrt{\beta(\beta - 1)}}$, when $\beta \geq 1$, we have:

$$\beta \frac{\Delta t}{2\Delta x} \sqrt{\frac{2 \max \varepsilon}{3m}} \leq C. \quad (\text{A.9})$$

This condition is called CFL stability criterion, where C depends on the particular time-integration method and space discretization. In our simulations, C is set to 0.1.

APPENDIX B

PumpKin algorithm

Thought is only a flash between two long nights, but this flash is everything.

– HENRI POINCARÉ

Prediction is very difficult, especially about the future.

– NIELS BOHR

In this section we briefly describe the algorithm underlying PumpKin. For a more detailed description and discussion about the algorithm we refer to [103].

B.1 Basic definitions

We assume the chemical reactions R_j , $j = 1, \dots, n_R$, involving species S_i , $i = 1, \dots, n_S$. Beside of R_j , it is assumed that the stoichiometric coefficients s_{ij} , which represent the number of molecules of species S_i produced (or negative number of molecules of S_i consumed) by reaction R_j , are given. For simplicity, PumpKin assumes only unidirectional reactions and in case of reversible reactions, it is the responsibility of the user to split them into forward and backward steps, incorporating external sources and sinks as “pseudo-reactions”.

We assume that the user has already integrated the chemical model, following the temporal evolution of species S_i during the time interval $[0, T]$ which was divided, in general non-uniformly, into n_T parts. That is, for every species S_i and reaction R_j we know the concentrations $c_i(t_l)$ and the reaction rates $r_j(t_l)$, where $l = 1, \dots, n_T$.

For a given time interval $[t_0, t_{end}] \subseteq [0, T]$ we can calculate

$$\Delta c_i = c_i(t_{end}) - c_i(t_0), \quad i = 1, \dots, n_S, \quad (\text{B.1})$$

$$c_i = \frac{1}{\Delta t} \cdot \int_{t_0}^{t_{end}} c_i(t) dt, \quad i = 1, \dots, n_S, \quad (\text{B.2})$$

$$r_j = \frac{1}{\Delta t} \cdot \int_{t_0}^{t_{end}} r_j(t) dt, \quad j = 1, \dots, n_R, \quad (\text{B.3})$$

where $\Delta t = t_{end} - t_0$, Δc_i and c_i are, respectively, the change of the concentration and the mean concentration of species S_i in the time window $[t_0, t_{end}]$; r_j is the mean rate of the reaction R_j in the time interval $[t_0, t_{end}]$. In the rest of this paper we will use *rate* for r_j , omitting the attribute *mean*. In this work we assume that c_i has units of [molecules cm^{-3}] and that r_j has units of [molecules $\text{cm}^{-3} \text{s}^{-1}$].

Ideally, we should have conservation of the concentration changes Δc_i

$$\Delta c_i = \sum_{j=1}^{n_R} s_{ij} \cdot r_j \cdot \Delta t, \quad \text{for every } i = 1, \dots, n_S, \quad (\text{B.4})$$

but, due to numerical inaccuracies in the kinetic solver and to the finite time steps, the conservation (B.4) will usually be violated within the user's input. We take as the definition of Δc_i the formula (B.4), instead of (B.2).

One of the key questions that we want to answer is: *How, i.e., by the interaction of which reactions, are certain species produced or destroyed?* Obviously, we can determine the reactions that produce (or destroy) the species directly. But if such a reaction consumes (or produces) another specie whose chemical lifetime is shorter than the time scale of interest, then it is necessary to follow the chemical 'fate' of that species. This leads to the idea of forming *pathways*, i.e. reaction sequences, that produce (or destroy) a chemical species of interest.

Let us denote by P_k , where $k = 1, \dots, n_P$, the set of pathways. The given pathway P_k is described by the set $\{x_{jk}, m_{ik}, f_k\}$, where

- x_{jk} is the multiplicity of reaction R_j in the pathway P_k (zero if R_j does not occur in P_k), $j = 1, \dots, n_R$, $k = 1, \dots, n_P$,
- m_{ik} is the positive (negative) number of molecules of S_i produced (consumed) by the pathway P_k , $i = 1, \dots, n_S$, $k = 1, \dots, n_P$,
- f_k is the rate of pathway P_k , $k = 1, \dots, n_P$.

Then, by the definition of x_{jk} and the stoichiometric coefficients s_{ij} , we have

$$m_{ik} = \sum_{j=1}^{n_R} s_{ij} \cdot x_{jk}. \quad (\text{B.5})$$

If we multiply both sides of (B.5) by f_k , we get

$$m_{ik} \cdot f_k = \sum_{j=1}^{n_R} s_{ij} \cdot (x_{jk} \cdot f_k), \quad (\text{B.6})$$

which illustrates that $x_{jk} \cdot f_k$ is the portion of the rate r_j of reaction R_j associated with the pathway P_k .

We take into account the effects of deleted pathways with small rates (in next section). For this, we introduce the additional variables \tilde{r}_j , which represent the part of the rate of reaction R_j associated with the deleted pathways, and \tilde{p}_i (and \tilde{d}_i) representing the rate of the production (and destruction) of species S_i by deleted pathways. In this case, the rate of each reaction will be totally distributed to pathways, including the effect of the deleted ones

$$r_j = \tilde{r}_j + \sum_{k=1}^{n_P} x_{jk} \cdot f_k. \quad (\text{B.7})$$

On the other hand, the total rate of production p_i and destruction d_i of a species S_i by all pathways, including the effect of deleted pathways, are

$$p_i = \tilde{p}_i + \sum_{\{k \mid m_{ik} > 0\}} m_{ik} \cdot f_k, \quad (\text{B.8})$$

$$d_i = \tilde{d}_i + \sum_{\{k \mid m_{ik} < 0\}} m_{ik} \cdot f_k. \quad (\text{B.9})$$

Although p_i , d_i , \tilde{p}_i and \tilde{d}_i are changed at different steps inside the algorithm, we always ensure that we don't violate the balance between the production, consumption and concentration change of a species (B.4) and the following holds at any point:

$$\Delta c_i = (p_i - d_i) \cdot \Delta t. \quad (\text{B.10})$$

The mean rate δ_i of the concentration change of species S_i is defined as $\Delta c_i / \Delta t$. Besides, we also need the auxiliary variable D_i defined as

$$D_i = \max\{p_i, d_i\} = \begin{cases} p_i = d_i + \delta_i & \text{if } \Delta c_i \geq 0, \\ d_i = p_i + |\delta_i| & \text{if } \Delta c_i < 0. \end{cases} \quad (\text{B.11})$$

A reaction sequence P'_k is called *sub-pathway* of a pathway P_l if all intermediate species, corresponding to the branching-points, are at steady state and the set of all reactions from P'_k is a subset of the set of reactions of P_l , i.e.

$$R(P'_k) \subset R(P_l), \quad (\text{B.12})$$

where $R(P_l) := \{j \in \{1, \dots, n_R\} \mid x_{jl} \neq 0\}$. A pathway is called *elementary* if it does not contain sub-pathways (condition(C3') from [200]).

B.2 Description of the algorithm

Algorithm 1 summarizes in pseudo-code the steps in the PumpKin code.

B.2.1 Initialization.

The algorithm starts with a list of pathways, each containing only one reaction:

$$x_{jk} = \begin{cases} 1 & \text{if } j = k, \\ 0 & \text{else,} \end{cases} \quad j, k = 1, \dots, n_R. \quad (\text{B.13})$$

Algorithm 1 PumpKin algorithm.

```

1: begin
2: read input files                                {Section 6.3.1}
3: initialize pathways := individual pathways      {Section B.2.1}
4: chose branching-point  $S_b$                       {Section B.2.2}
5: repeat
6:   merge pathways producing  $S_b$  with pathways consuming  $S_b$     {Section
   B.2.3}
7:   delete pathways with a rate less than  $f_{min}$                 {Section B.2.4}
8:   determine and split sub-pathways                  {Section B.2.5}
9: until the new branching-point  $S_b$  is found
10: ouput                                             {Section B.2.5}
11: end.

```

To each pathway we assign the rate of the corresponding reaction, i.e. $f_k = r_k$, $k = 1, \dots, n_R$. The book-keeping variables \tilde{r}_j , \tilde{p}_i and \tilde{d}_i are set equal to zero.

B.2.2 Branching-points.

Depending on the time scale of interest and the lifetime of species of interest, the user might need to exclude certain species from the list of branching points. For this, user can define lifetime threshold τ_{min} . In this case the species with lifetime greater than τ_{min} are considered as long-lived species and not used as branching points. Then, for every species S_i with a lifetime shorter than τ_{min} and that has not been a branching point yet, we calculate its lifetime τ_i with respect to the pathways constructed so far:

$$\tau_i = \frac{c_i}{d_i}, \quad (\text{B.14})$$

with c_i from (B.2) and d_i from (B.9). As the next branching point we choose the species with the shortest lifetime τ_i .

B.2.3 Merging pathways.

Let us assume that we are given branching-point species S_b and that so far we have constructed pathways P_k , $k = 1, \dots, n_P$. Then we perform the following steps:

- Every pathway P_k producing the species S_b is connected with each pathway P_l consuming S_b . Let us denote the resulting pathway by P_n . The number of molecules m_{in} of S_i and the corresponding multiplicities x_{jn} of the reactions R_j in the pathway P_n can be calculated as

$$m_{in} = m_{ik} \cdot |m_{bl}| + m_{il} \cdot m_{bk}, \quad i = 1, \dots, n_S, \quad (\text{B.15})$$

$$x_{jn} = x_{jk} \cdot |m_{bl}| + x_{jl} \cdot m_{bk}, \quad j = 1, \dots, n_R. \quad (\text{B.16})$$

Equation (B.15) ensures that the constructed pathway P_n fully recycles S_b , that is, it has no net production or consumption of S_b .

The rate f_n of the new pathway P_n is calculated using the branching probabilities discussed in [103] and reads

$$f_n = \frac{f_k \cdot f_l}{D_b}. \quad (\text{B.17})$$

- If $\Delta c_b \neq 0$, we store the contribution of P_k to Δc_b by introducing a new pathway P_n that is identical to P_k , but has a rate

$$f_n = \begin{cases} f_k \cdot \delta_b / D_b, & \text{if } \Delta c_b > 0 \\ f_k \cdot |\delta_b| / D_b, & \text{if } \Delta c_b < 0 \end{cases}. \quad (\text{B.18})$$

- We remove all the pathways that have been connected with all partners. Pathways that neither produce nor consume S_b are not affected.

B.2.4 Deletion of insignificant pathways.

Even when the total number of reactions is relatively low, PumpKin may generate an excessive number of pathways. To avoid this “combinatorial explosion”, we delete a newly formed pathway P_n if its rate f_n is less than the user-specified threshold f_{min} . To keep track of the contribution from the deleted pathways, we update equations (B.7)-(B.9) in the following way

$$\tilde{r}_j := \tilde{r}_j + x_{jn} \cdot f_n, \quad j = 1, \dots, n_R, \quad (\text{B.19})$$

$$\tilde{p}_i := \tilde{p}_i + m_{in} \cdot f_n, \quad \text{if } m_{in} > 0, \quad i = 1, \dots, n_S, \quad (\text{B.20})$$

$$\tilde{d}_i := \tilde{d}_i + m_{in} \cdot f_n, \quad \text{if } m_{in} < 0, \quad i = 1, \dots, n_S, \quad (\text{B.21})$$

where x_{jn} is the multiplicity of reaction R_j in P_n , and m_{in} is the number of molecules of S_i produced by P_n . More details are discussed in [103].

B.2.5 Sub-pathways.

In section B.2.4 we discussed the procedure to limit the growth of total number of pathways in our algorithm. On the other hand, when two pathways are connected, it may happen that the resulting reaction sequence is unnecessarily complicated, i.e. it contains other pathways as sub-pathways.

As described in section B.2.4, we often eliminate “insignificant” pathways; so it is not enough to check whether other pathways constructed so far are sub-pathways of P_n . Instead, for a given pathway P_n we determine all elementary sub-pathways P'_k , $k = 1, \dots, n_{P'}$, using the algorithm by Schuster and Schuster [103, 199]. This method has a limitation, namely, it requires that all intermediate species, i.e. branching-points, are at steady state

$$\sum_{j=1}^{n_R} x_{jn} \cdot s_{ij} = 0 \text{ for all } i \text{ for which } S_i \text{ has been a branching point.} \quad (\text{B.22})$$

The condition (B.22) can be enforced by adding “pseudo-reactions” to the pathway P_n , with multiplicity $|m_{in}|$ for all previous branching-points S_i ,

$$S_i \rightarrow \dots \quad \text{if } m_{in} > 0, \quad (\text{B.23})$$

$$S_i \leftarrow \dots \quad \text{if } m_{in} < 0. \quad (\text{B.24})$$

Once we have the sub-pathways P'_k , $k = 1, \dots, n_{P'}$, of a pathway P_n , then we represent P_n as a linear combination (with non-negative wights w_k) of these sub-pathways, i.e.

$$x_{jn} = \sum_{k=1}^{n_{P'}} w_k \cdot x'_{jk}, \quad j = 1, \dots, n_R, \quad (\text{B.25})$$

where x_{jn} and x'_{jk} are the multiplicities of reaction R_j in pathway P_n and sub-pathway P'_k , respectively. Such representation is justified in [200]. The rate f_n of P_n will be distributed to the sub-pathways according to

$$f'_k = w_k \cdot f_n, \quad k = 1, \dots, n_{P'}. \quad (\text{B.26})$$

The equation (B.25) leads to a linear optimization problem [103], which we solve by the simplex method employing the GPLK package [130]. Then, we search for the sub-pathways P'_k , $k = 1, \dots, n_{P'}$, in the list of pathways constructed so far by the main part of the algorithm. If P'_k is contained in that list, then we add f'_k to its rate, otherwise, we add P'_k as a new entry with rate f'_k .

APPENDIX C

List of reactions used in chemical model

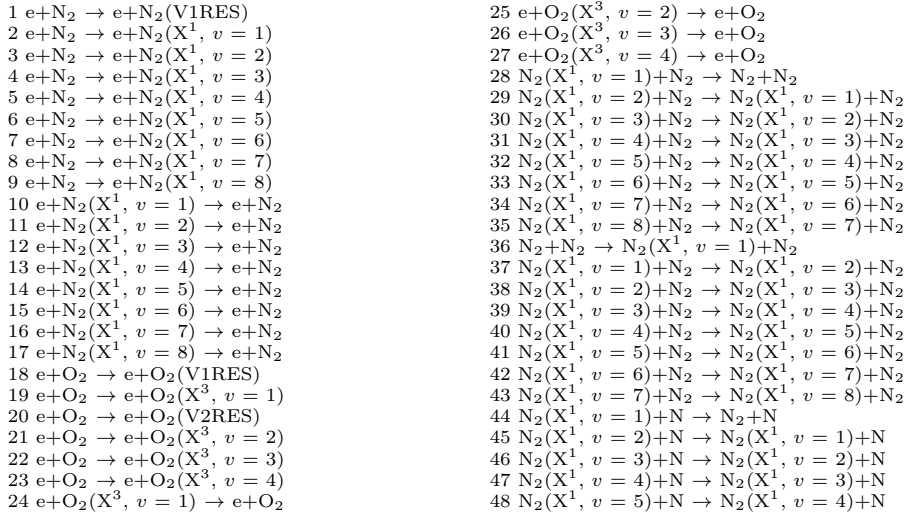
The creator of the universe works in mysterious ways. But he uses a base ten counting system and likes round numbers.

– SCOTT ADAMS

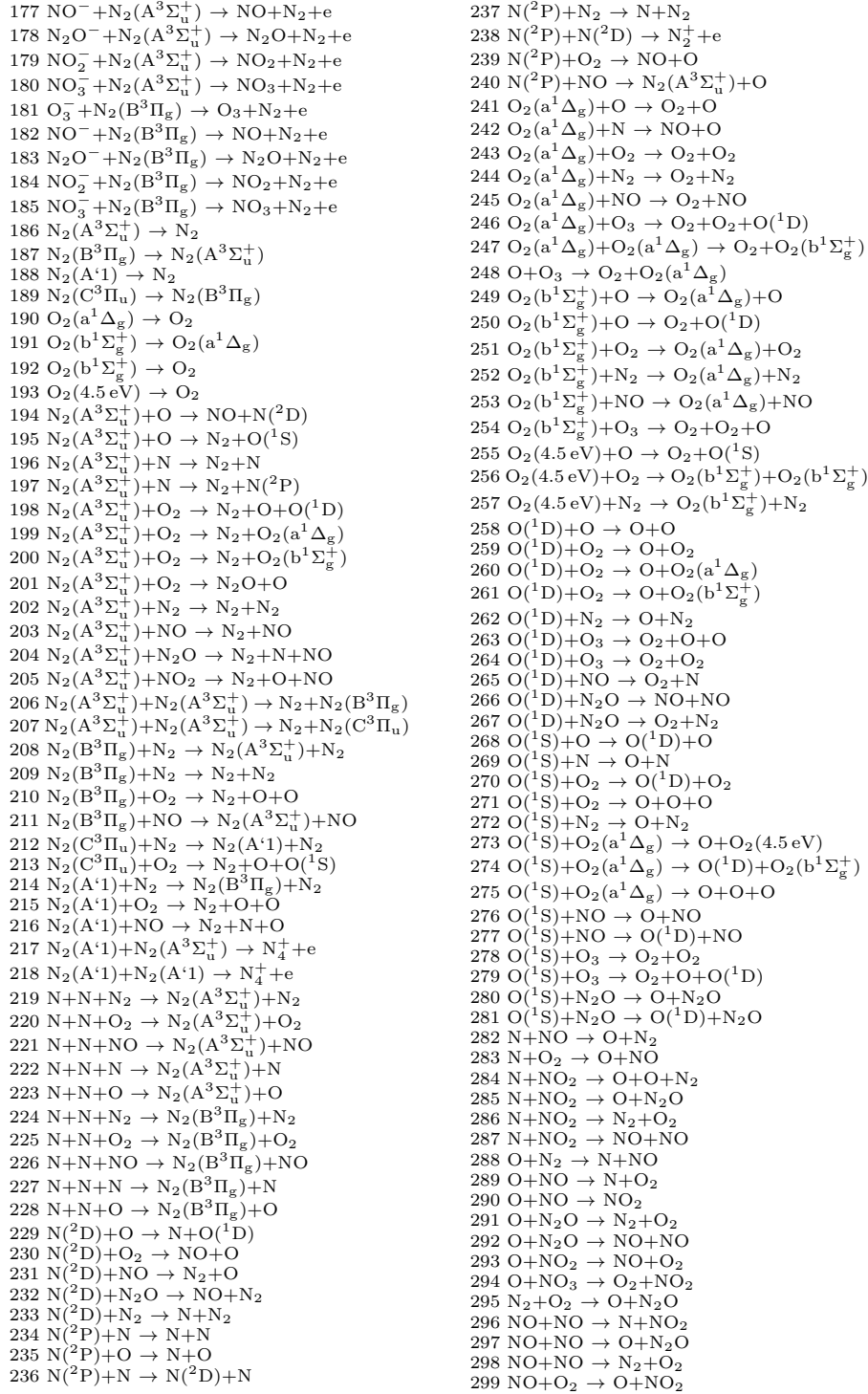
A complex system that works is invariably found to have evolved from a simple system that works.

– JOHN GAULE

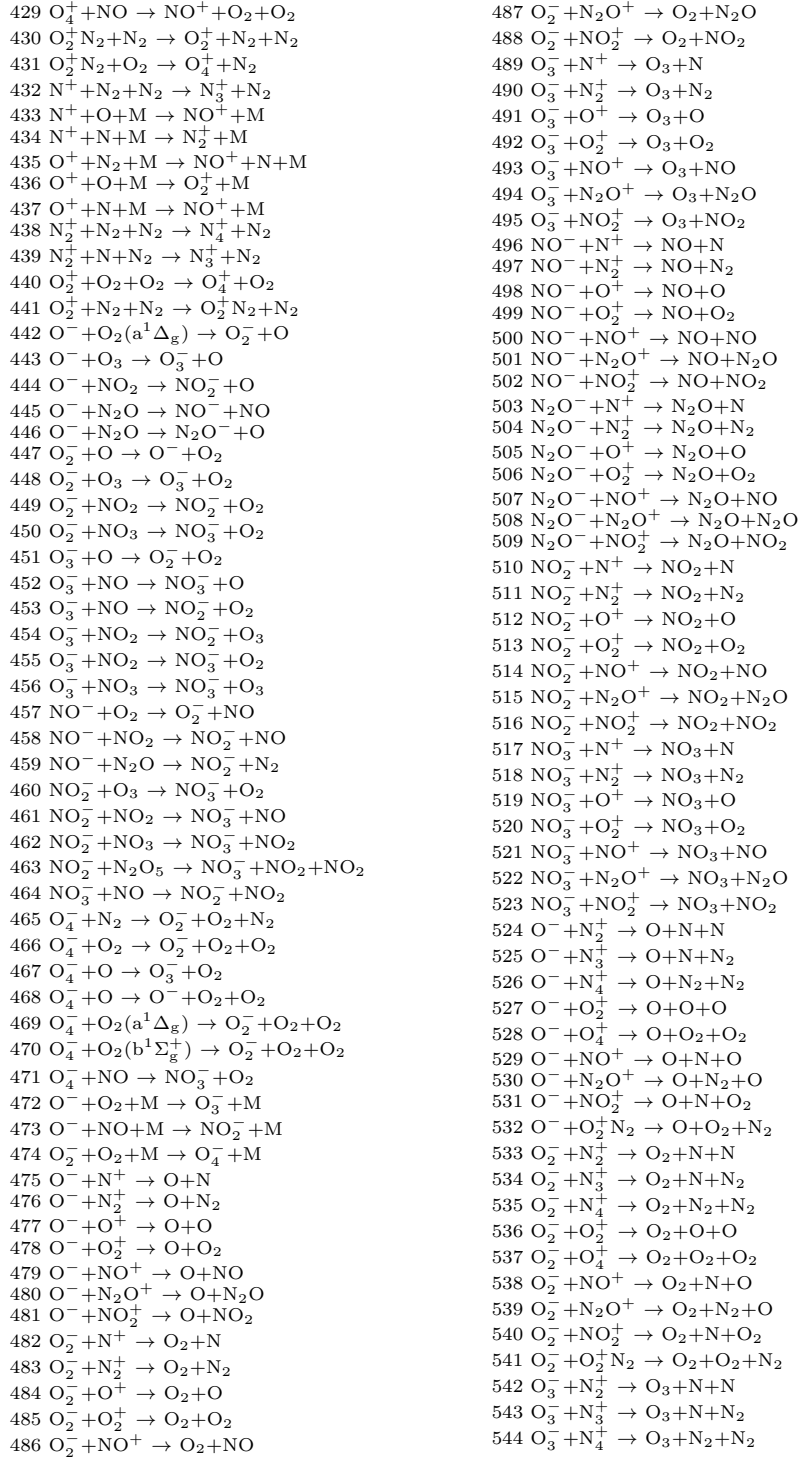
The list of reactions used in the chemical model (5.1). M denotes any neutral species.



- 49 $N_2(X^1, v=6)+N \rightarrow N_2(X^1, v=5)+N$
 50 $N_2(X^1, v=7)+N \rightarrow N_2(X^1, v=6)+N$
 51 $N_2(X^1, v=8)+N \rightarrow N_2(X^1, v=7)+N$
 52 $N_2+N \rightarrow N_2(X^1, v=1)+N$
 53 $N_2(X^1, v=1)+N \rightarrow N_2(X^1, v=2)+N$
 54 $N_2(X^1, v=2)+N \rightarrow N_2(X^1, v=3)+N$
 55 $N_2(X^1, v=3)+N \rightarrow N_2(X^1, v=4)+N$
 56 $N_2(X^1, v=4)+N \rightarrow N_2(X^1, v=5)+N$
 57 $N_2(X^1, v=5)+N \rightarrow N_2(X^1, v=6)+N$
 58 $N_2(X^1, v=6)+N \rightarrow N_2(X^1, v=7)+N$
 59 $N_2(X^1, v=7)+N \rightarrow N_2(X^1, v=8)+N$
 60 $N_2(X^1, v=1)+O \rightarrow N_2+O$
 61 $N_2(X^1, v=2)+O \rightarrow N_2(X^1, v=1)+O$
 62 $N_2(X^1, v=3)+O \rightarrow N_2(X^1, v=2)+O$
 63 $N_2(X^1, v=4)+O \rightarrow N_2(X^1, v=3)+O$
 64 $N_2(X^1, v=5)+O \rightarrow N_2(X^1, v=4)+O$
 65 $N_2(X^1, v=6)+O \rightarrow N_2(X^1, v=5)+O$
 66 $N_2(X^1, v=7)+O \rightarrow N_2(X^1, v=6)+O$
 67 $N_2(X^1, v=8)+O \rightarrow N_2(X^1, v=7)+O$
 68 $N_2+O \rightarrow N_2(X^1, v=1)+O$
 69 $N_2(X^1, v=1)+O \rightarrow N_2(X^1, v=2)+O$
 70 $N_2(X^1, v=2)+O \rightarrow N_2(X^1, v=3)+O$
 71 $N_2(X^1, v=3)+O \rightarrow N_2(X^1, v=4)+O$
 72 $N_2(X^1, v=4)+O \rightarrow N_2(X^1, v=5)+O$
 73 $N_2(X^1, v=5)+O \rightarrow N_2(X^1, v=6)+O$
 74 $N_2(X^1, v=6)+O \rightarrow N_2(X^1, v=7)+O$
 75 $N_2(X^1, v=7)+O \rightarrow N_2(X^1, v=8)+O$
 76 $O_2(X^3, v=1)+O_2 \rightarrow O_2+O_2$
 77 $O_2(X^3, v=2)+O_2 \rightarrow O_2(X^3, v=1)+O_2$
 78 $O_2(X^3, v=3)+O_2 \rightarrow O_2(X^3, v=2)+O_2$
 79 $O_2(X^3, v=4)+O_2 \rightarrow O_2(X^3, v=3)+O_2$
 80 $O_2+O_2 \rightarrow O_2(X^3, v=1)+O_2$
 81 $O_2(X^3, v=1)+O_2 \rightarrow O_2(X^3, v=2)+O_2$
 82 $O_2(X^3, v=2)+O_2 \rightarrow O_2(X^3, v=3)+O_2$
 83 $O_2(X^3, v=3)+O_2 \rightarrow O_2(X^3, v=4)+O_2$
 84 $O_2(X^3, v=1)+O \rightarrow O_2+O$
 85 $O_2(X^3, v=2)+O \rightarrow O_2(X^3, v=1)+O$
 86 $O_2(X^3, v=3)+O \rightarrow O_2(X^3, v=2)+O$
 87 $O_2(X^3, v=4)+O \rightarrow O_2(X^3, v=3)+O$
 88 $O_2+O \rightarrow O_2(X^3, v=1)+O$
 89 $O_2(X^3, v=1)+O \rightarrow O_2(X^3, v=2)+O$
 90 $O_2(X^3, v=2)+O \rightarrow O_2(X^3, v=3)+O$
 91 $O_2(X^3, v=3)+O \rightarrow O_2(X^3, v=4)+O$
 92 $e+N_2 \rightarrow e+N_2(A^3\Sigma_u^+)$
 93 $e+N_2 \rightarrow e+N_2(A^3\Sigma_u^+, v=5-9)$
 94 $e+N_2 \rightarrow e+N_2(A^3\Sigma_u^+, v=10)$
 95 $e+N_2 \rightarrow e+N_2(B^3\Pi_g)$
 96 $e+N_2 \rightarrow e+N_2(W3)$
 97 $e+N_2 \rightarrow e+N_2(B'3)$
 98 $e+N_2 \rightarrow e+N_2(A'1)$
 99 $e+N_2 \rightarrow e+N_2(A1)$
 100 $e+N_2 \rightarrow e+N_2(W1)$
 101 $e+N_2 \rightarrow e+N_2(C^3\Pi_u)$
 102 $e+N_2 \rightarrow e+N_2(E3)$
 103 $e+N_2 \rightarrow e+N_2(A''1)$
 104 $e+N_2 \rightarrow e+N_2(SUM)$
 105 $e+O_2 \rightarrow e+O_2(a^1\Delta_g)$
 106 $e+O_2 \rightarrow e+O_2(b^1\Sigma_g^+)$
 107 $e+O_2 \rightarrow e+O_2(4.5\text{ eV})$
 108 $e+O_2 \rightarrow e+O_2(6.0\text{ eV})$
 109 $e+O_2 \rightarrow e+O_2(8.4\text{ eV})$
 110 $e+O_2 \rightarrow e+O_2(9.97\text{ eV})$
 111 $e+O \rightarrow e+O(^1D)$
 112 $e+O \rightarrow e+O(^1S)$
 113 $e+N_2(A^3\Sigma_u^+) \rightarrow e+N_2$
 114 $e+O_2(a^1\Delta_g) \rightarrow e+O_2$
 115 $e+N \rightarrow 2e+N^+$
 116 $e+O \rightarrow 2e+O^+$
 117 $e+N_2 \rightarrow 2e+N_2^+$
 118 $e+O_2 \rightarrow 2e+O_2^+$
 119 $e+NO \rightarrow 2e+NO^+$
 120 $e+N_2O \rightarrow 2e+N_2O^+$
 121 $e+N_2^+ \rightarrow N+N$
 122 $e+N_2^+ \rightarrow N+N(^2D)$
 123 $e+N_2^+ \rightarrow N+N(^2P)$
 124 $e+O_2^+ \rightarrow O+O$
 125 $e+O_2^+ \rightarrow O+O(^1D)$
 126 $e+O_2^+ \rightarrow O+O(^1S)$
 127 $e+NO^+ \rightarrow O+N$
 128 $e+NO^+ \rightarrow O+N(^2D)$
 129 $e+N_3^+ \rightarrow N_2+N$
 130 $e+N_4^+ \rightarrow N_2+N_2$
 131 $e+N_2O^+ \rightarrow N_2+O$
 132 $e+NO_2^+ \rightarrow NO+O$
 133 $e+O_4^+ \rightarrow O_2+O_2$
 134 $e+O_2^+N_2 \rightarrow O_2+N_2$
 135 $e+N^++e \rightarrow N+e$
 136 $e+O^++e \rightarrow O+e$
 137 $e+N^++M \rightarrow N+M$
 138 $e+O^++M \rightarrow O+M$
 139 $e+O_2 \rightarrow O^-+O$
 140 $e+O_2+O_2 \rightarrow O_2^-+O_2$
 141 $e+NO_2 \rightarrow O^-+NO$
 142 $e+O+O_2 \rightarrow O^-+O_2$
 143 $e+O+O_2 \rightarrow O_2^-+O$
 144 $e+O_3+M \rightarrow O_3^-+M$
 145 $e+NO+M \rightarrow NO^-+M$
 146 $e+N_2O+M \rightarrow N_2O^-+M$
 147 $e+O_2+N_2 \rightarrow O_2^-+N_2$
 148 $O^-+O \rightarrow O_2+e$
 149 $O^-+N \rightarrow NO+e$
 150 $O^-+NO \rightarrow NO_2+e$
 151 $O^-+N_2 \rightarrow N_2O+e$
 152 $O^-+O_2 \rightarrow O_3+e$
 153 $O^-+O_2(a^1\Delta_g) \rightarrow O_3+e$
 154 $O^-+O_2(b^1\Sigma_g^+) \rightarrow O+O_2+e$
 155 $O^-+N_2(A^3\Sigma_u^+) \rightarrow O+N_2+e$
 156 $O^-+N_2(B^3\Pi_g) \rightarrow O+N_2+e$
 157 $O^-+O_3 \rightarrow O_2+O_2+e$
 158 $O_2^-+O \rightarrow O_3+e$
 159 $O_2^-+N \rightarrow NO_2+e$
 160 $O_2^-+O_2 \rightarrow O_2+O_2+e$
 161 $O_2^-+O_2(a^1\Delta_g) \rightarrow O_2+O_2+e$
 162 $O_2^-+O_2(b^1\Sigma_g^+) \rightarrow O_2+O_2+e$
 163 $O_2^-+N_2 \rightarrow O_2+N_2+e$
 164 $O_2^-+N_2(A^3\Sigma_u^+) \rightarrow O_2+N_2+e$
 165 $O_2^-+N_2(B^3\Pi_g) \rightarrow O_2+N_2+e$
 166 $O_3^-+O \rightarrow O_2+O_2+e$
 167 $NO^-+N \rightarrow N_2O+e$
 168 $O_3^-+N \rightarrow NO+O_2+e$
 169 $N_2O^-+N \rightarrow NO+N_2+e$
 170 $NO_2^-+N \rightarrow NO+NO+e$
 171 $NO_3^-+N \rightarrow NO+NO_2+e$
 172 $NO^-+O \rightarrow NO_2+e$
 173 $N_2O^-+O \rightarrow NO+NO+e$
 174 $NO_2^-+O \rightarrow NO+O_2+e$
 175 $NO_3^-+O \rightarrow NO+O_3+e$
 176 $O_3^-+N_2(A^3\Sigma_u^+) \rightarrow O_3+N_2+e$



- 300 $\text{NO} + \text{O}_3 \rightarrow \text{O}_2 + \text{NO}_2$
 301 $\text{NO} + \text{N}_2\text{O} \rightarrow \text{N}_2 + \text{NO}_2$
 302 $\text{NO} + \text{NO}_3 \rightarrow \text{NO}_2 + \text{NO}_2$
 303 $\text{O}_2 + \text{O}_2 \rightarrow \text{O} + \text{O}_3$
 304 $\text{O}_2 + \text{NO}_2 \rightarrow \text{NO} + \text{O}_3$
 305 $\text{NO}_2 + \text{NO}_2 \rightarrow \text{NO} + \text{NO} + \text{O}_2$
 306 $\text{NO}_2 + \text{NO}_2 \rightarrow \text{NO} + \text{NO}_3$
 307 $\text{NO}_2 + \text{O}_3 \rightarrow \text{O}_2 + \text{NO}_3$
 308 $\text{NO}_2 + \text{NO}_3 \rightarrow \text{NO} + \text{NO}_2 + \text{O}_2$
 309 $\text{NO}_3 + \text{O}_2 \rightarrow \text{NO}_2 + \text{O}_3$
 310 $\text{NO}_3 + \text{NO}_3 \rightarrow \text{O}_2 + \text{NO}_2 + \text{NO}_2$
 311 $\text{N} + \text{N} \rightarrow \text{N}_2^+ + \text{e}$
 312 $\text{N} + \text{O} \rightarrow \text{NO}^+ + \text{e}$
 313 $\text{N}_2 + \text{N}_2 \rightarrow \text{N} + \text{N} + \text{N}_2$
 314 $\text{N}_2 + \text{O}_2 \rightarrow \text{N} + \text{N} + \text{O}_2$
 315 $\text{N}_2 + \text{NO} \rightarrow \text{N} + \text{N} + \text{NO}$
 316 $\text{N}_2 + \text{O} \rightarrow \text{N} + \text{N} + \text{O}$
 317 $\text{N}_2 + \text{N} \rightarrow \text{N} + \text{N} + \text{N}$
 318 $\text{O}_2 + \text{N}_2 \rightarrow \text{O} + \text{O} + \text{N}_2$
 319 $\text{O}_2 + \text{O}_2 \rightarrow \text{O} + \text{O} + \text{O}_2$
 320 $\text{O}_2 + \text{O} \rightarrow \text{O} + \text{O} + \text{O}$
 321 $\text{O}_2 + \text{N} \rightarrow \text{O} + \text{O} + \text{N}$
 322 $\text{O}_2 + \text{NO} \rightarrow \text{O} + \text{O} + \text{NO}$
 323 $\text{NO} + \text{N}_2 \rightarrow \text{N} + \text{O} + \text{N}_2$
 324 $\text{NO} + \text{O}_2 \rightarrow \text{N} + \text{O} + \text{O}_2$
 325 $\text{NO} + \text{O} \rightarrow \text{N} + \text{O} + \text{O}$
 326 $\text{NO} + \text{N} \rightarrow \text{N} + \text{O} + \text{N}$
 327 $\text{NO} + \text{NO} \rightarrow \text{N} + \text{O} + \text{NO}$
 328 $\text{O}_3 + \text{N}_2 \rightarrow \text{O}_2 + \text{O} + \text{N}_2$
 329 $\text{O}_3 + \text{O}_2 \rightarrow \text{O}_2 + \text{O} + \text{O}_2$
 330 $\text{O}_3 + \text{N} \rightarrow \text{O}_2 + \text{O} + \text{N}$
 331 $\text{O}_3 + \text{O} \rightarrow \text{O}_2 + \text{O} + \text{O}$
 332 $\text{N}_2\text{O} + \text{N}_2 \rightarrow \text{N}_2 + \text{O} + \text{N}_2$
 333 $\text{N}_2\text{O} + \text{O}_2 \rightarrow \text{N}_2 + \text{O} + \text{O}_2$
 334 $\text{N}_2\text{O} + \text{NO} \rightarrow \text{N}_2 + \text{O} + \text{NO}$
 335 $\text{N}_2\text{O} + \text{N}_2\text{O} \rightarrow \text{N}_2 + \text{O} + \text{N}_2\text{O}$
 336 $\text{NO}_2 + \text{N}_2 \rightarrow \text{NO} + \text{O} + \text{N}_2$
 337 $\text{NO}_2 + \text{O}_2 \rightarrow \text{NO} + \text{O} + \text{O}_2$
 338 $\text{NO}_2 + \text{NO} \rightarrow \text{NO} + \text{O} + \text{NO}$
 339 $\text{NO}_2 + \text{NO}_2 \rightarrow \text{NO} + \text{O} + \text{NO}_2$
 340 $\text{NO}_3 + \text{N}_2 \rightarrow \text{NO}_2 + \text{O} + \text{N}_2$
 341 $\text{NO}_3 + \text{O}_2 \rightarrow \text{NO}_2 + \text{O} + \text{O}_2$
 342 $\text{NO}_3 + \text{NO} \rightarrow \text{NO}_2 + \text{O} + \text{NO}$
 343 $\text{NO}_3 + \text{N} \rightarrow \text{NO}_2 + \text{O} + \text{N}$
 344 $\text{NO}_3 + \text{O} \rightarrow \text{NO}_2 + \text{O} + \text{O}$
 345 $\text{NO}_3 + \text{N}_2 \rightarrow \text{NO} + \text{O}_2 + \text{N}_2$
 346 $\text{NO}_3 + \text{O}_2 \rightarrow \text{NO} + \text{O}_2 + \text{O}_2$
 347 $\text{NO}_3 + \text{NO} \rightarrow \text{NO} + \text{O}_2 + \text{NO}$
 348 $\text{NO}_3 + \text{N} \rightarrow \text{NO} + \text{O}_2 + \text{N}$
 349 $\text{NO}_3 + \text{O} \rightarrow \text{NO} + \text{O}_2 + \text{O}$
 350 $\text{N}_2\text{O}_5 + \text{M} \rightarrow \text{NO}_2 + \text{NO}_3 + \text{M}$
 351 $\text{N} + \text{N} + \text{N}_2 \rightarrow \text{N}_2 + \text{N}_2$
 352 $\text{N} + \text{N} + \text{O}_2 \rightarrow \text{N}_2 + \text{O}_2$
 353 $\text{N} + \text{N} + \text{NO} \rightarrow \text{N}_2 + \text{NO}$
 354 $\text{N} + \text{N} + \text{N} \rightarrow \text{N}_2 + \text{N}$
 355 $\text{N} + \text{N} + \text{O} \rightarrow \text{N}_2 + \text{O}$
 356 $\text{O} + \text{O} + \text{N}_2 \rightarrow \text{O}_2 + \text{N}_2$
 357 $\text{O} + \text{O} + \text{O}_2 \rightarrow \text{O}_2 + \text{O}_2$
 358 $\text{O} + \text{O} + \text{N} \rightarrow \text{O}_2 + \text{N}$
 359 $\text{O} + \text{O} + \text{O} \rightarrow \text{O}_2 + \text{O}$
 360 $\text{O} + \text{O} + \text{NO} \rightarrow \text{O}_2 + \text{NO}$
 361 $\text{N} + \text{O} + \text{N}_2 \rightarrow \text{NO} + \text{N}_2$
 362 $\text{N} + \text{O} + \text{O}_2 \rightarrow \text{NO} + \text{O}_2$
 363 $\text{N} + \text{O} + \text{N} \rightarrow \text{NO} + \text{N}$
 364 $\text{N} + \text{O} + \text{O} \rightarrow \text{NO} + \text{O}$
 365 $\text{N} + \text{O} + \text{NO} \rightarrow \text{NO} + \text{NO}$
 366 $\text{O} + \text{O}_2 + \text{N}_2 \rightarrow \text{O}_3 + \text{N}_2$
 367 $\text{O} + \text{O}_2 + \text{O}_2 \rightarrow \text{O}_3 + \text{O}_2$
 368 $\text{O} + \text{O}_2 + \text{NO} \rightarrow \text{O}_3 + \text{NO}$
 369 $\text{O} + \text{O}_2 + \text{N} \rightarrow \text{O}_3 + \text{N}$
 370 $\text{O} + \text{O}_2 + \text{O} \rightarrow \text{O}_3 + \text{O}$
 371 $\text{O} + \text{N}_2 + \text{M} \rightarrow \text{N}_2\text{O} + \text{M}$
 372 $\text{O} + \text{NO} + \text{N}_2 \rightarrow \text{NO}_2 + \text{N}_2$
 373 $\text{O} + \text{NO} + \text{O}_2 \rightarrow \text{NO}_2 + \text{O}_2$
 374 $\text{O} + \text{NO} + \text{NO} \rightarrow \text{NO}_2 + \text{NO}$
 375 $\text{O} + \text{NO}_2 + \text{N}_2 \rightarrow \text{NO}_3 + \text{N}_2$
 376 $\text{O} + \text{NO}_2 + \text{O}_2 \rightarrow \text{NO}_3 + \text{O}_2$
 377 $\text{O} + \text{NO}_2 + \text{N} \rightarrow \text{NO}_3 + \text{N}$
 378 $\text{O} + \text{NO}_2 + \text{O} \rightarrow \text{NO}_3 + \text{O}$
 379 $\text{O} + \text{NO}_2 + \text{NO} \rightarrow \text{NO}_3 + \text{NO}$
 380 $\text{NO}_2 + \text{NO}_3 + \text{M} \rightarrow \text{N}_2\text{O}_5 + \text{M}$
 381 $\text{N}^+ + \text{O} \rightarrow \text{N} + \text{O}^+$
 382 $\text{N}^+ + \text{O}_2 \rightarrow \text{O}_2^+ + \text{N}$
 383 $\text{N}^+ + \text{O}_2 \rightarrow \text{NO}^+ + \text{O}$
 384 $\text{N}^+ + \text{O}_2 \rightarrow \text{O}^+ + \text{NO}$
 385 $\text{N}^+ + \text{O}_3 \rightarrow \text{NO}^+ + \text{O}_2$
 386 $\text{N}^+ + \text{NO} \rightarrow \text{NO}^+ + \text{N}$
 387 $\text{N}^+ + \text{NO} \rightarrow \text{N}_2^+ + \text{O}$
 388 $\text{N}^+ + \text{NO} \rightarrow \text{O}^+ + \text{N}_2$
 389 $\text{N}^+ + \text{N}_2\text{O} \rightarrow \text{NO}^+ + \text{N}_2$
 390 $\text{O}^+ + \text{N}_2 \rightarrow \text{NO}^+ + \text{N}$
 391 $\text{O}^+ + \text{O}_2 \rightarrow \text{O}_2^+ + \text{O}$
 392 $\text{O}^+ + \text{O}_3 \rightarrow \text{O}_2^+ + \text{O}_2$
 393 $\text{O}^+ + \text{NO} \rightarrow \text{NO}^+ + \text{O}$
 394 $\text{O}^+ + \text{NO} \rightarrow \text{O}_2^+ + \text{N}$
 395 $\text{O}^+ + \text{N}(^2\text{D}) \rightarrow \text{N}^+ + \text{O}$
 396 $\text{O}^+ + \text{N}_2\text{O} \rightarrow \text{NO}^+ + \text{NO}$
 397 $\text{O}^+ + \text{N}_2\text{O} \rightarrow \text{N}_2\text{O}^+ + \text{O}$
 398 $\text{O}^+ + \text{N}_2\text{O} \rightarrow \text{O}_2^+ + \text{N}_2$
 399 $\text{O}^+ + \text{NO}_2 \rightarrow \text{NO}_2^+ + \text{O}$
 400 $\text{N}_2^+ + \text{O}_2 \rightarrow \text{O}_2^+ + \text{N}_2$
 401 $\text{N}_2^+ + \text{O} \rightarrow \text{NO}^+ + \text{N}$
 402 $\text{N}_2^+ + \text{O}_3 \rightarrow \text{O}_2^+ + \text{O} + \text{N}_2$
 403 $\text{N}_2^+ + \text{N} \rightarrow \text{N}^+ + \text{N}_2$
 404 $\text{N}_2^+ + \text{NO} \rightarrow \text{NO}^+ + \text{N}_2$
 405 $\text{N}_2^+ + \text{N}_2\text{O} \rightarrow \text{N}_2\text{O}^+ + \text{N}_2$
 406 $\text{N}_2^+ + \text{N}_2\text{O} \rightarrow \text{NO}^+ + \text{N} + \text{N}_2$
 407 $\text{O}_2^+ + \text{N}_2 \rightarrow \text{NO}^+ + \text{NO}$
 408 $\text{O}_2^+ + \text{N} \rightarrow \text{NO}^+ + \text{O}$
 409 $\text{O}_2^+ + \text{NO} \rightarrow \text{NO}^+ + \text{O}_2$
 410 $\text{O}_2^+ + \text{NO}_2 \rightarrow \text{NO}^+ + \text{O}_3$
 411 $\text{O}_2^+ + \text{NO}_2 \rightarrow \text{NO}_2^+ + \text{O}_2$
 412 $\text{N}_3^+ + \text{O}_2 \rightarrow \text{O}_2^+ + \text{N} + \text{N}_2$
 413 $\text{N}_3^+ + \text{O}_2 \rightarrow \text{NO}_2^+ + \text{N}_2$
 414 $\text{N}_3^+ + \text{N} \rightarrow \text{N}_2^+ + \text{N}_2$
 415 $\text{N}_3^+ + \text{NO} \rightarrow \text{NO}^+ + \text{N} + \text{N}_2$
 416 $\text{N}_3^+ + \text{NO} \rightarrow \text{N}_2\text{O}^+ + \text{N}_2$
 417 $\text{NO}_2^+ + \text{NO} \rightarrow \text{NO}^+ + \text{NO}_2$
 418 $\text{N}_2\text{O}^+ + \text{NO} \rightarrow \text{NO}^+ + \text{N}_2\text{O}$
 419 $\text{N}_4^+ + \text{N}_2 \rightarrow \text{N}_2^+ + \text{N}_2 + \text{N}_2$
 420 $\text{N}_4^+ + \text{O}_2 \rightarrow \text{O}_2^+ + \text{N}_2 + \text{N}_2$
 421 $\text{N}_4^+ + \text{O} \rightarrow \text{O}^+ + \text{N}_2 + \text{N}_2$
 422 $\text{N}_4^+ + \text{N} \rightarrow \text{N}^+ + \text{N}_2 + \text{N}_2$
 423 $\text{N}_4^+ + \text{NO} \rightarrow \text{NO}^+ + \text{N}_2 + \text{N}_2$
 424 $\text{O}_4^+ + \text{N}_2 \rightarrow \text{O}_2^+ + \text{N}_2 + \text{O}_2$
 425 $\text{O}_4^+ + \text{O}_2 \rightarrow \text{O}_2^+ + \text{O}_2 + \text{O}_2$
 426 $\text{O}_4^+ + \text{O}_2(\text{a}^1\Delta_g) \rightarrow \text{O}_2^+ + \text{O}_2 + \text{O}_2$
 427 $\text{O}_4^+ + \text{O}_2(\text{b}^1\Sigma_g^+) \rightarrow \text{O}_2^+ + \text{O}_2 + \text{O}_2$
 428 $\text{O}_4^+ + \text{O} \rightarrow \text{O}_2^+ + \text{O}_3$



Summary

Science may set limits to knowledge, but should not set limits to imagination.

– BERTRAND RUSSELL

Do not fear to be eccentric in opinion, for every opinion now accepted was once eccentric.

– BERTRAND RUSSELL

Modeling multiple time scales in streamer discharges

Aram H. Markosyan

The thesis focuses on modeling the various time scales in streamer development. Streamers are growing channels of ionized gas occurring in the first stages of electric breakdown. As such they play a fundamental role in natural phenomena such as lightning and sprite discharges as well as in technical applications like plasma medicine or plasma assisted combustion. In most gases, streamers are propagating with speeds of 10^5 m/s or more. In the streamer tip (also called streamer head) not only plasma, but many excited species are created. The further evolution of these species plays a crucial role in technical applications as well as in discharge phenomena in general. This makes the modeling of the whole process a very complicated task, as many different time scales are involved. Streamer propagation takes place on timescales of tens to hundreds of nanoseconds. But chemical reactions require time scales up to minutes or even days depending on the problem.

In the first part of the thesis we derive and test a high order fluid model for streamer discharges. Using momentum transfer theory, the fluid equations are obtained as velocity moments of the Boltzmann equation; they are closed in the local mean energy approximation and coupled to the Poisson equation for the space charge generated electric field. The high order tensor in the energy flux

equation is approximated by the product of two lower order moments to close the system. The average collision frequencies for momentum and energy transfer in elastic and inelastic collisions for electrons in molecular nitrogen are calculated from a multi term solution of the Boltzmann equation. We then discuss, in particular, (1) the correct implementation of transport data in streamer models; (2) the accuracy of the two term approximation for solving the Boltzmann equation in the context of streamer studies; and (3) the evaluation of the mean-energy-dependent collision rates for electrons required as an input in the high order fluid model, (4) comparisons of the simulation results with the high order model, with a PIC/MC (Particle in Cell/Monte Carlo) model and with the first order fluid model based on the hydrodynamic drift-diffusion approximation.

The second part of the thesis investigates streamer discharges created by two short electric pulses. S. Nijdam and E. Takahashi performed experiments in $\text{N}_2\text{-O}_2$ mixtures at 133 mbar and showed that for a sufficiently short interval between the pulses the second streamers would continue the paths of the first streamers. For nitrogen-oxygen mixtures at 133 mbar the experiments show that this time interval is maximal at 0.2% O_2 . We use a zero-dimensional plasma chemical model to describe the dynamics of 53 species subject to 650 chemical reactions. We explain the experimental observations by the loss of electrons and conductivity which is slowest at an oxygen concentration of about 0.2%.

In the third part a pathway reduction tool for complex plasma chemical models is described. Many fields of science increasingly demand complex chemical models. Thanks to the availability of cheap computing power, scientists routinely use models composed of hundreds, if not thousands, of interacting chemical species. Many of these models have a direct relevance for our society's most pressing problems; for example the chemical modeling of the atmosphere plays a significant role in the study of global climatic change. The demand for complex chemical models is also growing within the plasma physics community. This tendency arises from the recent development of plasma applications involving complex chemical processes, as well as a growing interest in the role of atmospheric electricity on the global chemical balance of our atmosphere. We have developed a software tool PumpKin (pathway reduction method for plasma kinetic models). PumpKin is a software package to find all principal pathways, i.e. the dominant reaction sequences, in chemical reaction systems. Although many tools are available to integrate numerically arbitrarily complex chemical reaction systems, few tools exist in order to analyze the results and interpret them in relatively simple terms. In particular, due to the large disparity in the lifetimes of the interacting components, it is often useful to group reactions into pathways that recycle the fastest species. Thus, the researcher can focus on the slow chemical dynamics, eliminating the shortest timescales. Based on the algorithm described by Lehmann [103], PumpKin automates the process of finding such pathways, allowing the user to analyze complex kinetics and understand the consumption and production of a certain species of interest. We designed PumpKin with an emphasis on plasma chemical systems but it can also be applied to atmospheric modeling and other application areas. The code and its user manual can be downloaded from the web site <http://www.pumpkin-tool.org>.

Acknowledgements

A teacher is one who makes himself progressively unnecessary.

– THOMAS CARRUTHERS

Liberty means responsibility. That is why most men dread it.

– GEORGE BERNARD SHAW

If you would be a real seeker after truth, it is necessary that at least once in your life you doubt, as far as possible, all things.

– RENE DESCARTES

It seems like it was only yesterday, when I entered the office of Prof. Ute Ebert at CWI for the first time. Since that very first moment I have met many people who have contributed to the research summarised in this thesis as well as to my personal development.

First of all, I would like to thank Ute for being such a great mentor encouraging me to pursue my academic career. I have received endless support from her in both my academic and personal life. Her door was always open for any type of discussion. Beside of being a great scientist and person, she is a visionary and a passionate leader. She gave me absolute freedom during these years. This was crucial for my development as an independent scientist. At the same time, I constantly felt her support and I always knew that if something went wrong she would know what to do. Ute, it was an honour and pleasure to work with you. Thank you very much for everything. I truly hope we can keep collaborating in the future.

Second, I would like to gratefully and respectfully thank my co-promotor and very good friend Sasha Dujko. We both started to work at CWI at the same time: Sasha as a PostDoc and me as a PhD student. From the initial days we were

I am grateful to Jannis and Mrunal for reading the initial version of this chapter very carefully.

spending our evenings together and were regularly making bicycle trips around Diemen. Very often we were having food at Flevopark while discussing practically everything. Sasha graduated from James Cook University, Australia under the supervision of Ron D. White, with whom we later published my first paper. Sasha liked to remember his Australian times and share his PhD experience with me. He used to repeat "Mate, a PhD is a journey... Be smart!". Sasha was an enormous source of knowledge, helping me fill the gaps in my physics education. In 2011, when he moved to Institute of Physics in Belgrade as an associate professor, we kept working together via Skype. Since then, he has been visiting CWI, almost regularly, one week per month. For longer discussions, I used to call him on Skype when he was at home (after 8 p.m. or during weekends) and then he liked to play guitar and sing while I was working. Often, during serious discussions, Sasha's funny little daughter Andrea was suddenly popping up in front of the screen with a very cute face (and without front teeth). I used to share all my worries with Sasha, and ask him for advice. Sasha has a talent for relaxing and encouraging me. He always had the right words for the right moment. I can say that one of the greatest things during this period of my life was our friendship. Sasha, thank you for your immense support and patience.

Furthermore, I would like to express my gratitude to Alejandro Luque and Francisco Gordillo Vázquez from the Institute for Astrophysics of Andalusia (IAA-CSIC), in Granada, Spain, whom I visited for 4 weeks in 2013. My visits were supported by 4 exchange grants (each for one week) from the European Research Networking Programme TEA-IS (Thunderstorm Effects on the Atmosphere - Ionosphere System). The initial purpose of my first visit was to learn about plasma chemistry, but after arriving Alejandro and Paco suggested me to work on the development of a tool which we later called PumpKin. I was working with Alejandro on a daily basis. I have never met such a brilliant physicist with deep knowledge in mathematics and scientific computing. I'm thankful to Alejandro for his enormous patience and willingness to help and support me. I would like to thank both Alejandro and Paco for our productive discussions and the warm hospitality during my visits. I look forward to continuing our collaboration.

The knowledge I got during my visits to Alejandro and Paco made possible my next collaboration with Sander Nijdam (TU/e) and Eiichi Takahashi (AIST, Japan). Working with Sander I have learned a lot about experiments. It was a unique experience for me to talk to an excellent experimentalist with a deep understanding of the theory. I am grateful to Sander for our discussions and the personal advice he gave me. I hope we can keep collaborating in the future.

I would also like to thank Jin Zhang (TU/e) for the very productive and nice time we spent working together. Jin, under the supervision of Bert van Heesch (TU/e), has designed a high voltage switch operating in supercritical nitrogen. Before meeting her, I knew nothing about switches. She had a background in electrical engineering, and together we had to come up with a numerical model for a supercritical switch. I learned a lot in this project and greatly enjoyed working with Jin. I would also like to express my deepest gratitude to Martin Seeger (ABB Switzerland Ltd, Corporate Research) for intense and fruitful discussions about

this project. Moreover, I am grateful to Martin for his very valuable advise and support related to my future.

I would like to thank Prof.dr. Nikolay L. Alexandrov (Moscow Institute of Physics and Technology), Prof.dr. Ralf Peter Brinkmann (Ruhr-Universität Bochum), prof.dr. Cornelis W. Oosterlee (TU Delft), prof.dr.ir. B. Koren (TU/e), prof.dr.ir. O.J. Luiten (TU/e) for being on the reading committee and prof.dr. H.J.H. Clercx (TU/e) for being the committee chairman.

I would like to thank my roommate and friend Mrunal Gawade with whom I lived in the shared apartment at Carolina MacGillavrylaan for 9 months. Mrunal, I greatly enjoyed our endless nightly discussions. I wish you a lot of success in your PhD and personal life.

Next I would like to express my deepest gratitude to my former college and friend Janis Bajars who has given me huge support from the first days I joined CWI. Janis has introduced me to many of our colleagues at CWI (Henk Roose, Maarten Dijkema, Georgiana Caltais, Behnaz Changizi etc.) and external colleagues whom we met at annual Woudschoten conferences in Zeist (Shavarsh Nurijanyan, Lilya Ghazaryan, David J. Lopez Penha, Mishra Chittaranjan, Valeriu Savcenco etc.). Janis I will miss our very intense scientific and personal discussions during the weekends.

Many thanks go, in particular, to Bram van Es who made my PhD life much easier and more enjoyable. Bram helped me getting a house in Haarlem at Vlammingstraat street where I lived for two years. Haarlem is one of the best places I have ever lived in. Bram, thanks for your daily support and for the enormous amount of fun that we had over the last four years. You were always a good friend (and never an ex-friend).

I would like to thank my friend Sergey Pancheshnyi from ABB Switzerland Ltd, Corporate Research, who always helped me move forward in the right direction. Sergey, during my PhD I knew that I could always call you for advice. I am grateful for the discussions about my future that we had at various conferences.

Next I would like to thank all my officemates at CWI: Gideon Wormeester (who could crash my MacBook with his presence), Anna Mozartova, Li Chao and Casper Rutjes. Casper, thanks for our nice discussions and all the support you gave me over the last year. I wish you a lot of success in your scientific and personal life.

I gratefully acknowledge the influence of the group-members of our MD (Multi-scale Dynamics) group (previously MAC3) on my research. I was honoured to know and work with all of you: Willem Hundsdorfer (thanks Willem for having your door open for any of my questions), Margreet Nool (I greatly enjoyed our discussions in the corridor), Jens Rademacher, Enrico Camporeale (thanks Enrico for your big support in such a short period. It was my pleasure to meet you), Christoph Köhn (my good friend Chris, before I leave we should drink Armenian brandy together), Jannis Teunissen (my friend and paranymp Jannis, we had a lot of fun moments during last years, for which I'm grateful to you. Stop teasing people and good luck!), Anbang Sun, Anna Dubinova, Ashutosh Agnihotri (Ashutosh, it is a great pity that we didn't have more time to spend together. I have greatly enjoyed all our discussions and I hope that we will keep in touch.

Mate don't forget to come to my wedding on June 21) and Valeria Ratushnaya. I would like to highlight the support of Nada Mitrovic, who let me be focused on my PhD without being stressed about administrative stuff and travelling declarations. Nada thank you for your endless kindness to me and for being so great at your job.

This research has been mostly carried out at CWI, and I would like to thank all my CWI colleagues/friends for helpful discussions and friendly working atmosphere. I would like to mention in particular: Barry Koren, Kees Oosterlee, Jan Verwer (1946-2011), Jason Frank, Daan Crommelin, Gunnar Klau, Joost Batenburg (Joost, I enjoyed our meetings and discussions in the train to CWI), Jeroen Witteveen (Jeroen, thanks for the advise you gave me about my career), Lech Grzelak (my friend Lech, thanks for making my Monday mornings alive and thanks for the interesting conversations we had), Sergiy Zhuk (thanks friend for our discussions), Benjamin Sanderse, Willem Haverkort, Igor Savostianov, Delyan Zhelyazov, Yunus Hassen, Jeroen Wackers, Shashi Jain, Wagner Fortes, Mohammed El-Kebir, Linda Plantagie, Marjon Ruijter, Qian Feng, Mohammed El-Kebir, Jesse Dorrestijn, Keith Myerscough, Marta Pou (Marta, thank you a lot for a tip for the ring), Wander Wadman, Davy Landman (my friend, thanks for making me laugh and be angry at the same time at every Praethuys), Vadim Zaytsev (my friend Vadim, thanks for the nice discussions during Praethuys), Waruzjan Shahbazian (thanks for everything), Gebre Gebremeskel (man, thanks for our interesting discussions), Niels Nes (thanks for your support), Eleni Petraki, Holger Pirk (Holgar, it was my pleasure to meet you), Yagiz Kargin (looking forward to seeing you in 'big politics'), Simon Gunkel (thanks mate for being such a quiet neighbour)...

I would like to express my deepest gratitude to the support staff of CWI: Bikkie Aldeias and Tilly Baas (you were the first people I met every morning, and thanks to you I was starting my day with a smile), Karin van Gemert, Irma van Lunenburg (thanks for your support and your kindness), Martine Anholt Gunzeln, Léon Ouwerkerk, Marlin van der Heijden, Angelique Schilder, Rick Ooteman, Margriet Brouwer, Huib van den Berg, Coby van Vonderen and Michael Smeding. I would like to thank Dubravka Tepsic (sorry for all the trouble, it was a pleasure to communicate with you), Maarten Dijkema and Henk Roose (thanks for your friendship and support). One of my favorite places at CWI was the library, where I have spent many hours. I would like to thank Hans Stoffel for our late night conversations and for his devoted work, as well as Lieke Schultze, Rob van Rooijen and Wouter Mettrop. Special thanks to Rob Korver for the very interesting (and funny) talks at 6 a.m. at CWI. Furthermore, I would like to acknowledge the fantastic health support from Margreet Lammertink and Ine Solleveld during the chair massage sessions two times a month at CWI. I must admit that every time I was desperately waiting for a massage. Very special thanks to Minnie Middelberg for all the warmth she gave me.

Due to my collaborations and frequent visits to the TU/e, I met many good colleagues and friends. I would like to thank several people: Pavlo Kochkin (Pasha, I'm waiting for your revenge for karting in Vienna), Anna Chvyreva, Guus Pemen, Wilfred Hoebe, Gerrit Kroesen, Chris Vasko (Hey Chris, I still

have the photos from the conference roof from Granada), Emile Carbone, Simon Hübner, Manuel Jimenez-Diaz (Manolo, do you remember New York?), Jan van Dijk and Diana Mihailova.

My greatest debts are to my family. My parents Henrik Markosyan and Karine Arzumanyan have dreamed about this day from the very early moments of my life. They have devoted their lives to educate me and to see me at this stage. I would like to mention my sister Anush Markosyan who gave me so much love and support. Not to forget my parents-in-law Arayik Stepanyan and Gohar Manvelyan whose constant support to Araks and me made our relations possible, and, hence, significantly contributed to my thesis. Finally, without my girlfriend, fiancée, official wife and best friend, Araks, I wouldn't been able to stay so strong during this journey. You shared every second of my last four years. Words wouldn't be enough to express your patience, love and encouragements to me.

I love you, *Araks!*

*Amsterdam, Haarlem, Yerevan
April 2014*

Aram Markosyan

Նախաբան

Կարծես երեկ լիներ. մորս հետ երթուղային տաքսիով իջնում էինք Երևանի պետական համալսարան (ԵՊՀ) ընդունելության դիմումն հանձնելու: Դեռ հստակ չէինք որոշել, թե որ բաժին եմ դիմելու: Քննարկել էինք մաթեմատիկայի ու կիրառական մաթեմատիկայի ֆակուլտետների տարբերակները և վերջ: Հայրս էլ այդ ժամանակ ծառայում էր ՀՀ պաշտպանության նախարարությունում և գործուղված էր զորամաս: Ճանապարհին, երբ հասնում էինք Ավան, ասացի, որ բան չկա, եթե չընդունվեմ պետպատվերով (վճարովի տարբերակը քննարկումից դուրս էր), ապա մյուս տարի կդիմեմ: Երբ հասանք ԵՊՀ, զգացի, որ մաթեմատիկայի ֆակուլտետ եմ ուզում դիմել: Այդպես էլ վարվեցի. դիմումի մեջ նշեցի միայն մաթեմատիկայի բաժինը: Մինչ այդ երևի մեկ կամ երկու անգամ էի տեսել ԵՊՀ-ի շենքը: Այսօրվա պես հիշում եմ, թե ինչ վեհ զգացողություն ունեցա:

Անցավ մի քանի ամիս, ես արդեն համալսարանի ուսանող էի: Մուսոյան, Պողոսյան, Բեգլարյան ... Այսօրվա պես հիշում եմ Պողոսյան Միքայելի հետ առաջին հանդիպումս, կարծեցի թե համակուրսեցիներ ենք: «Այդքան երիտասարդ ու արդեն մաթեմատիկական անալիզի գործնական է դասավանդում», - մտածեցի ես: Այնքան ինձ ոգևորեց այդ միտքն ու այդ կերպարը՝ երիտասարդ դասախոս: Մտածում էի. «Տեսնես ինչու՞ է շարունակում դասախոսել, եթե կարող էր ցանկացած արտասահմանյան ընկերությունում աշխատել շատ ավելի բարձր աշխատավարձով»: Հասկացա միայն 12 տարի անց, երբ ինքս պետք է նման որոշում կայացնեի:

Առաջին տարին շատ բարդ անցավ: Հիշում եմ մորս միշտ ասում էի, որ ծանրաբեռնվածությունը շատ է, որ ֆիզ. մաթ. թեքումով դպրոցներ ավարտած ուսանողների համար ամեն ինչ այնքան հեշտ է ստացվում: Մյուս կողմից էլ շատ հիասթափեցնող էր համատարած կաշառակերությունը, երբ վաճառքի առարկա էր դարձել ուսանողի առաջադիմությունը: Մայրս միշտ ասում էր, որ շարունակեմ աշխատել, ու որ ամեն ինչ լավ կլինի: Ինձ շատ էր օգնում իմ նախկին կրկնուսույցներ Աշոտ Հակոբյանի և Վարդան Մելքոնյանի ուսումնական մեթոդաբանությունը, որին հետևում եմ մինչ օրս:

Ավարտին էր մոտենում առաջին տարին: Այդ ժամանակ շատ մոտ էի երկու համակուրսեցիներին՝ Պողոսյան Վահրամի և Ջափարյան Արայիկի հետ, որոնք մինչև օրս էլ ընկերներս են: Արայիկը ի սկզբանե ուզում էր գնալ կիրառական մաթեմատիկայի ֆակուլտետ և այդպես էլ վարվեց: Վահրամի էլ մեր խմբից տեղափոխվեց «հատուկ խումբ», որին Մուսոյանը կատակով միշտ անվանում էր «թուլլերի խումբ»: Հատուկ խումբը 10 հոգանոց խումբ էր, որտեղ սովորում էին կուրսի լավագույն ուսանողները: Վահրամի պնդմամբ մտա դեկանատ և ասացի, որ ուզում եմ հատուկ խմբում սովորել: Հիշում եմ փոխդեկան Թապալքյանի անվատահ հայացքը, երբ հարցրեց թե արդյոք կարող եմ այդ խմբում սովորել: Այդ պահին, չգիտեմ էլ թե որտեղից այդքան ինքնավստահություն, պատասխանեցի, որ եթե թույլ տան, ապա կլինեմ այդ խմբի լավագույն ուսանողը: Այսպես հայտնվեցի հատուկ խմբում: Լավագույն տարիներն էին, ամբողջությամբ կլանված էի միայն ուսման մեջ, մասնակցում էի բոլոր գիտական ժողովներին: Շատ էի սիրում համալսարանի գրադարանը. այդքան աղքատիկ և այդքան հարագատ:

Անցավ ևս 5 տարի, և արդեն կայացած մագիստրոս էի: Ավարտել էի բակալավրը կարմիր դիպլոմով: Լսել էի Գեորգյանի, Առաքելյանի, Խաչատրյանի, Մովսիսյանի, Գրիգորյանի, Յավրյանի և այլոց ֆանտաստիկ դասախոսությունները: Աշխատում էի մագիստրոսական թեզիս վրա Միքայել Պողոսյանի ղեկավարությամբ: Խնդիրը առաջադրել էր Հ. Շահգեղյանը Ստեփանուի Տեխնոլոգիաների թագավորական ինստիտուտից: Որքան էի սիրում Միքայելի հետ հանդիպման օրերը, երբ ինչ-որ արդյունքի էինք հասնում: Նստում էինք մեր թվային մեթոդների և օպտիմալ կառավարման ամբիոնում և ժամերով քննարկում: Աշխատում էի օր ու գիշեր: Վաղեմի ընկերոջ՝ Մելքոնյան Ավետիքի (Մելքոնյան Վարդանի տղան) հորդորով ուսմանը զուգահեռ որոշեցի միանալ իրեն և ամառները աշխատել մի փոքրիկ սրճարանում որպես գանձապահ, որտեղ և հանդիպեցի Արտակին և Արթուրին: Շատ բան տեսա և սովորեցի այդ ընթացքում: Կարդում էի ամբողջ օրը (աշխատանքս ավարտվում էր կեսգիշերին ժ. 3-ին):

Վերջապես թեզս պատրաստ էր: Պաշտպանության ժամանակ Մովսիսյան Յուրան ասաց, որ իմ թեզը իր տեսած լավագույն թեզերից մեկն է: Անչափ ուրախ էի: Բայց ուրախությունս երկար չտևեց, քանի որ տեղեկացա, որ ինձ համար պետպատվերով ասպիրանտուրայի տեղ չի եկել կրթության և գիտության նախարարությունից: Այնքան վիրավորված էի: Շատ շուտով վիրավորանքս փոխարինվեց զայրույթով, երբ ընկերներս պարզեցին, որ ինձ ասպիրանտուրայի տեղ, այնուամենայնիվ, հատկացվել է: Իմացանք նաև, որ այդ տեղը նվիրել (վաճառել) էին ֆիզիկայի ֆակուլտետի մի ուսանողի, ում հայրը ֆիզիկայի ֆակուլտետի դասախոս էր: Գնացի դեկան Ա. Սահակյանի մոտ... Հայրս վրդովված գնաց մեր նախկին դեկան և դասախոս փոխդեկտոր Գեորգյանի մոտ, ով ինձ շատ լավ էր ճանաչում: Գեորգյանը հորս առաջարկեց, որ ասպիրանտուրան շարունակեմ Ռուսաստանի Դաշնությունում: Շատ մեծ աջակցություն ստացա Գեորգյանի կողմից, և վերջապես կարծես թե ստացվեց ամեն ինչ:

Դեռ մագիստրատուրան չավարտած մի օր դեկանատի պատին կարդացի հայտարարություն Փրանսիայի դեսպանատան կողմից այն մասին, որ Փրանսիայի կառավարությունը կրթաթոշակ է տրամադրում Փրանսիայում ուսանելու համար: Որոշեցի դիմել: Փրանսիայում էր բնակվում նախկին համակուրսեցիս և վաղեմի

ընկերն՝ Մարգարյան Մամիկոնը, ով էլ հենց օգնեց թղթաբանության հարցերում: Ընդունվեցի Փարիզի Պիեր և Մարի Կյուրիների համալսարանի (Փարիզ 6) մաթեմատիկա և կիրառությունների ֆակուլտետը՝ մագիստրատուրայի երկրորդ կուրս: Ընդունվելը հարցի միայն մի կողմն էր, պետք էին նաև ֆինանսներ, որպեսզի հասնեի այնտեղ: Այստեղ էլ օգնեց Արսենը, ում հայրը՝ Էդիկը, առանց ինձ հետ նախկինում ծանոթ լինելու, անմիջապես տրամադրեց ողջ գումարը:

Աննկարագրելի տպավորություն ունեի, երբ առաջին անգամ հասա Փարիզ 6 համալսարանը: Սարսափում էի մենակությունից և ֆրանսերենի չիմացությունից: Հակառակի պես էլ ամեն տեղ միայն ֆրանսերեն էին խոսում: Դասերն այնքան հագեցած ու խորն էին, որ հազիվ հասցնում էի գրի առնել լսածս ֆրանսերեն բառերը: Առաջին անգամ էի տանից հեռու, ամեն ինչ ուրիշ էր և օտար: Կարծես մեխանիկորեն էի ամեն ինչ անում: Պատահաբար մի անգամ օգնեցի մի երիտասարդի, ով, պարզվեց, իմ նոր հարևանն էր հանրակացարանում: Հարևանների մեծամասնությունը երիտասարդ արաբ ուսանողներ էին, ովքեր փախել էին Հյուսիսային Աֆրիկայի չքավորությունից և այդքան էլ չէին ուզում սովորել: Այնքան ուրախացա, երբ պարզվեց, որ նոր հարևանս մասամբ հայազգի վրացի է և եկել է, որ ավարտի մագիստրատուրայի երկրորդ կուրսը հոգեվերլուծաբան մասնագիտությամբ: Միանգամից դարձանք շատ մտերիմ ընկերներ: Նրա անունը Շալվա Մամինաշվիլի էր, նա ասաց, որ իրեն կոչեմ Գիգա: Այդ ժամանակ շատ էի հետաքրքրվում Ֆրեյդով, Ժան Լականով, Յունգով: Միանգամից հասկացա, որ գիտելիքների մի շտեմարան եմ գտել, և հաջորդ մեկուկես տարվա մեծ մասն անցավ հոգեվերլուծաբանական սեսիաների շուրջ: Սպունգի պես կլանում էի ամեն մի աննշան ինֆորմացիա: Հազվադեպ եմ հանդիպել այդքան գիտելիքներով հարուստ մարդու: Երբեք չեմ մոռանա, թե ինչպես էր սոված մնում և հավաքած գումարով գրքեր գնում:

Շատ դժվար անցան փարիզյան տարիները: Շատերն էին կողքիս, բայց քչերը գիտեին, թե իրականում ինչքան դժվար է: Իհարկե, ծնողներս միշտ աջակցում էին, ինչպես նաև հարազատներս: 2009-ի դեկտեմբերին թողեցի Փարիզը՝ առանց ապագայի մասին ինֆորմացիայի: Դիմել էի մի քանի տեղ ասպիրանտուրայի համար, բայց դեռ ոչ մի առաջարկություն չկար: Անցավ ևս երկու ամիս, և ահա հրավիրվեցի CWI, Ամստերդամ հարցազրույցի: CWI-ը Նիդեռլանդների մաթեմատիկայի և ինֆորմատիկայի ազգային կենտրոնն է: Պահանջվում էր ներկայացնել մագիստրոսական թեզերիցս որևէ մեկը: Ընտրեցի ԵՊՀ թեզը, քանի որ Փարիզինն այնքան էլ կապ չունեի այս խմբի թեմաների հետ, ովքեր, ի դեպ, զբաղվում էին կիրառական ֆիզիկայով: Չանցած երկու ամիս՝ 2010 թվականի մայիսին արդեն Ամստերդամում էի և պատրաստվում էի ինձ փորձել պլազմա ֆիզիկայի ոլորտում: Թե ինչպես ստացվեց, առաջարկում եմ ընթերցողին կարդալ թեզս:

Հիմա 2014 թվականի Մարտի 19-ն է: Ուղիղ երկու ամսից՝ Մայիսի 19-ին, կապաշտպանեմ չորս տարիների աշխատանքս և մի օր շուտ կգամ Հայաստան, որպեսզի կազմակերպենք հարսանեկան արարողությունս, որը տեղի է ունենալու հունիսին: Իսկ արդեն հուլիսին պետք է սկսեմ աշխատանքս Միչիգանի համալսարանում՝ Մարկ Կուշների խմբում, որտեղ ինձ հրավիրել է հենց ինքը՝ Մարկը: Գրեցի ամուսնանալու մասին և չասացի ամենակարևորը. ամուսնանում եմ իմ սիրելի Արաքս Ստեփանյանի հետ, ում հետ առաջին անգամ հանդիպեցի Ծաղկածորում 2008 թվականին միջազգային գիտաժողովի ժամանակ: Նի-

դեռ լանդներ գնալու առաջին իսկ օրերից միասին ենք ամեն երեկո Skype-ում: Երկու տարի է, ինչ նշանադրվել ենք և հունիսին կամուսնանանք ու միասին կտեղափոխվենք Միչիգան:

Վերջում ուզում եմ ջերմ շնորհակալություն հայտնել բոլոր նրանց, ովքեր աջակցում էին ինձ այս ամբողջ ընթացքում. հորս՝ Հենրիկ Մարկոսյանին, մորս՝ Կարինե Արզումանյանին, քրոջս՝ Անուշիկին, սիրելի հարսնացուիս՝ Արաքսին, և իր ընտանիքին՝ պարոն Ստեփանյանին, տիկին Գոհարին և վեց քույրերին (Անի, Արփի, Տաթևիկ, Լուսինե, Շողակաթ, Մարիամիկ) և նրանց ընտանիքներին, ինչպես նաև իմ հարազատներին՝ երեք քեռիներին՝ Աշոտին, Արայիկին, Դերոյին, և նրանց ընտանիքներին, հորաքույր Ջուլիկին, մորաքույր Մանիկին և նրանց ընտանիքներին, ընկերներ Աշոտին, Վահագնին, Արսենին, Ավետիք Մելքոնյանին, Վահրամին, Արայիկին, Ավետիք Առաքելյանին, Ինանց Արմենին, Միքայելին և այլն: Հատուկ շնորհակալություն Նիդեռլանդներում իմ ընկերներ Սարգիսին, Աշոտին, Վարուժանին և Շավարշին:

ՀԱՀ, Փափազյան գրադարան, Երևան
19 Մարտ 2014

Արամ Հ. Մարկոսյան

Curriculum Vitae

Good judgement comes from experience. Experience comes from bad judgement.

– UNKNOWN

I have never met a man so ignorant that I could not learn something from him.

– GALILEO GALILEI

Always and never are two words you should always remember never to use.

– WENDELL JOHNSON

If everything seems under control, you are not going fast enough.

– MARIO ANDRETTI

Aram H. Markosyan was born in Yerevan, Armenia on December 3, 1985. From 2002 to 2008 he studied Mathematics at Yerevan State University. He obtained his Bachelor of Science with honours, the latter in 2006 on a thesis titled 'An application of variational inequalities to the monotone operator theory', under supervision of Dr. G. Hakobyan. In 2008 he obtained the degree of Master of Science in Mathematics by defending his thesis entitled 'Existence of the minimal element of the class of super solutions in the one-phase parabolic free boundary problem in convex domain' under supervision of Dr. M. Poghosyan.

In late 2008 he moved to Paris and enrolled in the Master of Science & Technologies (M2) program of Mathematical Modeling, PDE and Numerical Analysis (in French: *M2 - Spécialité Mathématiques de la Modélisation, parcours 'Analyse numérique et équations aux dérivées partielles'*) at Jacques-Louis Lions Laboratory, University Pierre and Marie Curie (UPMC, Paris 6). In parallel to his studies, from the beginning of 2009 until the end of 2009, Aram H. Markosyan did his internship at Zeliade Systems under the supervision of CEO Dr. C. Mar-

tini. In late 2009, he defended his Master's thesis titled 'SVI implied variance parameterization' under supervision of Dr. C. Martini (Zeliade Systems), Prof. Dr. O. Pironneau (Paris 6) and Prof. Dr. H. Berestycki (Paris 6).

From 2010 to 2014 he performed PhD research under supervision of Prof. Dr. U. Ebert, Dr. S. Dujko and Prof. Dr. W. Hundsdorfer on modeling multiple time scales in streamer discharges, at the Centrum Wiskunde & Informatica (CWI, Amsterdam).

List of Publications

We judge ourselves by what we feel capable of doing, while others judge us by what we have already done.

– HENRY WADSWORTH LONGFELLOW

The trouble with being punctual is that nobody is there to appreciate it.

– FRANKLIN P. JONES

Publications associated with this thesis are:

Journal Publications

2014

- A.H. Markosyan, J. Teunissen, S. Dujko, U. Ebert. *Comparison of fluid models for streamer discharges*. Preprint to be submitted to Plasma Sources Sci. Technol.
- S. Dujko, A.H. Markosyan, U. Ebert. *Streamers in rare gases*. Preprint to be submitted to Plasma Sources Sci. Technol.
- J. Zhang, A.H. Markosyan, M. Seeger, E.M. van Veldhuizen, E.J.M. van Heesch, U. Ebert. *Numerical and experimental investigation of dielectric recovery in super-critical N₂*. Submitted to Plasma Sources Sci. Technol.
- S. Nijdam, E. Takahashi, A.H. Markosyan, U. Ebert. *Investigation of positive streamers by double pulse experiments, effects of repetition rate and gas mixtures*. *Plasma Sources Sci. Technol.* **23** 025008, 2014
- A.H. Markosyan, A. Luque, F. J. Gordillo-Vázquez, U. Ebert. *PumpKin: A tool to find principal pathways in plasma chemical models*. Submitted to Comput. Phys. Commun.

2013

- S. Dujko, A.H. Markosyan, R.D. White, U. Ebert. *High-order fluid model for streamer discharges: I. Derivation of model and transport data.* *J. Phys. D: Appl. Phys.* **46** 475202, 2013
- A.H. Markosyan, S. Dujko, U. Ebert. *High-order fluid model for streamer discharges: II. Numerical solution and investigation of planar fronts.* *J. Phys. D: Appl. Phys.* **46** 475203, 2013

Conference Papers

2014

- S. Dujko, D. Bošnjaković, J. Mirić, I. Simonović, Z.M. Raspopović, R.D. White, A.H. Markosyan, U. Ebert and Z.Lj. Petrović. *Recent results from studies of non-equilibrium electron transport in modeling of low-temperature plasmas and particle detectors.* Proceedings of the 9th EU-Japan Joint Symposium on Plasma Processing, JSPP2014, January 19-23, 2014, Bohinjska Bistrica, Slovenia (4 page paper).
- S. Dujko, A. Markosyan, U. Ebert. *High order fluid model for negative planar streamer fronts in rare gases.* Proceedings of the 9th EU-Japan Joint Symposium on Plasma Processing, JSPP2014, January 19-23, 2014, Bohinjska Bistrica, Slovenia (4 page paper).

2013

- A.H. Markosyan, A. Luque, F. J. Gordillo-Vázquez, U. Ebert. *Analyzing atmospheric kinetic pathways using PumpKin.* Proceedings of the European Planetary Science Congress 2013, EPSC2013, September 08-13, 2013, London, United Kingdom; Vol. 8, EPSC2013-655 (2 page paper and poster presentation).
- A.H. Markosyan, J. Zhang, B. van Heesch, U. Ebert. *Streamer to spark transition in supercritical N₂.* Proceedings of the XXth Symposium on Physics of Switching Arc, FSO 2013, September 2-6, 2013, Nove Mesto na Morave, Czech Republic (4 page paper and oral presentation).
- A.H. Markosyan, A. Luque, F. J. Gordillo-Vázquez, U. Ebert. *PumpKin: A tool to find principal pathways in plasma chemical models.* Proceedings of the XXXI International Conference on Phenomena in Ionized Gases, ICPIG 2013, July 14-19, 2013, Granada, Spain (2 page paper and poster presentation).

2012

- A. Markosyan, S. Dujko, U. Ebert. *Derivation and test of high order fluid model for streamer discharges.* Proceedings of the Scientific Computing in Electrical Engineering, SCIEE2012, September 11-14, 2012, ETH Zurich, Switzerland; pp. 107-108 (2 page paper and oral presentation).

- S. Dujko, A. Markosyan, R.D. White, U. Ebert. *High order fluid model for streamer discharges*. Proceedings of the 26th Summer School and International Symposium on the Physics of Ionized Gases, SPIG 2012, August 27-31, 2012, Zrenjanin, Serbia; ISBN: 978-86-7031-244-9, pp. 345-348 (4 page paper and poster presentation).
- A. Markosyan, S. Dujko, U. Ebert. *High order fluid model for ionization fronts in streamer discharges*. Proceedings of the XXI Europhysics Conference on Atomic and Molecular Physics of Ionized Gases, XXIth ESCAM-PIG, July 10-14, 2012, Viana do Castelo, Portugal (2 page paper and poster presentation).

Conference Talks and Posters

2014

- A.H. Markosyan, J. Teunissen, S. Dujko, U. Ebert. *Fluid models and the reality*. Proceedings of the 26th Symposium Plasma Physics & Radiation Technology, March 11 - 12, 2014, Lunteren, Netherlands (proceedings and poster presentation).
- A.H. Markosyan, A. Luque, F. J. Gordillo-Vázquez, U. Ebert. *PumpKin tool to find principal pathways in plasma chemical models*. Physics@FOM, January 21 - 22, 2014, Veldhoven, Netherlands (proceedings and oral presentation).

2013

- A.H. Markosyan, J. Zhang, B. van Heesch, U. Ebert. *Investigating streamer to spark transition in supercritical N₂*. Bulletin of the American Physical Society, 66th Annual Gaseous Electronics Conference, GEC 2013, September 30 - October 4, 2013, Princeton, New Jersey, USA; vol. 58, No. 8, p. 25 (proceedings and poster presentation).
- A.H. Markosyan, A. Luque, F. J. Gordillo-Vázquez, U. Ebert. *PumpKin: A tool to find principal pathways in plasma chemical models*. Bulletin of the American Physical Society, 66th Annual Gaseous Electronics Conference, GEC 2013, September 30 - October 4, 2013, Princeton, New Jersey, USA; vol. 58, No. 8, p. 72 (proceedings and oral presentation).
- A.H. Markosyan, J. Teunissen, S. Dujko, U. Ebert. *Comparing fluid models for streamer discharges*. Bulletin of the American Physical Society, 66th Annual Gaseous Electronics Conference, GEC 2013, September 30 - October 4, 2013, Princeton, New Jersey, USA; vol. 58, No. 8, p. 20 (proceedings and poster presentation).
- S. Nijdam, E. Takahashi, A.H. Markosyan, U. Ebert. *Investigation of positive streamers by double pulse experiments*. Bulletin of the American Physical

Society, 66th Annual Gaseous Electronics Conference, GEC 2013, September 30 - October 4, 2013, Princeton, New Jersey, USA; vol. 58, No. 8, p. 45 (proceedings).

- A.H. Markosyan, J. Zhang, B. van Heesch, U. Ebert. *Numerical investigation of voltage recovery after breakdown supercritical nitrogen*. Proceedings of the XXth Symposium on Physics of Switching Arc, FSO 2013, September 2-6, 2013, Nove Mesto na Morave, Czech Republic (proceedings and oral presentation).
- S. Dujko, Z.Lj. Petrović, R.D. White, D. Bošnjaković, J. Mirić, A.H. Markosyan, U. Ebert. *Non-conservative electron transport in gases and its application in modelling of non-equilibrium plasmas and particle detectors*. Proceedings of the XVII International Workshop on Low-Energy Positron and Positronium Physics and the XVIII International Symposium on Electron-Molecule Collisions and Swarms, POSMOL 2013, July 19-21, 2013, Kanazawa, Japan (proceedings).
- A.H. Markosyan, S. Dujko, R. U. Ebert. *High order fluid model for streamer discharges in rare gases*. Proceedings of the XVII International Workshop on Low-Energy Positron and Positronium Physics and the XVIII International Symposium on Electron-Molecule Collisions and Swarms, POSMOL 2013, July 19-21, 2013, Kanazawa, Japan (proceedings and poster presentation).
- A.H. Markosyan, S. Dujko, R. U. Ebert. *Challenges in fluid modeling of streamer discharges*. Proceedings of the Werkgemeenschap Scientific Computing spring meeting 2013, WSC Spring Meeting 2013, May 17, 2013, Amsterdam, Netherlands (proceedings and invited oral presentation).
- A.H. Markosyan, J. Zhang, B. van Heesch, U. Ebert. *Investigating heating dynamics in sparks*. Proceedings of the European Geoscience Union General Assembly 2013, EGU2013, April 07-12, 2013, Vienna, Austria (proceedings and poster presentation).
- A. Markosyan, S. Dujko, U. Ebert. *Numerical study of high order fluid model for streamer discharges*. Proceedings of the 25th Symposium Plasma Physics & Radiation Technology, March 5 - 6, 2013, Lunteren, Netherlands (proceedings and poster presentation).
- A. Markosyan, J. Zhang, B. van Heesch, U. Ebert. *On the heating dynamics in sparks*. Proceedings of the Physics@FOM, January 22 - 23, 2013, Veldhoven, Netherlands; p.41 (proceedings and poster presentation).

2012

- A. Markosyan, J. Zhang, B. van Heesch, U. Ebert. *Investigating voltage recovery after breakdown supercritical nitrogen*. Bulletin of the American Physical Society, 65th Annual Gaseous Electronics Conference, GEC 2012, October 22-26, 2012, Austin, Texas, USA; vol. 57, No. 8, p. 84 (proceedings and poster presentation).

- A. Markosyan, S. Dujko, R. White, J. Teunissen, U. Ebert. *High order fluid model for streamer discharges*. Bulletin of the American Physical Society, 65th Annual Gaseous Electronics Conference, GEC 2012, October 22-26, 2012, Austin, Texas, USA; vol. 57, No. 8, p. 53 (proceedings and oral presentation).
- A. Markosyan, S. Dujko, R. U. Ebert. *Why do we need high order fluid model for streamer discharges?*. Proceedings of the 37th Woudschoten conference, WSC Conference 2012, October 3-5, 2012, Zeist, Netherlands (proceedings and award for poster presentation).
- A. Markosyan, S. Dujko, R. U. Ebert. *High order fluid model for simulations of streamer and sprites*. Proceedings of the 1st Thunderstorm Effects on the Atmosphere-Ionosphere System Summer School, TEA-IS, June 17-22, 2012, Los Alamos, Torremolinos (Malaga), Spain (proceedings and poster presentation).
- S. Dujko, A. Markosyan, R.D. White, Z.Lj. Petrović, U. Ebert. *High-order fluid model of streamer discharges in molecular nitrogen*. Bulletin of the American Physical Society, 43rd Annual Meeting of the APS Division of Atomic, Molecular and Optical Physics, DAMOP 2012, June 4-8, 2012, Anaheim, California; vol. 57, No. 5, p. 118 (proceedings).
- A. Markosyan, S. Dujko, U. Ebert. *High order fluid model for ionization fronts in streamer discharges*. Proceedings of the 24 th Symposium Plasma Physics & Radiation Technology, March 6 - 7, 2012, Lunteren, Netherlands; p. B7 (proceedings and poster presentation).
- A. Markosyan, S. Dujko, W. Hundsdorfer, U. Ebert. *A high order density model for streamer discharges*. Proceedings of the Physics@FOM, January 17 - 18 2012, Veldhoven, Netherlands; p. 250 (proceedings and poster presentation).

2011

- A. Markosyan, S. Dujko, W. Hundsdorfer, U. Ebert. *A high order density model for streamer discharges*. Proceedings of the 14th Euregional WELTPP Workshop on the Exploration of Low Temperature Plasma Physics, December 1 - 2, 2011, Rolduc Kerkrade, Netherlands; p. P42 (proceedings and poster presentation).